Functional role of non-coding RNAs and extracellular matrix proteins in developmental processes and breast cancer

Zuzana Budková

Thesis for the degree of Philosophiae Doctor

Supervisors:
Prof. Dr. Þórarinn Guðjónsson
Dr. Gunnhildur Ásta Traustadóttir
Dr. Bylgja Hilmarsdóttir

Tutor (Supervisory teacher):
Dr. Þórarinn Guðjónsson

Doctoral committee:
Dr. Unnur Þorsteinsdóttir
Prof. Dr. Eiríkur Steingrímsson
Dr. Jón Þór Bergþórsson

April 2021

UNIVERSITY OF ICELAND
SCHOOL OF HEALTH SCIENCES
FACULTY OF MEDICINE

Hlutverk non-coding RNA sameinda og utanfrumupróteina í þroskun og sérhæfingu brjóstkirtilsfruma og í brjóstakrabbameinum

Zuzana Budková

Ritgerð til doktorsgráðu

Leiðbeinandi/leiðbeinendur:

Prof. Dr. Þórarinn Guðjónsson

Dr. Gunnhildur Ásta Traustadóttir

Dr. Bylgja Hilmarsdóttir

Umsjónarkennari

Prof. Dr. Þórarinn Guðjónsson

Doktorsnefnd:

Dr. Unnur Þorsteinsdóttir

Prof. Dr. Eiríkur Steingrímsson

Dr. Jón Þór Bergþórsson

Apríl 2021

UNIVERSITY OF ICELAND
SCHOOL OF HEALTH SCIENCES
FACULTY OF MEDICINE

ISBN 978-9935-9516-9-4

ORCID ID 0000-0002-9253-6587

Printing by Háskolarent ehf.

Reykjavik, Iceland 2021

Ágrip

Þekking á þroskun og sérhæfingu vefja gefur innsýn í gen og þroskunarferli sem einnig gegna hlutverki við myndun krabbameina og framþróun æxlisvaxtar. Í þessari ritgerð rannsakaði ég RNA sameindir sem ekki tjá fyrir próteinum (e. non-coding RNAs (microRNA og long noncoding RNA, lncRNA)) og hlutverk þeirra í þroskun og sérhæfingu brjóstkirtilsfruma. Ég skoðaði einkum hlutverk þeirra í bandvefsumbreytingu þekjufruma (e. epithelial to mesenchymal transition, EMT) og í greinóttri formgerð (e. branching morphogenesis). Auk þess rannsakaði ég hlutverk utanfrumupróteina í hegðun og svipgerð brjóstrabbameinsfruma og í nýæðamyndun. EMT og þekjuvefsumbreyting bandvefsfruma (e. mesenchymal to epithelial transition, MET) eru mikilvægir ferlar í fósturþroska og í sjúkdómum á borð við krabbamein þar sem þeir hafa verið tengdir við ífarandi vöxt og meinvarpamyndun. Greinótt formgerð í brjóstkirtlinum hefst að mestu við kynþroska kvenna og er kirtilinn í mikilli ummyndun í hverjum tíðarhring fram að tíðahvörfum. EMT og MET gegna mikilvægu hlutverki í myndun greinóttrar formgerðar í brjóstkirtli. Á síðustu árum hefur komið í ljós að non-coding RNAs hafa mikil áhrif á stjórnun EMT og MET þó enn sé margt á huldu varðandi hlutverk einstakra RNA sameinda í þessu ferli.

Rannsóknarmódelið sem ég notaði byggir á brjóstþekjufrumulínunni D492 og dótturlínum hennar. D492 er stofnfrumulína sem getur myndað greinótta formgerð í þrívíðri rækt. D492M er bandvefs-lik dótturlína frá D492 sem hefur undirgengist EMT. D492HER2 er einnig komin frá D492, en í þessari dótturlínu er HER2 æxlisgenið yfirtjáð; frumulína þessi getur myndað æxli í músum. Þessar línur hafa allar sama erfðabakgrunn en ólíka svipgerð og eru því hentugar til rannsókna á greinóttri formgerð, EMT og MET í eðlilegum og illkynja brjóstkirtli.

Meginmarkmið verkefnisins var að rannsaka tjáningu og hlutverk RNA sameinda sem ekki tjá fyrir próteinum, bæði microRNA og lncRNA, í greinóttri formgerð, EMT og MET í brjóstkirtli. Jafnframt var markmiðið að rannsaka áhrif utanfrumupróteina sem seytt er frá D492HER2 á æxlisvöxt, svipgerð og nýæðamyndun í frumurækt.

Í grein I kannaði ég hlutverk RNA sameinda sem eru staðsett á DLK1-DIO3 genasvæðinu (e. gene locus) á litningi 14 í EMT/MET, stjórnun svipgerðar frumna og í brjóstakrabbameinum. Helstu niðurstöður sýndu að RNA

sameindir þessar, þar með talið MEG3 lncRNA og microRNA á þessu genasvæði eru meira tjáð í bandvefsfrumum en þekjufrumum og jafnframt að tjáning þessara RNA sameinda hefur áhrif á sérhæfingu brjóstaþekjufruma yfir í bandvefsfrumur.

Í grein II var markmiðið að greina tjáningamynstur microRNA sameinda í greinóttri formgerð í þrívíðri rækt og EMT. Niðurstöður okkar sýna að tjáning microRNA 203a jókst margalt við myndun greinóttrar formgerðar í D492 en var lækkuð í D492M bandvefsfrumulínunni. Við sýndum einnig fram á að sameindin bælir tjáningu peroxidasin (PXDN) millifrumupróteinsins. Niðurstöður okkar benda til þess að microRNA203a sé mikilvægur stýrill við myndun greinóttrar formgerðar og í myndun grunnhimnu í brjóstkirtli og þá mögulega í gegnum PXDN.

Í grein III og IV var markmiðið að bera saman svipgerð D492 og D492M við D492HER2 frumulínuna sem ólíkt þeim fyrrnefndu myndar æxli í ónæmisbældum músum. Ólíkt D492M, sem hefur sterka EMT svipgerð, þá sýnir D492HER2 einungis EMT svipgerð að hluta (e. partial EMT) og breytir sinni svipgerð eftir ytri aðstæðum, ásamt því að tjá mun meira af þekjuvefstengdum microRNA sameindum en D492M. Auk þess sýnir D492HER2 mun meira skrið og ífarandi vaxtareiginleika en D492M. Með massagreiningu og RNA raðgreiningu greindum við utanfrumupróteinin YKL-40 og ECM1 sem prótein sem mögulega geta stuðlað að krabbameinseiginleikum D492HER2. Jafnframt hafa YKL-40 and ECM1 áhrif á nýmyndun æða í frumuræktunum.

Í ritgerð þessari hef ég rannsakað RNA sameindir sem ekki tjá fyrir próteinum frá DLK1-DIO3 genasvæðinu ásamt microRNA203a og hlutverk þeirra í greinóttri formgerð og í krabbameinum og sýnt fram á að þessar RNA sameindir gegna hlutverki í EMT/MET. Jafnframt hef ég unnið að rannsóknum á hlutverki YKL-40 og ECM1 utanfrumupróteinanna í brjóstakrabbameinum og sýnt fram á hlutverk þeirra í í skriði æxlisfruma og í nýæðamyndun.

Lykilorð:

Brjóstkirtill, non-coding RNA, Utanfrumuprótein, Bandvefsumbreyting þekjufruma, Greinótt formgerð D492, Brjóstakrabbamein

Abstract

A better understanding of normal organ development can give deeper insight into which genes are harnessed by aberrant cells during cancer formation and progression. In my thesis, I have investigated two seemingly different, however, related, developmental processes in the breast gland: epithelial-to-mesenchymal transition (EMT) and branching morphogenesis. EMT and its reverse process mesenchymal-to-epithelial transition (MET), are important processes during embryogenesis and in diseases, such as cancer, where evidence suggests that they mediate processes such as cell invasion and formation of metastasis. Branching morphogenesis is an essential developmental process that in the breast gland mostly takes place postnatally. Both processes are widely studied due to their importance in multiple fields. However, the involvement of non-coding RNAs in the regulation of gene expression during EMT and branching morphogenesis has recently been appreciated and is a challenging field of study.

In my experimental approach, I mainly took advantage of a well-defined series of cell lines referred to as the D492 cell lines, which include D492, D492M and D492HER2. D492 is a breast progenitor epithelial cell line and a model for branching morphogenesis. D492M is a non-tumorigenic cell line derived from D492 through endothelial-induced EMT, while D492HER2 is a tumorigenic cell line derived from D492 through oncogene-induced EMT. Together, D492 and D492M represent a unique *in vitro* cellular model, enabling research on the phenotypic and functional changes occurring during EMT, while D492M and D492HER2 allow us to study differences in tumorigenicity.

The primary aim of this thesis was to study the expression and functional role of non-coding RNAs during branching morphogenesis and EMT in the human breast gland using the D492 and D492M cell lines. The secondary aim was to study the role of extracellular matrix proteins secreted by D492HER2 on cancer growth and angiogenesis.

In paper #I, I addressed the role of non-coding RNAs from the DLK1-DIO3 locus in cellular plasticity, EMT and cancer. Here I used primary cells, cancer patient's cohorts and the D492 cell lines. Using the CRISPRi and CRISPRa approaches, we found out that this locus is a marker of mesenchymal cells and affects the cellular plasticity of adult breast epithelial cells.

Paper #II was focused on identifying miRNAs highly upregulated in D492 during branching morphogenesis but downregulated in D492M. We identified MIR203a as a novel suppressor of peroxidasin (PXDN), a collagen IV crosslinking agent. Our results indicate that MIR203a may be an essential regulator of branching morphogenesis and basement remodelling in the human breast gland, likely through its target PXDN.

Finally, in paper #III and IV, we compared the two D492 derived cell lines D492M and D492HER2. Compared to D492M, the tumorigenic D492HER2 has a partial EMT phenotype, seen by increased expression of epithelial miRNAs. D492HER2 shows higher migratory, invasive, proliferative and angiogenic properties compared to both D492 and D492M. By means of mass spectrometry and RNA sequencing analysis of D492M and D492HER2, we identified extracellular matrix protein YKL-40 and ECM1 as potential candidates contributing to tumorigenicity of D492HER2 and to be partially responsible for the functional differences between the cell lines. Moreover, we showed that ECM1 induces crosstalk with endothelial cells through Notch signalling.

Collectively, I have in my thesis partially uncovered the role of non-coding genes from the DLK1-DIO3 locus and MIR203a in EMT and branching morphogenesis. Furthermore, I have also, in collaboration with my co-workers, identified the ECM proteins YKL-40 and ECM1 as potential inducers of cancer growth and angiogenesis.

Keywords:

Mammary gland, non-coding RNA, extracellular matrix proteins, epithelial-to-mesenchymal transition, D492

Acknowledgements

Here, I would like to acknowledge all the people and institutions who helped me during the doctoral study.

I wish to express my sincere appreciation to my supervisor, Thorarinn Gudjonsson. First of all, for getting me the chance to come to Iceland and become part of his team. For being the exact supervisor whom I needed - for putting his trust in me, being supportive in making decisions and allowing me to find my own way. And last but not least, for showing me that science must be fun.

I wish to express my deepest gratitude to Gunnhildur Traustadottir and Bylgja Hilmarsdottir, my role models, not only as scientists. Thank you for being there to help whenever I needed it. Thank you, Gunnhildur, for being very patient and paying attention to details, both invaluable characteristics of a great scientist. Thank you, Bylgja, for your ability to put things into context, your excellent scientific overview, bright ideas, and invaluable help with the MEG3 story.

I would like to thank the other members of my doctoral committee: Jón Þór Bergþórsson, Eiríkur Steingrímsson and Unnur Þorsteinsdóttir. It was an honour for me. Special thanks to Magnus Karl Magnusson, a great person and scientist.

I would like to pay my special regards to all the present and past SCRU crew – my work family: Anna Karen, Ari, Arna, Arni, Bryndis, Eirikur, Halla, Hildur, Kata, Jennifer, Jon Petur, Saevar, Snaevar, Sigga, Tobias … I felt very well among you, each and every one of you exceptional personalities, making together such a fun and professional team to work with. Special thanks to all my office fellows during all the years: Alex, Amaranta, Erika, Paulina and Sophie, for the friendly environment and the discussions, both in and outside the workplace.

I wish to thank all the people from the labs from BMC. EM lab, GHG lab, Erikurs lab, namely to Andrea, Arsalan, Fatih, Iwona, Kimberley and Marjorie, for always willingly providing material support and great friendship.

I wish to acknowledge the support and great love of my family, my parents, my husband Jan, my daughters Doubravka Eydís and Mlada Lóa. Biggest thanks belong to Jan, who was my generous emotional, technical and scientific

support. They all kept me going on, and this work would not have been possible without their love.

Acknowledgements also belong to the bodies, who financially supported the research. This work was supported by grants from Landspitali University Hospital - Science Fund, University of Iceland - Research Fund, Rannis - Grant of Excellence, "Vísindasjóður Krabbameinsfélagsins" (Icelandic Cancer Society Science Fund) and "Göngum saman", a supportive group for breast cancer research in Iceland (www.gongumsaman.is).

Content

List of abbreviations

2D	two-dimensional
3D	three-dimensional
3'-UTR	3’ untranslated region
ALDH1A3	aldehyde dehydrogenase 1 family member A3
BRENCS	breast endothelial cells
C14MC	chromosome 14 microRNA cluster
CAGE	cap analysis of gene expression
cAMP	cyclic adenosine monophosphate
CD	cluster of differentiation
CHI3L1	Chitinase 3 like 1
Chip-seq	chromatin immunoprecipitation followed by sequencing
CRE	cAMP response element
CRISPRa	clustered regularly interspaced short palindromic repeats - activation
CRISPRi	clustered regularly interspaced short palindromic repeats - inhibition
CSCs	cancer stem cells
DAPT	N-[N-(3,5-Difluorophenacetyl)-L-alanyl]-S-phenylglycine t-butyl ester
dCas9	dead CRISPR associated protein 9
DCIS	ductal carcinoma in situ
DIO3	iodothyronine deiodinase type III
DLK1	delta like non-canonical Notch ligand 1
DMR	differentially methylated region,
DNA	deoxyribonucleic acid
ECM	extracellular matrix
ECM1	extracellular matrix protein 1
EHS	Engelbreth-Holm-Swarm
EMT	epithelial-to-mesenchymal transition

ENCODE	encyclopaedia of DNA elements
EndoMT	endothelial-to-mesenchymal transition
EpCAM	epithelial cell adhesion molecule
ER+	estrogen receptor-positive
ES	embryonic stem
FGF	fibroblast growth factor
GATA6	GATA-binding factor 6
GOBO	gene expression-based outcome for breast cancer online
GSEA	gene set enrichment analysis
GTL2	gene trap locus 2
H3K27me3	trimethylation of lysine 27 on histone H3 protein subunit
HER2+	human epidermal growth factor receptor 2 positive
HGF	hepatocyte growth factor
HMLE	human mammary epithelial cells
HUVEC	human umbilical vein endothelial cells
IDC	invasive ductal carcinoma
IG-DMR	intergenic DMR
iPCS	induced pluripotent stem cell
ITGα6	Integrin alpha 6
JARID2	Jumonji/AT-rich interactive domain 2
kb	kilo-base
KRAB	Krüppel-associated box
KRT	keratin
LEP	luminal epithelial cells
lncRNA	long non-coding RNA
LOI	loss of imprinting
MASC	mammary stem cells
MDM2	murine/human double minute 2
MEP	myoepithelial cells
MET	mesenchymal-to-epithelial transition

MG50	melanoma gene 50
CM	conditioned media
miRNA	microRNA
MMP	matrix metalloproteinases
MMTV-PyMT	mouse mammary tumor virus - polyoma middle T oncoprotein
MRE	miRNA response element
Muc1	mucin 1
ncRNA	non-coding RNA
NES	normalized enrichment score
nt	nucleotide
piRNAs	piwi-interacting RNAs
polyA	poly-adenylated
PR+	progesterone receptor-positive
PRC2	polycomb repressive complex 2
PVDF	polyvinylidene fluoride membrane
PXDN	peroxidasin
RB	retinoblastoma
rBM	reconstituted basement membrane
RNA	ribonucleic acid
RNA-seq	RNA sequencing
Rtl1	retrotransposon-like 1
scRNAseq	single-cell mRNA sequencing
SMAD	small drosophila mothers against decapentaplegic
SNORD	small nucleolar RNAs, C/D box
snRNA	small nucleolar RNA
SPRY2	sprouty homolog 2
TDLU	terminal duct lobular units
TGFβ	transforming growth factor β
TIMP	tissue inhibitor metalloproteinases
TNBC	triple negative breast cancer
TNFα	tumor necrosis factor

TP63	tumor protein 63
tRNAs	transfer RNAs
TSS	transcription start site
UPD	paternal uniparental disomy
VIM	vimentin
ZEB1	zinc finger E-box binding homeobox 1
ZEB2	zinc finger E-box binding homeobox 2
*α*SMA	alpha smooth muscle actin

List of figures

List of tables

List of original papers

I. Expression of ncRNAs on the DLK1-DIO3 locus is associated with basal and mesenchymal phenotype in breast epithelial progenitor cells.

Zuzana Budkova, Anna Karen Sigurdardottir, Eirikur Briem, Jon Thor Bergthorsson, Snævar Sigurdsson, Magnus Karl Magnusson, Gunnhildur Traustadottir, Thorarinn Gudjonsson and Bylgja Hilmarsdottir

(Front Cell Dev Biol, 2020 June)

II. MiR-203a is differentially expressed during branching morphogenesis and EMT in breast progenitor cells and is a repressor of peroxidasin.

Eirikur Briem, Zuzana Budkova, Anna Karen Sigurdardottir, Bylgja Hilmarsdottir, Jennifer Kricker, Winston Timp, Magnus Karl Magnusson, Gunnhildur Asta Traustadottir and Thorarinn Gudjonsson

(Mech Dev. , 2019 February)

III. YKL-40/CHI3L1 facilitates migration and invasion in HER2 overexpressing breast epithelial progenitor cells and generates a niche for capillary-like network formation.

Erika Morera, Sarah Sophie Steinhauser, Zuzana Budkova, Saevar Ingthorsson, Jennifer Kricker, Aileen Krueger, Gunnhildur Asta Traustadottir and Thorarinn Gudjonsson

(In Vitro Cell Dev Biol Anim., 2019 September)

IV. ECM1 secreted by HER2-overexpressing breast cancer cells generates vascular niche that accelerates migration and invasion of cancer cells.

Sarah Sophie Steinhauser, Erika Morera, Zuzana Budkova, Wang, Q., Rolfsson, O., Riedel, A., Aileen Krueger, Bylgja Hilmarsdottir, Maelandsmo, G.M., Agnarsson, B.A., Jonasson, J.G., Ingthorsson, S., Gunnhildur Asta Traustadottir, Oskarsson, T. and Thorarinn Gudjonsson.

(*Lab Invest, 100*(7), 2020 March)

V. Mammary organoids and 3D cell cultures: Old dogs with new tricks.

Jakub Sumbal, Zuzana Budkova, Gunnhildur Asta Traustadottir, Zuzana Koledova

(J Mammary Gland Biol Neoplasia, 2020 November)

In addition, unpublished data are presented.

All papers are reprinted by kind permission of the publishers.

Declaration of contribution

I. Expression of ncRNAs on the DLK1-DIO3 locus is associated with basal and EMT phenotype in breast epithelial progenitor cells.

This paper is dedicated to the examination of non-coding RNAs from the imprinted locus DLK1-DIO3 and its role in the EMT process. This paper is the main part and focus of my PhD project. Here I am the first author, and I contributed to the conceptualisation and design of the study, data acquisition, analysis and writing of the manuscript. I joined this project when part of the story and data was already generated, mainly by Dr Bylgja Hilmarsdottir, the last author of the paper. After I overtook the project, I continued with the initial ideas and conceptualised new ideas. I spent a considerable amount of time with optimisation of CRISPRi and CRISPRa methods for creating gain and loss of function of *MEG3* in D492 and D492M, respectively. I functionally (using assays such as proliferation, apoptosis, migration, invasion or 3D cultures) and molecularly (using qRT–PCR and western blot) characterised the newly generated cell lines. I prepared the samples for RNA sequencing and contributed to the analysis and interpretation of the sequencing data. Moreover, I drafted the manuscript and, together with other authors, performed the tasks needed for finalising the manuscript. In addition to the published data and material, I have also collected other preliminary data, which are a part of the thesis.

II. MiR-203a is differentially expressed during branching morphogenesis and EMT in breast progenitor cells and is a repressor of peroxidasin.

In this paper, we describe the role of MIR203a in branching morphogenesis and EMT in the breast gland and identified its novel target gene peroxidasin (PXDN). My contribution to this paper, where I am the second author, is performing laboratory work, including optimisations of various experiments. I performed multiple qRT–PCR, immunostaining, functional assays (proliferation assay, apoptosis assay, anchorage-independent growth assay, migration assay, invasion assay), transient transfections with miRNA mimics and inhibitors, optimisation of luciferase assay, and finally silencing PXDN

with siRNAs and subsequent functional assays (proliferation and apoptosis). I have also generated other cell lines with overexpression of MIR203a in addition to the published data and material (PMC42^{miR203a} and D492HER2^{miR203a}) using lentiviral overexpression. Finally, I also contributed to the finalisation of the manuscript.

III. YKL-40/CHI3L1 facilitates migration and invasion in HER2 overexpressing breast epithelial progenitor cells and generates a niche for capillary-like network formation

In this paper, we functionally and molecularly compared the two EMT-derived cell lines called D492M and D492HER2, and we identified YKL-40 as a facilitator of migration and invasion. I am the third author in this study, and I contributed to the study with help in laboratory work: qRT–PCR for analysing the miRNAs expression, the analysis and optimisation of the newly established CRISPR cell lines. I also performed angiogenesis assays, viability assay and some of the 3D cultures. I also contributed to the finalisation of the manuscript and general cell culture work.

IV. ECM1 secreted by HER2-overexpressing breast cancer cells generates vascular niche that accelerates migration and invasion of cancer cells.

In this paper, we identified secreted protein ECM1 as an essential player in angiogenesis in HER2-overexpressing cell lines. I am the third author of this study, and I contributed with laboratory work such as angiogenesis assays, qRT–PCR, design of the gRNAs for CRISPRi/a and general cell culture work.

V. Mammary organoids and 3D cell cultures: Old dogs with new tricks.

In this review, we summarise the 3D cell culture methods used in the mammary gland field. The review comprises a wide range of topics, including the comparison of mouse and human models, the methods allowing to study processes like mammary gland development, branching morphogenesis, lactation, and tumorigenesis in a physiological context. I am a co-author in this review, and my focus was on the parts related to breast cancer research and modern 3D technology such as bioprinting and microfluidics.

1 Introduction

1.1 Human mammary gland

The mammary gland is a determining organ for the class *Mammalia*, which can produce milk to feed the offspring. Unlike the development of other organs, the female mammary gland is an organ undergoing significant cellular changes postnatally, with the main periods of development during puberty, pregnancy, lactation, and involution. The human breast gland is composed of branching epithelial ducts surrounded by stromal tissue.

1.1.1 Epithelium

The mammary gland is made up of highly branching epithelial ducts, extending from the nipple and terminating in the functional units called terminal duct lobular units (TDLUs). TDLUs consist of two main epithelial cell types. The inner layer is composed of luminal epithelial cells, which synthesise milk. The outer layer comprises myoepithelial cells, whose contractions help to push out the milk during lactation. Myoepithelial cells also contribute to the formation of the basement membrane that surrounds the epithelial ducts. The histological changes are enabled by breast progenitor cells with regenerative capacity, located between luminal and myoepithelial cells (Gudjonsson et al., 2002; Hammond et al., 1984; Shackleton et al., 2006) (**Figure 1**).

Several markers can distinguish breast epithelial cell types. Among characteristic markers of luminal epithelial cells are keratin 8 (KRT8), keratin 19 (KRT19), EpCAM, and GATA3. In contrast, the myoepithelial cells are characterised by markers such as keratin 5 (KRT5), keratin 14 (KRT14), P-cadherin (CDH3), p63 (TP63), alpha-smooth muscle actin (αSMA), and vimentin (VIM) (Adriance et al., 2005; Gudjonsson et al., 2005; Gudjonsson et al.,2002). Recently, further heterogeneity within the two epithelial cell types of the breast has been revealed. Nguyen et al. (2018) reported, using single-cell RNA sequencing, three distinct mammary epithelial cell clusters, one basal and two luminal cell types, which were derived from the basal population. Moreover, Fridriksdottir et al. (2017) revealed spatial heterogeneity in myoepithelial progenitor cells.

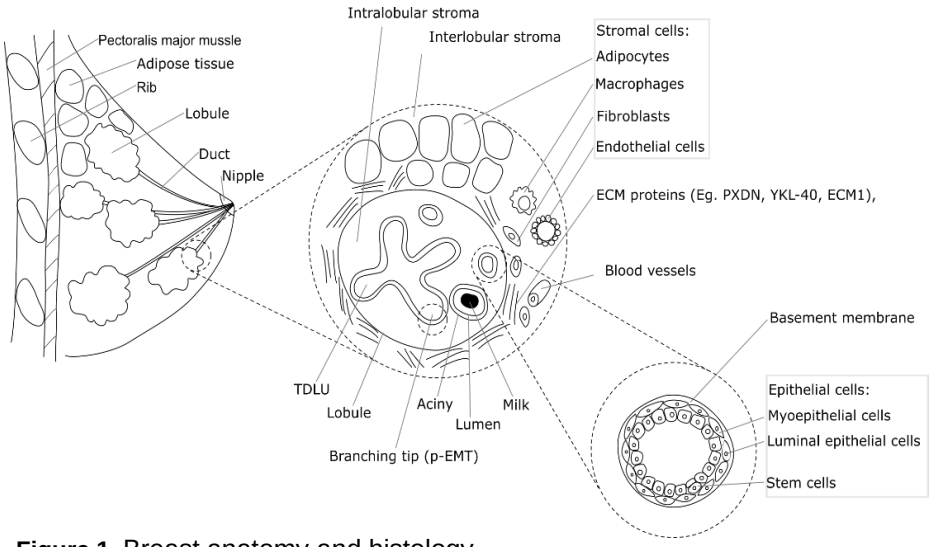

Figure 1. Breast anatomy and histology.

The breast gland is created by epithelial ductal tree surrounded by cellular rich stromal tissue. Epithelial tissue includes the ducts and lobules. Each TDLU is composed of myoepithelial and luminal epithelial cells, as well as of small percentage of mammary stem cells. Stroma comprises the area between lobes (interlobular stroma) and inside the lobes (intralobular stroma) and is formed by extracellular matrix (ECM) and stromal cells (fibroblasts, adipocytes, macrophages, endothelial cells). Each cell type can be distinguished by specific markers.

A small percentage of basal cells forms the mammary stem cells (MASCs), the tissue progenitor cells with the ability to generate the breast's functional units (Eirew et al., 2008). Mammary stem cells enable continuous tissue remodelling throughout the lifetime, known as branching morphogenesis (Arendt & Kuperwasser, 2015). In general, stem cells are defined by asymmetrical division, unlimited self-renewal capacity and the ability to give rise to more differentiated cells and are characterised by drug resistance, quiescence (dormancy) and slow proliferation (Dean et al., 2005; Mikkers & Frisen, 2005; Sottocornola & Lo Celso, 2012). It has been shown that breast stem cells can be identified by $CD44^{+}/CD24^{-/low}$, CD49f (ITGα6), EpCAM and ALDH1A3 (Aldehyde Dehydrogenase 1 Family Member A3) (Al-Hajj et al., 2003; Makarem et al., 2013; Spike et al., 2012; Vassalli, 2019). In the human mammary gland, mammary stem cells were found to be located in terminal ducts near differentiated cells (Villadsen et al., 2007). Such specific localisation is mediated by the crosstalk of stem cells and the stem cell niche. Stem cell niche is a tissue-specific 3D microenvironment, which has a determining role on stem cell properties.

1.1.2 Stroma

Stroma forms the microenvironment for the functional tissue and directly affects the epithelial cells' cell fate (Ghajar & Bissell, 2008; Kleinman et al., 2003; Wiesen et al., 1999). The ratio of stromal to epithelial compartment changes during mammary gland development (Polyak & Kalluri, 2010). The breast gland's stroma is composed of extracellular matrix (ECM) and stromal cells. The human mammary stroma's cellular elements are represented by fibroblasts, adipocytes, immune cells, and vascular endothelial cells. The most common type of stromal cells are fibroblasts, which synthesise many ECM proteins (Unsworth et al., 2014). The second most common cell type is mammary gland-associated adipocytes, which serve as an energy reservoir for milk production (Neville et al., 1998). Our research group has mainly focused on endothelial cells and their role in the differentiation of mammary epithelial cells. Endothelial cells line the luminal side of blood and lymph vessels, and their primary function is providing nutrients and oxygen and removing the waste products. However, as we and others have shown, the role of endothelial cells goes beyond that. Endothelial cells follow the dynamic of the mammary gland during the lifetime and support the branching and growth of cells (Bergthorsson et al., 2013; Ingthorsson et al., 2010). Vasculogenesis, which takes place during embryogenesis, is followed by angiogenesis, where the blood vessels are formed.

Epithelial cells are separated from interstitial ECM by a basement membrane, a specialised structure essential for tissue polarity (Bonnans et al., 2014). The basement membrane is a sheet-like extracellular matrix, which encapsulates the mammary gland epithelium. It is composed of collagen IV, laminins, perlecan and nidogen, while interstitial ECM is rich in proteins such as collagen I, fibronectin, decorin and biglycan, and altogether of more than 300 molecules (Hynes & Naba, 2012; Insua-Rodríguez & Oskarsson, 2016).

The communication between epithelium and stroma is enabled by a network of biochemical factors. The main biochemical components include soluble proteins, growth factors, along with enzymes responsible for ECM remodelling (matrix metalloproteinases - MMPs or tissue inhibitor metalloproteinases - TIMPs). In this thesis, I, together with my co-workers, identified secreted extracellular matrix proteins peroxidasin (PXDN), YKL-40 and extracellular matrix protein 1 (ECM1) playing an important role in various properties, increasing the metastatic potential of epithelial cells. PXDN is a secreted protein that facilitates crosslinking between collagen IV fibres by catalysis of sulfilimine bonds and is involved in extracellular matrix formation (Bhave et al., 2012; Cummings et al., 2016; Péterfi & Geiszt, 2014). YKL-40, also called Chitinase 3 like 1 (CHI3L1), is a secreted glycoprotein, approximate

40 KDa in size, associated with various biological functions and diseases, such as inflammation or asthma (Erturk et al., 2017; Johansen et al., 2007; Kastrup, 2012). ECM1 is a secreted and transmembrane glycoprotein with a size of about 85 kDa. In previous studies, it has been involved in many biologic processes and functions, such as differentiation and angiogenesis (Wu et al., 2018).

1.1.3 Branching morphogenesis

Crosstalk of epithelium and stroma plays a vital role in a developmental program called branching morphogenesis. Unlike the branching development in other organs such as lung, kidney or salivary gland, the human mammary gland's branching develops in stages (Lu et al., 2006). The development starts during embryogenesis with the rudimentary ductal tree. Later stages of development, occurring during puberty and pregnancy, are hormone (estrogen and progesterone) dependent. At puberty, the rudimentary tree develops further into more elaborated branching structures. When pregnancy occurs, the branching morphogenesis further progresses and reaches the maximum differentiation stage during lactation. The arborisation of the mammary gland is an effective way of the spatial distribution of ducts and lobules. Branching is a combination of cell proliferation, differentiation, migration and invasion (Myllymaki & Mikkola, 2019; Zhang et al., 2014). Besides the principal role of hormones, branching is coordinated by local bi-directional epithelial-stromal crosstalk and by soluble factors from ECM (Fata et al., 2004; Kim & Nelson, 2012). For example, stromal transforming growth factor β (TGFβ) directs branch point generation as an inhibitory morphogen by different concentrations at duct and lobules (Nelson et al., 2006). Another important growth factor is fibroblast growth factor 2 (FGF2), which controls the ductal elongation process, while FGF10 regulates the branch initiation process (Unsworth et al., 2014). Epithelial invasion is also facilitated by matrix metalloproteinases (MMPs) (Nelson et al., 2000). The unique postnatal developmental properties of the mammary gland, which includes cycles of cell growth and death, and the invasive essence, allow looking for parallels between normal mammary gland development and breast cancer progression (Ghajar & Bissell, 2008). Also, signalling pathways governing branching morphogenesis can be hijacked by cancer cells that use these processes for invasion and metastasis (Lanigan et al., 2007). Understanding the mechanism of branching morphogenesis is essential to understand metastatic spreading in breast cancer.

1.1.4 Angiogenesis

Vessel morphogenesis can be viewed as a parallel to mammary morphogenesis in terms of processes involved in forming new sprouts/branches. Vessels are formed by a single inner layer of endothelial cells, which are wrapped by pericytes. Pericytes maintain the maturation of endothelial cells and sustain the blood-brain barrier (Bergers & Song, 2005). Endothelial cells can be distinguished by markers such as CD31, VE-cadherin or VEGFR (Goncharov et al., 2017). In sprouting angiogenesis, there are three kinds of specialised endothelial cells, called 'tip, stalk, and phalanx cells', which differ in their role and marker expression. The 'tip cell' receives the pro-angiogenic signal and release proteases that break down the vessel wall in order to escape (migrate) to the extracellular matrix (Chappell et al., 2011). 'Tip cells' are, among others, characterised by filopodia (Gerhardt et al., 2003). The 'stalk cell' is called the cell behind the 'tip cell' and is proliferating, causing the elongation of the sprout as a response to a pro-angiogenic signal. A new vessel fragment is formed when the 'tip cell' fuses with an existing vessel, and a lumen is formed. The quiescent endothelial cells are called 'phalanx cells' and ensure a tight barrier of the vessel.

Various stimuli act as pro-angiogenic factors, such as VEGF, FGF1, FGF2, angiopoietins, MMPs. One of the most critical factors driving angiogenesis is Notch signalling. It coordinates 'stalk/tip cell' specification, where it is inhibited in the 'tip cell', whereas it is activated in the 'stalk cell' (Gridley, 2010).

1.2 Breast cancer

Breast cancer is the most diagnosed cancer in women, and the second most common type of cancer overall (Ghoncheh et al., 2016). In the USA, approximately 1,7 million cases are diagnosed per year, with approximately 0,5 million cancer-related death annually (Siegel et al., 2019).

Breast carcinoma originates in epithelial cells; however, epithelium only comprises about 50 % of a tumour's cell mass (Lewis & Pollard, 2006). Tumour tissue is usually very heterogeneous, formed by different amounts of malignant cells and tumour microenvironment. The stromal compartment within the tumour mass can be created by both normal and cancer-associated cells; among them are tumour-associated macrophages (TAMs), carcinoma-associated fibroblast (CAFs), cancer-associated adipocytes, immune cells and endothelial cells (Conklin & Keely, 2012; Denton et al., 2018) (**Figure 2**).

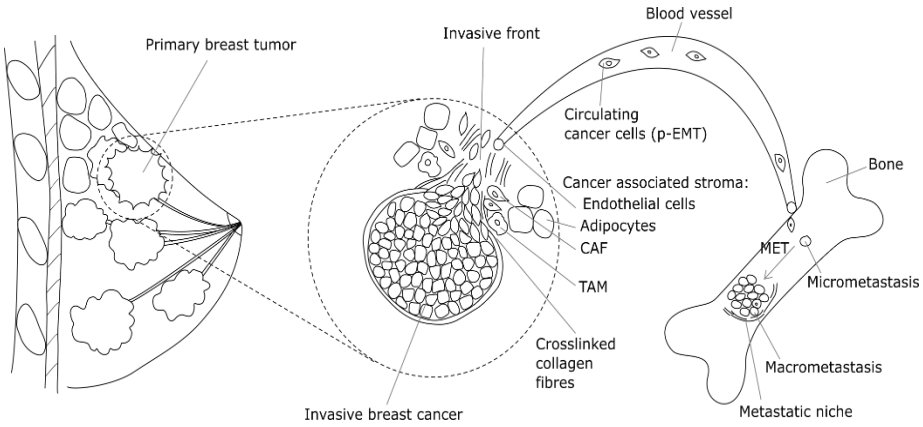

Figure 2. Breast cancer and formation of metastasis.

Cancer cells from a primary tumor can invade the circulatory system and establish metastasis. The invasion occurs at the invasive front, in a stiff microenvironment, and is a result of crosstalk of epithelial cells with stromal cells. Cancer-associated stroma is created by a cell such as CAFs (carcinoma-associated fibroblasts), adipocytes, TAMs (tumor-associated macrophages) and endothelial cells. The cancer cells can travel through the body in a circulatory system (eg. blood vessels) as circulating cancer cells. A cancer cell can reside in a breast metastatic site, such as bone, in a dormant state as micrometastasis or grow out as macrometastases when the conditions formed by the metastatic niche are convenient.

Every specific cell type can bring a particular advantage to the tumour. CAFs, characterised by α-smooth muscle actin, are predominantly in the wound healing state, producing greater amounts of matrix proteins than normal fibroblasts (Mao et al., 2013). CAFs may have various cellular origin. Besides normal fibroblast, they can arise from epithelial cells, endothelial or mesenchymal stem cells (Chen & Song, 2019; Mishra et al., 2008; Zeisberg et al., 2007). Also, endothelial cells play an important role in promoting the survival of cancer cells, for example, through secretion of tumour necrosis factor α (TNFα) (Bussard et al., 2016; De Palma et al., 2017) or have the ability to induce EMT (Ingthorsson et al.,2016; Sigurdsson et al., 2011). Increased angiogenesis is a crucial ability of tumourigenic cells and one of the tumour hallmarks (Hanahan & Weinberg, 2011). Blocking the angiogenesis has been proposed numerous times as anti-tumour therapy and is already being used in clinical practice (monoclonal antibody to VEGF, bevacizumab) (Carmeliet & Jain, 2011). The blood supply is essential for the tumour to grow beyond 1–2 mm^3, with hypoxia as one of the best-known inducers of angiogenesis. During metastasis formation, blood/lymph circulation serves as a highway for the malignant cell towards the metastatic site. The abnormal ratio of pro-and anti-angiogenic stimuli can result in chaotic and leaky vessels (McDonald &

Baluk, 2002). In general, the crosstalk between tumour cells and tumour-adjacent cells can create a convenient environment for tumour progression (Quail & Joyce, 2013).

The heterogeneity of the tumour manifests itself in the treatment as mosaics of cancer cells, with different sensitivity to the anti-cancer therapies (Cojoc et al., 2015). The development of resistance to chemotherapy is one of the biggest issues of current medicine. Intra-tumour heterogeneity arises from genomic instability and selective pressure (such as microenvironmental - acidic pH, lack of oxygen), resulting in spatial and temporal tumoral heterogeneity (Martelotto et al., 2014).

Inter-tumour heterogeneity, representing patient to patient differences, is commonly categorised into molecular subtypes based on hormone receptors' expression or based on gene expression. Categorisation of breast tumours enables targeted treatment (Turashvili & Brogi, 2017) (**Figure 3**).

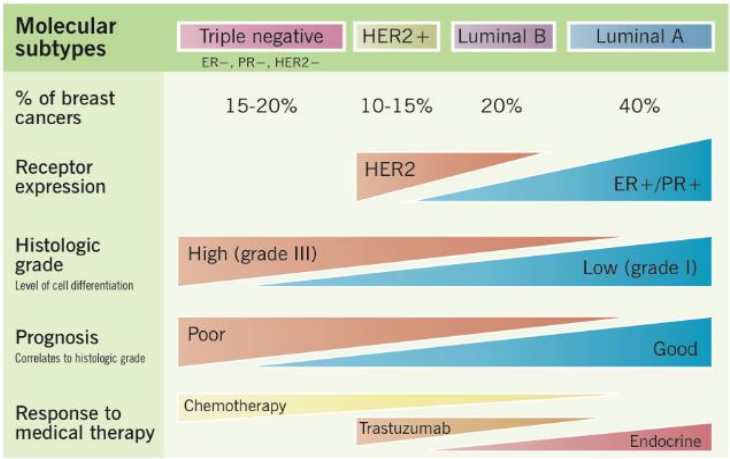

Figure 3. Molecular subtypes of breast cancer.
About 60 % of all breast cancers are estrogen receptor-positive (ER+). About 40 % of these are also progesterone receptor-positive (PR+). About 10 - 15 % of breast cancers are Human Epidermal growth factor Receptor 2 positive (HER2+). About 15 - 20 % are known as triple-negative breast cancer (TNBC). Adapted from: http://www.pathophys.org/wp-content/uploads/2012/12/breastcancer-copy.png

The most commonly recognised breast cancer groups are triple-negative (including basal-like and claudin-low), HER2, luminal A, luminal B and normal-like (Perou, 2010; Perou et al., 2000; Sorlie et al., 2001). The basal-like group can be further divided by marker expression into two subgroups: basal A (KRT5 and KRT14-positive) and basal B (VIM-positive) (Blick et al., 2010; Neve et al., 2006). TNBC is a heterogeneous group and hard to treat, especially once it has spread due to the lack of specific drug targets. It may be associated

with an inherited mutation in BRCA1 and has the same incidence in young and older women. Normal-like tumours have a high proportion of normal tissue and low tumour cellularity, therefore resembles normal breast tissue in gene expression (Prat & Perou, 2011; Yersal & Barutca, 2014).

Breast tumours samples can be classified using the PAM50 gene signature. It is a 50-gene predictor panel in which normal and tumour tissue have markedly different expression patterns (Elloumi et al., 2011; Troester et al., 2009). Based on the PAM50, a genetic test called Prosigna assay is used, which reports a risk of recurrence.

1.2.1 Carcinogenesis

Carcinogenesis is a process of transformation of normal cells into cancer cells. There are two main concepts of carcinogenesis. The first model is based on a clonal selection of cells with advantageous mutations (Greaves & Maley, 2012). The cellular origin must accumulate mutations in DNA or/and epimutations in oncogenes and tumour suppressors, which drive carcinogenesis. The second model is based on cell hierarchy, giving rise to the cancer stem cell model (CSCs) (Meacham & Morrison, 2013). CSCs show resistance to chemotherapy and radiotherapy, leading to relapse and formation of metastasis (Vidal et al., 2014). One of the proteins associated with the resistance of these cells is aldehyde dehydrogenase (ALDH), an enzyme capable of metabolising drugs (Sakakibara et al., 2012). Cancer stem cells share characteristic traits with normal stem cells, including the determining role of the stem cell niche. It is not clear whether the cancer cell of origin gained/acquired (from a differentiated cell) or inherited the capabilities (from normal stem cell) leading to cancerous phenotype, but probably both concepts can support carcinogenesis in the same tumour. In any case, the microenvironment plays a vital role in carcinogenesis and potential subsequent metastatic formation. In the case of breast cancer, the invasive transition from ductal carcinoma in situ (DCIS) to invasive ductal carcinoma (IDC) is also driven by genetic and epigenetic alternations and by tumour stroma (Cowell et al., 2013; Sung et al., 2013).

1.2.2 Metastatic formation

The metastatic formation is a process of spreading the primary tumour into secondary sites. Early metastatic formation steps occur at the invasive front, where the cells are in direct contact with stromal cells, supporting the importance of the crosstalk of epithelium and stroma (Brabletz et al., 2001). The invasive front is a stiff part of a tumour that has been suggested to contain putative cancer stem cells (Acerbi et al., 2015; Costa et al., 2015; Hermann et al., 2007). Tumour cells can escape from the primary tumour mass, invade the surrounding tissue, and intravasate into the blood or lymphatic vessels.

Subsequently, cancer cells can colonise distant organs upon extravasation and may remain as dormant micro-metastases or grow out as macro-metastases (Nieto et al., 2016) (**Figure 2**). The most common sites of breast cancer's distant spread are bone, lungs, regional lymph nodes, liver and brain (Tungsukruthai et al., 2018). Despite the fact that distant metastasis formation causes over 90 % of cancer-related deaths, there is a lack of treatment preventing metastasis formation and treatments targeting the dormant disseminated tumour cells (Ben-Jacob et al., 2012; Mehlen & Puisieux, 2006).

1.3 Epithelial to mesenchymal transition

One of the parallels between normal breast development and breast cancer progression is a developmental program termed epithelial to mesenchymal transition (EMT) and its reverse process mesenchymal to epithelial transition (MET).

In the mammary gland, EMT takes place during branching morphogenesis. Transient and partial EMT generates epithelial plasticity necessary for the invasiveness of cells into ECM during the formation of new branch points (Chakrabarti et al., 2012). One of the crucial regulators of branching morphogenesis and EMT in the mammary gland is SPRY2 (Sprouty homolog 2) (Sigurdsson et al., 2013).

In cancer, EMT is proposed to be one of the processes leading to formation the of metastasis in carcinomas (Moustakas & Heldin, 2007; Radisky et al., 2007; Tsai & Yang, 2013; Zeisberg & Kalluri, 2004). EMT enables cells to acquire increased migration, invasive properties, resistance to apoptosis, anoikis and contributes to the gain of stem cell properties and drug resistance (Cao et al., 2016; Celia-Terrassa et al., 2012; May et al., 2011; Meacham & Morrison, 2013; Ye & Weinberg, 2015). EMT/MET leads to changes in morphology, polarity and cell contacts, as summarised in **Table 1**.

EMT is a multi-stage reversible process, having on one end full epithelial phenotype and on the other end full mesenchymal phenotype, with many intermediate phenotypes (Ingthorsson et al., 2016; Meyer-Schaller et al., 2019). The intermediate stages of EMT have been connected to epithelial plasticity, stemness and increased metastatic risk (Grosse-Wilde et al., 2015). Cellular plasticity can be described as a certain degree of differentiation or dedifferentiation and serves for the dynamic adaptation of cells to the microenvironment (Varga & Greten, 2017). The terms such as plasticity, hybrid epithelial-mesenchymal phenotype or partial EMT all refer to a state with the potential to lead to the metastatic formation and gain of stem cell properties (Brabletz et al., 2018; Mani et al., 2008; Pastushenko et al., 2018; Polyak & Weinberg, 2009) (**Figure 4**).

Table 1. Differences characterising epithelial and mesenchymal cells.

	Epithelial characteristics	**Mesenchymal characteristics**
Morphology	cuboidal shape	spindle shape
Polarity	polarised (apico-basal polarity)	non-polarized (front-back elongated)
Adhesion	adhere to each other (with cell-cell contacts: adherent junctions, tight junctions, integrins)	separated or loosely attached
Motility	non-motile	motile (migratory), invasive
Sensitivity to apoptosis	sensitive to apoptosis, anoikis	increased resistance to apoptosis and anoikis

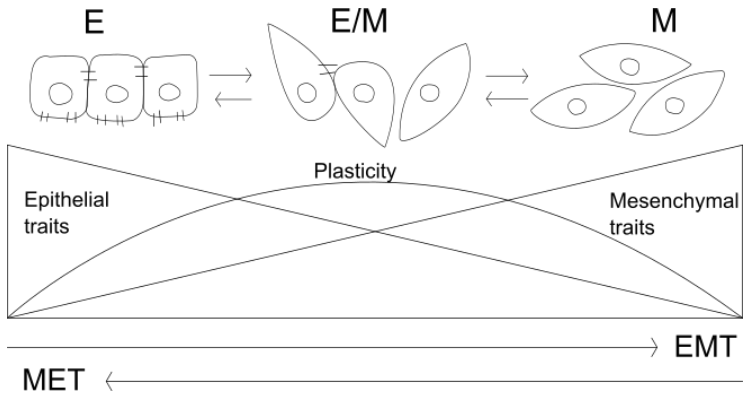

Figure 4. The spectrum of EMT.
Epithelial (E) cells can undergo transition through hybrid stages epithelial/mesenchymal (E/M) and mesenchymal/epithelial (M/E), also called partial EMT, into cells with mesenchymal (M) phenotype. During this transition, cells acquire mesenchymal characteristics and loose epithelial characteristics. There is a hypothesis that partial EMT goes together with the acquisition of plasticity/stemness. Adapted from Li and Kang (2016).

Targeting both EMT/MET, depending on the stage of cancer progression, could represent one of the approaches for treating cancer's complexity (Grosse-Wilde et al., 2015) (**Figure 5**).

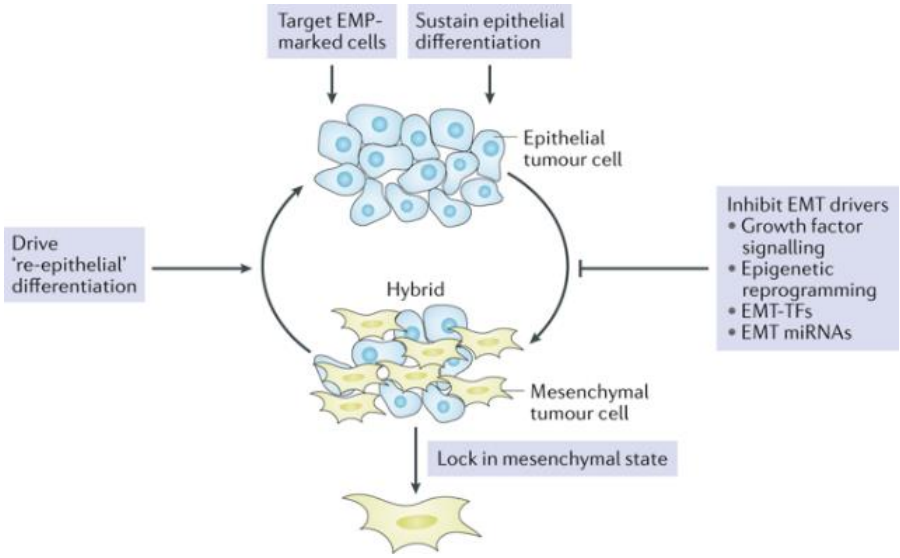

Figure 5. Potential targets to inhibit cellular plasticity.
The various states of plasticity produced during EMT provide several opportunities to target cancer progression. In the early stages, it could be to sustain the epithelial differentiation through blocking the EMT process, while in later stages of cancer progression, it could be preventing MET and locking the cells in a mesenchymal state. Further options might be to develop therapies that specifically target the unique aspects of the hybrid epithelial-mesenchymal phenotype. Adapted from Williams et al. (2019a).

There are many different types of stimuli, which can induce EMT (**Figure 6**). Important inducers of EMT are intrinsic factors such as transcription factors (TF: SNAI1, SNAI2, TWIST1, ZEB1 or ZEB2), which can lead to a fundamental event in EMT, the cadherin switch from E-cadherin to N-cadherin. Among inducers of EMT are also epigenetic mechanisms or non-coding RNAs, as discussed in the following chapter. Several extrinsic factors or their signalling pathways may also induce EMT, such as TGFβ, epidermal growth factor (EGF), FGFs, hepatocyte growth factor (HGF) or Wnt signalling factors (Moustakas & Heldin, 2007; Peinado et al., 2007; Wang & Zhou, 2013; Williams et al., 2019b). Other researchers have studied the EMT process induced by stromal cells, and herein our research group has contributed significantly (Sigurdsson et al., 2011; Soon et al., 2013). It has been shown that different levels of EMT inducers enable different phenotypes, leading to cellular heterogeneity (Lu et al., 2013).

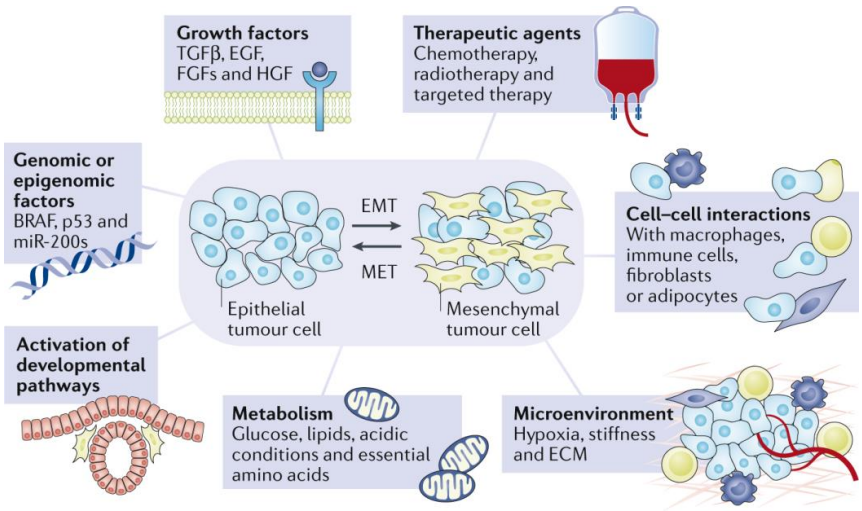

Figure 6. Types of EMT/MET stimuli.
EMT can be promoted by interaction with stromal cells, by microenvironmental factors (for example, hypoxia, matrix stiffness), by metabolic factors, growth factors, by activation of developmental pathways or by increase expression of non-coding genes or by chemotherapeutic agents. Adapted from Williams et al. (2019a).

It is important to note that the action of EMT/MET in cancer progression is still debated. Some of the reasons for raising the discussions are that the EMT/MET is challenging to detect *in vivo*, as the cells are indistinguishable from mesenchymal cells in the body. Furthermore, its complexity and plasticity, together with the transient nature of the process and suboptimal experimental models, make it a complicated object to study. From the *in vivo* observations, it has been shown, using mouse models (MMTV-PyMT), that the partial EMT of cancer cells leads to metastasis and chemoresistance (Pastushenko et al., 2018; Shibue & Weinberg, 2017). The most aggressive subtypes of breast cancer are enriched for cells co-expressing epithelial and mesenchymal markers and have more cancer circulating cells, indicating a strong association between aggressiveness and partial EMT phenotype (Fedele et al., 2017; Prat et al., 2010; Yu et al., 2013). Another evidence for EMT being the actual dissemination process are sarcomas, which are cancers that originate directly from stromal cells and are characterised by early metastasis formation (Williams et al., 2019a). The EMT process has been very much studied *in vitro*, most commonly induced by EMT-TF, which were however, shown to be tissue-specific and have a pleiotropic role (Tran et al., 2014; Zheng et al., 2015).

Other cases of EMT/MET presence are in fibrosis or wound healing, and for that reason, tumours have also been nicknamed wounds that fail to heal (Schafer and Werner, 2008).

1.3.1 Endothelial to mesenchymal transition

In addition to epithelial cells, endothelial cells have the potential to differentiate into the mesenchymal cell through endothelial to mesenchymal transition (EndoMT), a specific form of EMT (Kovacic et al., 2019). Similarly to EMT, also EndoMT gives rise to cells with the mesenchymal phenotype and helps to acquire invasive characteristics (Nakajima et al., 2000). Such process is proposed to be an important source of CAFs in cancer or as a source of fibroblasts in fibrosis (Kalluri & Zeisberg, 2006; Potenta et al., 2008; Widyantoro et al., 2010; Zeisberg et al., 2008) or contribute to heart valve formation (Armstrong & Bischoff, 2004). Interestingly, the partial endothelial to mesenchymal transition has also been connected with the transition from 'stalk-to-tip cell' during angiogenesis (Welch-Reardon et al., 2014; Welch-Reardon et al., 2015). 'Tip cell' gains mesenchymal properties, such as migratory ability, loses apical-basal polarity, ability to degrade ECM, but retain cell-cell contact. It is suggested that the endothelial transition of the 'stalk-to-tip cell' is regulated by the balance of pro-angiogenic and anti-angiogenic factors (Carmeliet & Jain, 2000; De Smet et al., 2009). The 'tip cell' in angiogenesis could be another potential targetable site against cancer.

1.4 Non-coding RNA

Non-coding RNAs (ncRNAs) have been reported to be potential diagnostic and prognostic biomarkers in tumours, including breast cancer (Huang et al., 2018; Tong et al., 2015; Wang et al., 2016; Wang et al., 2012). Non-coding RNAs are defined by no protein-coding potential and weak Kozak sequence for protein translation initiation (Miyoshi et al., 2000). In the past, RNAs (besides rRNAs and tRNAs) were commonly considered only as intermediates between DNA and proteins. The gene regulatory function of RNA, without involvement in gene translation, was revealed with the advance of RNA sequencing (Lander, 2011). The projects of systematic characterisation of gene function (such as ENCODE - encyclopaedia of DNA elements or FANTOM projects) has shown that at least 80 % of the human genome can be transcribed with no protein-coding capability. In comparison, only 3 % of the genes contain segments of coding sequences (ENCODE Project Consortium, 2012, Hon et al., 2017). Moreover, the complexity of the organism increases with the proportion of ncRNAs in the genome, rather than with the number of coding genes (Taft et al., 2007). The ncRNAs are commonly subdivided into short and long ncRNAs (lncRNAs). To the group of short RNAs, with less than 200 nucleotides (nt), belong small nucleolar RNA (snRNA), piwi-interacting RNAs (piRNAs), micro RNAs (miRNAs) and transfer RNAs (tRNAs), among others. Conversely, lncRNAs are defined by transcripts longer than 200 nt. MiRNAs

and lncRNAs have been the most widely studied ncRNAs in recent decades and are also the focus of this thesis.

1.4.1 Micro RNAs

Micro RNAs (miRNAs) are 22 nt long RNA molecules that post-transcriptionally regulate gene expression and are crucial regulators of branching morphogenesis and EMT in the breast (Briem et al., 2019; Hilmarsdottir et al., 2015). The human genome may encode thousands of miRNAs, targeting about 60 % of the genes (Friedman et al., 2009). The biogenesis and action of miRNAs have been described in considerable detail. The miRNA genes are transcribed by RNA polymerase II (pol II) and contain 5′ end cap and are poly-adenylated (polyA) on a 3′ end. The pri-miRNA, which can consist of multiple miRNA gene transcripts, is processed by the enzyme Drosha to about 70 nt long double-stranded RNA (dsRNA) in the nucleus. This RNA molecule is then exported to the cytoplasm as pre-miRNA, where the enzyme Dicer further processes the transcript to 22 nt mature double-stranded miRNAs. Subsequently, one strand is incorporated into the RNA-induced silencing complex (RISC), together with Argonaute (AGO) protein as the essential component that binds miRNAs. MiRNAs suppress gene expression by targeting the 3′ untranslated regions (3′ - UTRs) of target mRNA through sequence complementarity in the miRNA response element (MREs) (**Figure 7**) (Macfarlane & Murphy, 2010). MiRNAs target multiple genes and can induce broad downstream and feedback effects simultaneously. MiRNAs also regulate EMT (Bullock et al., 2012; Nicoloso et al., 2009; Shimono et al., 2009). An example of the important interplay of miRNAs and TF in EMT, is the reciprocal feedback loop between ZEB family and miR200 family (Brabletz & Brabletz, 2010; Nicoloso et al., 2009; Schubert & Brabletz, 2011). Our research group previously demonstrated the importance of miR200 family in maintaining epithelial integrity during the EMT process (Hilmarsdottir et al., 2015).

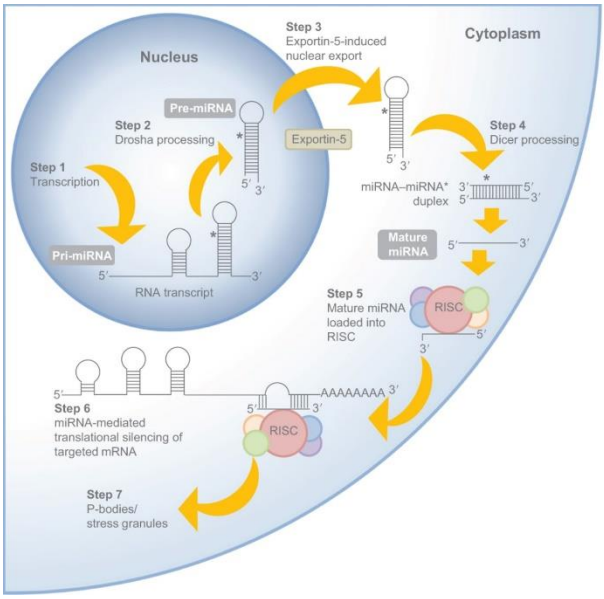

Figure 7. The biogenesis pathway of miRNAs.

The biogenesis starts in the nucleus as pri-miRNA and is processed by Drosha to pre-miRNA, which is exported to the cytoplasm and further processed by Dicer to mature miRNA, which can enter the RISC and act as a transcriptional repressor of the mRNA. Adapted from Biggar and Storey (2015).

1.4.2 Long non-coding RNAs

Unlike miRNAs, lncRNAs are a heterogeneous group defined by the transcript's size being longer than 200 nt with non-coding potential. Rarely, lncRNAs can code for small peptides (Hubé & Francastel, 2018). LncRNAs are 5′ capped, have polyA tail at 3′ end and are transcribed by RNA polymerase II (Eades et al., 2014). Over 60 000 lncRNA have been identified, with tens of thousands of them identified in mammals (Kopp & Mendell, 2018). Despite recent extensive research carried on the role of lncRNAs, fewer than 2 % of lncRNAs have been ascribed to a particular biological role (Hon et al., 2017). LncRNAs can interact with other biological molecules like DNA, RNA or proteins to regulate diverse cellular processes such as cell growth, survival, migration, invasion or differentiation (Derrien et al., 2012; Di Gesualdo et al., 2014; Mercer et al., 2009; Sun et al., 2013). They can fold into complex three-dimensional (3D) structures and act both in the cytoplasm and nucleus (Batista & Chang, 2013). It has been shown that lncRNA has high tissue specificity (Kadota et al., 2006). LncRNA can regulate gene expression at different levels, and there are numerous ways of action of lncRNA, such as guide RNA, scaffolds, decoys (sponges) for miRNA and mediation of antisense

interference for coding mRNA (Shibue & Weinberg, 2017 (**Figure 8**) (Fico et al., 2019; Li et al., 2017; Wang & Chang, 2011).

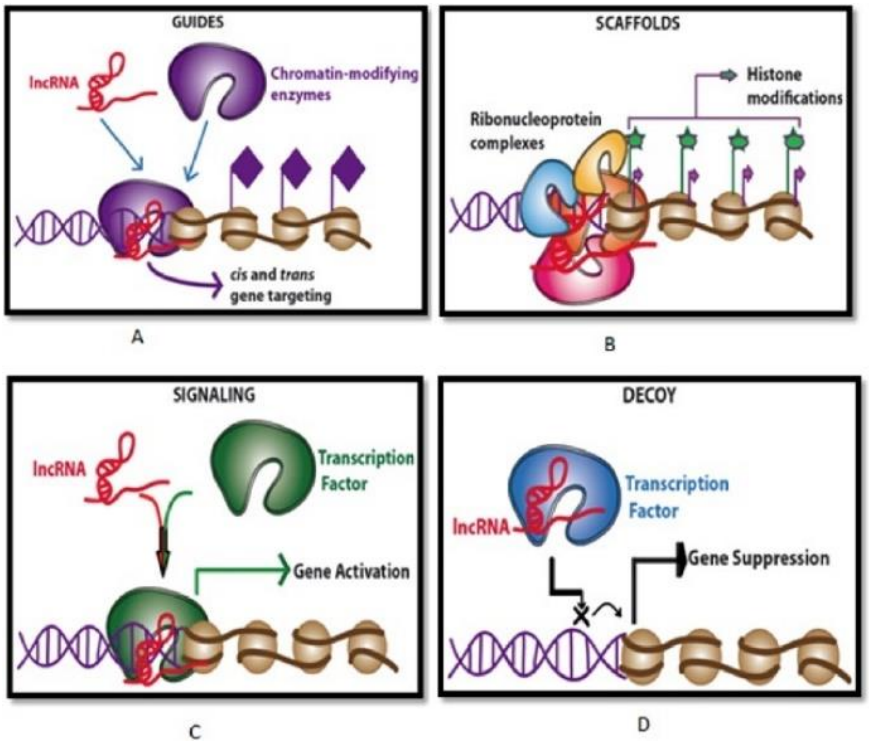

Figure 8. LncRNAs have multiple modes of action.
LncRNAs can act in both nucleus and cytoplasm. In nucleus it can guide proteins to DNA. And in cytoplasm can act as scaffold, decoy, or binding partner. Adapted from Bhat et al. (2016).

1.4.3 Epigenetics and imprinting

As with coding genes, epigenetic modifications have been shown to regulate the expression of non-coding RNAs (Vrba et al., 2010). Epigenetic inheritance (also called cell memory) is a heritable alteration in a cell or organism′s phenotype that are not caused by changes in the DNA sequence but from DNA marks. These marks include DNA methylation at CpG sites and modifications at core histone tails (Edwards & Ferguson-Smith, 2007). The modification of histones has a prominent role in organising the accessibility of chromatin, and so influences the transcription of DNA. Particularly, the methylation of lysine (K) of histone H3 is highly studied due to its importance in gene regulation. The outcome of regulation depends, however, on which of the lysin residues are methylated. Methylations of K4, K36 or K79 on H3 are associated with active

chromatin, while methylations of K9 or K27 are linked to gene repression. Especially, the aberrant regulation of H3K27 methylation by Polycomb repressive complex-2 (PRC2) was shown to be prominent for the EMT-inducing gene expression programs in malignancy (Oktyabri et al., 2014).

Epigenetic modifications also regulate imprinting, where a gene is marked and expressed according to its parental origin. The expression of most genes in somatic cells is bi-allelic, where both copies of the gene are transcribed. However, a fraction of mammalian genes is subject to imprinting, which results in monoallelic expression. This phenomenon applies to about 300 imprinted genes in the human genome, located in clusters, regulated by differentially methylated regions (DMR) (Barlow & Bartolomei, 2014).

1.4.4 DLK1-DIO3 locus

The imprinted DLK1-DIO3 locus is located on mouse chromosome 12 and human chromosome 14 (Gubina et al., 1999, 2000). The DLK1-DIO3 locus is flanked by and named after the paternally expressed protein-coding genes Delta Like Non-Canonical Notch Ligand 1 (DLK1) and Iodothyronine Deiodinase type III (DIO3). The entire locus is approximately 1 Mb long. It contains three paternally expressed protein-coding genes: DLK1, Retrotransposon-like 1 (RTL1), and DIO3 and maternally expressed non-coding genes, including lncRNA Maternally expressed gene 3 (*MEG3*), *MEG8*, *MEG9*, an antisense transcript to RTL1, numerous small RNAs belonging to the Small nucleolar RNAs, C/D box (SNORD) and more than 50 miRNAs (Baulina et al., 2019; Dill & Naya, 2018; Zerbino et al., 2018; Zhang et al., 2010). In humans, miRNAs from this locus are collectively called Chromosome 14 MicroRNA Cluster (C14MC), and most of them are grouped into two genomic regions: the miR-127/miR-136 cluster (also called Cluster A) and the miR-379/miR-410 cluster (also called cluster B) located upstream and downstream from the SNORD gene cluster, respectively (**Figure 9**).

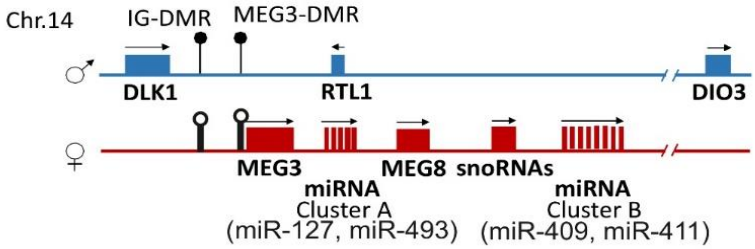

Figure 9. Schematic figure of DLK1-DIO3 locus.

This locus is imprinted and is located on chromosome 14 in humans. It contains paternally expressed protein-coding genes (DLK1, RTL, DIO3) and maternally expressed non-coding genes, among them lncRNA *MEG3*, *MEG8*, two clusters of miRNAs: cluster A - among them MIR127 and MIR493 and cluster B - MIR409 and MIR411 and numerous C/D-box-containing small nucleolar RNAs (snoRNAs). There are also two main DMRs: IG-DMR and MEG3-DMR, regulating the expression of those genes. DMR-differentially methylated region, filled circles represent methylated DMRs, and unfilled circles represent unmethylated DMRs.

The imprinting of the locus is controlled by two key differentially methylated regions (DMRs), one germline-derived primary intergenic DMR (IG-DMR), located about 13 kilo-base (kb) upstream of the *MEG3* transcription start site (TSS) and the post-fertilisation-derived secondary (MEG3-DMR) overlapping with the *MEG3* promoter region (Benetatos et al., 2008; da Rocha et al., 2008; Kagami et al., 2010).

Dysregulation of genes at the DLK1-DIO3 region has been documented to cause several developmental disorders in the embryo and placenta and defects in adult metabolism and brain function (da Rocha et al., 2008). Mice with paternal uniparental disomy (UPD) of 12q die prenatally, unlike the phenotype of knockout of maternal gene trap locus 2 (GTL2), mouse equivalent for *MEG3,* which dies perinatally (Takahashi et al., 2009). Loss of imprinting (LOI) of DLK1-DIO3 in humans leads to Kagami-Ogata syndrome (Kagami et al., 2010; Ogata & Kagami, 2016) or Temple syndrome (Ioannides et al., 2014). Interestingly, the activity of the DLK1-DIO3 locus is essential to maintain pluripotency of induced pluripotent stem cell (iPSCs), and its reduced expression is associated with incomplete iPSC reprogramming (Liu et al., 2010; Stadtfeld et al., 2010). Moreover, ncRNAs from DLK1-DIO3 locus were correlated with the developmental potential of iPSCs (Kang et al., 2009; Stadtfeld et al., 2010; Zhao et al., 2009), and the miRNAs from the DLK1-DIO3 locus promoted pluripotency by inhibition of differentiation and stimulated self-renewal in mouse embryonic stem cells (Moradi et al., 2017).

1.4.4.1 MEG3

Human *MEG3* is a lncRNA of about 1700 nt with multiple isoforms (Schuster-Gossler et al., 1998; Zhang et al., 2010). In 2010 Zhang and colleagues identified 12 isoforms of *MEG3*; nevertheless, currently, there are 50 splice variants identified in the Ensemble database with transcript IDs. *MEG3* is a single copy, intergenic lncRNA and has been found located in both nucleus (Mondal et al., 2015) and cytoplasm (Zha et al., 2019) of cells. *MEG3* is expressed in many normal tissues with higher expression in the brain and the epithelia of salivary glands, pancreas, and kidney (Schmidt et al., 2000). *MEG3* RNA folds into three central motifs, M1, M2, and M3. Motif M2 is essential for TP53-mediated transactivation (Zhang et al., 2010).

MEG3 regulators

Multiple factors can regulate *MEG3* expression. An underlying cause of *MEG3* down-regulation is promoter hyper-methylation (X. Cui et al., 2018; Li et al., 2016). On the other hand, cyclic adenosine monophosphate (cAMP) was found to stimulate the expression of *MEG3* by binding to the cAMP response element (CRE) in the promotor of *MEG3* (Zhao et al., 2006). *MEG3* can also be regulated at the post-transcriptional level by several miRNAs (Cui et al., 2018).

Role of *MEG3* on a molecular level

MiRNAs are also putative downstream targets of *MEG3*, which can act as competing endogenous RNA (ceRNA), or sponging RNA for a number of them (Chen et al., 2020; Moradi et al., 2019; Peng et al., 2015; Qin et al., 2017; Wang et al., 2019; Wu et al., 2020; Xu et al., 2020; Zha et al., 2019; Zhang et al., 2016; Zhang & Feng, 2017). On the molecular level, various actions of *MEG3* have been described. *MEG3* regulates the expression TP53 tumour suppressor gene through MDM2 or directly affecting TP53 (Sun et al., 2016; Uroda et al., 2019; Zhou et al., 2007). *MEG3* overexpression acts as the inhibitor of Akt pathway (Li et al., 2019; Zhang et al., 2017). Also, *MEG3* acts as a guide for Polycomb Repressive Complex 2 (PRC2) to specific DNA sequences establishing facultative heterochromatin marked by repressive H3K27me3 modification (Kaneko, Bonasio, Saldana-Meyer, et al., 2014; Mondal et al., 2015). *MEG3* directly interacts with subunits of PRC2, EZH2 (Jin et al., 2018; Zhou et al., 2020), or JARID 2 (Kaneko et al., 2014). The specific target is recognised via RNA-DNA triplex formation, binding through GA-rich repetitive motif (Kuo et al., 2019; Mondal et al., 2015). An epigenetic function of *MEG3* has been reported in breast and lung cancer cells, suppressing TGFβ-related genes to modulate their invasive properties (Mondal et al., 2015;

Terashima et al., 2017). *MEG3* was shown to be an important player in the EMT of ovarian cancer (Mitra et al., 2017) and lung cancer (Terashima et al., 2017). Genome-wide mapping showed that *MEG3* binding sites were present in 73% of genes related to EMT (Mitra et al., 2017). In lung cancer cell lines, knockdown of *MEG3* inhibited changes caused by TGFβ on gene expression and functional level (Terashima et al., 2017).

The functional role of *MEG3*

MEG3 is an object of numerous recent works reporting its pro and anti-cancer activity, depending on the context. Moreover, *MEG3* is dysregulated in other diseases, such as diabetes or rheumatoid arthritis (Li et al., 2019; You et al., 2016; Zhu et al., 2016). Functional studies have demonstrated that *MEG3* inhibits cell proliferation and promotes cell apoptosis (Wang et al., 2012; Zhang et al., 2010; Zhang et al., 2003) and has been connected to both promotion and inhibition of cell migration and invasion (Ma et al., 2018; Zhang et al., 2018).

1.4.4.2 miRNAs from the DLK1-DIO3 locus

Liu et al. (2010) revealed that the miRNAs from the DLK1-DIO3 cluster are only presented in mammalian genomes and are highly conserved, indicating their specific and crucial role in regulating mammalian development. A large number of miRNAs located at the DLK1-DIO3 locus make it challenging to study the whole locus's function collectively. When an entire cluster of genes is upregulated, it is challenging to narrow down single genes' contribution (Valdmanis et al., 2015). Therefore, the role of those miRNAs at the DLK1-DIO3 locus is mostly unknown. Besides, each miRNA can have many different functions by targeting multiple genes. Some miRNAs have been shown to have a role in the EMT process, such as MIR127, whose increased expression shifted cancer cells phenotype from the epithelial to the mesenchymal (Shi et al., 2017).

1.5 The D492 cell lines

D492 is a cell line of suprabasal origin, derived from MUC1-negative and EpCAM-positive primary breast epithelial cells with the ability to establish both luminal and myoepithelial cells (Gudjonsson et al., 2002) (**Figure 10**). D492 was immortalised with the E6/E7 oncogenes from the HPV16 (human papillomavirus 16), targeting TP53 and Rb (retinoblastoma), respectively. D492 has proven a valuable tool to investigate branching morphogenesis *in vitro*, as it can grow colonies from single cells and form structures resembling TDLUs (Briem et al., 2019; Briem et al., 2019; Hilmarsdottir et al., 2015). Such process of branching morphogenesis can be examined during approximately

21 days. D492 at day 7 forms small colonies, at day 14, the branching has begun and at day 21, D492 has formed fully branching colonies. Furthermore, when the D492 cell line is co-cultured with endothelial cells, some of the colonies undergo EMT and form spindle-shaped cells in 3D rBM culture. From one such spindle-shaped colony, mesenchymal cell line called D492M was isolated (Sigurdsson et al., 2011). D492M is a phenotypically stable mesenchymal cell line. Endothelial cells near D492, induced heritable effects that maintain the mesenchymal state of D492M even after EMT initiating signals are no longer present.

Together, D492 and D492M form a unique model for EMT; therefore, we have used them as main cell lines in this thesis's first two papers (paper #I and paper #II). D492 co-expresses both luminal and myoepithelial keratins, while D492M has lost epithelial markers such as keratins, E-cadherin and transcription factors such as TP63 and gained mesenchymal markers including N-cadherin, vimentin and alpha-smooth muscle actin (*α*SMA) (Sigurdsson et al., 2011). D492M is non-tumorigenic but has acquired specific phenotypic properties of cancer stem cells such as increased CD44/CD24 ratio, anchorage-independent growth, resistance to apoptosis and increased migration/invasion (Sigurdsson et al., 2011). Both cell lines are diploid. D492 and D492M cells also differ in the metabolomics and the placement of the mitochondria (in D492 the mitochondria are closer to the nucleus as compared to D492M). Moreover, D492 proliferates faster than D492M (Halldorsson et al., 2017). The transition of D492M back to the epithelial state of D492 was achieved by overexpression of miR200c together with TP63 in D492M (Hilmarsdottir et al., 2015).

D492HER2 is the third main cell line I used during my PhD studies, with more focus in paper #III and paper #IV. The D492HER2 cell line was established by overexpression of the HER2 oncogene in the D492 cell line (Ingthorsson et al., 2016). The activation of HER2 in D492 cells recapitulates the malignant process, and the cells are tumorigenic in mice. As is the case for D492M, D492HER2 has a mesenchymal phenotype. D492HER2 has reduced expression of TP63, KRT14 and KRT19 as well as E-cadherin and P-cadherin and increased expression of mesenchymal markers such as N-cadherin and Axl.

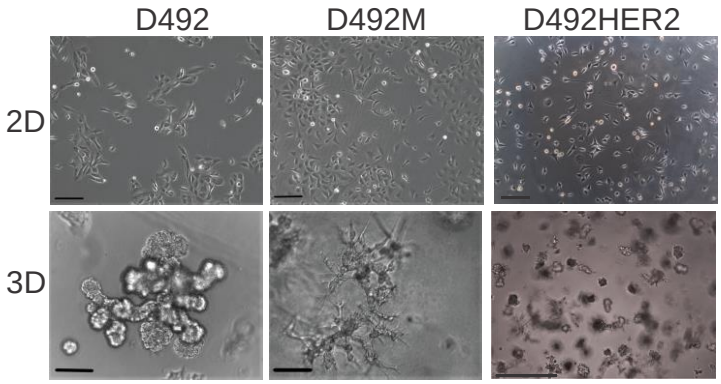

Figure 10. D492 has epithelial phenotype, while D492M and D492HER2 have mesenchymal phenotype.
2D: D492 forms cuboidal-shaped cells, while D492M and D492HER2 form spindle-shaped cells. In 3D: D492 forms branching structures, D492M forms mesenchymal structures and D492HER2 forms mix of grape-like structures and mesenchymal structures. Scale bar = 100 μm.

2 Aims

Developmental processes driving branching morphogenesis in the breast gland are related to events occurring in cancer progression where these pathways go awry. Therefore, it is possible to gain a valuable understanding of how breast cancer originates and progresses by studying normal breast development. Epithelial to mesenchymal transition (EMT) and mesenchymal to epithelial transition (MET) govern important phenotypic changes in both the normal and malignant breast gland. Enhanced understanding of these processes can lead to the finding of improved treatment options for breast cancer patients. Moreover, identifying important molecular components involved in EMT and MET could serve as valuable biomarkers and help stratify patients towards more personalised medicine. Studying the differences between tumorigenic and non-tumorigenic cell lines of the same origin can help identify key molecular factors contributing to tumorigenicity and plasticity. In my PhD project, I have used the D492 cell lines that reflect the spectrum from non-malignant to cancer phenotype. In my main project, the focus has been on the non-coding RNAs and their role in branching morphogenesis and EMT (aim 1 and 2). A substantial focus of my PhD studies was on extracellular matrix proteins and their function in malignant HER2 overexpressing cell lines (aim 3). These specific aims reflect the papers that form the basis of my PhD thesis.

The specific aims include:

1. **Analysing expression pattern and functional role of non-coding RNAs from the DLK1-DIO3 locus in EMT/MET.** (paper #I)
2. **Analysing expression pattern and functional role of miRNA 203a in branching morphogenesis and EMT/MET.** (paper #II)
3. **Comparing isogenic non-malignant and malignant cell lines with EMT phenotype and identify extracellular matrix proteins with a putative role in promoting malignancy.** (paper #III and #IV)

3 Materials and methods

In this chapter, I will list and describe the materials and methods I used in my experiments which are presented in the chapter “Results and discussion”. A more detailed discussion about the optimisation and inscrutability of the methods can be found in the chapter “Technical considerations“. Finally, a detailed description of methods used in the published papers can be found in the material and methods paragraphs of each paper.

3.1 Cell culture

Monolayer (2D) culture

I have used mostly three cell lines D492, D492M and D492HER2. All three were maintained in H14 medium, as described previously (Gudjonsson et al., 2002; Sigurdsson et al., 2011) in tissue treated T25 Falcon flasks (BD Biosciences) coated with collagen I (Advanced BioMatrix, 5005-B). H14 is a chemically defined medium, with a base of Dulbecco’s Modified Eagle Medium (DMEM): F12 with HEPES and L-Glutamine (Gibco, 31330), supplemented with penicillin and streptomycin (Gibco, 15070-063) and the growth factors with their final concentrations: 250 ng/ml Insulin (Sigma, I1882), 10 ng/ml EGF (Peprotech, AF-100-15), 10 µg/ml Transferrin (Sigma, T1147), 2,6 ng/ml NaSel (BD Biosciences, 534201), 0,1 nM Estradiol (Sigma, E2758), 500 ng/ml Hydrocortisone (Sigma, H0888), 0,15 IU Prolactin (Sigma, L6520). Luminal epithelial cell line D382 was also cultured in H14 media.

HEK-293T (Human embryonic kidney 293) cells were cultured in DMEM high glucose GlutaMAX™, pyruvate (Gibco, 31966), supplemented with 10 % Fetal bovine serum (FBS), penicillin and streptomycin (Gibco, 15140-122). HMLE (human mammary epithelial cells) (Elenbaas et al., 2001) is an epithelial progenitor cell line, from which a mesenchymal cell line HMLEmes was derived by sorting for the Thy1-positive population. HMLE, and HMLEmes were cultured in chemically defined media called HMLE media, containing DMEM/F12 supplemented with penicillin and streptomycin and growth factors: 10 µg/ml Insulin (Sigma, I1882), 10 ng/ml EGF (Peprotech, AF-100-15) and 500 ng/ml Hydrocortisone (Sigma, H0888).

For experimental treatment with TGFβ, recombinant human TGFβ in the concentration of 10 ng/ml (RD systems) was used.

Primary breast cells were acquired from Landspitali, University Hospital in Reykjavik, Iceland (with informed consent from the donor, approved by the Icelandic National Bioethics Committee VSN-13-057), from reduction mammoplasty. Primary human luminal-epithelial cells, myoepithelial cells, endothelial cell, fibroblast and organoids (epithelial cells) were isolated from breast reduction mammoplasties as previously described and maintained in chemically defined medium 3 (CDM3) and chemically defined medium 4 (CDM4) as previously described (Ingthorsson et al., 2010; Pechoux et al., 1999; Sigurdsson et al., 2006). Primary human umbilical vein endothelial cells (HUVECs) were received from Landspitali, University Hospital in Reykjavik, Iceland (with informed consent, approved by Landspitali Ethical Committee No. 35/2013). HUVECs were cultured in Endothelial Growth Medium 2 (EGM2) media (Lonza, CC-3162) enriched with growth factors and 5 % FBS, further called EGM5 medium. All cells were grown at 5 % CO_2 at 37 °C.

Despite coating culture flasks with collagen type I, the main component of ECM, this strategy does not faithfully recapitulate the behaviour of cells within tissues, which demand not only a 3D format but also an ECM that can be readily remodelled.

Three dimensional (3D) cultures

3D cell cultures were performed in reduced reconstituted basement membrane rBM (further called with its commercial name Matrigel). Matrigel is extracted from the Engelbreth-Holm-Swarm (EHS) mouse sarcoma, a tumour rich in extracellular matrix proteins, specifically in collagen IV and laminin. 3D experiments were carried out in a 48-well plate format, where 5-10 x 10^3 of cells were embedded in 150 µl of Matrigel per well. The plate was incubated in 5 % CO_2 at 37 °C for 15 min to solidify the Matrigel, and then 300 µl of H14 media was added on top. The cultures were imaged using the EVOS FL Auto 2 Cell Imaging System (Thermo Fisher Scientific) for three weeks. Fresh media was added three times per week. The colonies were quantified on day 14. The total number of cells was converted into a percentage.

For co-culture experiments, 0,5 x 10^3 of the epithelial cells were seeded together with 1 x 10^5 of endothelial cells (HUVECs) and were resuspended in 150 µl of Matrigel. The plate was incubated in 5 % CO_2 at 37 °C for 15 min to solidify the Matrigel, and then 300 µl EGM5 media was added on top. Endothelial cells cultured in Matrigel are viable, however dormant, having a supporting function in the epithelial cells' proliferation. The colonies were quantified by counting all colonies greater than 100 µm.

3.2 Functional assays

Cell proliferation assay

Cell proliferation assay was performed on the IncuCyte Zoom microscope (Essen Bioscience) according to the manufacturer's protocol. Cells were plated at a density 10 x 10^3 / well in a 96-well plate. Cell culture media was changed three times per week.

Alternatively, the cells' proliferation was assessed by staining with crystal violet in a 24-well plate format. The cells were plated, and then every 24 hours, three wells (technical triplicate) were fixed with 3,7 % formaldehyde in PBS for 10 min, washed with 1 x PBS and dyed with 0,1 % crystal violet in ethanol for 15 min. The cells were then washed four times with 1 x PBS, and crystal violet was solubilised with 10 % acetic acid, and the optic density was measured at 595 nm using a spectrometer.

Cell viability

Cell viability was assessed using PrestoBlue Cell Viability Reagent (ThermoFisher Scientific, A13261), according to the manufacturer's instructions. Three thousand cells/well cells were plated in H14 media in a 96-well plate in 90 µl/well of media and cultured for four days. Ten µl/well of prestoBlue was added to each well and incubated for 4 hours. The absorbance was measured at 570 nm and 595 nm on a spectrophotometer.

Cell migration assay and cell invasion assays

Cell migration and invasion were examined by using trans-well Boyden chambers with an 8 µm pore size (Corning, 353097). An additional layer of diluted Matrigel (1:10 with H14 media) was added in case of invasion. Briefly, 3 x 10^3 cells were resuspended in 250 µl H14 medium and seeded on the trans-well inserts in a 24-well plate (Corning, 353047) or placed on top of Matrigel in case of invasion assay. 500 µl H14 media with 10 % FBS was added to the lower chamber below the filter. Cells were incubated for 48 hours in 5 % CO_2 at 37 °C. After incubation, non-migratory cells from the upper part of the filter were discharged with a cotton swab and washed 3 x with 1 x PBS. In case of invasion, the Matrigel was discharged as well. The filters were then fixed with methanol and stained with DAPI (diluted 1:5000; Sigma, D9542-1MG). Cells were photographed in three random fields using the EVOS FL Auto 2 Cell Imaging System (Thermo Fisher Scientific). Pictures were analysed with ImageJ software. Besides, cell migration was assessed using the wound healing assay.

Wound healing assay was performed on the IncuCyte instrument (Essen Bioscience), according to the manufacturer's guidance. 6 x 10^3 cells/well were seeded to be 100 % confluent the following day into the 96-well plate ImageLock Plate (Essen Bioscience, 4379). Woundmaker (Essen Bioscience, 4493) was used to do the scratch wound. The images were taken every two hours and were analysed as *Relative Wound Density (%)* in the IncuCyte software.

Apoptosis assay

Resistance to chemically induced apoptosis was examined by inducing the cells with 10 µM camptothecin (CPT, Sigma-Aldrich, C9911) and quantified using IncuCyte Caspase-3/7 Reagents (Essen Bioscience, 4440) on IncuCyte Zoom (Essen Bioscience), according to the manufacturer's protocol.

Low attachment assay/mammosphere formation assay

Anchorage-independent growth was analysed using 24-well ultra-low attachment plates (Corning, 3473). Summarily, the cells were single-cell filtered and seeded in a density of 500 cells/well into EGM5 media and cultured for 9 days. The growth of colonies was quantified under the EVOS FL Auto 2 Cell Imaging System (Thermo Fisher Scientific) microscope, counting all the colonies greater than 40 µm.

Angiogenesis assay

Tube formation assay was examined measuring four specific parameters (master junction - three or more branches coming out of one point, master segment - parts connecting two master junctions, total master segments lengths and meshes - closed areas) of net formation of HUVEC cells. Briefly, the conditioned media (CM) was collected from cells after being for 48 hours on the 80 % confluent cells. Ten µl/well of Matrigel was placed on a µ-plate angiogenesis 96-well plate (IBIDI, 89646), then 35 µl of CM/well was added and another 35 µl with 6 000/well of HUVEC cell (early passage up to passage 3). Pictures were taken at the 4 h, 24 h and 48 h time-point of the network formation, using the EVOS FL Auto 2 Cell Imaging System (Thermo Fisher Scientific) and interpreted with ImageJ Angiogenesis plug-in.

3.3 Techniques of molecular biology

3.3.1 Gene expression techniques

Total RNA-sequencing and analysis of the data

The RNA was extracted using Trizol (Thermo Fisher Scientific, AM9738) from

five replicates of each cell line. The Whole Transcriptome sequencing of D492M$^{KD\text{-}CTRL}$ and D492M$^{KD\text{-}MEG3}$ was performed in deCODE genetics (Reykjavik, Iceland). Data have been deposited in NCBI's Gene Expression Omnibus and are accessible through the GEO Series accession number GSE142268. Sequence alignment of raw reads to the reference genome (Ensembl primary assembly, version GRCh38) was performed using STAR version 2.6.1 (Dobin et al., 2013). The program htseq-count (Anders et al., 2015) was used to quantify how many reads match each gene in an annotation file (Ensemble version GRCh38.96). The data from htseq-count were imported into R (Team, 2015) and differential expression (DE) analysis on D492M$^{KD\text{-}CTRL}$ vs D492$^{KD\text{-}MEG3}$ was done using DESeq2 (Love et al., 2014). *P* values were corrected for multiple testing using the false discovery rate (FDR) method. *P* value cut off 0,05 was applied. Genes with a reading below two in both D492M$^{KD\text{-}CTRL}$ and D492M$^{KD\text{-}MEG3}$ were excluded due to weak expression. The Volcano plot overall data (P < 0,05) was created in “R“ using the EnhancedVolcano package from BioConductor. Gene Set Enrichment Analysis (GSEA) was utilised to identify enrichment of gene signatures. Comparative analysis was investigated using the “Hallmark” database, where each "Hallmark" category consists of a defined gene set describing a given biological process. The list of significantly expressed pathways was displayed as a bar plot, with a FDR *q* value bellow 0,05 are considered statistically significant.

The GSEA analysis intends to settle whether the gene list members tend to occur towards the top or bottom of the ranked list “L“. Firstly, all genes from the RNA sequencing analysis were ranked using the formula: log10(*q* value) x (log2 fold change) and then uploaded into the GSEA database using the "Hallmark" dataset. The second step is the Enrichment Score (ES) calculation, which reveals whether the genes from the list are found more towards the top or bottom of the ranked list “L“. Randomly distributed genes will appear more towards the centre of the list, with ES closer to zero. Non-randomly distributed genes will appear towards the top or bottom of the list “L“, with ES number relatively high (either positive or negative). The normalized enrichment score (NES) accounts for the size of the set. False FDR estimates the probability that a set with a given NES represents a false positive. All pathways with significant (P < 0,05) positive or negative normalised enrichment scores were put into the barplot.

Quantitative RT-PCR analysis

Total RNA was extracted with Trizol (Thermo Fisher Scientific, AM9738). One µg of RNA per specimen was reverse transcribed into complementary DNA (cDNA), using Random Hexamers (Thermo Fisher Scientific, N8080127) and SuperScript IV Reverse Transcriptase (Thermo Fisher Scientific,18090-200) kit and used in quantitative real-time PCR (qRT-PCR) using pre-designed primer pairs: Sybr Green dye Luna® Universal qPCR Master Mix (NEB, M3003L) or TaqMan probes Luna® Universal Probe qPCR Master Mix (NEB, M3004L) according to manufacturer's guidance. Normalization was done with the GAPDH reference gene. Reference gene mRNAs should be stably expressed, and their abundances should show a strong correlation with the total amounts of mRNA present in the samples. The $2^{-\Delta\Delta Ct}$ was used to calculate each gene's relative expression using the ABI 7500 instrument (Applied Biosystems). Primers are listed in **Table 2**.

Table 2. List of primers for Quantitative RT-PCR analysis

Gene symbol	Producer, Assay ID
ZEB1	ThermoFisher Scientific, Hs00232783_m1
ZEB2	ThermoFisher Scientific, Hs00207691_m1
SNAI1	ThermoFisher Scientific, Hs00195591_m1
SNAI2	ThermoFisher Scientific, Hs00950344_m1
TWIST	ThermoFisher Scientific, Hs01675818_s1
GAPDH	ThermoFisher Scientific, 4326317E
KRT14	IDT, Hs.PT.58.4592110
KRT19	IDT,Hs.PT.58.4188708
MEG3 ex 10-11	IDT, Hs.PT.58.25190740
GAPDH	IDT, Hs.PT.39a.22214836
TP63	IDT, HS.PT.58.38930512
ALDH1A3	IDT, Hs.PT.56a.657970
PXDN	IDT, Hs.PT.58.630748
KRT5	IDT, Hs.PT.58.14446018
TP63	IDT, Hs.PT.58.2966111
CDH3 (P CAD)	IDT, Hs.PT.58.39234242
ITGα6	IDT, Hs.PT.58.453862

miRNA qRT PCR

Total RNA was extracted with Trizol (Thermo Fisher Scientific, AM9738). The RNA was reverse transcribed with the miRCURY LNA RT Kit (Qiagen, 339340) for cDNA synthesis reactions, according to the manufacturer's protocol. QRT-PCR analysis of miRNAs was conducted using miRCURY LNA SYBR Green PCR Kit (Qiagen, 339346), according to the manufacturer's protocol. Primers are listed in **Table 3**. The $2^{-\Delta\Delta Ct}$ method was utilised to calculate each gene's relative expression determined using the ABI 7500 instrument (Applied Biosystems).

Table 3. List of primers for miRNA qRT PCR

Gene symbol	Producer, Assay ID
hsa-miR-200c-3p	Qiagen, YP00204482
hsa-miR-205-5p	Exiqon, 204487
hsa-miR-203a	Exiqon, 205914
hsa-miR-127-3p	Qiagen, YP00204048
hsa-miR-409-3p	Qiagen, YP00204358
hsa-miR-411-5p	Qiagen, YP00204531
hsa-miR-493-3p	Qiagen, YP00204557
U6	Qiagen, YP00203907

Western blot assay

For harvesting the protein, cells were washed with cold Phosphate Buffered Saline (PBS) and lysed in radioimmunoprecipitation assay (RIPA) buffer supplemented with phosphatase and protease inhibitors (Halt Protease Inhibitor Cocktail, Thermo Fisher Scientific, 78430) for 10 min on ice and scraped with a cell scraper. Protein concentration was measured utilizing the Bradford reagent (BioRad, 5000002). Samples were denatured utilizing mercaptoethanol at 95 °C for 10 min. Equivalent amounts (5 µg-15 µg) of protein were separated on NuPage 10 % Bis-Tris gels (Invitrogen, NP0301PK2) with NuPage MES (2-(N-Morpholino) ethanesulfonic acid) running buffer (Thermo Fisher Scientific, NP0002). Samples were subsequently transferred with NuPage Transfer buffer (Thermo Fisher Scientific, NP0006-1) to polyvinylidene fluoride (PVDF) membrane Millipore Imobilion-FL transfer membrane, pore size 0,45 µM (Millipore, IPFL00010). The membranes were blocked with Odyssey Blocking buffer (TBS) (LiCor,

927-500) and incubated with primary antibodies overnight at 4 °C. Proteins were detected using secondary antibodies IRDey (Li-Cor 926-32213 - mouse, 926-32212 -rabbit) diluted to 1:10 000 for 1 hour at room temperature (RT) and detected and quantified using the Odyssey Infrared Imaging System (Li-Cor). The fluorescent signal was converted to greyscale. Antibodies used for western blot (WB) are listed in **Table 4**. Actin was used as a loading control.

Table 4. List of primary antibodies

Gene symbol	Producer, Assay ID	Methods
CDH1	BD Transduction Labs, 610182	WB, DAB
CDH2	BD Transduction Labs, 610921	WB, DAB
KRT14	Abcam, ab15461	WB
KRT14	Abcam, ab7800	DAB
KRT19	Abcam, ab7754	WB, DAB
TP63	Abcam, Ab124762	WB
KRT5/6	Invitrogen, 180267	WB
CDH3	Cell signalling, CS2130	WB
Actin	Licor, 926-42212	WB

DAB staining

DAB staining is an immunohistochemical method based on DAB (3,3′-Diaminobenzidine), a derivative of benzene. The oxidized DAB forms a brown precipitate at the area of the HRP (horseradish peroxidase), which can be observed with light microscopy (Leica DMI3000 B inverted microscope. Antibodies used for DAB staining are listed in **Table 4.**

3.3.2 Techniques for preparation of material (transfections, cloning, sorting)

Transient transfections

Transient transfection was used for transfection with small interfering (siRNAs) and miRNA mimics/ inhibitors. For transient transfection with siRNA targeting PXDN, cells (D492M) were transfected with 10 nm final concentration of negative control siRNA (Ambion, SilencerSelect siRNA 4390843) and siRNA targeting the gene of interest (PXDN) (Ambion, SilencerSelect siRNA 4427037), using Lipofectamine RNAiMAX (ThermoFisher Scientific, 13778075), according to the manufacturer's protocol. Cells were incubated for 48 hours, and the knockdown was confirmed by qRT-PCR. A mimics are

double-stranded RNAs that mimic the endogenous miRNA of the cell, which enable functional studies of upregulation. Inhibitors are single-stranded RNAs that bind to the target miRNA and thereby downregulate it. Cells were separately transfected first with mimics/inhibitors or its negative controls and then used in the luciferase assay (see Luciferase assay). miRNA mimics (ThermoFisher Scientific, 4464066, Assay ID MC10152), inhibitors (ThermoFisher Scientific, 4464084, Assay ID MH10152) and negative controls for miRNA mimics (ThermoFisher Scientific, 4464058) and inhibitor control (ThermoFisher Scientific, 4464076) were used in the concentration of 50 pmol and transfected using RNAiMAX (ThermoFisher Scientific, 13778075), according to manufacturer's instructions.

Luciferase assay

The dual-luciferase assay is a sensitive gene reporter assay based on bioluminescence allowing to study of gene regulation. Reporter expression is under the control of regulatory elements of a gene of our interest. Here, we were studying the binding (regulation) of MIR203a to protein PXDN (its 3' UTRs). For this purpose, 3' UTR of the potential target genes was cloned into the luciferase vector. If the miRNA binds to its potential target gene, luciferase translation is inhibited, and less light is produced. Firefly luciferase reporter gene construct and Renilla luciferase constructs (as internal transfection control) were co-transfected with or without the MIR203a mimics into HEK-293T cells. Hsa-miR203a-3p mimics (mirVana™ miRNA Mimics, Thermo Fisher Scientific, 4464070) with a final concentration of 100 nM, using Lipofec tamine RNAiMAX (Thermo Fisher Scientific, 13778150) transfection reagent (according to manufacturer's instructions, with minor changes: using serum-free and antibiotic-free high glucose DMEM medium instead of Opti-MEM Medium). 24 h after transfection with miRNA mimics, cells were transfected (according to manufacturer's guidance) with 200 ng/well luciferase plasmids (pmirGLO constructs), using Lipofectamine 3000 (Thermo Fisher Scientific, L3000015). Luciferase activity was measured using the Luciferase assay kit (Promega, E4030) by luminometer Modulus TM II (Turner Biosystems) after 24 hours. The results were presented as a ratio of Firefly luciferase over Renilla activity.

Plasmid construction

I performed the plasmid construction in various projects, such as for luciferase assay with miR203a or for lentiviral transfection with *MEG3*. To construct the plasmid, first, the gradient PCR was performed to find out the best annealing temperature with forward and reverse primers. The optimal

annealing temperature was used to amplify the cDNA. The band with amplified cDNA was cut out and extracted from the gel using a Monarch Gel extraction kit (NEB, T1020S). The amplicon was cloned into the vector using the Gibson Assembly cloning kit (NEB, E5510S), according to the manufacturer's protocol. The vector was transformed into competent bacteria NEB 5 α (NEB, C2987) and inserts were confirmed with colony PCR. Vector was isolated from the bacteria using a Plasmid miniprep kit (Thermo Fisher Scientific, K0502). The cloned insert was confirmed by DNA sequencing (Eurofins Genomics).

Lentivirus packaging and transfection

The packaging of the expression vector into pseudo viral particles was done using the psPAX2 (Addgene, 12260) and PMDG.2 (Addgene, 12259) plasmids in the presence of Turbofect (Thermo Fisher Scientific, R05319) transfection reagent in HEK-293T cells. The supernatant was collected after 48 and 72 hours and filtered through a 0,45 µm pore filter. For infection, cells were plated on T25 flasks to be 70-80 % confluent the next day and were infected with a mixture of 1 ml of viral particles and 1 ml of fresh media in the presence of 2 µl of 8 µg/ml polybrene. Lentivirus-transduced cells were selected with antibiotics or sorted by FACS (Sony SH800), based on fluorescent dye, to obtain a stable pool of clones. The altered expression of *MEG3* was determined by qRT-PCR. The plasmids used in the study and their selection markers (with a used concentration in case of antibiotics) were: PWPI-MEG3 (GFP fluorescence), pLenti_sgRNA(MS2)_zeo (Zeocin Invitrogen 4 µl/ml), pLenti_dCas9-VP64_Blast (Blasticidin, 2 µg/ml), pLenti_dCas9-KRAB_mCherry (mCherry fluorescence) and SAM MS2-P65-HSF1 Plasmids (Hygromycin 1 µl/ml).

CRISPRi/CRISPRa

To perform CRISPRi (Clustered Regularly Interspaced Short Palindromi c Repeats - inhibition) and CRISPRa (activation), two the vector system was used. First, a vector with dCas9 (dead CRISPR associated protein 9) with effector domain KRAB (pLenti_dCas9-VP64_Blast, Genscript) and VP64 (pLenti_dCas9-VP64_Blast, Genscript) effector domain for CRISPRi and CRISPRa, respectively, was incorporated, using lentiviral transfection. Subsequently, in the second round of lentiviral transfection, the vector with designed gRNA targeting a specific site of our gene of interest *MEG3* was incorporated. In case of gain of function studies with CRISPRa, one additional helper plasmid SAM (SAM MS2-P65-HSF1 Plasmids, Genscript) was used to increase activation further. The gRNAs for our gene of interest and the gRNAs for negative control were cloned into pLenti_sgRNA(MS2)_zeo (Genscript)

(**Table 5**). The stability of the CRISPRed cell population was verified in various passages by the percentage of mCherry-positive cells on FACS.

Table 5. gRNAs used for CRISPRi/a

gRNA for overexpression (gRNA A)	GCTCTCCGCCGTCTGCGCTA
gRNA for downregulation (gRNA B)	GCGGGTGAGGGATCCTCTCGT
negative control	GCTTAGTTACGCGTGGACGA

Cell sorting

D492 were sorted on EpCAM^{high} and EpCAM^{low} (NCL-ESA, Novocastra), using FACS (Sony SH800). Cells were trypsinised and resuspended in 500 µl 5 % FBS in PBS. Primary antibody was added in 1:100 dilution to the 0,5 ml cell suspension. Cells were incubated for 30 min at 4 °C in the dark, centrifuged and washed 3 x with cold PBS. Secondary fluorophore-conjugated antibody (Invitrogen) was added in 1:1000 dilution to 500 µl of cells in 5 % FBS in PBS and incubated for 20-30 min at 4 °C in the dark. Subsequently, cells were centrifuged, washed 3 x with cold PBS, single-cell filtered and stored in the dark until analysed.

3.4 Statistical analysis

A number of biological replications is indicated in figure legend as “n”. *P* values below 0,05 were considered significant (*p ≤ 0,05; **p ≤ 0,01; ***p ≤ 0,001; ****p ≤ 0,0001). The statistical analysis was performed in GraphPad Prism.

4 Technical consideration

During my PhD study, I have encountered several technical issues. In this chapter, I address a few key points related to the rationale for selecting methods, optimising the processes and hurdles I encountered, which I think could be beneficial for others. Moreover, an overview of 3D culture methods used in mammary gland research can be found in our recent review (paper #V).

4.1 Cell culture

Cell culture is the basis of many experiments. Knowing the cells well (the phenotype, doubling time, optimal splitting ratio, key markers) is crucial for every successful cell culture experiment. The use of established cell lines brings the possibility to have a homogeneous genetic background and an almost unlimited source of the material. However, there are also considerable disadvantages, such as change of genotype to some degree by introducing the immortalisation, the limited possibility of the available cell types (not all cell types are suitable or easily immortalised). The use of primary cells brings a higher level of complexity and heterogeneity to research. I have used primary cells as a tool for the validation of results from cell lines. Another level of complexity is brought using 3D cultures, while 2D modelling is a simple starting point for most cancer models. The benefits of 3D culture compared to 2D culture are undoubted, getting closer to *in vivo* conditions in terms of partially including (mimicking) the cells' microenvironment, such as acidity, hypoxia and stiffness (Simian & Bissell, 2017). 3D cultures also compensate for some of the weaknesses of 2D cultures associated with crosstalk, discussed in more detail in our review (paper #V). Culturing cells in 3D or 3D co-cultures allows cells to perform better their transcriptomic potential due to the activation of a unique set of transcription factors (Bellis et al., 2013; Neville & Daniel, 1987).

D492, D492M and D492HER2 were the primary cell lines used in this thesis. Each of them has a different splitting ratio and doubling time. For D492 the splitting ratio is 1:10, for D492M 1:5 and for D492HER2 1:20. Especially in the case of D492, it is essential to keep this ratio when maintaining the cells because of their stem cell characteristics (the ability to self-renew and give rise to more differentiated cells). When D492 is cultured, it comprises a heterogeneous population - cells with progenitor capacity to generate both luminal and myoepithelial cells. D492M cell line was generated from a single

cell and does not have the progenitor capacity as D492, so all the cells are homogenous.

Another critical issue to have in mind to achieve successful repetition of experiments with branching potential or clonogenic capacity in 3D culture, is to optimise the cell number for each batch of Matrigel (due to batch-to-batch variability).

4.2 Selection of functional assays

To better understand the function of the selected genes in our cell models, I have used multiple functional assays, such as proliferation, migration, invasion, apoptosis, cell attachment independent growth and angiogenesis. Cell migration and invasion are among the most crucial abilities of disseminating cells. *In vitro* assays for migration and invasion are models detecting the metastatic capacity of cells. Migratory properties usually go in hand with invasive properties, but not exclusively. Boyden chamber is a suitable tool to study chemotaxis, evaluating cell migration and invasion. Cell attachment independent growth can be examined with various assays, such as low attachment assay/mammosphere assay. Apoptosis assays give us information about cells' survivability, ability assigned to cells with EMT phenotype, and stem cells. To date, no *in vitro* method fully represents *in vivo* situation in breast tissue. Only about 5 % of the oncological drugs from phase one trial are approved for clinical use (Thomas et al., 2016). Therefore, there is a need to use more physiologically relevant 3D culture models, covering the complexity of breast cancer microenvironment (paper #V). Co-culture methods enable partial recapitulation of the breast microenvironment. We used co-culture as a strategy to determine the role of interactions between stromal and epithelial cells. The three standard methods for studying heterotypic interactions *in vitro are* conditioned media transfer, direct co-culture, and indirect co-culture. The use of conditioned media allows one-way signalling from effector to responder. Direct co-culture is when different cell types are cultured within a single compartment, allowing reciprocal interaction. On the other hand, indirect co-culture is when two physically separated cell types are cultured in shared media, using transwell filters, communicating through soluble signals in the shared media (Regier et al., 2016). The angiogenesis assay is detecting heterotypic interactions between epithelial and endothelial cells. It measures the impact of soluble factors, from epithelial cells, on tube formation of endothelial cells.

4.3 Optimizations and the use of controls

It is essential to use positive and negative controls to know that each step works as it should and be sure about the correct procedure. Here, I will list

three methods with which I spent considerable time in my studies.

4.3.1 Cloning into lentiviral plasmid

Cloning is a multi-step process, which also means plenty of room for mistakes and failures. For visualization of the process and design of the primers, I used the software SNAPgene, which makes the work easier and clearer. From my experience, a good practice is to run the electrophoresis gel, after every possible step, to verify that the plasmid has correct conformation, size and is not degraded.

4.3.2 Luciferase assay

With luciferase assay, we aimed to elucidate the binding of MIR203a to PXDN. Here I would like to illustrate how we went through the optimisation process, using different kits for this assay. First, we used a kit (from Genocopeia), where the whole 3´UTR of PXDN was cloned into a plasmid with the luciferase gene. The technical problem we were dealing with was an unstable expression of luciferase from the control plasmid between the cell lines we were comparing

(3´UTR PXDN with negative ctrl mimics vs Scr 3´UTR with negative ctrl mimics). (**Figure 11**). As this was critical for the interpretation of the result, we could not continue using this kit. Next, we decided to use another kit (Promega) where we cloned just the binding site of MIR203a into the plasmid. We did not see any change in the luciferase signal. To be sure that the method was working, we used a positive control - TP63 for binding MIR203a (Lena et al., 2008) (**Figure 12**). We ended up cloning eight plasmids, from which six were negative controls. However, we again did not see any change in the luciferase signal.

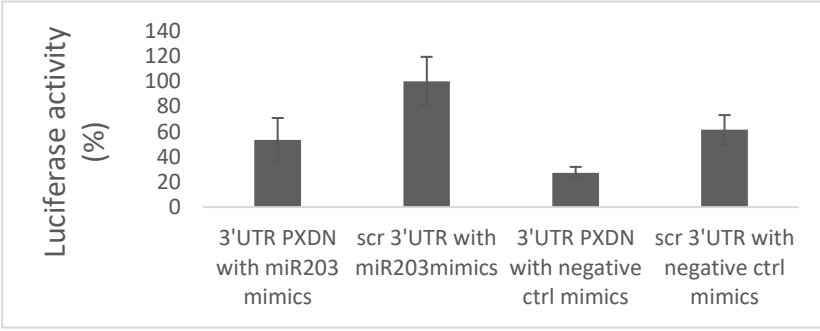

Figure 11. Unstable expression of luciferase from control plasmids.
(3´UTR PXDN with negative ctrl mimics vs Scr 3´UTR with negative ctrl mimics).

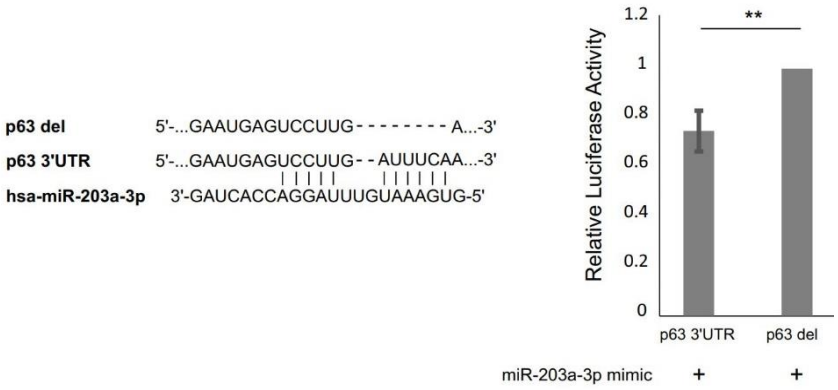

Figure 12. MIR203a binds to 3´UTR of TP63.
Results of luciferase assay confirm the correct use of the luciferase method with positive control – binding MIR203a to the 3´UTR of TP63.

Then we assessed the transfection efficiency using a GFP plasmid and found out that the cells were not getting transfected. Therefore, instead of using D492M^{miR203a} we switched to a cell line that is efficiently transfected – HEK293T cell line. This cell line has been used efficiently by many laboratories for transfections (Thomas & Smart, 2005). We optimized and coordinated the transfection of miRNA mimics and plasmids in the HEK293T cells, where the transfections' timing was critical due to the nature of the double transient transfection. Also, the confluence at the time of transfection was necessary for the maximal transfections' efficacy. With the optimised procedure, we could confirm that MIR203a binds to both 3´ UTR of TP63 and peroxidasin (PXDN).

4.3.3 CRISPRi/a

The purpose of CRISPRa (activation) or CRISPRi (inhibition) is the regulation of the genome instead of modification. Using this system, we can either activate or repress gene expression. The technique relies on two components: catalytically dead Cas9 (dCas9), without the endonuclease activity, and a guide molecule that directs dCas9 to a specific target like a genetic GPS. dCas9 can be fused to a Krüppel-associated box (KRAB) for repression or an activation domain, like VP64, for activation of a target gene (**Figure 13**).

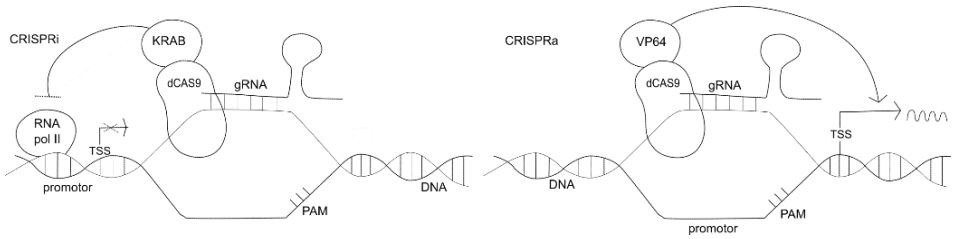

Figure 13. Molecular mechanism of CRISPRi and CRISPRa.
Protein dCaS9 is fused to effector domain: KRAB domain for CRISPRi and VP64 domain for CRISPRa. In CRISPRi, RNA pol II binding is blocked due to heterochromatinization, which makes it impossible to start the transcription of the gene. Conversely, the CRISPRa, enhances transcription as an artificial transcription factor. The location of gRNA is chosen in relevance to the protospacer adjacent motif (PAM), the transcriptional start site (TSS) and the uniqueness in the (human) genome, among other factors.

The most critical step for the CRISPRi/a approach is the first step - designing the gRNA. The design of the gRNA depends on its application. The appropriate position of gRNA(s) in CRISPRi/a might be different from the appropriate position of gRNA(s) intended to be used in the generation of a knockout or knock-in. For CRISPRi/a, the gRNAs need to be targeted in such a way that dCas9 can repress/activate transcription. Not all gRNAs work equally well, and the outcome depends on the effectiveness of the gRNA. I designed the binding of gRNA around the TSS (transcriptional start site): up to 200 nt upstream from TSS for the activation of the target gene and up to 200 nt downstream from TSS for the repression of the target gene (Gilbert et al., 2014; Smith et al., 2016). A critical step for long non-coding RNA, was the use of the database with accurately identified 5' end of the transcript. Data from FANTOM5 cap analysis of gene expression (CAGE) were used to build an atlas of human lncRNAs with accurate 5' ends to identify a genuine TSS (Hon et al., 2017). For the design of the gRNA itself, I used two online design tools Genscript and Crispr.mit.edu. Also, I applied the knowledge that the gRNA complementary to the non-template strand (sequence of the gRNA is the same as template strand) more strongly represses transcription (Rossi et al., 2015), and the sequence should start with the G nucleotide for efficient expression from the U6 promoter. The candidate gRNAs were ranked based on various parameters, among them the minimal off-target binding. Off-target effects of Cas9 is a major concern for the application of this technique, as it could lead to undesired mutations. Specifically, for the dCas9 technique, the frequency of off-target binding to essential (functional) exons is very low (Boyle et al., 2017). There are various reasons for low off-target binding, like the specificity of gRNA, the dependence on the protospacer adjacent motif (PAM) sequence, and importantly, the efficiency of effector domains (the KRAB and VP64) is limited to the area around TSS. A good practice is to validate the efficiency of CRISPRi/a methods with two pools of the same gRNA(s).

I selected three different gRNAs, one binding right at the TSS, the second binding upstream and the third binding downstream of TSS. Additionally, I used two negative controls (**Figure 14**). Based on multiple qRT-PCR results, I chose the gRNAs providing the most significant difference in gene expression, one for the activation and one for the repression of *MEG3*. However, later it turned out that the gene expression of *MEG3* was not stable and therefore not reproducible. I speculated that it might be a consequence of inefficient knockdown of *MEG3* or that the cells were losing dCas9 KRAB mCherry plasmid over time, which turned out to be the case. FACS sorting confirmed that the number of mCherry expressing cells was unstable. The instability caused a fluctuation of *MEG3* expression and loss of the knockdown with increasing passages. Even after multiple cycles of sorting mCherry positive cells to increase the proportion of dCas9 KRAB expressing cells, I could not get a clean mCherry positive population. Cells with high levels of *MEG3* expression (without the dCas9 KRAB plasmid) were overtaking the culture. I overcame this problem by increasing the transfection efficiency from about the original 1-2 % to over 90 % by using more of the virus supernatant when transducing the cells. Another way to solve the problem would be to use plasmid with different selection markers – instead of fluorescent protein, use antibiotic selection markers, or grow single-cell colonies from the mCherry positive cells. During the optimization process, I used negative controls to see whether the lentiviral transfection with dCas9 KRAB mCherry plasmid itself causes a significant effect on *MEG3* expression. My results stress the importance of generating a control cell line, which goes through the same technical process as a cell line targeting the gene of interest (**Figure 15**).

The overexpression of *MEG3* in D492 was not the priority right from the beginning since the endogenous expression of *MEG3* in D492 is relatively high already. *MEG3* expression in D492 following transfection with the CRISPRa plasmid was increased and relatively stable, however not high compared to D492 control. Therefore, I decided to switch from a plasmid from OriGene to a plasmid from Genscript with the option of using a helper plasmid with additional activation domains to help increase the expression, which significantly increased expression of *MEG3* to levels comparable in D492M.

A

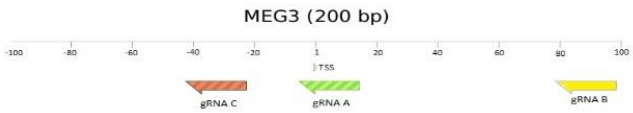

B

Guide 1 (gRNA A): GCTCTCCGCCGTCTGCGCTA
Guide 2 (gRNA B): GCGGGTGAGGGATCCTCTCGT
Guide 3 (gRNA C): GTTTATATGGAGGCGCAGAA
Negative control I: GCACTACCAGAGCTAACTCA
Negative control II: GCTTAGTTACGCGTGGACGA

Figure 14. Design of binding of gRNA to *MEG3*.
(A) Three gRNA binding around TSS of *MEG3*. **(B)** The nucleotide sequences of the gRNAs.

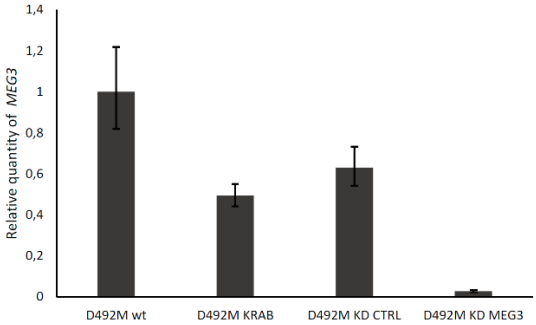

Figure 15. The importance of the use of proper negative control cell line.
D492M^{KRAB} and D492M$^{KD\ CTRL}$ have lower *MEG3* expression compared to D492M

5 Results and discussion

In this chapter, I will present and discuss published and unpublished data generated in my PhD studies. I will discuss breast gland development and cancer progression from the perspective of non-coding RNAs and include some retrospective thoughts into the discussion. Original publications are enclosed with this thesis.

5.1 Paper #I. Expression of ncRNAs on the DLK1-DIO3 locus is associated with basal and EMT phenotype in breast epithelial progenitor cells.

This work's objective was to elucidate how non-coding RNAs from the DLK1-DIO3 locus affect the process of epithelial to mesenchymal transition. This work forms the central part of my PhD thesis, published in Budkova et al. (2020).

5.1.1 The DLK1-DIO3 locus is upregulated in breast epithelial progenitor cells undergoing EMT.

In order to reveal differences in gene expression following the EMT transition from D492 to D492M, we performed gene expression profiling of these two cell lines. A number of miRNAs from the DLK1-DIO3 locus was highly upregulated in D492M. Long non-coding RNAs from DLK1-DIO3 locus were also upregulated in D492M, with *MEG3* being the most differentially expressed (Figure 1 in paper #I). This prompted us to ask whether non-coding RNAs from DLK1-DIO3 locus play a role in EMT.

We selected four representative miRNAs (MIR127, MIR493, MIR409 and MIR411) and the long non-coding RNA *MEG3* to verify the expression of non-coding RNAs from the DLK1-DIO3 locus by qRT-PCR. These non-coding RNAs were confirmed to be upregulated in D492M compared to D492 (**Figure 16A**). Besides, we showed that ncRNAs from the locus are upregulated in another EMT model, the HMLEmes cell line, a mesenchymal subline of the breast epithelial cell line HMLE (**Figure 16B**).

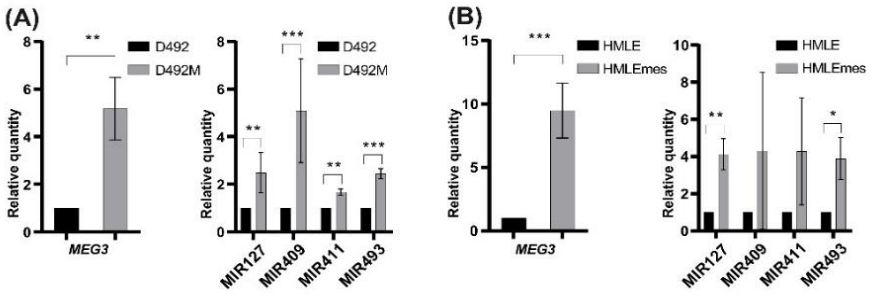

Figure 16. Upregulation of ncRNA from the DLK1-DIO3 locus in two cell lines with a mesenchymal phenotype.
(A) qRT-PCR shows higher expression of *MEG3* (left) and four miRNAs - MIR127, MIR493, MIR409 and MIR411 (right) in D492M compared to D492. Results are shown as mean ± SD. Unpaired t-test; n = 3. **(B)** ncRNAs from the DLK1-DIO3 locus are also upregulated in HMLEmes. qRT-PCR shows higher expression of *MEG3* (left) and miRNAs - MIR127, MIR493, MIR409 and MIR411 (right) in HMLEmes compared to HMLE. Results are shown as mean ± SD. Unpaired t-test; n = 3. (Adapted from Figure 1E and 1F in paper #I).

Compared to cell lines, the transcriptome of primary cells and organoids resembles more closely gene expression in breast tissue (K. Liu et al., 2019). Therefore, we were intrigued to study the expression of ncRNAs from the DLK1-DIO3 locus in primary tissue using sorted cell types from normal breast biopsies. Our data showed that the expression of ncRNAs from the DLK1-DIO3 locus was increased in the stromal compartment compared to the epithelial compartment of breast primary tissue. Moreover, we noted that the expression of *MEG3* is high in fibroblasts and whole tissue lysates from the breast, whereas it is low in the epithelial cell types (**Figure 17**). Considering the differential *MEG3* expression in fibroblasts and in whole tissue, our data clearly indicates that the expression in whole tissue lysates is primarily derived from stromal cells, the prevalent part of normal breast tissue. Therefore, any comparison of *MEG3* expression in normal breast tissue compared to breast cancer tissue should be done cautiously. This is discussed further later in this chapter.

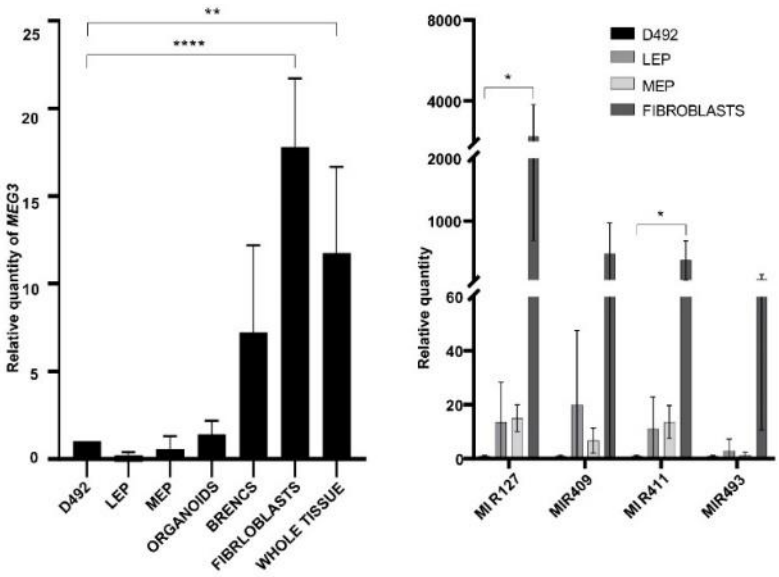

Figure 17. The ncRNAs from the DLK1-DIO3 locus are highly expressed in stromal cells and whole tissue compared to epithelial cells.
qRT-PCR shows that *MEG3* expression is higher in breast fibroblasts and whole tissue than in D492 (left). Results are shown as mean + SD. One-way ANOVA with Dunnett's multiple comparisons test; n = 3. Expression of MIR127 and MIR411 from the DLK1-DIO3 locus is higher in breast fibroblast than in D492 (right). Results are shown as mean ± SD. One-way ANOVA with Dunnett's multiple comparisons test; n = 3. (LEP - luminal epithelial cells, MEP - myoepithelial cells, BRENCs - breast endothelial cells). (Adapted from Figure 2 in paper #I).

Our observation of increased expression of non-coding RNAs in the stromal compartment was consolidated by the data from the online dataset GOBO (Gene expression-based Outcome for Breast Cancer Online), where *MEG3* expression correlates with expression of extracellular matrix genes in breast cancer (Supplemental Figure 2A in paper #I). Moreover, using the online resource MiPanda (Niknafs et al., 2018), we confirmed a positive correlation of *MEG3* expression with many commonly used EMT markers in healthy and cancerous breast tissue (Supplemental Figure 2B in paper #I).

5.1.2 *MEG3* expression negatively correlates with breast cancer prognosis.

EMT plays a fundamental role in understanding the metastatic behaviour of epithelia-originating cancer and treatment resistance (Creighton et al., 2009). However, the cell lines recapitulate the biology of tumour samples only to some extent (Gillet et al., 2011). We intended to translate our observations of *MEG3* involvement in cell lines into more clinically relevant outcome with patients'

cohorts, using breast tumour samples. *MEG3* expression is significantly higher in the breast cancer group classified as the normal-like (NL) (Figure 4A in paper #I), which resembles the expression of *MEG3* in normal tissue shown in **Figure 17**. Numerous papers suggest that the samples that fall into the normal-like group have a high proportion of normal tissue and low tumour cellularity (Elloumi et al., 2011; Prat et al., 2010) and they are therefore often excluded from the analysis. To ensure the quality of results representing tumour tissue, requiring a minimal percentage of malignant cells in a tumour sample (Elloumi et al., 2011), we omitted the normal-like tumours from the analysis of the effect of *MEG3* on the survival of breast cancer patients. Survival analysis showed lower overall survival in patients with high *MEG3* expression. These findings were corroborated in the GOBO database (Ringnér et al., 2011) (Figure 4B in paper #I), where *MEG3* expression negatively correlates with survival in breast cancer, exclusively in grade 3 tumours and the luminal B subtype. Together, we have shown in two independent cohorts that *MEG3* negatively correlates with survival. Our data underscore the necessity of further studies where subgroups are analysed.

As we have shown previously (**Figure 17**), by comparing primary breast cell types, high *MEG3* expression in normal breast tissue comes from stromal cells. In the clinic, genomic profiling is typically performed from bulk samples, so we cannot conclude whether the expression in tumour samples comes from infiltrated stromal cells or elevated expression in tumour cells. Nevertheless, both events could affect the prognosis of patients. Indeed, there are many proofs showing that the stroma is a major regulator of tumour progression (Bremnes et al., 2011; Conklin & Keely, 2012; Place et al., 2011).

The vast majority of cancer oriented papers describe lncRNA *MEG3* as a tumour suppressor, based on expressional studies comparing tumour tissue with relatively lower expression of *MEG3* versus adjacent normal tissue with relatively higher expression of *MEG3* (Chak et al., 2017; Molina-Pinelo et al., 2018; Sheng et al., 2014; Sun et al., 2016; Yin et al., 2015). However, as carcinoma (including breast cancer) originates from epithelial cells, it would be expected to see lower levels of *MEG3* expression in tumour samples, as they are comprised of a relatively higher number of epithelial cells, compared to normal tissue. Single-cell sequencing or in situ hybridization would provide a better way to understand the heterogeneity of breast tumours and the origin of expression of *MEG3*.

In my opinion, the classification of a gene as a tumour suppressor cannot be based on expression level but rather on the survival analysis. As such, survival analysis can tell if the gene is a positive/negative prognostic factor for the given cancer. To the best of my knowledge, there is only one paper related

to breast cancer, by Yao et al. (2019), where high *MEG3* expression was identified as a negative prognostic marker for breast cancer. On the other hand, most research papers on survival analysis with *MEG3* in breast cancer have shown conflicting results (Binabaj et al., 2018; X. Cui et al., 2018; Tian et al., 2018).

A major tumour suppressor role of *MEG3* is through stabilization of TP53 level, one of the most critical genetic alterations in human cancers (Sun et al., 2016; Uroda et al., 2019; Zhou et al., 2007). More than 50 % of tumours have direct inactivation in TP53 or its pathway. Our D492 cell lines with inactive TP53 offers another, perhaps more relevant view, on the role of *MEG3,* for such tumours with inactive TP53. The effect of TP53 can be studied on cell proliferation and cell cycle assays. We did not see the change in proliferation rate in our cell lines with the altered expression of *MEG3*. A recent paper by (Uroda et al.,2019) may support a different role of *MEG3* than tumour suppressor in our cellular model, as they state that cell cycle arrest by *MEG3* is exclusively TP53-dependent. Moreover, Chang et al. (2011) showed that TP53 inhibits EMT and stemness properties in mammary epithelial cells through transcriptional activation of the MIR200c gene. There, loss of TP53 leads to decreased expression of MIR200c and activated EMT program, accompanied by an increase in the mammary stem cell population. However, in D492, MIR200c is not lost, although TP53 is inactive (Hilmarsdottir et al., 2015). TP53 loss has also been correlated with the acquisition of self-renewal ability in normal and tumour mammary stem cells (Cicalese et al., 2009; Gatza et al., 2008). These findings emphasise the importance of studying the relation of *MEG3* and TP53 and the context-dependent role of *MEG3* in tumour progression.

5.1.3 *MEG3* as a marker of DLK1-DIO3 locus

To gain further insight into EMT regulation by *MEG3*, we established a cellular model for studying the effects of gain and loss of function with the CRISPRi/a approach (**Figure 18A**). Using this model, we showed concomitant expression of miRNAs from the DLK1-DIO3 locus with *MEG3*, suggesting that *MEG3* and miRNAs from the same locus are regulatory dependents (**Figure 18B**). These results were corroborated with data from The Cancer Genome Atlas (TCGA), where 75 % of miRNAs with positive correlation were located at the DLK1-DIO3 locus (table 1 in paper #I). Researchers have demonstrated that the maternally inherited unmethylated copy is essential for maintaining repression of protein-coding genes and activation of the ncRNAs (da Rocha et al., 2008; Lin et al., 2003). Previous studies have shown that the *MEG3* promoter, specifically MEG3-DMR, regulate the expression of all maternally expressed

genes from the DLK1-DIO3 locus (Ioannides et al., 2014; Sanli et al., 2018; Tierling et al., 2006; Zhu et al., 2019). Our results and the results of others suggest that *MEG3* expression is indicative for the expression of all the ncRNAs at the locus and may therefore be accepted as a marker for the expression of ncRNAs from the DLK1-DIO3 locus.

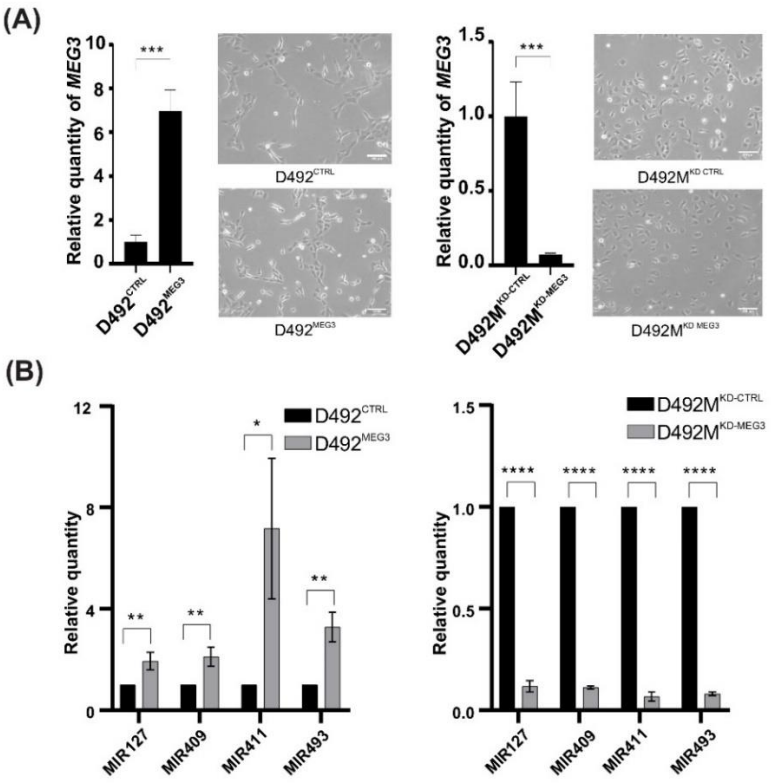

Figure 18. Concomitant expression of non-coding RNAs from DLK-DIO3 locus with *MEG3*.
(A) Cellular model of altered expression of *MEG3* was generated using CRISPR activation (CRISPRa) in D492 and CRISPR inhibition (CRISPRi) in D492M for upregulating and downregulation of *MEG3*, respectively. Upregulation of *MEG3* in D492 ($D492^{MEG3}$) compared to D492 with scrambled control ($D492^{CTRL}$; left), with phase-contrast pictures of $D492^{CTRL}$ and $D492^{MEG3}$ (below). Knockdown of *MEG3* in D492M ($D492M^{KD\text{-}MEG3}$) compared to D492M with scrambled control ($D492M^{KD\text{-}CTRL}$; right), with phase contrast-pictures of $D492M^{KD\text{-}CTRL}$ and $D492M^{KD\text{-}MEG3}$ (below). Results are shown as qRT-PCR with mean ± SD. Unpaired t-test; n = 3. Scale bar = 100 µm. **(B)** miRNAs from the DLK1-DIO3 locus are upregulated with overexpression of *MEG3* and downregulated with knockdown of *MEG3*. qRT-PCR shows increased expression of four representative miRNAs from the DLK1-DIO3 locus in $D492^{MEG3}$ compared to $D492^{CTRL}$ (left) and their decreased expression in $D492M^{KD\text{-}MEG3}$ compared to $D492M^{KD\text{-}CTRL}$ (right). Results are shown as mean ± SD. Unpaired t-test; n = 3. (Adapted from Figure 5 in paper #I).

To study gene expression changes induced by *MEG3*, we performed RNA sequencing of D492M with knockdown of *MEG*3. Gene Set Enrichment Analysis, using the Hallmark dataset, supported our hypothesis that non-coding RNAs from DLK1-DIO3 locus play a role in EMT. The epithelial-to-mesenchymal transition was one of the significantly deregulated gene sets by *MEG3* (Figure 6A in paper #I).

5.1.4 *MEG3* induce partial EMT

Existing literature regarding the role of *MEG3* in EMT is conflicting. We have shown that many mesenchymal and basal markers follow the *MEG3* expression (Figure 7 in paper #I). Nevertheless, we did not see a complete EMT phenotype, including the classical E- to N-cadherin switch when *MEG3* was overexpressed in D492 (Supplementary Figure 4 in paper #I). We have obtained comparable findings using another cell line with the mesenchymal phenotype (HMLEmes), indicating a positive correlation of *MEG3* with mesenchymal markers (**Figure 19**), and conversely, using luminal epithelial cell line (D382), we have seen a negative correlation of *MEG3* with luminal epithelial markers (**Figure 20**). Our data indicate that *MEG3* expression shifts the cells towards basal/mesenchymal phenotype. It has been shown already that myoepithelial cells, epithelial to mesenchymal transition-derived cells and stromal cells share common markers (Petersen et al., 2001).

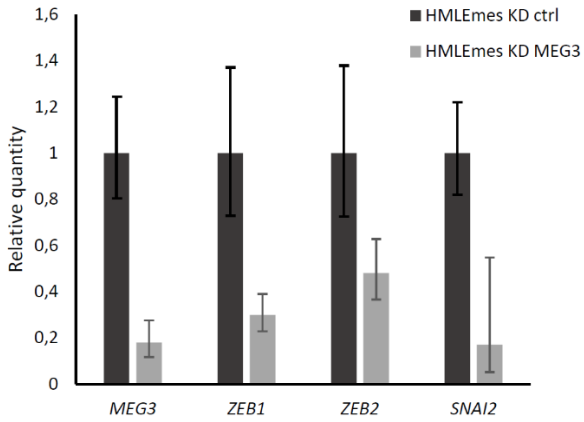

Figure 19. Transcription factors related to EMT were downregulated after *MEG3* knockdown in HMLEmes cell line.
qRT-PCR data confirms downregulation of *MEG3* in HMLEmes KD MEG3 cell line compared to control cell line HMLEmes KD ctrl and shows downregulation of TF *ZEB1*, *ZEB2* and *SNAI2* in HMLEmes KD MEG3 cell line compared to control cell line HMLEmes KD ctrl. Results show unpublished preliminary data.

.

.

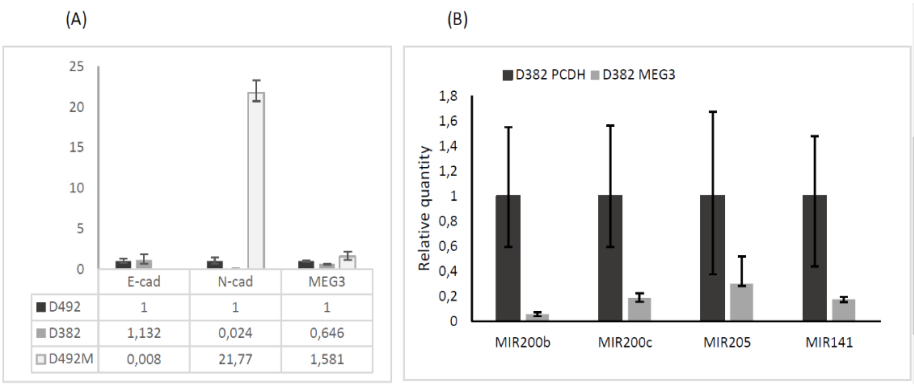

Figure 20. *MEG3* is negatively associated with the luminal phenotype.
(A) *MEG3* has low expression in luminal epithelial cells (D382) compared to epithelial (D492) and mesenchymal (D492M) cells. **(B)** Lentiviral overexpression of *MEG3* in D382 resulting in D382 MEG3 decreases luminal markers – MIR200b, MIR200c, MIR205, MIR141 compared to its control with empty vector D382 PCDH. Results show unpublished preliminary data.

Our results suggest that *MEG3* is a novel inducer of EMT in breast tissue, in contrast to the majority of studies that have shown an inhibitory role of *MEG3* in EMT in cancers (Seip et al., 2016; Xu et al., 2018). Nevertheless, our data are supported by studies, where *MEG3* was found to have an inducing role in the EMT in ovarian cancer (Mitra et al., 2017; Wang et al., 2019), lung cancer (Terashima et al., 2018; Terashima et al., 2017), hepatocellular carcinoma (Zhang et al., 2018) or glioma (Yang et al., 2020). *MEG3* plays a promoting role in the tumorigenesis and angiogenesis of lung adenocarcinoma through the Akt pathway (Li et al., 2019). Also, *MEG3* has been revealed to contribute to osteosarcoma expansion through enhanced migration, invasion, and reduced apoptosis (Wang & Kong, 2018). Furthermore, plasma samples from colorectal cancer patients have shown higher levels of *MEG3* compared to healthy controls (H. Liu et al., 2019). Moreover, *MEG3* siRNA decreased cell migration and proliferation, and conversely, overexpression of *MEG3* increased cell migration and proliferation in Hirschsprung‘s disease (Li et al., 2017). *MEG3* was also found to promote pulmonary, cardiac and kidney fibrosis (Gokey et al., 2018; Piccoli et al., 2017; Zha et al., 2019). A few EMT related studies are also dedicated to the role of miRNAs from the DLK1-DIO3 locus. MiRNAs from the DLK1-DIO3 locus have been linked to EMT in metastatic prostate cancer (Gururajan et al., 2014). Milosevic et al. (2012) found that most of the miRNAs upregulated in IPF (idiopathic pulmonary fibrosis) patients belonged to the DLK1-DIO3 locus.

One of the best-known inducers of EMT is TGFβ (Xu et al., 2009), a key regulator of mammary branching and regulator of gene expression in various

cell types (Nelson et al., 2006; Willis & Borok, 2007). *MEG3* and miRNAs from the DLK1-DIO3 locus were induced in cells after TGFβ1 stimulation (Milosevic et al., 2012; Terashima et al., 2017), which was also the case in our cellular model (**Figure 21**). *MEG3* binding sites revealed that *MEG3* modulates the activity of TGFβ - responsive genes by binding to distal regulatory elements (Mondal et al., 2015). TGFβ has a dual role in cancer - it can act as a tumour suppressor by inhibiting growth and promoting apoptosis at the early stages of cancer initiation, or in later stages, act as tumour promotor by inducing metastasis formation (Kim et al., 2000; Lebrun, 2012; Millet & Zhang, 2007; Xu et al., 2009). Such a dual role of TGFβ and its connection to *MEG3* could be another possible reason for the conflicting data about *MEG3* in the literature. However, the possible time-dependent role and detailed connection of *MEG3* with TGFβ during the EMT process remains to be elucidated.

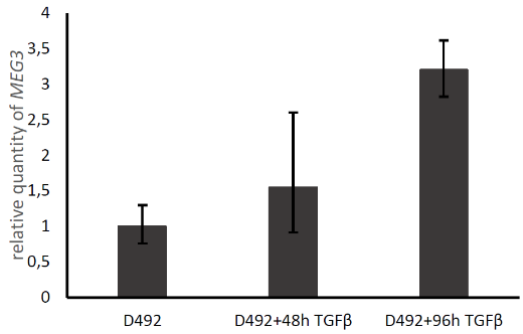

Figure 21. *MEG3* expression increases after treatment with TGFβ1.
qRT-PCR shows a time-dependent increase of *MEG3* expression after treatment with TGFβ1. Results show unpublished preliminary data.

5.1.5 *MEG3* induces mesenchymal properties and stemness

Several indications lead us to focus on the role of the DLK1-DIO3 locus in stemness. First of all, partial EMT phenotype is associated with stemness (Grosse-Wilde et al., 2015). Furthermore, several papers previously connected the expression of genes from the locus to pluripotency (Kang et al., 2009; Liu et al., 2010; Moradi et al., 2017; Stadtfeld et al., 2010; Zhao et al., 2009).

To revise the role of DLK1-DIO3 locus in inducing stemness in our cell model, we have studied stem cell markers and performed functional assays describing stem cell properties. Stemness is commonly quantified using specific markers like $CD44^{+}/CD24^{-/low}$ (Al-Hajj et al., 2003), integrin alpha 6 (ITGα6 or CD49f) or aldehyde dehydrogenase (ALDH1) (Ginestier et al., 2007; Krebsbach & Villa-Diaz, 2017; Resetkova et al., 2010). Our results showed a positive correlation of *MEG3* with stem cell markers ITGα6, ALDH1

(Supplementary Figure 6 in paper #I) and a negative correlation with CD24 (**Figure 22).** From the functional studies, we observed the association of *MEG3* with increased migration, resistance to apoptosis and sphere formation capacity, properties typically associated with the mesenchymal phenotype (Figure 8 in paper #I and Supplementary Figure 5 in paper #I). We also observed a bigger size of colonies and less branching in correlation with *MEG3* expression. A similar effect on branching potential, however, in the lung, was described in another study, where epithelial cells with overexpression of MIR127, one of the most studied miRNAs from the DLK1-DIO3 locus, led to fewer terminal buds (Bhaskaran et al., 2009). On the other hand, a recent study by Deocesano-Pereira et al. (2019) focused on the role of *MEG3* in breast cancer obtained different results compared to us. Similarly to our study, they performed CRISPR knockout of *MEG3* and studied the phenotypic and functional changes. Despite finding high expression of *MEG3* in the triple-negative metastatic breast cancer cell line Hs578T, their results showed that *MEG3* deletion promoted cell proliferation, anchorage-independent cell growth and migration. On the other hand, *MEG3* deletion also led to decreased cell invasiveness and promoted the expression of TGFβ and N-cadherin (Deocesano-Pereira et al., 2019).

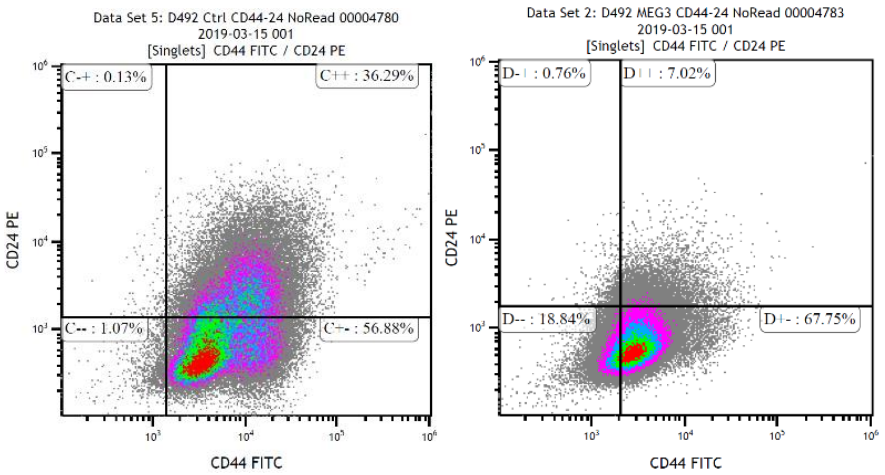

Figure 22. *MEG3* expression negatively correlates with the CD24 marker.
FACS analysis shows D492^{MEG3} (7,09 %) (right) has decreased expression of CD24 compared to D492^{CTRL} (36,42 %) (left), while the proportion of CD44 positive cells remain similar in both cell lines. Results show unpublished preliminary data.

In summary, in this study, we focused on non-coding RNAs with high expression levels in mesenchymal cells. Our interest was miRNAs and

lncRNAs on the imprinted DLK1-DIO3 locus, which showed high expression in D492M compared to D492. We explored the functional role of the locus in cellular phenotype using CRISPR and pinpointed its role in inducing partial EMT, therefore plasticity. Gain and loss of function studies showed concomitant expression of the lncRNA *MEG3* with miRNAs from the locus and its association with a basal and mesenchymal phenotype.

5.2 Paper #2. MiR203a is differentially expressed during branching morphogenesis and EMT in breast progenitor cells and is a repressor of peroxidasin.

A comparison of D492 and D492M in 2D and 3D culture in terms of miRNAs expression was the main project of a previous PhD student in our lab, Dr. Eirikur Briem (Briem et al., 2019). MIR203a, MIR141, MIR200c, MIR203a and MIR205 were the most differentially expressed miRNAs, with higher expression in epithelial cells (D492) compared to the mesenchymal cells (D492M) (Figure 1 in paper #II). Those miRNAs have been found to have high expression in epithelial cells, and their loss of expression has been shown to occur during EMT (Gregory et al., 2008; Moes et al., 2012; Tran et al., 2013). Our group has previously shown that MIR200c and MIR141 play an important role in maintaining epithelial integrity during the EMT process and, together with TP63, are required to achieve branching potential when overexpressed in D492M (Hilmarsdottir et al., 2015). Numerous studies have implicated specific miRNAs in EMT and cancer; among them is the study by Meyer-Schaller et al. (2019), where 13 miRNAs critically important for EMT progression were identified with miR200 family among them. Our study focused on MIR203a as a potential candidate, having a role in the cell lines' epithelial phenotype. To elucidate the role of epithelial miRNAs in branching morphogenesis, we compared their expression in three different time-points in 3D culture. Uniquely, MIR203a was increasingly expressed with advancing branching morphogenesis (Figure 3B in paper #II). Our results show MIR203a consistently associated with the epithelial and particularly luminal phenotype (Figure 3C in paper #II), corresponding to MIR203a being activated during luminal epithelial differentiation (DeCastro et al., 2013).

To elucidate the role of MIR203a in our EMT model, we stably overexpressed this miRNA in the D492M cell line, using lentiviral transduction, resulting in a new cell line D492M^{miR203a} along with the control cell line D492M^{Empty}, transduced with an empty vector. Initial characterization of D492M^{miR203a} demonstrated subtle changes towards cuboidal epithelial cells in 2D and more compact colonies in 3D, compared to the control D492M^{Empty}. We have found that MIR203a slows down the proliferation and negatively affects the phenotype typically associated with mesenchymal cells, such as resistance to apoptosis, anchorage-independent growth, migration, and invasion (Figure 4 in paper #II). The effect of MIR203a on the abilities mentioned above is consistent with previous studies in various cancer types, including breast cancers (Ding et al., 2013; Taube et al., 2013; Wang et al., 2014). Also, on the molecular level, MIR203a expression contributes to the epithelial phenotype. MIR203a increases the expression of epithelial markers such as E-cadherin (CDH1), KRT14 or KRT19, while expression of mesenchymal N-cadherin (CDH2) is decreased (Figure 4 in paper #II).

Several MIR203a target genes were revealed, suggesting that MIR203a may play a role in multiple signalling pathways. Among MIR203a target genes is the EMT- inducer SMAD3, oncogene SRC or stemness markers TP63 and GATA6 (GATA-binding factor 6) (DeCastro et al., 2013; Ding et al., 2013; Huang et al., 2020; Lai et al., 2020), which is overall in line with our findings that MIR203a expression suppresses characteristics of EMT/stemness. Further clarification of MIR203a target genes is important for understanding its entire regulatory network. By RNA sequencing of D492M^{miR203a} and D492M^{empty}, and corroborating bioinformatic predictions, we identified a potential novel target gene of MIR203a, peroxidasin (PXDN). PXDN is an ECM protein with peroxidase activity and a collagen IV crosslinker, important for the basement membrane's integrity (Peterfi et al., 2009). To confirm PXDN as a target of MIR203a, we have shown that PXDN expression is affected when cells are treated with MIR203a mimics and inhibitors (**Figure 23A**). Also, using

the luciferase assay, we established that MIR203a interacts with a specific region of the 3´ UTR of PXDN (**Figure 23B**).

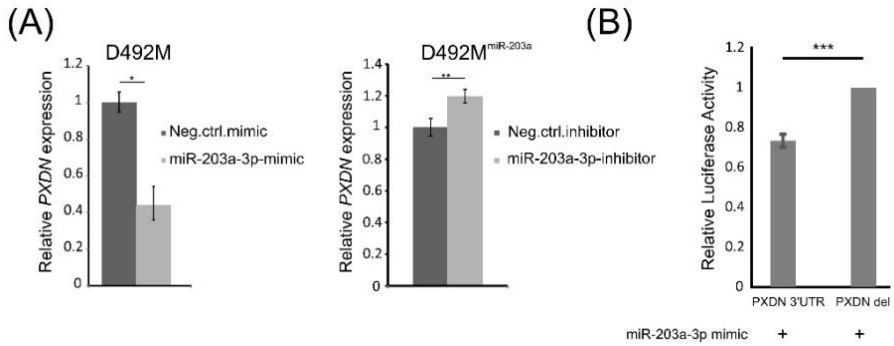

Figure 23. MIR203a regulates PXDN expression.
(A) D492M cells treated with MIR203a mimic have reduced expression of PXDN, whereas D492M$^{miR\text{-}203a}$ cells treated with MIR203a inhibitor have increased expression of PXDN. qRT-PCR results shown as mean ± SD, n = 3. **(B)** MIR203a directly binds to its target sequence on PXDN 3′ UTR. Luciferase results show as mean ± SD. Two-tailed student t-test, n = 3. (Adapted from Figure 5 in paper #II).

Increased PXDN expression has been associated with various diseases and developmental stages, such as renal fibrosis (Peterfi et al., 2009), during embryonic development of the eye (Yan et al., 2014), in melanoma cancer (PXDN has also been previously called MG50 - melanoma gene 50) (Mitchell et al., 2000) and ovarian cancer (Zheng & Liang, 2018). This demonstrates an association of PXDN with the EMT process. To determine whether PXDN is responsible for the effects seen by overexpression of MIR203a in D492M, we performed a transient knockdown of PXDN in D492M using siRNA. We have shown that decreased PXDN expression slows down the proliferation and decreases the resistance to apoptosis (Figure 6 in paper #II). Those results are in concordance with another study, where PXDN knockdown led to an increase in reactive oxygen species associated with decreased cell viability and increased apoptosis (Dougan et al., 2019).

Data from public online databases shows that patients with HER2 positive breast cancer and high PXDN expression have significantly lower overall survival (**Figure 24**). There are currently no published studies on the role of PXDN in HER2 positive breast cancer, but this subtype-specific effect on survival suggests that it is an interesting subject to study further. HER2-positive and triple-negative breast tumours are prominent by progressive stiffening of breast tissue (Acerbi et al., 2015; Chang et al., 2013). The stiffening of tumours is associated with ECM deposition and crosslinking (Butcher et al., 2009; Levental et al., 2009). Stiffness of the breast positively correlates with breast

cancer risk (Boyd et al., 2014) and negatively correlates with responsiveness to chemotherapy (Hayashi et al., 2012). The exact molecular mechanism of how stiffness promotes aggressiveness of breast tumours is not known. MIR203a was shown to be decreased as a response to high stiffness in breast tumours, followed by Robo/Slit regulatory pathway leading to maturation of focal adhesion, helping the cell to adjust to the stiffness (Le et al., 2016). Further characterization of downstream effects of MIR203a on PXDN and investigations on the role of PXDN in HER2 positive breast cancers is ongoing in our lab by another PhD student, Anna Karen Sigurdardottir.

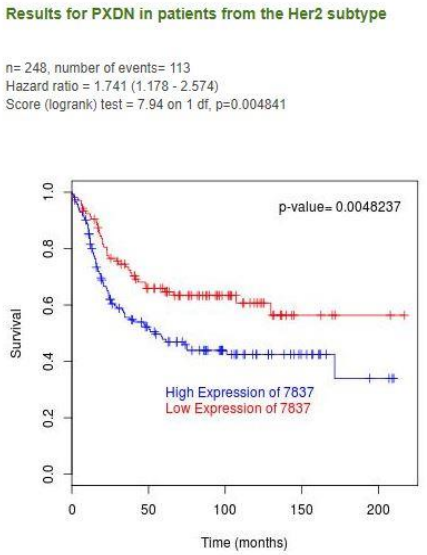

Figure 24. Patients with HER2 positive breast cancer with high PXDN expression has significantly lower overall survival.
Kaplan-Meier graph from BreastMark database.

Collectively, in this study, we explored the role of MIR203a as a regulator of branching morphogenesis and mesenchymal to epithelial transition, contributing to epithelial properties. Furthermore, we identified MIR203a as a novel suppressor of peroxidasin (PXDN). Unravelling MIR203a effects on EMT/MET, and their downstream target PXDN could help to uncover novel biomarkers for breast cancer.

5.3 Paper #III and IV. Comparison of isogenic non-malignant and malignant cell lines with EMT phenotype and identification of YKL-40 and ECM1 with a putative role in promoting malignancy.

Here, I will summarise findings from paper #III and #IV. In paper #III, we focused on identifying functional and molecular differences between two isogenic cell lines with differences in their ability to cause metastasis, whereas

paper #IV is focused on the heterotypic interaction of endothelial cells with cancer cells. In these two studies, we identified extracellular matrix proteins YKL-40 and ECM1 as important players in mediating the tumorigenicity of HER2 breast tumours. The characterization of the YKL-40 gene and the comparison of the cell lines (paper #III) was the main research questions of former PhD student in our group, Dr. Erika Morera (Morera et al., 2019), while the ECM1 study (paper #IV) was the main research question of Dr. Sophie Steinhauser (Steinhaeuser et al., 2020), also a previous PhD student in our group.

The main interest from the perspective of non-coding RNAs was to identify changes in miRNAs expression under conditions of tumorigenicity. We determined (in paper #II): MIR200c, MIR203a, and MIR205, as the most differentially expressed miRNAs between D492 and D492M, with high expression in epithelial cells. When D492M and D492HER2 are compared, the higher expression of those miRNAs in D492HER2 indicates stronger epithelial integrity of D492HER2 compared to D492M (**Figure 25**). The hybrid epithelial/mesenchymal phenotype of D492HER2 provides plasticity to the cells. The plasticity of cells is one of the proprieties of metastatic cells (Jolly et al., 2015; Jordan et al., 2011; Ye & Weinberg, 2015), as previously discussed in the introduction of this thesis.

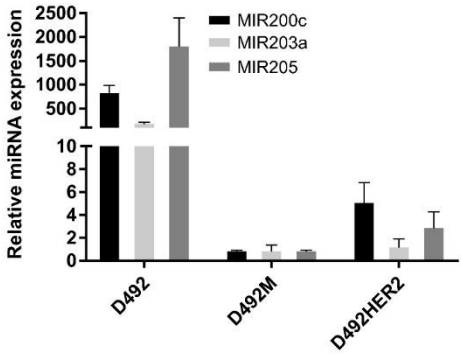

Figure 25. D492M and D492HER2 show a reduction in the expression of epithelial microRNAs.
However, D492HER2 has about 2-5 times higher expression of MIR200c, MIR203a, and MIR205 miRNAs compared to D492M. qRT-PCR results shown as mean ± SD, n = 2). (Adapted from Figure 1C in paper #III).

By studying functional differences of those D492 - derived cell lines, D492HER2 has shown increased migration, invasion, proliferation, viability, and sensitivity to apoptosis compared to D492M and D492 (Figure 1 in paper #III). In angiogenesis assay, we identified increased tube formation of endothelial cells after their induction with conditioned media from D492HER2

cells (Figure 1B in paper #IV). These aggressive traits of tumorigenic D492HER2 and its partial EMT phenotype goes in hand with the higher risk of cells with partial EMT phenotype to cause metastasis (Grosse-Wilde et al., 2015; Ye & Weinberg, 2015). However, we cannot distinguish whether the observed functions of D492HER2 are primarily caused by the HER2 oncogene or the partial EMT phenotype.

The importance of the interaction between the malignant epithelial cells and the surrounding stromal cells is widely recognised. Moreover, the specific receptivity of the metastatic niche was first identified more than 30 years ago (Allinen et al., 2004; Conklin & Keely, 2012; Paget, 1989). Here, we focused on the role of the endothelial cells. There are many ways that endothelial cells affect tumour growth. The vasculature is a key component in tumour growth and metastasis, not only because circulating cancer cells migrate through blood vessels (Junttila & de Sauvage, 2013), but also, endothelial cells are a vital component in enhancing the drug resistance of tumours. For example, endothelial cells have been suspected of having control over cancer progression through the expression of Nidogen-1 (Ferraro et al., 2019).

We studied epithelial-endothelial interactions, using co-cultures of epithelial cells with HER2 overexpression and endothelial cells or conditioned media thereof. To investigate possible feedback reactions between endothelial cells and epithelial cells, we applied co-culture methods such as conditioned media transfer and indirect co-culture (Figure 1D and 1F in paper #IV). Our results showed increased migration and invasion of tumorigenic cells towards endothelial cells compared to non-tumorigenic cell lines. Moreover, direct co-culture, both in 2D and 3D, showed that the morphogenetic and the mechanistic role of endothelial cells are possibly important in the pathogenesis and progression of tumours. Here we have shown that the migration of epithelial cells is directed towards endothelial cells (Figure 2 in paper #IV). Altogether, we observed that D492HER2 triggers endothelial cells in releasing a feedback response attracting epithelial cells towards them.

To identify specific secreted proteins responsible for the aggressivity of D492HER2 and its crosstalk with endothelial cells, we profiled conditioned media (CM) from D492HER2. We identified two candidate molecules YKL-40 and ECM1, contributing to the D492HER2 cell´s phenotype (Figure 2D in paper #IV).

5.3.1 YKL-40/CHI3L1 facilitates migration and invasion in HER2 overexpressing breast epithelial progenitor cells and generates a niche for capillary-like network formation.

Elevated expression of YKL-40 has been found in numerous cancers, including breast cancer (Liu et al., 2014; Roslind et al., 2007). Analysis of YKL-40 expression in breast cancer revealed a significant association with decreased overall survival and distant metastasis-free survival (Wan et al., 2017; Zhao et al., 2020). YKL-40 has also been linked to the EMT process in non-small cell lung carcinoma (Jefri et al., 2015). Moreover, the function of YKL-40 has been connected to supporting angiogenesis through VEGF stimulation (Ngernyuang et al., 2014; Shao, 2013; Shao et al., 2009), prevention of apoptosis (Lee et al., 2009) or involvement in inflammation (Kzhyshkowska et al., 2007). We aimed to decipher YKL-40 protein' role in D492 - derived cell lines with gain and loss of function studies (Figure 3 in paper #III). Both transient (using siRNA) silencing and stable (using CRISPR) repression of YKL-40 in D492HER2 have shown decreased migration and invasion upon repression of YKL-40. Similarly, the overexpression (using CRISPRa) of YKL-40 in D492 and D492M led to increased migration and invasion in both cell lines (**Figure 26**). Jensen et al. (2003) have shown a supportive role of YKL-40 in breast tumours' aggressiveness. They found that high expression of HER2 and YKL-40 in serum independently correlated with metastatic breast cancer patients with a poor prognosis.

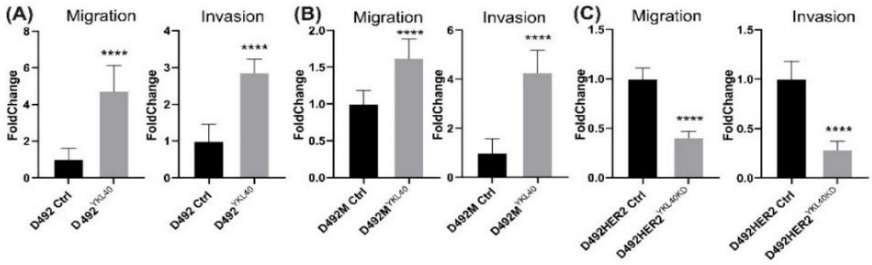

Figure 26. YKL-40 induces migration and invasion in D492 cell lines.

(A) Overexpression of YKL-40 in D492 and **(B)** D492M using the CRISPRa system increased their ability to migrate and invade. **(C)** Knockdown of YKL-40 in D492HER2 in stable cell lines generated by CRISPR/Cas9 reduced the ability of D492HER2 to migrate and invade. Results are shown as mean ± SD. Unpaired t-test, n = 8. (Adapted from Figure 3E, F and G in paper #III).

The supporting role of YKL-40 in angiogenesis has been observed in previous studies, with molecular signalling through syndecan 1, present on

endothelial cells (Shao, 2013) or through increased migration of endothelial cells (Malinda et al., 1999). Therefore, we were interested in elucidating the role of YKL-40 in angiogenesis in our cell model. Using conditioned media transfer, we showed that increased YKL-40 expression induces the potential to stimulate angiogenesis (Figure 4B in paper #III). Alternatively, when the monoclonal antibody against YKL-40 was added to CM of D492HER2, the formed HUVEC network was significantly reduced. However, when a recombinant YKL-40 protein was added to CM of D492HER2, the phenotype of the network structure was rescued (Figure 4A in paper #III). Together, our results indicate that the secreted YKL-40 induces angiogenesis.

Moreover, YKL-40 dramatically influences the phenotype of D492HER2 cells in 3D culture, contributing to the formation of grape-like colonies (Figure 5 in paper #III).

Collectively, in paper #III, we have analysed the role of YKL-40 in metastatic formation and show an increase in migration, invasion, and angiogenesis. Our data demonstrate that YKL-40 may contribute to the D492HER2 cell´s plasticity and aggressiveness by increasing the migratory, invasive, and angiogenetic abilities of cancer cells.

5.3.2 ECM1 secreted by HER2-overexpressing breast cancer cells generates vascular niche that accelerates migration and invasion of cancer cells

ECM1 has been shown to be essential for adhesion and invasion of breast cancer cells and promoting the formation of metastasis (Wu et al., 2018). Furthermore, ECM1 has been identified as a poor prognostic marker in patients with breast cancer (Lal et al., 2009) and having an effect on endothelial cells, promoting angiogenesis (Han et al., 2001; Sercu et al., 2008). ECM1 might represent a promising therapeutic target for decreasing the therapeutics' resistance or targeting the hallmark of metastatic cancer – angiogenesis. However, the mechanism of how ECM1 supports endothelial cells is not well understood on the molecular level. Currently, the principal treatment for HER2-positive breast cancer is the monoclonal antibody trastuzumab. Lee et al. (2014) have shown that trastuzumab resistance is often raised in breast cancer with ECM1 overexpression.

Using recombinant ECM1 protein and cell lines with stable overexpression, we have determined its direct role on endothelial cells, increasing angiogenesis (Figure 3B and Figure 4B in paper #IV). Conversely, the knockdown of ECM1 resulted in a decrease in angiogenesis (Figure 4B in paper #IV). Furthermore, conditioned media transfer from such treated endothelial cells back on epithelial cells revealed increased migration and invasion (**Figure 27**). This effect was also confirmed with the use of stable

knockdown of ECM1 in D492HER2, decreasing migration and invasion (Figure 4D, F in paper #IV).

On the molecular level, the results from RNA microarrays have revealed the importance of Notch signalling in the epithelial-endothelial crosstalk induced by ECM1. Obtained results were further validated by qRT-PCR and immunofluorescence staining (Figure 5A in paper #IV). Inhibition of the Notch pathway with γ-secretase inhibitor (DAPT- N-[N-(3,5-Difluorophenacetyl)-L-alanyl]-S-phenyl glycine t-butyl ester) confirmed its role in ECM1-mediated promotion of migration and invasion (**Figure 27**). We have shown that ECM1 induces endothelial feedback promoting migration of cancer cells towards them through Notch signalling. Notch signalling is very complex and is a known key player in endothelial cells and angiogenesis in both normal development and diseases, including breast cancer (Dufraine et al., 2008; Ghiabi et al., 2015; Iso et al., 2003; Miloudi et al., 2019). Notch is also known inducer of EMT and metastatic spreading in breast cancer (Lamouille et al., 2014; Reedijk, 2012).

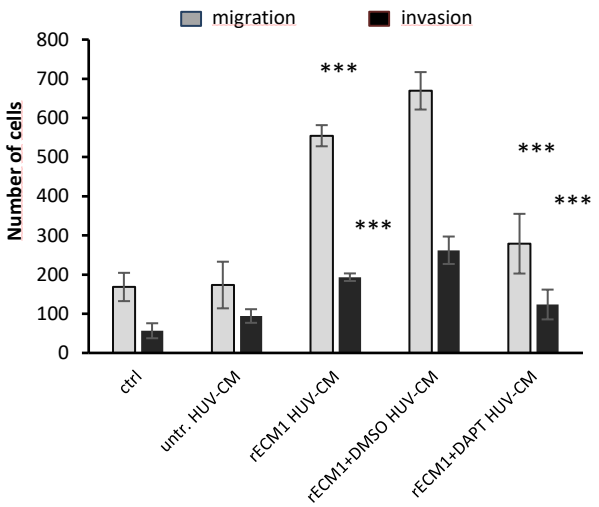

Figure 27. Recombinant ECM1 induces endothelial feedback increasing migration and invasion via Notch signalling pathway.
When the Notch inhibitor (DAPT) is added, the migration and invasion are decreased. Conditioned media from recombinant-ECM1 induced endothelial cells (rECM1 HUV-CM) promote migration and invasion of D492HER2 compared to untreated control (untr. HUV-CM). Conditioned media from recombinant-ECM1 induced endothelial cells treated with Notch inhibitor (DAPT) (rECM1+DAPT HUV-CM) reduce migration and invasion of D492HER2 cells compared to control (rECM1+DMSO HUV-CM). Student t-test, n = 3. (Adapted from Figure 5E in paper #IV).

Collectively, in paper #IV, we identified ECM1 as a mediator of endothelial-epithelial crosstalk with a role of supporting metastasis formation through Notch signalling. Upregulation of Notch is meditating positive feedback in promoting migration and invasion of breast cancer cells.

6 Future perspectives

The research described in this thesis is raising several questions, which answers would help to further elucidate the role of studied molecules in breast gland development and cancer. Therefore, I would like to mention here the ideas and proposals for the further continuation of the projects.

In our experimental set up with loss/gain of function of *MEG3,* we applied CRISPRi at the TSS of *MEG3*, which suppressed the transcription of ncRNAs from the DLK1-DIO3 locus. Therefore, we investigated the role of the whole ncRNAs from the DLK1-DIO3 locus. We used *MEG3* as a marker of the DLK1-DIO3 locus expression, but *MEG3* does not necessarily have a causative role in EMT in our model. Further studies are needed to dissect whether the observed molecular and functional effect is caused by *MEG3*, miRNA or a combination of more ncRNAs from the DLK1-DIO3 locus. This could be done by studying the gain and loss of function of single ncRNA at the time, with another approach than CRISPRi/a, such as lentiviral overexpression with cDNA vector or downregulation with shRNA vector. In our lab, we have previously tried to knockdown *MEG3* using shRNA and siRNA; however, we did not succeed using these methods. Another attempt, using targeting sequences from other published articles (Shi, 2020), would be worth pursuing.

Another future aspect should be decoding the relationship of *MEG3* and TP53 by comparison of two cell lines with the same genetic background but different methods of immortalisation, leading to functional and dysfunctional TP53. Among other issues remaining to be elucidated is the relationship of *MEG3* and TGFβ and, last but not least, the role of specific isoforms of *MEG3* in our EMT model.

One of the proposed function of *MEG3* is inducing heterochromatinization through the PRC2 complex (Kaneko et al., 2014). One aspect that would contribute to knowledge not only about *MEG3* downstream effects in our cellular model but also about the D492 cell lines´ general regulation of gene expression would be to study epigenetic alternations using ChIP-seq (chromatin immunoprecipitation followed by sequencing).

From the results in paper #II, one of the hypotheses to be studied further is whether a reorganisation of the extracellular matrix by PXDN potentially leads to stiffening and promoting the invasion of the cells and if the PXDN-stiffness axis is involved in HER2 breast cancer.

Joining the findings from paper #III and #IV together could also bring more information on the signalling pathway behind the aggressiveness of the D492HER2 cell line. YKL-40 and ECM1 seem to have a similar function in D492HER2 by supporting angiogenesis. However, we revealed vital differences, such as that YKL-40 has an effect on the proliferation of endothelial cells, while ECM1 does not and that YKL-40 acts probably through known pro-angiogenic factors VEGFR2, while ECM1 does not. This indicates that those two proteins act through different mechanisms. It would therefore be interesting to see whether the double knockdown of YKL-40 and ECM1 in D492HER2 would, even more, decrease the angiogenic potential. Although we studied the function of YKL-40 and ECM1 in HER2 overexpressing cell lines, its direct molecular connection to HER2 pathways remains to be elucidated. And last but not least, going from a fully controlled cellular model to *in vivo* setting, assaying tumorigenicity and metastatic potential of YKL-40 and ECM1 would lead the project closer to clinical relevance.

Moreover, in paper #IV, we identified the feedback effect of endothelial cells on epithelial cells through Notch signalling. The Notch signalling pathway also has a vital role in CSCs characteristics, including chemoresistance (Akil et al., 2021). It would be interesting to study further the feedback response from the endothelial cells on D492HER2, and study, whether Notch signalling has any effect on other stem cell characteristics of the cell line besides increased migration and invasion. So far, our group has unpublished data showing a negative correlation of ECM1 with GATA3, a transcription factor driving luminal differentiation, connected with a better prognosis of HER2 breast cancer patients. These findings require further investigation, such as testing whether the overexpression of GATA3 in the D492HER2 cell line would decrease its tumorigenicity.

Collectively, endothelial cells were quite in the spotlight in this thesis as part of the microenvironment playing a role in breast development and cancer. Using our cellular models of D492, we have studied the endothelial-induced EMT and the heterotypic interaction between endothelial and epithelial cells. Endothelial cells form the basic building blocks for blood vessels. Interestingly, the possible shared developmental mechanism of mammary branching and angiogenesis can be found in partial EMT and partial EndoMT, respectively. To the best of my knowledge, the involvement of EndoMT in developmental angiogenesis is an almost unexplored field, as its existence was just recently discovered (Welch-Reardon et al., 2015) and even more unexplored is the role of non-coding RNAs. Similarly, it applies to the involvement of partial EMT in mammary branching morphogenesis from the point of view of non-coding RNAs, which is also quite understudied, although our group has contributed

significantly to that topic (Briem et al., 2019; Hilmarsdottir et al., 2015). Therefore, the gained knowledge of non-coding RNAs and extracellular matrix proteins could be vice versa relevant in those processes. Precisely, the role of ncRNAs from DLK1-DIO3 locus and MIR203a in angiogenesis or YKL-40 and ECM1 in branching morphogenesis. Future research is also needed in this area.

Nevertheless, there are studies dealing with the role of members of the DLK1-DIO3 locus in angiogenesis. *MEG3* has been found to be highly expressed in endothelial cells (Michalik et al., 2014) involved in angiogenesis (Ruan et al., 2018). Increased *MEG3* expression in HUVECs was induced by HIF1α and promoted angiogenic sprouting, whereas knockdown of *MEG3* inhibited the sprouting by decreasing levels of VEGFR2 (Ruan et al., 2018). On the other hand, the inhibition of miRNAs from the DLK1-DIO3 locus has been shown to increase vascularisation after ischemia (Welten et al., 2014) or *MEG3* was negatively correlated with angiogenesis in other studies (He et al., 2017; Zhan et al., 2017; Zhang et al., 2017).

Finally, linking all presented projects together by implementing findings of the role of ncRNAs in D492M into the perspective of tumorigenicity of D492HER2 could strengthen the data. For example, to study whether the overexpression of epithelial miRNAs or downregulation of *MEG3* has an effect on the plasticity/tumorigenicity/angiogenesis of D492HER2. And last but not least, whether the increase in expression of YKL-40/ECM1 would make D492M more tumorigenic.

7 Summary and conclusions

In this chapter, I will summarise the importance of the research topic in my thesis for biomedical sciences, draw conclusions for each aim of the thesis and outline how the obtained results helped address the research questions. Moreover, I will delineate the future perspectives of individual projects.

My PhD thesis's main research topic is non-coding RNAs and their role in branching morphogenesis and epithelial-to-mesenchymal transition in breast epithelial cells. Our goal was to identify non-coding RNAs that govern cellular plasticity in the human mammary gland. My thesis's secondary focus was identifying extracellular matrix proteins contributing to the cellular plasticity and tumorigenic properties of breast epithelial cells. The research was conducted on D492 - derived cell lines. The D492 cell lines represent a highly relevant and useful model to study biological concepts, including EMT, branching morphogenesis, and tumorigenic properties.

In the first part of this thesis (paper #I and paper #II), the focus was on the non-coding RNAs from both sides of the EMT spectrum. The identified candidate molecules, lncRNA *MEG3* and MIR203a, play a role in the balance of EMT/MET. Extensive *in vitro* evidence has delineated the involvement of EMT/MET in branching morphogenesis and the formation of tumour metastasis (Chakrabarti et al., 2012; Sarrió et al., 2008). EMT is an important event contributing to drug resistance, leading to increased heterogeneity and plasticity of the cells within tumours. There is a lack of therapies that can efficiently prevent metastasis as well as effective prognostic markers to anticipate clinical outcome and treatment response. Identifying key molecules, such as *MEG3* and MIR203a, involved in EMT/MET and their mechanisms of action could be important for reducing breast cancer patient's mortality. In the second part of the thesis (in paper #III and paper #IV), we looked at the parallels and differences between tumorigenic and non-tumorigenic cell lines and the role of endothelial cells on both normal breast cells and cancer cells. The stroma's critical function during malignant transformation and progression suggests that targeting it in conjunction with the carcinoma cells may be a synergistic therapeutic intervention strategy. We identified two candidate extracellular matrix proteins YKL-40 and ECM1, secreted by breast cancer cells, promoting angiogenesis, migration and invasion (**Figure 28**).

The focus of paper #I was on one of the biggest clusters of non-coding RNAs in the human genome, the DLK1-DIO3 locus. In this study, we addressed the role of this locus in cellular plasticity and its association with

breast cancer. For this purpose, we used the D492 cellular EMT model, primary cell cultures and cancer patient cohorts. The study showed that DLK1-DIO3 might be a novel regulator of plasticity in breast epithelial progenitor cells. We used the expression of the long non-coding RNA *MEG3* as a marker for the expression of all non-coding RNAs from the DLK1-DIO3 locus. We suggested that the functional role of *MEG3* is increasing plasticity, therefore, promoting EMT. Our results object to other publications, where *MEG3* has been extensively reported as a tumour suppressor gene in different types of cancer, including breast cancer (Zhang et al., 2019). However, a few studies support our hypothesis of a role for *MEG3* in EMT induction, such as those by Mitra et al. (2017) or Terashima et al. (2017). The literature about *MEG3* indicates the complexity of its role in mammary gland development. Collectively, DLK1-DIO3 is a large and complex locus, and much remains to be discovered about these ncRNAs' individual versus joint function (Dill et al., 2020).

In paper #II, we addressed the role of MIR203a in branching morphogenesis and EMT. We identified increased expression of MIR203a during the branching process as well as its role in the MET process through maintaining the epithelial integrity. Furthermore, we revealed a novel mechanism of action of MIR203a by its ability to repress the expression of the collagen IV crosslinker, peroxidasin (PXDN).

In paper #III, we compared two isogenic EMT-derived cell lines with different abilities to cause metastasis. We demonstrated that the aggressiveness of the tumorigenic cell line (D492HER2) is mediated by functional abilities such as increased migration, invasion, proliferation or angiogenic potential, compared to the non-tumorigenic cell line (D492M). There is also a difference in expression of epithelial miRNAs, which is higher in D492HER2 than D492M, demonstrating the hybrid epithelial/mesenchymal phenotype of D492HER2. Furthermore, in this project, we identified extracellular matrix protein YKL-40 as a candidate causing significant differences between D492HER2 and D492M. Our results imply that YKL-40 may provide D492HER2 with increased aggressiveness, evidenced by enhanced migration and invasion. YKL-40 may also support cancer progression by facilitating angiogenesis and may be of interest as a therapeutic target in HER2-positive breast cancer.

Paper #IV aimed at investigating tumour-stroma interactions. Herein, ECM1 was identified as a breast cancer secreted protein promoting tube formation of endothelial cell (angiogenesis), which in turn promote migration and invasion of cancer cells. We identified a molecular pathway, through Notch signalling,

involved in breast tumour cell-endothelial interaction. Thereby, we show an alternative role for endothelial cells, supporting breast cancer spreading, independent of their vascular functions. Moreover, endothelial cells enhanced the migrative and invasive abilities of HER2 overexpressing breast cancer cells. Our data provide evidence that the tumour microenvironment, represented here by endothelial cells, directly affects cancer cells. With this study, we enhanced the understanding of tumour ECM and breast cancer microenvironments. Targeting ECM1 could lead to reduced tumour growth and metastasis dissemination.

Collectively, in this thesis, I identified non-coding RNAs and extracellular matrix proteins conveying cellular plasticity to breast epithelial cells and studied the underlying mechanisms causing cancer cell plasticity. I contributed to the exploration of the differences among epithelial cell line D492 and two cell lines with EMT phenotype D492M and D492HER2. I identified upregulated non-coding RNAs in both D492 and D492M. The results suggest the importance of both miRNAs and lncRNAs in a wide variety of processes and their contribution to the process of branching morphogenesis and EMT/MET by regulating gene expression. We identified non-coding RNAs from the DLK1-DIO3 locus, showed their correlation with mesenchymal genes and contribution to plasticity. Conversely, the identified MIR203a is an important player in the branching process and a contributor to epithelial integrity. Finally, we suggest that extracellular matrix proteins YKL-40 and ECM1 are candidates that might play a role in tumorigenicity.

Increased understanding of branching morphogenesis is essential not only to know how the breast gland develops but also to understand the aetiology of breast cancer.

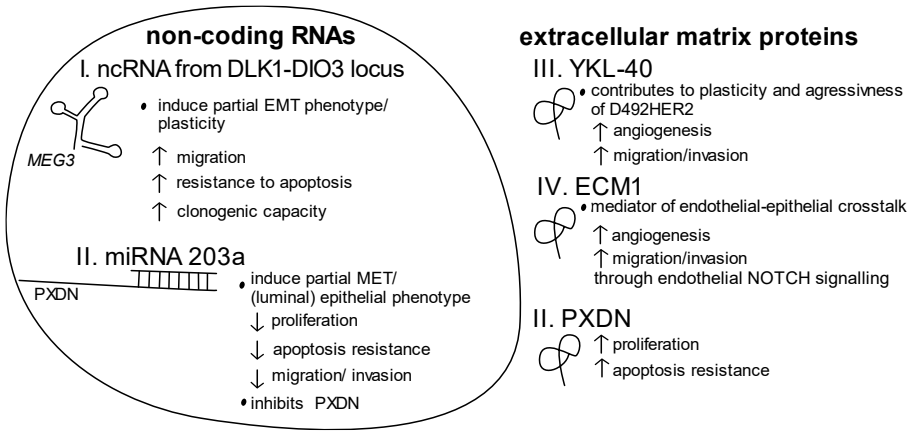

Figure 28. Graphical summary of results from the thesis.
The central part of the thesis is dedicated to ncRNA. Our results suggest that ncRNAs from the DLK1-DIO3 locus, with its marker *MEG3*, is a novel inducer of partial EMT in breast tissue through the functions such as increasing migration, resistance to apoptosis and clonogenic capacity. Conversely, the miRNA 203a induces partial MET and epithelial, particularly luminal, phenotype, through decreasing proliferation, increasing sensitivity to apoptosis and decreasing migration and invasion. Moreover, we identified its target gene peroxidasin. PXDN, on the other hand, enhances the proliferation and resistance to apoptosis. In this thesis, I, together with my co-workers, identified secreted extracellular matrix proteins peroxidasin (PXDN), YKL-40 and extracellular matrix protein 1 (ECM1) as potential inducers of cancer growth. YKL-40 may contribute to D492HER2 cell´s plasticity and aggressiveness by increasing the migratory, invasive and angiogenetic abilities of cancer cells. ECM1 is a mediator of epithelial-endothelial crosstalk with proangiogenic properties and inducing increased migration and invasion through endothelial Notch signalling.

8 References

Acerbi, I., Cassereau, L., Dean, I., Shi, Q., Au, A., Park, C., Chen, Y. Y., Liphardt, J., Hwang, E. S., & Weaver, V. M. (2015, Oct). Human breast cancer invasion and aggression correlates with ECM stiffening and immune cell infiltration. *Integr Biol (Camb), 7*(10), 1120-1134. https://doi.org/10.1039/c5ib00040h

Adriance, M. C., Inman, J. L., Petersen, O. W., & Bissell, M. J. (2005). Myoepithelial cells: good fences make good neighbors. *Breast Cancer Res, 7*(5), 190-197. https://doi.org/10.1186/bcr1286

Akil, A., Gutiérrez-García, A. K., Guenter, R., Rose, J. B., Beck, A. W., Chen, H., & Ren, B. (2021). Notch Signaling in Vascular Endothelial Cells, Angiogenesis, and Tumor Progression: An Update and Prospective. *Front Cell Dev Biol, 9*, 642352. https://doi.org/10.3389/fcell.2021.642352

Al-Hajj, M., Wicha, M. S., Benito-Hernandez, A., Morrison, S. J., & Clarke, M. F. (2003, Apr 1). Prospective identification of tumorigenic breast cancer cells. *Proc Natl Acad Sci U S A, 100*(7), 3983-3988. https://doi.org/10.1073/pnas.0530291100

Allinen, M., Beroukhim, R., Cai, L., Brennan, C., Lahti-Domenici, J., Huang, H., Porter, D., Hu, M., Chin, L., Richardson, A., Schnitt, S., Sellers, W. R., & Polyak, K. (2004, Jul). Molecular characterization of the tumor microenvironment in breast cancer. *Cancer Cell, 6*(1), 17-32. https://doi.org/10.1016/j.ccr.2004.06.010

Anders, S., Pyl, P. T., & Huber, W. (2015, Jan 15). HTSeq--a Python framework to work with high-throughput sequencing data. *Bioinformatics, 31*(2), 166-169. https://doi.org/10.1093/bioinformatics/btu638

Arendt, L. M., & Kuperwasser, C. (2015, Jun). Form and function: how estrogen and progesterone regulate the mammary epithelial hierarchy. *J Mammary Gland Biol Neoplasia, 20*(1-2), 9-25. https://doi.org/10.1007/s10911-015-9337-0

Armstrong, E. J., & Bischoff, J. (2004, Sep 3). Heart valve development: endothelial cell signaling and differentiation. *Circ Res, 95*(5), 459-470. https://doi.org/10.1161/01.RES.0000141146.95728.da

Barlow, D. P., & Bartolomei, M. S. (2014, Feb 1). Genomic imprinting in mammals. *Cold Spring Harb Perspect Biol, 6*(2). https://doi.org/10.1101/cshperspect.a018382

Batista, P. J., & Chang, H. Y. (2013, Mar 14). Long noncoding RNAs: cellular address codes in development and disease. *Cell, 152*(6), 1298-1307. https://doi.org/10.1016/j.cell.2013.02.012

Baulina, N., Osmak, G., Kiselev, I., Popova, E., Boyko, A., Kulakova, O., & Favorova, O. (2019, Feb 8). MiRNAs from DLK1-DIO3 Imprinted Locus at 14q32 are Associated with Multiple Sclerosis: Gender-Specific Expression and Regulation of Receptor Tyrosine Kinases Signaling. *Cells, 8*(2). https://doi.org/10.3390/cells8020133

Bellis, A. D., Bernabé, B. P., Weiss, M. S., Shin, S., Weng, S., Broadbelt, L. J., & Shea, L. D. (2013, Feb). Dynamic transcription factor activity profiling in 2D and 3D cell cultures. *Biotechnol Bioeng, 110*(2), 563-572. https://doi.org/10.1002/bit.24718

Ben-Jacob, E., Coffey, D. S., & Levine, H. (2012, Sep). Bacterial survival strategies suggest rethinking cancer cooperativity. *Trends Microbiol, 20*(9), 403-410. https://doi.org/10.1016/j.tim.2012.06.001

Benetatos, L., Dasoula, A., Hatzimichael, E., Georgiou, I., Syrrou, M., & Bourantas, K. L. (2008, Jun). Promoter hypermethylation of the MEG3 (DLK1/MEG3) imprinted gene in multiple myeloma. *Clin Lymphoma Myeloma, 8*(3), 171-175. https://doi.org/10.3816/CLM.2008.n.021

Bergers, G., & Song, S. (2005, Oct). The role of pericytes in blood-vessel formation and maintenance. *Neuro Oncol, 7*(4), 452-464. https://doi.org/10.1215/s1152851705000232

Bergthorsson, J. T., Magnusson, M. K., & Gudjonsson, T. (2013, Jun). Endothelial-rich microenvironment supports growth and branching morphogenesis of prostate epithelial cells. *Prostate, 73*(8), 884-896. https://doi.org/10.1002/pros.22634

Bhaskaran, M., Wang, Y., Zhang, H., Weng, T., Baviskar, P., Guo, Y., Gou, D., & Liu, L. (2009, May 13). MicroRNA-127 modulates fetal lung development. *Physiol Genomics, 37*(3), 268-278. https://doi.org/10.1152/physiolgenomics.90268.2008

Bhat, S. A., Ahmad, S. M., Mumtaz, P. T., Malik, A. A., Dar, M. A., Urwat, U., Shah, R. A., & Ganai, N. A. (2016, Oct). Long non-coding RNAs: Mechanism of action and functional utility. *Noncoding RNA Res, 1*(1), 43-50. https://doi.org/10.1016/j.ncrna.2016.11.002

Bhave, G., Cummings, C. F., Vanacore, R. M., Kumagai-Cresse, C., Ero-Tolliver, I. A., Rafi, M., Kang, J. S., Pedchenko, V., Fessler, L. I., Fessler, J. H., & Hudson, B. G. (2012, Sep). Peroxidasin forms sulfilimine chemical bonds using hypohalous acids in tissue genesis. *Nat Chem Biol, 8*(9), 784-790. https://doi.org/10.1038/nchembio.1038

Biggar, K. K., & Storey, K. B. (2015). Insight into post-transcriptional gene regulation: stress-responsive microRNAs and their role in the environmental stress survival of tolerant animals. *The Journal of Experimental Biology, 218*(9), 1281-1289. https://doi.org/10.1242/jeb.104828

Binabaj, M. M., Bahrami, A., Bahreyni, A., Shafiee, M., Rahmani, F., Khazaei, M., Soleimanpour, S., Ghorbani, E., Fiuji, H., Ferns, G. A., Ryzhikov, M., Avan, A., & Hassanian, S. M. (2018, Nov). The prognostic value of long noncoding RNA MEG3 expression in the survival of patients with cancer: A meta-analysis. *J Cell Biochem, 119*(11), 9583-9590. https://doi.org/10.1002/jcb.27276

Blick, T., Hugo, H., Widodo, E., Waltham, M., Pinto, C., Mani, S. A., Weinberg, R. A., Neve, R. M., Lenburg, M. E., & Thompson, E. W. (2010, Jun). Epithelial mesenchymal transition traits in human breast cancer cell lines parallel the CD44(hi/)CD24 (lo/-) stem cell phenotype in human breast cancer. *J Mammary Gland Biol Neoplasia, 15*(2), 235-252. https://doi.org/10.1007/s10911-010-9175-z

Bonnans, C., Chou, J., & Werb, Z. (2014, Dec). Remodelling the extracellular matrix in development and disease. *Nat Rev Mol Cell Biol, 15*(12), 786-801. https://doi.org/10.1038/nrm3904

Boyd, N. F., Li, Q., Melnichouk, O., Huszti, E., Martin, L. J., Gunasekara, A., Mawdsley, G., Yaffe, M. J., & Minkin, S. (2014). Evidence that breast

tissue stiffness is associated with risk of breast cancer. *PLoS One, 9*(7), e100937. https://doi.org/10.1371/journal.pone.0100937

Boyle, E. A., Andreasson, J. O. L., Chircus, L. M., Sternberg, S. H., Wu, M. J., Guegler, C. K., Doudna, J. A., & Greenleaf, W. J. (2017, May 23). High-throughput biochemical profiling reveals sequence determinants of dCas9 off-target binding and unbinding. *Proc Natl Acad Sci U S A, 114*(21), 5461-5466. https://doi.org/10.1073/pnas.1700557114

Brabletz, S., & Brabletz, T. (2010, Sep). The ZEB/miR-200 feedback loop--a motor of cellular plasticity in development and cancer? *EMBO Rep, 11*(9), 670-677. https://doi.org/10.1038/embor.2010.117

Brabletz, T., Jung, A., Reu, S., Porzner, M., Hlubek, F., Kunz-Schughart, L. A., Knuechel, R., & Kirchner, T. (2001, Aug 28). Variable beta-catenin expression in colorectal cancers indicates tumor progression driven by the tumor environment. *Proc Natl Acad Sci U S A, 98*(18), 10356-10361. https://doi.org/10.1073/pnas.171610498

Brabletz, T., Kalluri, R., Nieto, M. A., & Weinberg, R. A. (2018, Feb). EMT in cancer. *Nat Rev Cancer, 18*(2), 128-134. https://doi.org/10.1038/nrc.2017.118

Bremnes, R. M., Dønnem, T., Al-Saad, S., Al-Shibli, K., Andersen, S., Sirera, R., Camps, C., Marinez, I., & Busund, L. T. (2011, Jan). The role of tumor stroma in cancer progression and prognosis: emphasis on carcinoma-associated fibroblasts and non-small cell lung cancer. *J Thorac Oncol, 6*(1), 209-217. https://doi.org/10.1097/JTO.0b013e3181f8a1bd

Briem, E., Budkova, Z., Sigurdardottir, A. K., Hilmarsdottir, B., Kricker, J., Timp, W., Magnusson, M. K., Traustadottir, G. A., & Gudjonsson, T. (2019, Feb). MiR-203a is differentially expressed during branching morphogenesis and EMT in breast progenitor cells and is a repressor of peroxidasin. *Mech Dev, 155*, 34-47. https://doi.org/10.1016/j.mod.2018.11.002

Briem, E., Ingthorsson, S., Traustadottir, G. A., Hilmarsdottir, B., & Gudjonsson, T. (2019, Jan 25). Application of the D492 Cell Lines to Explore Breast Morphogenesis, EMT and Cancer Progression in 3D Culture. *J Mammary Gland Biol Neoplasia*. https://doi.org/10.1007/s10911-018-09424-w

Budkova, Z., Sigurdardottir, A. K., Briem, E., Bergthorsson, J. T., Sigurdsson, S., Magnusson, M. K., Traustadottir, G. A., Gudjonsson, T., & Hilmarsdottir, B. (2020). Expression of ncRNAs on the DLK1-DIO3 Locus Is Associated With Basal and Mesenchymal Phenotype in Breast Epithelial Progenitor Cells. *Front Cell Dev Biol, 8*, 461. https://doi.org/10.3389/fcell.2020.00461

Bullock, M. D., Sayan, A. E., Packham, G. K., & Mirnezami, A. H. (2012, Jan). MicroRNAs: critical regulators of epithelial to mesenchymal (EMT) and mesenchymal to epithelial transition (MET) in cancer progression. *Biol Cell, 104*(1), 3-12. https://doi.org/10.1111/boc.201100115

Bussard, K. M., Mutkus, L., Stumpf, K., Gomez-Manzano, C., & Marini, F. C. (2016, Aug 11). Tumor-associated stromal cells as key contributors to the tumor microenvironment. *Breast Cancer Res, 18*(1), 84. https://doi.org/10.1186/s13058-016-0740-2

Butcher, D. T., Alliston, T., & Weaver, V. M. (2009, Feb). A tense situation: forcing tumour progression. *Nat Rev Cancer, 9*(2), 108-122. https://doi.org/10.1038/nrc2544

Cao, Z., Livas, T., & Kyprianou, N. (2016). Anoikis and EMT: Lethal "Liaisons" during Cancer Progression. *Crit Rev Oncog, 21*(3-4), 155-168. https://doi.org/10.1615/CritRevOncog.2016016955

Carmeliet, P., & Jain, R. K. (2000, Sep 14). Angiogenesis in cancer and other diseases. *Nature, 407*(6801), 249-257. https://doi.org/10.1038/35025220

Carmeliet, P., & Jain, R. K. (2011, May 19). Molecular mechanisms and clinical applications of angiogenesis. *Nature, 473*(7347), 298-307. https://doi.org/10.1038/nature10144

Celia-Terrassa, T., Meca-Cortes, O., Mateo, F., Martinez de Paz, A., Rubio, N., Arnal-Estape, A., Ell, B. J., Bermudo, R., Diaz, A., Guerra-Rebollo, M., Lozano, J. J., Estaras, C., Ulloa, C., Alvarez-Simon, D., Mila, J., Vilella, R., Paciucci, R., Martinez-Balbas, M., de Herreros, A. G., Gomis, R. R., Kang, Y., Blanco, J., Fernandez, P. L., & Thomson, T. M. (2012, May). Epithelial-mesenchymal transition can suppress major attributes of human epithelial tumor-initiating cells. *J Clin Invest, 122*(5), 1849-1868. https://doi.org/10.1172/jci59218

Cojoc, M., Mäbert, K., Muders, M. H., & Dubrovska, A. (2015, Apr). A role for cancer stem cells in therapy resistance: cellular and molecular mechanisms. *Semin Cancer Biol, 31*, 16-27. https://doi.org/10.1016/j.semcancer.2014.06.004

Conklin, M. W., & Keely, P. J. (2012, May-Jun). Why the stroma matters in breast cancer: insights into breast cancer patient outcomes through the examination of stromal biomarkers. *Cell Adh Migr, 6*(3), 249-260. https://doi.org/10.4161/cam.20567

Costa, L. C., Leite, C. F., Cardoso, S. V., Loyola, A. M., Faria, P. R., Souza, P. E., & Horta, M. C. (2015, Mar-Apr). Expression of epithelial-mesenchymal transition markers at the invasive front of oral squamous cell carcinoma. *J Appl Oral Sci, 23*(2), 169-178. https://doi.org/10.1590/1678-775720140187

Cowell, C. F., Weigelt, B., Sakr, R. A., Ng, C. K., Hicks, J., King, T. A., & Reis-Filho, J. S. (2013, Oct). Progression from ductal carcinoma in situ to invasive breast cancer: revisited. *Mol Oncol, 7*(5), 859-869. https://doi.org/10.1016/j.molonc.2013.07.005

Creighton, C. J., Li, X., Landis, M., Dixon, J. M., Neumeister, V. M., Sjolund, A., Rimm, D. L., Wong, H., Rodriguez, A., Herschkowitz, J. I., Fan, C., Zhang, X., He, X., Pavlick, A., Gutierrez, M. C., Renshaw, L., Larionov, A. A., Faratian, D., Hilsenbeck, S. G., Perou, C. M., Lewis, M. T., Rosen, J. M., & Chang, J. C. (2009, Aug 18). Residual breast cancers after conventional therapy display mesenchymal as well as tumor-initiating features. *Proc Natl Acad Sci U S A, 106*(33), 13820-13825. https://doi.org/10.1073/pnas.0905718106

Cui, H. B., Ge, H. E., Wang, Y. S., & Bai, X. Y. (2018, Sep). MiR-208a enhances cell proliferation and invasion of gastric cancer by targeting SFRP1 and negatively regulating MEG3. *Int J Biochem Cell Biol, 102*, 31-39. https://doi.org/10.1016/j.biocel.2018.06.004

Cui, X., Yi, Q., Jing, X., Huang, Y., Tian, J., Long, C., Xiang, Z., Liu, J., Zhang, C., Tan, B., Li, Y., & Zhu, J. (2018). Mining Prognostic Significance of MEG3 in Human Breast Cancer Using Bioinformatics Analysis. *Cell Physiol Biochem, 50*(1), 41-51. https://doi.org/10.1159/000493956

Cummings, C. F., Pedchenko, V., Brown, K. L., Colon, S., Rafi, M., Jones-Paris, C., Pokydeshava, E., Liu, M., Pastor-Pareja, J. C., Stothers, C., Ero-Tolliver, I. A., McCall, A. S., Vanacore, R., Bhave, G., Santoro, S., Blackwell, T. S., Zent, R., Pozzi, A., & Hudson, B. G. (2016, May 23). Extracellular chloride signals collagen IV network assembly during basement membrane formation. *J Cell Biol, 213*(4), 479-494. https://doi.org/10.1083/jcb.201510065

da Rocha, S. T., Edwards, C. A., Ito, M., Ogata, T., & Ferguson-Smith, A. C. (2008, Jun). Genomic imprinting at the mammalian Dlk1-Dio3 domain. *Trends Genet, 24*(6), 306-316. https://doi.org/10.1016/j.tig.2008.03.011

De Palma, M., Biziato, D., & Petrova, T. V. (2017, Aug). Microenvironmental regulation of tumour angiogenesis. *Nat Rev Cancer, 17*(8), 457-474. https://doi.org/10.1038/nrc.2017.51

De Smet, F., Segura, I., De Bock, K., Hohensinner, P. J., & Carmeliet, P. (2009, May). Mechanisms of vessel branching: filopodia on endothelial tip cells lead the way. *Arterioscler Thromb Vasc Biol, 29*(5), 639-649. https://doi.org/10.1161/atvbaha.109.185165

Dean, M., Fojo, T., & Bates, S. (2005, Apr). Tumour stem cells and drug resistance. *Nat Rev Cancer, 5*(4), 275-284. https://doi.org/10.1038/nrc1590

DeCastro, A. J., Dunphy, K. A., Hutchinson, J., Balboni, A. L., Cherukuri, P., Jerry, D. J., & DiRenzo, J. (2013, Feb 28). MiR203 mediates subversion of stem cell properties during mammary epithelial differentiation via repression of DeltaNP63alpha and promotes mesenchymal-to-epithelial transition. *Cell Death Dis, 4*, e514. https://doi.org/10.1038/cddis.2013.37

Denton, A. E., Roberts, E. W., & Fearon, D. T. (2018). Stromal Cells in the Tumor Microenvironment. *Adv Exp Med Biol, 1060*, 99-114. https://doi.org/10.1007/978-3-319-78127-3_6

Deocesano-Pereira, C., Machado, R. A. C., De Jesus-Ferreira, H. C., Marchini, T., Pereira, T. F., Carreira, A. C. O., & Sogayar, M. C. (2019, Dec). Functional impact of the long non-coding RNA MEG3 deletion by CRISPR/Cas9 in the human triple negative metastatic Hs578T cancer

cell line. *Oncol Lett, 18*(6), 5941-5951. https://doi.org/10.3892/ol.2019.10969

Derrien, T., Johnson, R., Bussotti, G., Tanzer, A., Djebali, S., Tilgner, H., Guernec, G., Martin, D., Merkel, A., Knowles, D. G., Lagarde, J., Veeravalli, L., Ruan, X., Ruan, Y., Lassmann, T., Carninci, P., Brown, J. B., Lipovich, L., Gonzalez, J. M., Thomas, M., Davis, C. A., Shiekhattar, R., Gingeras, T. R., Hubbard, T. J., Notredame, C., Harrow, J., & Guigo, R. (2012, Sep). The GENCODE v7 catalog of human long noncoding RNAs: analysis of their gene structure, evolution, and expression. *Genome Res, 22*(9), 1775-1789. https://doi.org/10.1101/gr.132159.111

Di Gesualdo, F., Capaccioli, S., & Lulli, M. (2014, Nov 30). A pathophysiological view of the long non-coding RNA world. *Oncotarget, 5*(22), 10976-10996. https://doi.org/10.18632/oncotarget.2770

Dill, T. L., Carroll, A., Pinheiro, A., Gao, J., & Naya, F. J. (2020, Dec 9). The long noncoding RNA Meg3 regulates myoblast plasticity and muscle regeneration through epithelial-mesenchymal transition. *Development*. https://doi.org/10.1242/dev.194027

Dill, T. L., & Naya, F. J. (2018, Jul 10). A Hearty Dose of Noncoding RNAs: The Imprinted DLK1-DIO3 Locus in Cardiac Development and Disease. *J Cardiovasc Dev Dis, 5*(3). https://doi.org/10.3390/jcdd5030037

Ding, X., Park, S. I., McCauley, L. K., & Wang, C. Y. (2013, Apr 12). Signaling between transforming growth factor beta (TGF-beta) and transcription factor SNAI2 represses expression of microRNA miR-203 to promote epithelial-mesenchymal transition and tumor metastasis. *J Biol Chem, 288*(15), 10241-10253. https://doi.org/10.1074/jbc.M112.443655

Dobin, A., Davis, C. A., Schlesinger, F., Drenkow, J., Zaleski, C., Jha, S., Batut, P., Chaisson, M., & Gingeras, T. R. (2013, Jan 1). STAR: ultrafast universal RNA-seq aligner. *Bioinformatics, 29*(1), 15-21. https://doi.org/10.1093/bioinformatics/bts635

Dougan, J., Hawsawi, O., Burton, L. J., Edwards, G., Jones, K., Zou, J., Nagappan, P., Wang, G., Zhang, Q., Danaher, A., Bowen, N., Hinton, C., & Odero-Marah, V. A. (2019, Jun 21). Proteomics-Metabolomics

Combined Approach Identifies Peroxidasin as a Protector against Metabolic and Oxidative Stress in Prostate Cancer. *Int J Mol Sci, 20*(12). https://doi.org/10.3390/ijms20123046

Dufraine, J., Funahashi, Y., & Kitajewski, J. (2008, Sep 1). Notch signaling regulates tumor angiogenesis by diverse mechanisms. *Oncogene, 27*(38), 5132-5137. https://doi.org/10.1038/onc.2008.227

Eades, G., Zhang, Y. S., Li, Q. L., Xia, J. X., Yao, Y., & Zhou, Q. (2014, May 10). Long non-coding RNAs in stem cells and cancer. *World J Clin Oncol, 5*(2), 134-141. https://doi.org/10.5306/wjco.v5.i2.134

Edwards, C. A., & Ferguson-Smith, A. C. (2007, Jun). Mechanisms regulating imprinted genes in clusters. *Curr Opin Cell Biol, 19*(3), 281-289. https://doi.org/10.1016/j.ceb.2007.04.013

Eirew, P., Stingl, J., Raouf, A., Turashvili, G., Aparicio, S., Emerman, J. T., & Eaves, C. J. (2008, Dec). A method for quantifying normal human mammary epithelial stem cells with in vivo regenerative ability. *Nat Med, 14*(12), 1384-1389. https://doi.org/10.1038/nm.1791

Elenbaas, B., Spirio, L., Koerner, F., Fleming, M. D., Zimonjic, D. B., Donaher, J. L., Popescu, N. C., Hahn, W. C., & Weinberg, R. A. (2001, Jan 1). Human breast cancer cells generated by oncogenic transformation of primary mammary epithelial cells. *Genes Dev, 15*(1), 50-65. https://doi.org/10.1101/gad.828901

Elloumi, F., Hu, Z., Li, Y., Parker, J. S., Gulley, M. L., Amos, K. D., & Troester, M. A. (2011, Jun 30). Systematic bias in genomic classification due to contaminating non-neoplastic tissue in breast tumor samples. *BMC Med Genomics, 4*, 54. https://doi.org/10.1186/1755-8794-4-54

Erturk, K., Tas, F., Serilmez, M., Bilgin, E., & Yasasever, V. (2017, May 1). Clinical Significance of Serum Ykl-40 (Chitinase-3-Like-1 Protein) as a Biomarker in Melanoma: an Analysis of 112 Turkish Patients. *Asian Pac J Cancer Prev, 18*(5), 1383-1387. https://doi.org/10.22034/apjcp.2017.18.5.1383

Fata, J. E., Werb, Z., & Bissell, M. J. (2004). Regulation of mammary gland branching morphogenesis by the extracellular matrix and its remodeling enzymes. *Breast Cancer Res, 6*(1), 1-11. https://doi.org/10.1186/bcr634

Fedele, M., Cerchia, L., & Chiappetta, G. (2017, Sep 30). The Epithelial-to-Mesenchymal Transition in Breast Cancer: Focus on Basal-Like Carcinomas. *Cancers (Basel), 9*(10). https://doi.org/10.3390/cancers9100134

Ferraro, D. A., Patella, F., Zanivan, S., Donato, C., Aceto, N., Giannotta, M., Dejana, E., Diepenbruck, M., Christofori, G., & Buess, M. (2019, Apr 4). Endothelial cell-derived nidogen-1 inhibits migration of SK-BR-3 breast cancer cells. *BMC Cancer, 19*(1), 312. https://doi.org/10.1186/s12885-019-5521-8

Fico, A., Fiorenzano, A., Pascale, E., Patriarca, E. J., & Minchiotti, G. (2019, Apr). Long non-coding RNA in stem cell pluripotency and lineage commitment: functions and evolutionary conservation. *Cell Mol Life Sci, 76*(8), 1459-1471. https://doi.org/10.1007/s00018-018-3000-z

Fridriksdottir, A. J., Villadsen, R., Morsing, M., Klitgaard, M. C., Kim, J., Petersen, O. W., & Ronnov-Jessen, L. (2017, Nov 21). Proof of region-specific multipotent progenitors in human breast epithelia. *Proc Natl Acad Sci U S A, 114*(47), E10102-e10111. https://doi.org/10.1073/pnas.1714063114

Friedman, R. C., Farh, K. K., Burge, C. B., & Bartel, D. P. (2009, Jan). Most mammalian mRNAs are conserved targets of microRNAs. *Genome Res, 19*(1), 92-105. https://doi.org/10.1101/gr.082701.108

Gerhardt, H., Golding, M., Fruttiger, M., Ruhrberg, C., Lundkvist, A., Abramsson, A., Jeltsch, M., Mitchell, C., Alitalo, K., Shima, D., & Betsholtz, C. (2003, Jun 23). VEGF guides angiogenic sprouting utilizing endothelial tip cell filopodia. *J Cell Biol, 161*(6), 1163-1177. https://doi.org/10.1083/jcb.200302047

Ghajar, C. M., & Bissell, M. J. (2008, Dec). Extracellular matrix control of mammary gland morphogenesis and tumorigenesis: insights from imaging. *Histochem Cell Biol, 130*(6), 1105-1118. https://doi.org/10.1007/s00418-008-0537-1

Ghiabi, P., Jiang, J., Pasquier, J., Maleki, M., Abu-Kaoud, N., Halabi, N., Guerrouahen, B. S., Rafii, S., & Rafii, A. (2015, Jan 27). Breast cancer cells promote a notch-dependent mesenchymal phenotype in

endothelial cells participating to a pro-tumoral niche. *J Transl Med, 13*, 27. https://doi.org/10.1186/s12967-015-0386-3

Ghoncheh, M., Pournamdar, Z., & Salehiniya, H. (2016). Incidence and Mortality and Epidemiology of Breast Cancer in the World. *Asian Pac J Cancer Prev, 17*(S3), 43-46. https://doi.org/10.7314/apjcp.2016.17.s3.43

Gilbert, L. A., Horlbeck, M. A., Adamson, B., Villalta, J. E., Chen, Y., Whitehead, E. H., Guimaraes, C., Panning, B., Ploegh, H. L., Bassik, M. C., Qi, L. S., Kampmann, M., & Weissman, J. S. (2014, Oct 23). Genome-Scale CRISPR-Mediated Control of Gene Repression and Activation. *Cell, 159*(3), 647-661. https://doi.org/10.1016/j.cell.2014.09.029

Gillet, J. P., Calcagno, A. M., Varma, S., Marino, M., Green, L. J., Vora, M. I., Patel, C., Orina, J. N., Eliseeva, T. A., Singal, V., Padmanabhan, R., Davidson, B., Ganapathi, R., Sood, A. K., Rueda, B. R., Ambudkar, S. V., & Gottesman, M. M. (2011, Nov 15). Redefining the relevance of established cancer cell lines to the study of mechanisms of clinical anti-cancer drug resistance. *Proc Natl Acad Sci U S A, 108*(46), 18708-18713. https://doi.org/10.1073/pnas.1111840108

Ginestier, C., Hur, M. H., Charafe-Jauffret, E., Monville, F., Dutcher, J., Brown, M., Jacquemier, J., Viens, P., Kleer, C. G., Liu, S., Schott, A., Hayes, D., Birnbaum, D., Wicha, M. S., & Dontu, G. (2007, Nov). ALDH1 is a marker of normal and malignant human mammary stem cells and a predictor of poor clinical outcome. *Cell Stem Cell, 1*(5), 555-567. https://doi.org/10.1016/j.stem.2007.08.014

Gokey, J. J., Snowball, J., Sridharan, A., Speth, J. P., Black, K. E., Hariri, L. P., Perl, A. T., Xu, Y., & Whitsett, J. A. (2018, Sep 6). MEG3 is increased in idiopathic pulmonary fibrosis and regulates epithelial cell differentiation. *JCI Insight, 3*(17). https://doi.org/10.1172/jci.insight.122490

Goncharov, N. V., Nadeev, A. D., Jenkins, R. O., & Avdonin, P. V. (2017). Markers and Biomarkers of Endothelium: When Something Is Rotten in the State. *Oxid Med Cell Longev, 2017*, 9759735. https://doi.org/10.1155/2017/9759735

Greaves, M., & Maley, C. C. (2012, Jan 18). Clonal evolution in cancer. *Nature, 481*(7381), 306-313. https://doi.org/10.1038/nature10762

Gregory, P. A., Bert, A. G., Paterson, E. L., Barry, S. C., Tsykin, A., Farshid, G., Vadas, M. A., Khew-Goodall, Y., & Goodall, G. J. (2008, May). The miR-200 family and miR-205 regulate epithelial to mesenchymal transition by targeting ZEB1 and SIP1. *Nat Cell Biol, 10*(5), 593-601. https://doi.org/10.1038/ncb1722

Gridley, T. (2010). Notch signaling in the vasculature. *Curr Top Dev Biol, 92*, 277-309. https://doi.org/10.1016/s0070-2153(10)92009-7

Grosse-Wilde, A., Fouquier d'Hérouël, A., McIntosh, E., Ertaylan, G., Skupin, A., Kuestner, R. E., del Sol, A., Walters, K. A., & Huang, S. (2015). Stemness of the hybrid Epithelial/Mesenchymal State in Breast Cancer and Its Association with Poor Survival. *PLoS One, 10*(5), e0126522. https://doi.org/10.1371/journal.pone.0126522

Gubina, E., Ruiz-Hidalgo, M. J., Baladrón, V., & Laborda, J. (1999). Assignment of DLK1 to human chromosome band 14q32 by in situ hybridization. *Cytogenet Cell Genet, 84*(3-4), 206-207. https://doi.org/10.1159/000015259

Gubina, E., Ruiz-Hidalgo, M. J., Baladrón, V., & Laborda, J. (2000). Assignment of dlk (Dlk1) to mouse chromosome band 12E-F1 by in situ hybridization. *Cytogenet Cell Genet, 88*(3-4), 322-323. https://doi.org/10.1159/000015519

Gudjonsson, T., Adriance, M. C., Sternlicht, M. D., Petersen, O. W., & Bissell, M. J. (2005, Jul). Myoepithelial cells: their origin and function in breast morphogenesis and neoplasia. *J Mammary Gland Biol Neoplasia, 10*(3), 261-272. https://doi.org/10.1007/s10911-005-9586-4

Gudjonsson, T., Rønnov-Jessen, L., Villadsen, R., Rank, F., Bissell, M. J., & Petersen, O. W. (2002, Jan 1). Normal and tumor-derived myoepithelial cells differ in their ability to interact with luminal breast epithelial cells for polarity and basement membrane deposition. *J Cell Sci, 115*(Pt 1), 39-50.

Gudjonsson, T., Villadsen, R., Nielsen, H. L., Ronnov-Jessen, L., Bissell, M. J., & Petersen, O. W. (2002, Mar 15). Isolation, immortalization, and characterization of a human breast epithelial cell line with stem cell

properties. *Genes Dev, 16*(6), 693-706. https://doi.org/10.1101/gad.952602

Gururajan, M., Josson, S., Chu, G. C., Lu, C. L., Lu, Y. T., Haga, C. L., Zhau, H. E., Liu, C., Lichterman, J., Duan, P., Posadas, E. M., & Chung, L. W. (2014, Dec 15). miR-154* and miR-379 in the DLK1-DIO3 microRNA mega-cluster regulate epithelial to mesenchymal transition and bone metastasis of prostate cancer. *Clin Cancer Res, 20*(24), 6559-6569. https://doi.org/10.1158/1078-0432.Ccr-14-1784

Halldorsson, S., Rohatgi, N., Magnusdottir, M., Choudhary, K. S., Gudjonsson, T., Knutsen, E., Barkovskaya, A., Hilmarsdottir, B., Perander, M., Maelandsmo, G. M., Gudmundsson, S., & Rolfsson, O. (2017, Jun 28). Metabolic re-wiring of isogenic breast epithelial cell lines following epithelial to mesenchymal transition. *Cancer Lett, 396*, 117-129. https://doi.org/10.1016/j.canlet.2017.03.019

Hammond, S. L., Ham, R. G., & Stampfer, M. R. (1984, Sep). Serum-free growth of human mammary epithelial cells: rapid clonal growth in defined medium and extended serial passage with pituitary extract. *Proc Natl Acad Sci U S A, 81*(17), 5435-5439. https://doi.org/10.1073/pnas.81.17.5435

Han, Z., Ni, J., Smits, P., Underhill, C. B., Xie, B., Chen, Y., Liu, N., Tylzanowski, P., Parmelee, D., Feng, P., Ding, I., Gao, F., Gentz, R., Huylebroeck, D., Merregaert, J., & Zhang, L. (2001, Apr). Extracellular matrix protein 1 (ECM1) has angiogenic properties and is expressed by breast tumor cells. *Faseb j, 15*(6), 988-994. https://doi.org/10.1096/fj.99-0934com

Hanahan, D., & Weinberg, R. A. (2011, Mar 4). Hallmarks of cancer: the next generation. *Cell, 144*(5), 646-674. https://doi.org/10.1016/j.cell.2011.02.013

Hayashi, M., Yamamoto, Y., Ibusuki, M., Fujiwara, S., Yamamoto, S., Tomita, S., Nakano, M., Murakami, K., Iyama, K., & Iwase, H. (2012, Sep). Evaluation of tumor stiffness by elastography is predictive for pathologic complete response to neoadjuvant chemotherapy in patients with breast cancer. *Ann Surg Oncol, 19*(9), 3042-3049. https://doi.org/10.1245/s10434-012-2343-1

He, C., Yang, W., Yang, J., Ding, J., Li, S., Wu, H., Zhou, F., Jiang, Y., Teng, L., & Yang, J. (2017, Jun). Long Noncoding RNA MEG3 Negatively Regulates Proliferation and Angiogenesis in Vascular Endothelial Cells. *DNA Cell Biol, 36*(6), 475-481. https://doi.org/10.1089/dna.2017.3682

Hermann, P. C., Huber, S. L., Herrler, T., Aicher, A., Ellwart, J. W., Guba, M., Bruns, C. J., & Heeschen, C. (2007, Sep 13). Distinct populations of cancer stem cells determine tumor growth and metastatic activity in human pancreatic cancer. *Cell Stem Cell, 1*(3), 313-323. https://doi.org/10.1016/j.stem.2007.06.002

Hida, K., Maishi, N., Annan, D. A., & Hida, Y. (2018, Apr 24). Contribution of Tumor Endothelial Cells in Cancer Progression. *Int J Mol Sci, 19*(5). https://doi.org/10.3390/ijms19051272

Hilmarsdottir, B., Briem, E., Sigurdsson, V., Franzdottir, S. R., Ringner, M., Arason, A. J., Bergthorsson, J. T., Magnusson, M. K., & Gudjonsson, T. (2015, Jul 15). MicroRNA-200c-141 and Np63 are required for breast epithelial differentiation and branching morphogenesis. *Dev Biol, 403*(2), 150-161. https://doi.org/10.1016/j.ydbio.2015.05.007

Hon, C. C., Ramilowski, J. A., Harshbarger, J., Bertin, N., Rackham, O. J., Gough, J., Denisenko, E., Schmeier, S., Poulsen, T. M., Severin, J., Lizio, M., Kawaji, H., Kasukawa, T., Itoh, M., Burroughs, A. M., Noma, S., Djebali, S., Alam, T., Medvedeva, Y. A., Testa, A. C., Lipovich, L., Yip, C. W., Abugessaisa, I., Mendez, M., Hasegawa, A., Tang, D., Lassmann, T., Heutink, P., Babina, M., Wells, C. A., Kojima, S., Nakamura, Y., Suzuki, H., Daub, C. O., de Hoon, M. J., Arner, E., Hayashizaki, Y., Carninci, P., & Forrest, A. R. (2017, Mar 9). An atlas of human long non-coding RNAs with accurate 5' ends. *Nature, 543*(7644), 199-204. https://doi.org/10.1038/nature21374

Huang, S. K., Luo, Q., Peng, H., Li, J., Zhao, M., Wang, J., Gu, Y. Y., Li, Y., Yuan, P., Zhao, G. H., & Huang, C. Z. (2018, Apr 23). A Panel of Serum Noncoding RNAs for the Diagnosis and Monitoring of Response to Therapy in Patients with Breast Cancer. *Med Sci Monit, 24*, 2476-2488. https://doi.org/10.12659/msm.909453

Huang, W., Wu, Y., Cheng, D., & He, Z. (2020, Feb). Mechanism of epithelialmesenchymal transition inhibited by miR203 in nonsmall cell

lung cancer. *Oncol Rep, 43*(2), 437-446. https://doi.org/10.3892/or.2019.7433

Hubé, F., & Francastel, C. (2018). Coding and Non-coding RNAs, the Frontier Has Never Been So Blurred. *Front Genet, 9*, 140. https://doi.org/10.3389/fgene.2018.00140

Hynes, R. O., & Naba, A. (2012, Jan 1). Overview of the matrisome--an inventory of extracellular matrix constituents and functions. *Cold Spring Harb Perspect Biol, 4*(1), a004903. https://doi.org/10.1101/cshperspect.a004903

Chak, W. P., Lung, R. W., Tong, J. H., Chan, S. Y., Lun, S. W., Tsao, S. W., Lo, K. W., & To, K. F. (2017, Mar). Downregulation of long non-coding RNA MEG3 in nasopharyngeal carcinoma. *Mol Carcinog, 56*(3), 1041-1054. https://doi.org/10.1002/mc.22569

Chakrabarti, R., Hwang, J., Andres Blanco, M., Wei, Y., Lukačišin, M., Romano, R. A., Smalley, K., Liu, S., Yang, Q., Ibrahim, T., Mercatali, L., Amadori, D., Haffty, B. G., Sinha, S., & Kang, Y. (2012, Nov). Elf5 inhibits the epithelial-mesenchymal transition in mammary gland development and breast cancer metastasis by transcriptionally repressing Snail2. *Nat Cell Biol, 14*(11), 1212-1222. https://doi.org/10.1038/ncb2607

Chang, C. J., Chao, C. H., Xia, W., Yang, J. Y., Xiong, Y., Li, C. W., Yu, W. H., Rehman, S. K., Hsu, J. L., Lee, H. H., Liu, M., Chen, C. T., Yu, D., & Hung, M. C. (2011, Mar). p53 regulates epithelial-mesenchymal transition and stem cell properties through modulating miRNAs. *Nat Cell Biol, 13*(3), 317-323. https://doi.org/10.1038/ncb2173

Chang, J. M., Park, I. A., Lee, S. H., Kim, W. H., Bae, M. S., Koo, H. R., Yi, A., Kim, S. J., Cho, N., & Moon, W. K. (2013, Sep). Stiffness of tumours measured by shear-wave elastography correlated with subtypes of breast cancer. *Eur Radiol, 23*(9), 2450-2458. https://doi.org/10.1007/s00330-013-2866-2

Chappell, J. C., Wiley, D. M., & Bautch, V. L. (2011, Dec). Regulation of blood vessel sprouting. *Semin Cell Dev Biol, 22*(9), 1005-1011. https://doi.org/10.1016/j.semcdb.2011.10.006

Chen, P. Y., Hsieh, P. L., Peng, C. Y., Liao, Y. W., Yu, C. H., & Yu, C. C. (2020, Oct 2). LncRNA MEG3 inhibits self-renewal and invasion abilities of oral cancer stem cells by sponging miR-421. *J Formos Med Assoc*. https://doi.org/10.1016/j.jfma.2020.09.006

Chen, X., & Song, E. (2019, Feb). Turning foes to friends: targeting cancer-associated fibroblasts. *Nat Rev Drug Discov, 18*(2), 99-115. https://doi.org/10.1038/s41573-018-0004-1

Ingthorsson, S., Andersen, K., Hilmarsdottir, B., Maelandsmo, G. M., Magnusson, M. K., & Gudjonsson, T. (2016, Aug 11). HER2 induced EMT and tumorigenicity in breast epithelial progenitor cells is inhibited by coexpression of EGFR. *Oncogene, 35*(32), 4244-4255. https://doi.org/10.1038/onc.2015.489

Ingthorsson, S., Briem, E., Bergthorsson, J. T., & Gudjonsson, T. (2016, Dec). Epithelial Plasticity During Human Breast Morphogenesis and Cancer Progression. *J Mammary Gland Biol Neoplasia, 21*(3-4), 139-148. https://doi.org/10.1007/s10911-016-9366-3

Ingthorsson, S., Sigurdsson, V., Fridriksdottir, A., Jr., Jonasson, J. G., Kjartansson, J., Magnusson, M. K., & Gudjonsson, T. (2010, Jul 7). Endothelial cells stimulate growth of normal and cancerous breast epithelial cells in 3D culture. *BMC Res Notes, 3*, 184. https://doi.org/10.1186/1756-0500-3-184

Insua-Rodríguez, J., & Oskarsson, T. (2016, Feb 1). The extracellular matrix in breast cancer. *Adv Drug Deliv Rev, 97*, 41-55. https://doi.org/10.1016/j.addr.2015.12.017

An integrated encyclopedia of DNA elements in the human genome. (2012, Sep 6). *Nature, 489*(7414), 57-74. https://doi.org/10.1038/nature11247

Ioannides, Y., Lokulo-Sodipe, K., Mackay, D. J., Davies, J. H., & Temple, I. K. (2014, Aug). Temple syndrome: improving the recognition of an underdiagnosed chromosome 14 imprinting disorder: an analysis of 51 published cases. *J Med Genet, 51*(8), 495-501. https://doi.org/10.1136/jmedgenet-2014-102396

Iso, T., Hamamori, Y., & Kedes, L. (2003, Apr 1). Notch signaling in vascular development. *Arterioscler Thromb Vasc Biol, 23*(4), 543-553. https://doi.org/10.1161/01.Atv.0000060892.81529.8f

Jefri, M., Huang, Y. N., Huang, W. C., Tai, C. S., & Chen, W. L. (2015, Aug 15). YKL-40 regulated epithelial-mesenchymal transition and migration/invasion enhancement in non-small cell lung cancer. *BMC Cancer, 15*, 590. https://doi.org/10.1186/s12885-015-1592-3

Jensen, B. V., Johansen, J. S., & Price, P. A. (2003, Oct 1). High levels of serum HER-2/neu and YKL-40 independently reflect aggressiveness of metastatic breast cancer. *Clin Cancer Res, 9*(12), 4423-4434.

Jin, L., Cai, Q., Wang, S., Wang, S., Mondal, T., Wang, J., & Quan, Z. (2018, Oct 3). Long noncoding RNA MEG3 regulates LATS2 by promoting the ubiquitination of EZH2 and inhibits proliferation and invasion in gallbladder cancer. *Cell Death Dis, 9*(10), 1017. https://doi.org/10.1038/s41419-018-1064-1

Johansen, J. S., Jensen, B. V., Roslind, A., & Price, P. A. (2007, Feb). Is YKL-40 a new therapeutic target in cancer? *Expert Opin Ther Targets, 11*(2), 219-234. https://doi.org/10.1517/14728222.11.2.219

Jolly, M. K., Boareto, M., Huang, B., Jia, D., Lu, M., Ben-Jacob, E., Onuchic, J. N., & Levine, H. (2015). Implications of the Hybrid Epithelial/Mesenchymal Phenotype in Metastasis. *Front Oncol, 5*, 155. https://doi.org/10.3389/fonc.2015.00155

Jordan, N. V., Johnson, G. L., & Abell, A. N. (2011, Sep 1). Tracking the intermediate stages of epithelial-mesenchymal transition in epithelial stem cells and cancer. *Cell Cycle, 10*(17), 2865-2873. https://doi.org/10.4161/cc.10.17.17188

Junttila, M. R., & de Sauvage, F. J. (2013, Sep 19). Influence of tumour micro-environment heterogeneity on therapeutic response. *Nature, 501*(7467), 346-354. https://doi.org/10.1038/nature12626

Kadota, K., Ye, J., Nakai, Y., Terada, T., & Shimizu, K. (2006, Jun 12). ROKU: a novel method for identification of tissue-specific genes. *BMC Bioinformatics, 7*, 294. https://doi.org/10.1186/1471-2105-7-294

Kagami, M., O'Sullivan, M. J., Green, A. J., Watabe, Y., Arisaka, O., Masawa, N., Matsuoka, K., Fukami, M., Matsubara, K., Kato, F., Ferguson-Smith, A. C., & Ogata, T. (2010, Jun 17). The IG-DMR and the MEG3-DMR at human chromosome 14q32.2: hierarchical interaction and distinct functional properties as imprinting control centers. *PLoS Genet, 6*(6), e1000992. https://doi.org/10.1371/journal.pgen.1000992

Kalluri, R., & Zeisberg, M. (2006, May). Fibroblasts in cancer. *Nat Rev Cancer, 6*(5), 392-401. https://doi.org/10.1038/nrc1877

Kaneko, S., Bonasio, R., Saldana-Meyer, R., Yoshida, T., Son, J., Nishino, K., Umezawa, A., & Reinberg, D. (2014, Jan 23). Interactions between JARID2 and noncoding RNAs regulate PRC2 recruitment to chromatin. *Mol Cell, 53*(2), 290-300. https://doi.org/10.1016/j.molcel.2013.11.012

Kaneko, S., Bonasio, R., Saldaña-Meyer, R., Yoshida, T., Son, J., Nishino, K., Umezawa, A., & Reinberg, D. (2014, Jan 23). Interactions between JARID2 and noncoding RNAs regulate PRC2 recruitment to chromatin. *Mol Cell, 53*(2), 290-300. https://doi.org/10.1016/j.molcel.2013.11.012

Kang, L., Wang, J., Zhang, Y., Kou, Z., & Gao, S. (2009, Aug 7). iPS cells can support full-term development of tetraploid blastocyst-complemented embryos. *Cell Stem Cell, 5*(2), 135-138. https://doi.org/10.1016/j.stem.2009.07.001

Kastrup, J. (2012, May). Can YKL-40 be a new inflammatory biomarker in cardiovascular disease? *Immunobiology, 217*(5), 483-491. https://doi.org/10.1016/j.imbio.2011.04.007

Kim, H. Y., & Nelson, C. M. (2012, Apr-Jun). Extracellular matrix and cytoskeletal dynamics during branching morphogenesis. *Organogenesis, 8*(2), 56-64. https://doi.org/10.4161/org.19813

Kim, S. J., Im, Y. H., Markowitz, S. D., & Bang, Y. J. (2000, Mar-Jun). Molecular mechanisms of inactivation of TGF-beta receptors during carcinogenesis. *Cytokine Growth Factor Rev, 11*(1-2), 159-168.

Kleinman, H. K., Philp, D., & Hoffman, M. P. (2003, Oct). Role of the extracellular matrix in morphogenesis. *Curr Opin Biotechnol, 14*(5), 526-532. https://doi.org/10.1016/j.copbio.2003.08.002

Kopp, F., & Mendell, J. T. (2018, Jan 25). Functional Classification and Experimental Dissection of Long Noncoding RNAs. *Cell, 172*(3), 393-407. https://doi.org/10.1016/j.cell.2018.01.011

Kovacic, J. C., Dimmeler, S., Harvey, R. P., Finkel, T., Aikawa, E., Krenning, G., & Baker, A. H. (2019, Jan 22). Endothelial to Mesenchymal Transition in Cardiovascular Disease: JACC State-of-the-Art Review. *J Am Coll Cardiol, 73*(2), 190-209. https://doi.org/10.1016/j.jacc.2018.09.089

Krebsbach, P. H., & Villa-Diaz, L. G. (2017, Aug 1). The Role of Integrin α6 (CD49f) in Stem Cells: More than a Conserved Biomarker. *Stem Cells Dev, 26*(15), 1090-1099. https://doi.org/10.1089/scd.2016.0319

Kuo, C. C., Hanzelmann, S., Senturk Cetin, N., Frank, S., Zajzon, B., Derks, J. P., Akhade, V. S., Ahuja, G., Kanduri, C., Grummt, I., Kurian, L., & Costa, I. G. (2019, Apr 8). Detection of RNA-DNA binding sites in long noncoding RNAs. *Nucleic Acids Res, 47*(6), e32. https://doi.org/10.1093/nar/gkz037

Kzhyshkowska, J., Gratchev, A., & Goerdt, S. (2007, May 3). Human chitinases and chitinase-like proteins as indicators for inflammation and cancer. *Biomark Insights, 2*, 128-146.

Lai, H. T., Tseng, W. K., Huang, S. W., Chao, T. C., & Su, Y. (2020, Mar). MicroRNA-203 diminishes the stemness of human colon cancer cells by suppressing GATA6 expression. *J Cell Physiol, 235*(3), 2866-2880. https://doi.org/10.1002/jcp.29192

Lal, G., Hashimi, S., Smith, B. J., Lynch, C. F., Zhang, L., Robinson, R. A., & Weigel, R. J. (2009, Aug). Extracellular matrix 1 (ECM1) expression is a novel prognostic marker for poor long-term survival in breast cancer: a Hospital-based Cohort Study in Iowa. *Ann Surg Oncol, 16*(8), 2280-2287. https://doi.org/10.1245/s10434-009-0533-2

Lamouille, S., Xu, J., & Derynck, R. (2014, Mar). Molecular mechanisms of epithelial-mesenchymal transition. *Nat Rev Mol Cell Biol, 15*(3), 178-196. https://doi.org/10.1038/nrm3758

Lander, E. S. (2011, Feb 10). Initial impact of the sequencing of the human genome. *Nature, 470*(7333), 187-197. https://doi.org/10.1038/nature09792

Lanigan, F., O'Connor, D., Martin, F., & Gallagher, W. M. (2007, Dec). Molecular links between mammary gland development and breast cancer. *Cell Mol Life Sci, 64*(24), 3159-3184. https://doi.org/10.1007/s00018-007-7386-2

Le, L. T., Cazares, O., Mouw, J. K., Chatterjee, S., Macias, H., Moran, A., Ramos, J., Keely, P. J., Weaver, V. M., & Hinck, L. (2016, Mar 14). Loss of miR-203 regulates cell shape and matrix adhesion through ROBO1/Rac/FAK in response to stiffness. *J Cell Biol, 212*(6), 707-719. https://doi.org/10.1083/jcb.201507054

Lebrun, J. J. (2012). The Dual Role of TGFbeta in Human Cancer: From Tumor Suppression to Cancer Metastasis. *ISRN Mol Biol, 2012*, 381428. https://doi.org/10.5402/2012/381428

Lee, C. G., Hartl, D., Lee, G. R., Koller, B., Matsuura, H., Da Silva, C. A., Sohn, M. H., Cohn, L., Homer, R. J., Kozhich, A. A., Humbles, A., Kearley, J., Coyle, A., Chupp, G., Reed, J., Flavell, R. A., & Elias, J. A. (2009, May 11). Role of breast regression protein 39 (BRP-39)/chitinase 3-like-1 in Th2 and IL-13-induced tissue responses and apoptosis. *J Exp Med, 206*(5), 1149-1166. https://doi.org/10.1084/jem.20081271

Lee, K. M., Nam, K., Oh, S., Lim, J., Kim, Y. P., Lee, J. W., Yu, J. H., Ahn, S. H., Kim, S. B., Noh, D. Y., Lee, T., & Shin, I. (2014, Dec 11). Extracellular matrix protein 1 regulates cell proliferation and trastuzumab resistance through activation of epidermal growth factor signaling. *Breast Cancer Res, 16*(6), 479. https://doi.org/10.1186/s13058-014-0479-6

Levental, K. R., Yu, H., Kass, L., Lakins, J. N., Egeblad, M., Erler, J. T., Fong, S. F., Csiszar, K., Giaccia, A., Weninger, W., Yamauchi, M., Gasser, D. L., & Weaver, V. M. (2009, Nov 25). Matrix crosslinking forces tumor progression by enhancing integrin signaling. *Cell, 139*(5), 891-906. https://doi.org/10.1016/j.cell.2009.10.027

Lewis, C. E., & Pollard, J. W. (2006, Jan 15). Distinct role of macrophages in different tumor microenvironments. *Cancer Res, 66*(2), 605-612. https://doi.org/10.1158/0008-5472.Can-05-4005

Li, G., Liu, Y., Meng, F., Xia, Z., Wu, X., Fang, Y., Zhang, C., Zhang, Y., & Liu, D. (2019, Oct). LncRNA MEG3 inhibits rheumatoid arthritis through miR-141 and inactivation of AKT/mTOR signalling pathway. *J Cell Mol Med, 23*(10), 7116-7120. https://doi.org/10.1111/jcmm.14591

Li, H., Li, B., Zhu, D., Xie, H., Du, C., Xia, Y., & Tang, W. (2017, Sep 19). Downregulation of lncRNA MEG3 and miR-770-5p inhibit cell migration and proliferation in Hirschsprung's disease. *Oncotarget, 8*(41), 69722-69730. https://doi.org/10.18632/oncotarget.19207

Li, H., Wang, J., Lv, S., Zhang, Y., Zhang, C., Lige, B., Dan, S., & Sun, Y. (2019, Jun 18). Long noncoding RNA MEG3 plays a promoting role in the proliferation, invasion, and angiogenesis of lung adenocarcinoma cells through the AKT pathway. *J Cell Biochem*. https://doi.org/10.1002/jcb.28895

Li, J., Bian, E. B., He, X. J., Ma, C. C., Zong, G., Wang, H. L., & Zhao, B. (2016, Feb). Epigenetic repression of long non-coding RNA MEG3 mediated by DNMT1 represses the p53 pathway in gliomas. *Int J Oncol, 48*(2), 723-733. https://doi.org/10.3892/ijo.2015.3285

Li, W., & Kang, Y. (2016, Feb). Probing the Fifty Shades of EMT in Metastasis. *Trends Cancer, 2*(2), 65-67. https://doi.org/10.1016/j.trecan.2016.01.001

Lin, S. P., Youngson, N., Takada, S., Seitz, H., Reik, W., Paulsen, M., Cavaille, J., & Ferguson-Smith, A. C. (2003, Sep). Asymmetric regulation of imprinting on the maternal and paternal chromosomes at the Dlk1-Gtl2 imprinted cluster on mouse chromosome 12. *Nat Genet, 35*(1), 97-102. https://doi.org/10.1038/ng1233

Liu, H., Ye, D., Chen, A., Tan, D., Zhang, W., Jiang, W., Wang, M., & Zhang, X. (2019, Jun 26). A pilot study of new promising non-coding RNA diagnostic biomarkers for early-stage colorectal cancers. *Clin Chem Lab Med, 57*(7), 1073-1083. https://doi.org/10.1515/cclm-2019-0052

Liu, K., Newbury, P. A., Glicksberg, B. S., Zeng, W. Z. D., Paithankar, S., Andrechek, E. R., & Chen, B. (2019, May 15). Evaluating cell lines as models for metastatic breast cancer through integrative analysis of genomic data. *Nat Commun, 10*(1), 2138. https://doi.org/10.1038/s41467-019-10148-6

Liu, L., Luo, G. Z., Yang, W., Zhao, X., Zheng, Q., Lv, Z., Li, W., Wu, H. J., Wang, L., Wang, X. J., & Zhou, Q. (2010, Jun 18). Activation of the imprinted Dlk1-Dio3 region correlates with pluripotency levels of mouse stem cells. *J Biol Chem, 285*(25), 19483-19490. https://doi.org/10.1074/jbc.M110.131995

Liu, X., Zhang, Y., Zhu, Z., Ha, M., & Wang, Y. (2014, Aug). Elevated pretreatment serum concentration of YKL-40: an independent prognostic biomarker for poor survival in patients with colorectal cancer. *Med Oncol, 31*(8), 85. https://doi.org/10.1007/s12032-014-0085-6

Love, M. I., Huber, W., & Anders, S. (2014). Moderated estimation of fold change and dispersion for RNA-seq data with DESeq2. *Genome Biol, 15*(12), 550. https://doi.org/10.1186/s13059-014-0550-8

Lu, M., Jolly, M. K., Levine, H., Onuchic, J. N., & Ben-Jacob, E. (2013, Nov 5). MicroRNA-based regulation of epithelial-hybrid-mesenchymal fate determination. *Proc Natl Acad Sci U S A, 110*(45), 18144-18149. https://doi.org/10.1073/pnas.1318192110

Lu, P., Sternlicht, M. D., & Werb, Z. (2006, Oct). Comparative mechanisms of branching morphogenesis in diverse systems. *J Mammary Gland Biol Neoplasia, 11*(3-4), 213-228. https://doi.org/10.1007/s10911-006-9027-z

Ma, L., Wang, F., Du, C., Zhang, Z., Guo, H., Xie, X., Gao, H., Zhuang, Y., Kornmann, M., Gao, H., Tian, X., & Yang, Y. (2018, Mar). Long non-coding RNA MEG3 functions as a tumour suppressor and has prognostic predictive value in human pancreatic cancer. *Oncol Rep, 39*(3), 1132-1140. https://doi.org/10.3892/or.2018.6178

Macfarlane, L. A., & Murphy, P. R. (2010, Nov). MicroRNA: Biogenesis, Function and Role in Cancer. *Curr Genomics, 11*(7), 537-561. https://doi.org/10.2174/138920210793175895

Makarem, M., Kannan, N., Nguyen, L. V., Knapp, D. J., Balani, S., Prater, M. D., Stingl, J., Raouf, A., Nemirovsky, O., Eirew, P., & Eaves, C. J. (2013). Developmental changes in the in vitro activated regenerative activity of primitive mammary epithelial cells. *PLoS Biol, 11*(8), e1001630. https://doi.org/10.1371/journal.pbio.1001630

Malinda, K. M., Ponce, L., Kleinman, H. K., Shackelton, L. M., & Millis, A. J. (1999, Jul 10). Gp38k, a protein synthesized by vascular smooth muscle cells, stimulates directional migration of human umbilical vein endothelial cells. *Exp Cell Res, 250*(1), 168-173. https://doi.org/10.1006/excr.1999.4511

Mani, S. A., Guo, W., Liao, M. J., Eaton, E. N., Ayyanan, A., Zhou, A. Y., Brooks, M., Reinhard, F., Zhang, C. C., Shipitsin, M., Campbell, L. L., Polyak, K., Brisken, C., Yang, J., & Weinberg, R. A. (2008, May 16). The epithelial-mesenchymal transition generates cells with properties of stem cells. *Cell, 133*(4), 704-715. https://doi.org/10.1016/j.cell.2008.03.027

Mao, Y., Keller, E. T., Garfield, D. H., Shen, K., & Wang, J. (2013, Jun). Stromal cells in tumor microenvironment and breast cancer. *Cancer Metastasis Rev, 32*(1-2), 303-315. https://doi.org/10.1007/s10555-012-9415-3

Martelotto, L. G., Ng, C. K., Piscuoglio, S., Weigelt, B., & Reis-Filho, J. S. (2014, May 20). Breast cancer intra-tumor heterogeneity. *Breast Cancer Res, 16*(3), 210. https://doi.org/10.1186/bcr3658

May, C. D., Sphyris, N., Evans, K. W., Werden, S. J., Guo, W., & Mani, S. A. (2011, Feb 8). Epithelial-mesenchymal transition and cancer stem cells: a dangerously dynamic duo in breast cancer progression. *Breast Cancer Res, 13*(1), 202. https://doi.org/10.1186/bcr2789

McDonald, D. M., & Baluk, P. (2002, Sep 15). Significance of blood vessel leakiness in cancer. *Cancer Res, 62*(18), 5381-5385.

Meacham, C. E., & Morrison, S. J. (2013, Sep 19). Tumour heterogeneity and cancer cell plasticity. *Nature, 501*(7467), 328-337. https://doi.org/10.1038/nature12624

Mehlen, P., & Puisieux, A. (2006, Jun). Metastasis: a question of life or death. *Nat Rev Cancer, 6*(6), 449-458. https://doi.org/10.1038/nrc1886

Mercer, T. R., Dinger, M. E., & Mattick, J. S. (2009, Mar). Long non-coding RNAs: insights into functions. *Nat Rev Genet, 10*(3), 155-159. https://doi.org/10.1038/nrg2521

Meyer-Schaller, N., Cardner, M., Diepenbruck, M., Saxena, M., Tiede, S., Luond, F., Ivanek, R., Beerenwinkel, N., & Christofori, G. (2019, Feb 25). A Hierarchical Regulatory Landscape during the Multiple Stages of EMT. *Dev Cell, 48*(4), 539-553.e536. https://doi.org/10.1016/j.devcel.2018.12.023

Michalik, K. M., You, X., Manavski, Y., Doddaballapur, A., Zörnig, M., Braun, T., John, D., Ponomareva, Y., Chen, W., Uchida, S., Boon, R. A., & Dimmeler, S. (2014, Apr 25). Long noncoding RNA MALAT1 regulates endothelial cell function and vessel growth. *Circ Res, 114*(9), 1389-1397. https://doi.org/10.1161/circresaha.114.303265

Mikkers, H., & Frisen, J. (2005, Aug 3). Deconstructing stemness. *Embo j, 24*(15), 2715-2719. https://doi.org/10.1038/sj.emboj.7600749

Millet, C., & Zhang, Y. E. (2007). Roles of Smad3 in TGF-beta signaling during carcinogenesis. *Crit Rev Eukaryot Gene Expr, 17*(4), 281-293. https://doi.org/10.1615/critreveukargeneexpr.v17.i4.30

Milosevic, J., Pandit, K., Magister, M., Rabinovich, E., Ellwanger, D. C., Yu, G., Vuga, L. J., Weksler, B., Benos, P. V., Gibson, K. F., McMillan, M., Kahn, M., & Kaminski, N. (2012, Dec). Profibrotic role of miR-154 in pulmonary fibrosis. *Am J Respir Cell Mol Biol, 47*(6), 879-887. https://doi.org/10.1165/rcmb.2011-0377OC

Miloudi, K., Oubaha, M., Ménard, C., Dejda, A., Guber, V., Cagnone, G., Wilson, A. M., Tétreault, N., Mawambo, G., Binet, F., Chidiac, R., Delisle, C., Buscarlet, M., Cerani, A., Crespo-Garcia, S., Bentley, K., Rezende, F., Joyal, J. S., Mallette, F. A., Gratton, J. P., Larrivée, B., & Sapieha, P. (2019, Mar 5). NOTCH1 signaling induces pathological vascular permeability in diabetic retinopathy. *Proc Natl Acad Sci U S A, 116*(10), 4538-4547. https://doi.org/10.1073/pnas.1814711116

Mishra, P. J., Mishra, P. J., Humeniuk, R., Medina, D. J., Alexe, G., Mesirov, J. P., Ganesan, S., Glod, J. W., & Banerjee, D. (2008, Jun 1). Carcinoma-associated fibroblast-like differentiation of human mesenchymal stem cells. *Cancer Res, 68*(11), 4331-4339. https://doi.org/10.1158/0008-5472.Can-08-0943

Mitchell, M. S., Kan-Mitchell, J., Minev, B., Edman, C., & Deans, R. J. (2000, Nov 15). A novel melanoma gene (MG50) encoding the interleukin 1

receptor antagonist and six epitopes recognized by human cytolytic T lymphocytes. *Cancer Res, 60*(22), 6448-6456.

Mitra, R., Chen, X., Greenawalt, E. J., Maulik, U., Jiang, W., Zhao, Z., & Eischen, C. M. (2017, Nov 17). Decoding critical long non-coding RNA in ovarian cancer epithelial-to-mesenchymal transition. *Nat Commun, 8*(1), 1604. https://doi.org/10.1038/s41467-017-01781-0

Miyoshi, N., Wagatsuma, H., Wakana, S., Shiroishi, T., Nomura, M., Aisaka, K., Kohda, T., Surani, M. A., Kaneko-Ishino, T., & Ishino, F. (2000, Mar). Identification of an imprinted gene, Meg3/Gtl2 and its human homologue MEG3, first mapped on mouse distal chromosome 12 and human chromosome 14q. *Genes Cells, 5*(3), 211-220.

Moes, M., Le Bechec, A., Crespo, I., Laurini, C., Halavatyi, A., Vetter, G., Del Sol, A., & Friederich, E. (2012). A novel network integrating a miRNA-203/SNAI1 feedback loop which regulates epithelial to mesenchymal transition. *PLoS One, 7*(4), e35440. https://doi.org/10.1371/journal.pone.0035440

Molina-Pinelo, S., Salinas, A., Moreno-Mata, N., Ferrer, I., Suarez, R., Andres-Leon, E., Rodriguez-Paredes, M., Gutekunst, J., Jantus-Lewintre, E., Camps, C., Carnero, A., & Paz-Ares, L. (2018, Jan 12). Impact of DLK1-DIO3 imprinted cluster hypomethylation in smoker patients with lung cancer. *Oncotarget, 9*(4), 4395-4410. https://doi.org/10.18632/oncotarget.10611

Mondal, T., Subhash, S., Vaid, R., Enroth, S., Uday, S., Reinius, B., Mitra, S., Mohammed, A., James, A. R., Hoberg, E., Moustakas, A., Gyllensten, U., Jones, S. J., Gustafsson, C. M., Sims, A. H., Westerlund, F., Gorab, E., & Kanduri, C. (2015, Jul 24). MEG3 long noncoding RNA regulates the TGF-beta pathway genes through formation of RNA-DNA triplex structures. *Nat Commun, 6*, 7743. https://doi.org/10.1038/ncomms8743

Moradi, M. T., Fallahi, H., & Rahimi, Z. (2019, Mar). Interaction of long noncoding RNA MEG3 with miRNAs: A reciprocal regulation. *J Cell Biochem, 120*(3), 3339-3352. https://doi.org/10.1002/jcb.27604

Moradi, S., Sharifi-Zarchi, A., Ahmadi, A., Mollamohammadi, S., Stubenvoll, A., Gunther, S., Salekdeh, G. H., Asgari, S., Braun, T., & Baharvand, H. (2017, Dec 12). Small RNA Sequencing Reveals Dlk1-Dio3 Locus-

Embedded MicroRNAs as Major Drivers of Ground-State Pluripotency. *Stem Cell Reports, 9*(6), 2081-2096. https://doi.org/10.1016/j.stemcr.2017.10.009

Morera, E., Steinhäuser, S. S., Budkova, Z., Ingthorsson, S., Kricker, J., Krueger, A., Traustadottir, G. A., & Gudjonsson, T. (2019, Dec). YKL-40/CHI3L1 facilitates migration and invasion in HER2 overexpressing breast epithelial progenitor cells and generates a niche for capillary-like network formation. *In Vitro Cell Dev Biol Anim, 55*(10), 838-853. https://doi.org/10.1007/s11626-019-00403-x

Moustakas, A., & Heldin, C. H. (2007, Oct). Signaling networks guiding epithelial-mesenchymal transitions during embryogenesis and cancer progression. *Cancer Sci, 98*(10), 1512-1520. https://doi.org/10.1111/j.1349-7006.2007.00550.x

Myllymaki, S. M., & Mikkola, M. L. (2019, Aug 3). Inductive signals in branching morphogenesis - lessons from mammary and salivary glands. *Curr Opin Cell Biol, 61*, 72-78. https://doi.org/10.1016/j.ceb.2019.07.001

Nakajima, Y., Yamagishi, T., Hokari, S., & Nakamura, H. (2000, Feb 1). Mechanisms involved in valvuloseptal endocardial cushion formation in early cardiogenesis: roles of transforming growth factor (TGF)-beta and bone morphogenetic protein (BMP). *Anat Rec, 258*(2), 119-127. https://doi.org/10.1002/(sici)1097-0185(20000201)258:2<119::Aid-ar1>3.0.Co;2-u

Nelson, A. R., Fingleton, B., Rothenberg, M. L., & Matrisian, L. M. (2000, Mar). Matrix metalloproteinases: biologic activity and clinical implications. *J Clin Oncol, 18*(5), 1135-1149. https://doi.org/10.1200/jco.2000.18.5.1135

Nelson, C. M., Vanduijn, M. M., Inman, J. L., Fletcher, D. A., & Bissell, M. J. (2006, Oct 13). Tissue geometry determines sites of mammary branching morphogenesis in organotypic cultures. *Science, 314*(5797), 298-300. https://doi.org/10.1126/science.1131000

Neve, R. M., Chin, K., Fridlyand, J., Yeh, J., Baehner, F. L., Fevr, T., Clark, L., Bayani, N., Coppe, J. P., Tong, F., Speed, T., Spellman, P. T., DeVries, S., Lapuk, A., Wang, N. J., Kuo, W. L., Stilwell, J. L., Pinkel, D., Albertson, D. G., Waldman, F. M., McCormick, F., Dickson, R. B., Johnson, M. D., Lippman, M., Ethier, S., Gazdar, A., & Gray, J. W.

(2006, Dec). A collection of breast cancer cell lines for the study of functionally distinct cancer subtypes. *Cancer Cell, 10*(6), 515-527. https://doi.org/10.1016/j.ccr.2006.10.008

Neville, M. C., & Daniel, C. W. (1987). *The mammary gland: development, regulation, and function*. Plenum Publishing Corporation.

Neville, M. C., Medina, D., Monks, J., & Hovey, R. C. (1998, Apr). The mammary fat pad. *J Mammary Gland Biol Neoplasia, 3*(2), 109-116. https://doi.org/10.1023/a:1018786604818

Ngernyuang, N., Francescone, R. A., Jearanaikoon, P., Daduang, J., Supoken, A., Yan, W., Shao, R., & Limpaiboon, T. (2014, Jun). Chitinase 3 like 1 is associated with tumor angiogenesis in cervical cancer. *Int J Biochem Cell Biol, 51*, 45-52. https://doi.org/10.1016/j.biocel.2014.03.021

Nguyen, Q. H., Pervolarakis, N., Blake, K., Ma, D., Davis, R. T., James, N., Phung, A. T., Willey, E., Kumar, R., Jabart, E., Driver, I., Rock, J., Goga, A., Khan, S. A., Lawson, D. A., Werb, Z., & Kessenbrock, K. (2018, May 23). Profiling human breast epithelial cells using single cell RNA sequencing identifies cell diversity. *Nat Commun, 9*(1), 2028. https://doi.org/10.1038/s41467-018-04334-1

Nicoloso, M. S., Spizzo, R., Shimizu, M., Rossi, S., & Calin, G. A. (2009, Apr). MicroRNAs--the micro steering wheel of tumour metastases. *Nat Rev Cancer, 9*(4), 293-302. https://doi.org/10.1038/nrc2619

Nieto, M. A., Huang, R. Y., Jackson, R. A., & Thiery, J. P. (2016, Jun 30). EMT: 2016. *Cell, 166*(1), 21-45. https://doi.org/10.1016/j.cell.2016.06.028

Niknafs, Y. S., Pandian, B., Gajjar, T., Gaudette, Z., Wheelock, K., Maz, M. P., Achar, R. K., Song, M., Massaro, C., Cao, X., & Chinnaiyan, A. M. (2018, Nov). MiPanda: A Resource for Analyzing and Visualizing Next-Generation Sequencing Transcriptomics Data. *Neoplasia, 20*(11), 1144-1149. https://doi.org/10.1016/j.neo.2018.09.001

Ogata, T., & Kagami, M. (2016, Feb). Kagami-Ogata syndrome: a clinically recognizable upd(14)pat and related disorder affecting the chromosome 14q32.2 imprinted region. *J Hum Genet, 61*(2), 87-94. https://doi.org/10.1038/jhg.2015.113

Oktyabri, D., Tange, S., Terashima, M., Ishimura, A., & Suzuki, T. (2014, Oct 10). EED regulates epithelial-mesenchymal transition of cancer cells induced by TGF-beta. *Biochem Biophys Res Commun, 453*(1), 124-130. https://doi.org/10.1016/j.bbrc.2014.09.082

Paget, S. (1989, Aug). The distribution of secondary growths in cancer of the breast. 1889. *Cancer Metastasis Rev, 8*(2), 98-101.

Pastushenko, I., Brisebarre, A., Sifrim, A., Fioramonti, M., Revenco, T., Boumahdi, S., Van Keymeulen, A., Brown, D., Moers, V., Lemaire, S., De Clercq, S., Minguijon, E., Balsat, C., Sokolow, Y., Dubois, C., De Cock, F., Scozzaro, S., Sopena, F., Lanas, A., D'Haene, N., Salmon, I., Marine, J. C., Voet, T., Sotiropoulou, P. A., & Blanpain, C. (2018, Apr). Identification of the tumour transition states occurring during EMT. *Nature, 556*(7702), 463-468. https://doi.org/10.1038/s41586-018-0040-3

Pechoux, C., Gudjonsson, T., Ronnov-Jessen, L., Bissell, M. J., & Petersen, O. W. (1999, Feb 1). Human mammary luminal epithelial cells contain progenitors to myoepithelial cells. *Dev Biol, 206*(1), 88-99. https://doi.org/10.1006/dbio.1998.9133

Peinado, H., Olmeda, D., & Cano, A. (2007, Jun). Snail, Zeb and bHLH factors in tumour progression: an alliance against the epithelial phenotype? *Nat Rev Cancer, 7*(6), 415-428. https://doi.org/10.1038/nrc2131

Peng, W., Si, S., Zhang, Q., Li, C., Zhao, F., Wang, F., Yu, J., & Ma, R. (2015, Aug 8). Long non-coding RNA MEG3 functions as a competing endogenous RNA to regulate gastric cancer progression. *J Exp Clin Cancer Res, 34*, 79. https://doi.org/10.1186/s13046-015-0197-7

Perou, C. M. (2010). Molecular stratification of triple-negative breast cancers. *Oncologist, 15 Suppl 5*, 39-48. https://doi.org/10.1634/theoncologist.2010-S5-39

Perou, C. M., Sorlie, T., Eisen, M. B., van de Rijn, M., Jeffrey, S. S., Rees, C. A., Pollack, J. R., Ross, D. T., Johnsen, H., Akslen, L. A., Fluge, O., Pergamenschikov, A., Williams, C., Zhu, S. X., Lonning, P. E., Borresen-Dale, A. L., Brown, P. O., & Botstein, D. (2000, Aug 17). Molecular portraits of human breast tumours. *Nature, 406*(6797), 747-752. https://doi.org/10.1038/35021093

Peterfi, Z., Donko, A., Orient, A., Sum, A., Prokai, A., Molnar, B., Vereb, Z., Rajnavolgyi, E., Kovacs, K. J., Muller, V., Szabo, A. J., & Geiszt, M. (2009, Aug). Peroxidasin is secreted and incorporated into the extracellular matrix of myofibroblasts and fibrotic kidney. *Am J Pathol, 175*(2), 725-735. https://doi.org/10.2353/ajpath.2009.080693

Péterfi, Z., & Geiszt, M. (2014, Jul). Peroxidasins: novel players in tissue genesis. *Trends Biochem Sci, 39*(7), 305-307. https://doi.org/10.1016/j.tibs.2014.05.005

Petersen, O. W., Lind Nielsen, H., Gudjonsson, T., Villadsen, R., Rønnov-Jessen, L., & Bissell, M. J. (2001). The plasticity of human breast carcinoma cells is more than epithelial to mesenchymal conversion. *Breast Cancer Res, 3*(4), 213-217. https://doi.org/10.1186/bcr298

Piccoli, M. T., Gupta, S. K., Viereck, J., Foinquinos, A., Samolovac, S., Kramer, F. L., Garg, A., Remke, J., Zimmer, K., Batkai, S., & Thum, T. (2017, Aug 18). Inhibition of the Cardiac Fibroblast-Enriched lncRNA Meg3 Prevents Cardiac Fibrosis and Diastolic Dysfunction. *Circ Res, 121*(5), 575-583. https://doi.org/10.1161/circresaha.117.310624

Place, A. E., Jin Huh, S., & Polyak, K. (2011). The microenvironment in breast cancer progression: biology and implications for treatment. *Breast Cancer Res, 13*(6), 227. https://doi.org/10.1186/bcr2912

Polyak, K., & Kalluri, R. (2010, Nov). The role of the microenvironment in mammary gland development and cancer. *Cold Spring Harb Perspect Biol, 2*(11), a003244. https://doi.org/10.1101/cshperspect.a003244

Polyak, K., & Weinberg, R. A. (2009, Apr). Transitions between epithelial and mesenchymal states: acquisition of malignant and stem cell traits. *Nat Rev Cancer, 9*(4), 265-273. https://doi.org/10.1038/nrc2620

Potenta, S., Zeisberg, E., & Kalluri, R. (2008, Nov 4). The role of endothelial-to-mesenchymal transition in cancer progression. *Br J Cancer, 99*(9), 1375-1379. https://doi.org/10.1038/sj.bjc.6604662

Prat, A., Parker, J. S., Karginova, O., Fan, C., Livasy, C., Herschkowitz, J. I., He, X., & Perou, C. M. (2010). Phenotypic and molecular characterization of the claudin-low intrinsic subtype of breast cancer. *Breast Cancer Res, 12*(5), R68. https://doi.org/10.1186/bcr2635

Prat, A., & Perou, C. M. (2011, Feb). Deconstructing the molecular portraits of breast cancer. *Mol Oncol, 5*(1), 5-23. https://doi.org/10.1016/j.molonc.2010.11.003

Qin, N., Tong, G. F., Sun, L. W., & Xu, X. L. (2017, Nov 2). Long Noncoding RNA MEG3 Suppresses Glioma Cell Proliferation, Migration, and Invasion by Acting as a Competing Endogenous RNA of miR-19a. *Oncol Res, 25*(9), 1471-1478. https://doi.org/10.3727/096504017x14886689179993

Quail, D. F., & Joyce, J. A. (2013, Nov). Microenvironmental regulation of tumor progression and metastasis. *Nat Med, 19*(11), 1423-1437. https://doi.org/10.1038/nm.3394

Radisky, D. C., Kenny, P. A., & Bissell, M. J. (2007, Jul 1). Fibrosis and cancer: do myofibroblasts come also from epithelial cells via EMT? *J Cell Biochem, 101*(4), 830-839. https://doi.org/10.1002/jcb.21186

Reedijk, M. (2012). Notch signaling and breast cancer. *Adv Exp Med Biol, 727*, 241-257. https://doi.org/10.1007/978-1-4614-0899-4_18

Regier, M. C., Alarid, E. T., & Beebe, D. J. (2016, Jun 13). Progress towards understanding heterotypic interactions in multi-culture models of breast cancer. *Integr Biol (Camb), 8*(6), 684-692. https://doi.org/10.1039/c6ib00001k

Resetkova, E., Reis-Filho, J. S., Jain, R. K., Mehta, R., Thorat, M. A., Nakshatri, H., & Badve, S. (2010, Aug). Prognostic impact of ALDH1 in breast cancer: a story of stem cells and tumor microenvironment. *Breast Cancer Res Treat, 123*(1), 97-108. https://doi.org/10.1007/s10549-009-0619-3

Ringnér, M., Fredlund, E., Häkkinen, J., Borg, Å., & Staaf, J. (2011, Mar 21). GOBO: gene expression-based outcome for breast cancer online. *PLoS One, 6*(3), e17911. https://doi.org/10.1371/journal.pone.0017911

Roslind, A., Johansen, J. S., Junker, N., Nielsen, D. L., Dzaferi, H., Price, P. A., & Balslev, E. (2007, Dec). YKL-40 expression in benign and malignant lesions of the breast: a methodologic study. *Appl Immunohistochem Mol Morphol, 15*(4), 371-381. https://doi.org/10.1097/01.pai.0000213146.77772.6a

Rossi, A., Kontarakis, Z., Gerri, C., Nolte, H., Holper, S., Kruger, M., & Stainier, D. Y. (2015, Aug 13). Genetic compensation induced by deleterious mutations but not gene knockdowns. *Nature, 524*(7564), 230-233. https://doi.org/10.1038/nature14580

Ruan, W., Zhao, F., Zhao, S., Zhang, L., Shi, L., & Pang, T. (2018, Apr 5). Knockdown of long noncoding RNA MEG3 impairs VEGF-stimulated endothelial sprouting angiogenesis via modulating VEGFR2 expression in human umbilical vein endothelial cells. *Gene, 649*, 32-39. https://doi.org/10.1016/j.gene.2018.01.072

Sakakibara, M., Fujimori, T., Miyoshi, T., Nagashima, T., Fujimoto, H., Suzuki, H. T., Ohki, Y., Fushimi, K., Yokomizo, J., Nakatani, Y., & Miyazaki, M. (2012, Aug 15). Aldehyde dehydrogenase 1-positive cells in axillary lymph node metastases after chemotherapy as a prognostic factor in patients with lymph node-positive breast cancer. *Cancer, 118*(16), 3899-3910. https://doi.org/10.1002/cncr.26725

Sanli, I., Lalevee, S., Cammisa, M., Perrin, A., Rage, F., Lleres, D., Riccio, A., Bertrand, E., & Feil, R. (2018, Apr 10). Meg3 Non-coding RNA Expression Controls Imprinting by Preventing Transcriptional Upregulation in cis. *Cell Rep, 23*(2), 337-348. https://doi.org/10.1016/j.celrep.2018.03.044

Sarrió, D., Rodriguez-Pinilla, S. M., Hardisson, D., Cano, A., Moreno-Bueno, G., & Palacios, J. (2008, Feb 15). Epithelial-mesenchymal transition in breast cancer relates to the basal-like phenotype. *Cancer Res, 68*(4), 989-997. https://doi.org/10.1158/0008-5472.Can-07-2017

Seip, K., Fleten, K. G., Barkovskaya, A., Nygaard, V., Haugen, M. H., Engesæter, B., Mælandsmo, G. M., & Prasmickaite, L. (2016, Apr 12). Fibroblast-induced switching to the mesenchymal-like phenotype and PI3K/mTOR signaling protects melanoma cells from BRAF inhibitors. *Oncotarget, 7*(15), 19997-20015. https://doi.org/10.18632/oncotarget.7671

Sercu, S., Zhang, L., & Merregaert, J. (2008, May). The extracellular matrix protein 1: its molecular interaction and implication in tumor progression. *Cancer Invest, 26*(4), 375-384. https://doi.org/10.1080/07357900701788148

Shackleton, M., Vaillant, F., Simpson, K. J., Stingl, J., Smyth, G. K., Asselin-Labat, M. L., Wu, L., Lindeman, G. J., & Visvader, J. E. (2006, Jan 5). Generation of a functional mammary gland from a single stem cell. *Nature, 439*(7072), 84-88. https://doi.org/10.1038/nature04372

Shao, R. (2013). YKL-40 acts as an angiogenic factor to promote tumor angiogenesis. *Front Physiol, 4*, 122. https://doi.org/10.3389/fphys.2013.00122

Shao, R., Hamel, K., Petersen, L., Cao, Q. J., Arenas, R. B., Bigelow, C., Bentley, B., & Yan, W. (2009, Dec 17). YKL-40, a secreted glycoprotein, promotes tumor angiogenesis. *Oncogene, 28*(50), 4456-4468. https://doi.org/10.1038/onc.2009.292

Sheng, X., Li, J., Yang, L., Chen, Z., Zhao, Q., Tan, L., Zhou, Y., & Li, J. (2014, Jul). Promoter hypermethylation influences the suppressive role of maternally expressed 3, a long non-coding RNA, in the development of epithelial ovarian cancer. *Oncol Rep, 32*(1), 277-285. https://doi.org/10.3892/or.2014.3208

Shi, L., Wang, Y., Lu, Z., Zhang, H., Zhuang, N., Wang, B., Song, Z., Chen, G., Huang, C., Xu, D., Zhang, Y., Zhang, W., & Gao, Y. (2017, Mar 23). miR-127 promotes EMT and stem-like traits in lung cancer through a feed-forward regulatory loop. *Oncogene, 36*(12), 1631-1643. https://doi.org/10.1038/onc.2016.332

Shi, Y. (2020, Jun). MEG3 regulates apoptosis of adipose-derived stem cells. *Mol Med Rep, 21*(6), 2435-2442. https://doi.org/10.3892/mmr.2020.11059

Shibue, T., & Weinberg, R. A. (2017, Oct). EMT, CSCs, and drug resistance: the mechanistic link and clinical implications. *Nat Rev Clin Oncol, 14*(10), 611-629. https://doi.org/10.1038/nrclinonc.2017.44

Shimono, Y., Zabala, M., Cho, R. W., Lobo, N., Dalerba, P., Qian, D., Diehn, M., Liu, H., Panula, S. P., Chiao, E., Dirbas, F. M., Somlo, G., Pera, R. A., Lao, K., & Clarke, M. F. (2009, Aug 7). Downregulation of miRNA-200c links breast cancer stem cells with normal stem cells. *Cell, 138*(3), 592-603. https://doi.org/10.1016/j.cell.2009.07.011

Schmidt, J. V., Matteson, P. G., Jones, B. K., Guan, X. J., & Tilghman, S. M. (2000, Aug 15). The Dlk1 and Gtl2 genes are linked and reciprocally imprinted. *Genes Dev, 14*(16), 1997-2002.

Schubert, J., & Brabletz, T. (2011, May). p53 Spreads out further: suppression of EMT and stemness by activating miR-200c expression. *Cell Res, 21*(5), 705-707. https://doi.org/10.1038/cr.2011.62

Schuster-Gossler, K., Bilinski, P., Sado, T., Ferguson-Smith, A., & Gossler, A. (1998, Jun). The mouse Gtl2 gene is differentially expressed during embryonic development, encodes multiple alternatively spliced transcripts, and may act as an RNA. *Dev Dyn, 212*(2), 214-228. https://doi.org/10.1002/(sici)1097-0177(199806)212:2<214::Aid-aja6>3.0.Co;2-k

Siegel, R. L., Miller, K. D., & Jemal, A. (2019). Cancer statistics, 2019. *CA: A Cancer Journal for Clinicians, 69*(1), 7-34. https://doi.org/10.3322/caac.21551

Sigurdsson, V., Fridriksdottir, A. J., Kjartansson, J., Jonasson, J. G., Steinarsdottir, M., Petersen, O. W., Ogmundsdottir, H. M., & Gudjonsson, T. (2006, Nov-Dec). Human breast microvascular endothelial cells retain phenotypic traits in long-term finite life span culture. *In Vitro Cell Dev Biol Anim, 42*(10), 332-340. https://doi.org/10.1290/0602017.1

Sigurdsson, V., Hilmarsdottir, B., Sigmundsdottir, H., Fridriksdottir, A. J., Ringner, M., Villadsen, R., Borg, A., Agnarsson, B. A., Petersen, O. W., Magnusson, M. K., & Gudjonsson, T. (2011). Endothelial induced EMT in breast epithelial cells with stem cell properties. *PLoS One, 6*(9), e23833. https://doi.org/10.1371/journal.pone.0023833

Sigurdsson, V., Ingthorsson, S., Hilmarsdottir, B., Gustafsdottir, S. M., Franzdottir, S. R., Arason, A. J., Steingrimsson, E., Magnusson, M. K., & Gudjonsson, T. (2013). Expression and functional role of sprouty-2 in breast morphogenesis. *PLoS One, 8*(4), e60798. https://doi.org/10.1371/journal.pone.0060798

Simian, M., & Bissell, M. J. (2017, Jan 2). Organoids: A historical perspective of thinking in three dimensions. *J Cell Biol, 216*(1), 31-40. https://doi.org/10.1083/jcb.201610056

Smith, J. D., Suresh, S., Schlecht, U., Wu, M., Wagih, O., Peltz, G., Davis, R. W., Steinmetz, L. M., Parts, L., & St Onge, R. P. (2016, Mar 8). Quantitative CRISPR interference screens in yeast identify chemical-genetic interactions and new rules for guide RNA design. *Genome Biol, 17*, 45. https://doi.org/10.1186/s13059-016-0900-9

Soon, P. S. H., Kim, E., Pon, C. K., Gill, A. J., Moore, K., Spillane, A. J., Benn, D. E., & Baxter, R. C. (2013, 2013/02//). Breast cancer-associated fibroblasts induce epithelial-to-mesenchymal transition in breast cancer cells. *Endocrine-related cancer, 20*(1), 1-12. https://doi.org/10.1530/erc-12-0227

Sorlie, T., Perou, C. M., Tibshirani, R., Aas, T., Geisler, S., Johnsen, H., Hastie, T., Eisen, M. B., van de Rijn, M., Jeffrey, S. S., Thorsen, T., Quist, H., Matese, J. C., Brown, P. O., Botstein, D., Lonning, P. E., & Borresen-Dale, A. L. (2001, Sep 11). Gene expression patterns of breast carcinomas distinguish tumor subclasses with clinical implications. *Proc Natl Acad Sci U S A, 98*(19), 10869-10874. https://doi.org/10.1073/pnas.191367098

Sottocornola, R., & Lo Celso, C. (2012, Mar 19). Dormancy in the stem cell niche. *Stem Cell Res Ther, 3*(2), 10. https://doi.org/10.1186/scrt101

Spike, B. T., Engle, D. D., Lin, J. C., Cheung, S. K., La, J., & Wahl, G. M. (2012, Feb 3). A mammary stem cell population identified and characterized in late embryogenesis reveals similarities to human breast cancer. *Cell Stem Cell, 10*(2), 183-197. https://doi.org/10.1016/j.stem.2011.12.018

Stadtfeld, M., Apostolou, E., Akutsu, H., Fukuda, A., Follett, P., Natesan, S., Kono, T., Shioda, T., & Hochedlinger, K. (2010, May 13). Aberrant silencing of imprinted genes on chromosome 12qF1 in mouse induced pluripotent stem cells. *Nature, 465*(7295), 175-181. https://doi.org/10.1038/nature09017

Steinhaeuser, S. S., Morera, E., Budkova, Z., Schepsky, A., Wang, Q., Rolfsson, O., Riedel, A., Krueger, A., Hilmarsdottir, B., Maelandsmo, G. M., Valdimarsdottir, B., Sigurdardottir, A. K., Agnarsson, B. A., Jonasson, J. G., Ingthorsson, S., Traustadottir, G. A., Oskarsson, T., & Gudjonsson, T. (2020, Jul). ECM1 secreted by HER2-overexpressing breast cancer cells promotes formation of a vascular niche accelerating cancer cell migration and invasion. *Lab Invest, 100*(7), 928-944. https://doi.org/10.1038/s41374-020-0415-6

Sun, L., Li, Y., & Yang, B. (2016, Sep 9). Downregulated long non-coding RNA MEG3 in breast cancer regulates proliferation, migration and invasion by depending on p53's transcriptional activity. *Biochem Biophys Res Commun, 478*(1), 323-329. https://doi.org/10.1016/j.bbrc.2016.05.031

Sun, L., Luo, H., Liao, Q., Bu, D., Zhao, G., Liu, C., Liu, Y., & Zhao, Y. (2013, Apr). Systematic study of human long intergenic non-coding RNAs and their impact on cancer. *Sci China Life Sci, 56*(4), 324-334. https://doi.org/10.1007/s11427-013-4460-x

Sung, K. E., Su, X., Berthier, E., Pehlke, C., Friedl, A., & Beebe, D. J. (2013). Understanding the impact of 2D and 3D fibroblast cultures on in vitro breast cancer models. *PLoS One, 8*(10), e76373. https://doi.org/10.1371/journal.pone.0076373

Taft, R. J., Pheasant, M., & Mattick, J. S. (2007, Mar). The relationship between non-protein-coding DNA and eukaryotic complexity. *Bioessays, 29*(3), 288-299. https://doi.org/10.1002/bies.20544

Takahashi, N., Okamoto, A., Kobayashi, R., Shirai, M., Obata, Y., Ogawa, H., Sotomaru, Y., & Kono, T. (2009, May 15). Deletion of Gtl2, imprinted non-coding RNA, with its differentially methylated region induces lethal parent-origin-dependent defects in mice. *Hum Mol Genet, 18*(10), 1879-1888. https://doi.org/10.1093/hmg/ddp108

Taube, J. H., Malouf, G. G., Lu, E., Sphyris, N., Vijay, V., Ramachandran, P. P., Ueno, K. R., Gaur, S., Nicoloso, M. S., Rossi, S., Herschkowitz, J. I., Rosen, J. M., Issa, J. P., Calin, G. A., Chang, J. T., & Mani, S. A. (2013). Epigenetic silencing of microRNA-203 is required for EMT and cancer stem cell properties. *Sci Rep, 3*, 2687. https://doi.org/10.1038/srep02687

Team, R. C. (2015). R Foundation for Statistical Computing; Vienna, Austria: 2014. *R: A language and environment for statistical computing*, 2013.

Terashima, M., Ishimura, A., Wanna-Udom, S., & Suzuki, T. (2018, Nov 23). MEG8 long noncoding RNA contributes to epigenetic progression of the epithelial-mesenchymal transition of lung and pancreatic cancer cells. *J Biol Chem, 293*(47), 18016-18030. https://doi.org/10.1074/jbc.RA118.004006

Terashima, M., Tange, S., Ishimura, A., & Suzuki, T. (2017, Jan 6). MEG3 Long Noncoding RNA Contributes to the Epigenetic Regulation of Epithelial-Mesenchymal Transition in Lung Cancer Cell Lines. *J Biol Chem, 292*(1), 82-99. https://doi.org/10.1074/jbc.M116.750950

Thomas, D. W., Burns, J., Audette, J., Carroll, A., Dow-Hygelund, C., & Hay, M. (2016). Clinical development success rates 2006–2015. *BIO Industry Analysis, 1*, 16.

Thomas, P., & Smart, T. G. (2005, May-Jun). HEK293 cell line: a vehicle for the expression of recombinant proteins. *J Pharmacol Toxicol Methods, 51*(3), 187-200. https://doi.org/10.1016/j.vascn.2004.08.014

Tian, T., Wang, M., Lin, S., Guo, Y., Dai, Z., Liu, K., Yang, P., Dai, C., Zhu, Y., Zheng, Y., Xu, P., Zhu, W., & Dai, Z. (2018, Sep 7). The Impact of lncRNA Dysregulation on Clinicopathology and Survival of Breast Cancer: A Systematic Review and Meta-analysis. *Mol Ther Nucleic Acids, 12*, 359-369. https://doi.org/10.1016/j.omtn.2018.05.018

Tierling, S., Dalbert, S., Schoppenhorst, S., Tsai, C. E., Oliger, S., Ferguson-Smith, A. C., Paulsen, M., & Walter, J. (2006, Feb). High-resolution map and imprinting analysis of the Gtl2-Dnchc1 domain on mouse chromosome 12. *Genomics, 87*(2), 225-235. https://doi.org/10.1016/j.ygeno.2005.09.018

Tong, Y. S., Wang, X. W., Zhou, X. L., Liu, Z. H., Yang, T. X., Shi, W. H., Xie, H. W., Lv, J., Wu, Q. Q., & Cao, X. F. (2015, Jan 21). Identification of the long non-coding RNA POU3F3 in plasma as a novel biomarker for diagnosis of esophageal squamous cell carcinoma. *Mol Cancer, 14*, 3. https://doi.org/10.1186/1476-4598-14-3

Tran, H. D., Luitel, K., Kim, M., Zhang, K., Longmore, G. D., & Tran, D. D. (2014, Nov 1). Transient SNAIL1 expression is necessary for metastatic competence in breast cancer. *Cancer Res, 74*(21), 6330-6340. https://doi.org/10.1158/0008-5472.Can-14-0923

Tran, M. N., Choi, W., Wszolek, M. F., Navai, N., Lee, I. L., Nitti, G., Wen, S., Flores, E. R., Siefker-Radtke, A., Czerniak, B., Dinney, C., Barton, M., & McConkey, D. J. (2013, Feb 1). The p63 protein isoform DeltaNp63alpha inhibits epithelial-mesenchymal transition in human bladder cancer cells: role of MIR-205. *J Biol Chem, 288*(5), 3275-3288. https://doi.org/10.1074/jbc.M112.408104

Troester, M. A., Lee, M. H., Carter, M., Fan, C., Cowan, D. W., Perez, E. R., Pirone, J. R., Perou, C. M., Jerry, D. J., & Schneider, S. S. (2009, Nov 15). Activation of host wound responses in breast cancer microenvironment. *Clin Cancer Res, 15*(22), 7020-7028. https://doi.org/10.1158/1078-0432.Ccr-09-1126

Tsai, J. H., & Yang, J. (2013, Oct 15). Epithelial-mesenchymal plasticity in carcinoma metastasis. *Genes Dev, 27*(20), 2192-2206. https://doi.org/10.1101/gad.225334.113

Tungsukruthai, S., Petpiroon, N., & Chanvorachote, P. (2018, May). Molecular Mechanisms of Breast Cancer Metastasis and Potential Anti-metastatic Compounds. *Anticancer Res, 38*(5), 2607-2618. https://doi.org/10.21873/anticanres.12502

Turashvili, G., & Brogi, E. (2017). Tumor Heterogeneity in Breast Cancer. *Front Med (Lausanne), 4*, 227. https://doi.org/10.3389/fmed.2017.00227

Unsworth, A., Anderson, R., & Britt, K. (2014, Jul). Stromal fibroblasts and the immune microenvironment: partners in mammary gland biology and pathology? *J Mammary Gland Biol Neoplasia, 19*(2), 169-182. https://doi.org/10.1007/s10911-014-9326-8

Uroda, T., Anastasakou, E., Rossi, A., Teulon, J. M., Pellequer, J. L., Annibale, P., Pessey, O., Inga, A., Chillon, I., & Marcia, M. (2019, Aug 15). Conserved Pseudoknots in lncRNA MEG3 Are Essential for Stimulation of the p53 Pathway. *Mol Cell*. https://doi.org/10.1016/j.molcel.2019.07.025

Uroda, T., Anastasakou, E., Rossi, A., Teulon, J. M., Pellequer, J. L., Annibale, P., Pessey, O., Inga, A., Chillón, I., & Marcia, M. (2019, Sep 5). Conserved Pseudoknots in lncRNA MEG3 Are Essential for Stimulation of the p53 Pathway. *Mol Cell, 75*(5), 982-995.e989. https://doi.org/10.1016/j.molcel.2019.07.025

Valdmanis, P. N., Roy-Chaudhuri, B., Kim, H. K., Sayles, L. C., Zheng, Y., Chuang, C. H., Caswell, D. R., Chu, K., Zhang, Y., Winslow, M. M., Sweet-Cordero, E. A., & Kay, M. A. (2015, Jan 2). Upregulation of the microRNA cluster at the Dlk1-Dio3 locus in lung adenocarcinoma. *Oncogene, 34*(1), 94-103. https://doi.org/10.1038/onc.2013.523

Varga, J., & Greten, F. R. (2017, Oct). Cell plasticity in epithelial homeostasis and tumorigenesis. *Nat Cell Biol, 19*(10), 1133-1141. https://doi.org/10.1038/ncb3611

Vassalli, G. (2019). Aldehyde Dehydrogenases: Not Just Markers, but Functional Regulators of Stem Cells. *Stem Cells Int, 2019*, 3904645. https://doi.org/10.1155/2019/3904645

Vidal, S. J., Rodriguez-Bravo, V., Galsky, M., Cordon-Cardo, C., & Domingo-Domenech, J. (2014, Sep 4). Targeting cancer stem cells to suppress acquired chemotherapy resistance. *Oncogene, 33*(36), 4451-4463. https://doi.org/10.1038/onc.2013.411

Villadsen, R., Fridriksdottir, A. J., Rønnov-Jessen, L., Gudjonsson, T., Rank, F., LaBarge, M. A., Bissell, M. J., & Petersen, O. W. (2007, Apr 9). Evidence for a stem cell hierarchy in the adult human breast. *J Cell Biol, 177*(1), 87-101. https://doi.org/10.1083/jcb.200611114

Vrba, L., Jensen, T. J., Garbe, J. C., Heimark, R. L., Cress, A. E., Dickinson, S., Stampfer, M. R., & Futscher, B. W. (2010, Jan 13). Role for DNA methylation in the regulation of miR-200c and miR-141 expression in normal and cancer cells. *PLoS One, 5*(1), e8697. https://doi.org/10.1371/journal.pone.0008697

Wan, G., Xiang, L., Sun, X., Wang, X., Li, H., Ge, W., & Cao, F. (2017, Jan 17). Elevated YKL-40 expression is associated with a poor prognosis in breast cancer patients. *Oncotarget, 8*(3), 5382-5391. https://doi.org/10.18632/oncotarget.14280

Wang, C., Yu, J., Han, Y., Li, L., Li, J., Li, T., & Qi, P. (2016, Oct 25). Long non-coding RNAs LOC285194, RP11-462C24.1 and Nbla12061 in serum provide a new approach for distinguishing patients with colorectal cancer from healthy controls. *Oncotarget, 7*(43), 70769-70778. https://doi.org/10.18632/oncotarget.12220

Wang, K. C., & Chang, H. Y. (2011, Sep 16). Molecular mechanisms of long noncoding RNAs. *Mol Cell, 43*(6), 904-914. https://doi.org/10.1016/j.molcel.2011.08.018

Wang, L., Yu, M., & Zhao, S. (2019, Jun 3). lncRNA MEG3 modified epithelial-mesenchymal transition of ovarian cancer cells by sponging miR-

219a-5p and regulating EGFR. *J Cell Biochem*. https://doi.org/10.1002/jcb.29037

Wang, N., Liang, H., Zhou, Y., Wang, C., Zhang, S., Pan, Y., Wang, Y., Yan, X., Zhang, J., Zhang, C. Y., Zen, K., Li, D., & Chen, X. (2014). miR-203 suppresses the proliferation and migration and promotes the apoptosis of lung cancer cells by targeting SRC. *PLoS One, 9*(8), e105570. https://doi.org/10.1371/journal.pone.0105570

Wang, P., Ren, Z., & Sun, P. (2012, Jun). Overexpression of the long non-coding RNA MEG3 impairs in vitro glioma cell proliferation. *J Cell Biochem, 113*(6), 1868-1874. https://doi.org/10.1002/jcb.24055

Wang, Q., Huang, Z., Ni, S., Xiao, X., Xu, Q., Wang, L., Huang, D., Tan, C., Sheng, W., & Du, X. (2012). Plasma miR-601 and miR-760 are novel biomarkers for the early detection of colorectal cancer. *PLoS One, 7*(9), e44398. https://doi.org/10.1371/journal.pone.0044398

Wang, Y., & Kong, D. (2018, Jan). Knockdown of lncRNA MEG3 inhibits viability, migration, and invasion and promotes apoptosis by sponging miR-127 in osteosarcoma cell. *J Cell Biochem, 119*(1), 669-679. https://doi.org/10.1002/jcb.26230

Wang, Y., & Zhou, B. P. (2013, Mar). Epithelial-mesenchymal Transition---A Hallmark of Breast Cancer Metastasis. *Cancer Hallm, 1*(1), 38-49. https://doi.org/10.1166/ch.2013.1004

Welch-Reardon, K. M., Ehsan, S. M., Wang, K., Wu, N., Newman, A. C., Romero-Lopez, M., Fong, A. H., George, S. C., Edwards, R. A., & Hughes, C. C. (2014, May 1). Angiogenic sprouting is regulated by endothelial cell expression of Slug. *J Cell Sci, 127*(Pt 9), 2017-2028. https://doi.org/10.1242/jcs.143420

Welch-Reardon, K. M., Wu, N., & Hughes, C. C. (2015, Feb). A role for partial endothelial-mesenchymal transitions in angiogenesis? *Arterioscler Thromb Vasc Biol, 35*(2), 303-308. https://doi.org/10.1161/atvbaha.114.303220

Welten, S. M., Bastiaansen, A. J., de Jong, R. C., de Vries, M. R., Peters, E. A., Boonstra, M. C., Sheikh, S. P., La Monica, N., Kandimalla, E. R., Quax, P. H., & Nossent, A. Y. (2014, Sep 26). Inhibition of 14q32 MicroRNAs miR-329, miR-487b, miR-494, and miR-495 increases

neovascularization and blood flow recovery after ischemia. *Circ Res, 115*(8), 696-708. https://doi.org/10.1161/circresaha.114.304747

Widyantoro, B., Emoto, N., Nakayama, K., Anggrahini, D. W., Adiarto, S., Iwasa, N., Yagi, K., Miyagawa, K., Rikitake, Y., Suzuki, T., Kisanuki, Y. Y., Yanagisawa, M., & Hirata, K. (2010, Jun 8). Endothelial cell-derived endothelin-1 promotes cardiac fibrosis in diabetic hearts through stimulation of endothelial-to-mesenchymal transition. *Circulation, 121*(22), 2407-2418. https://doi.org/10.1161/circulationaha.110.938217

Wiesen, J. F., Young, P., Werb, Z., & Cunha, G. R. (1999). Signaling through the stromal epidermal growth factor receptor is necessary for mammary ductal development. *Development, 126*(2), 335-344. https://dev.biologists.org/content/develop/126/2/335.full.pdf

Williams, E. D., Gao, D., Redfern, A., & Thompson, E. W. (2019a, Oct 30). Controversies around epithelial-mesenchymal plasticity in cancer metastasis. *Nat Rev Cancer*. https://doi.org/10.1038/s41568-019-0213-x

Williams, E. D., Gao, D., Redfern, A., & Thompson, E. W. (2019b, Dec). Controversies around epithelial-mesenchymal plasticity in cancer metastasis. *Nat Rev Cancer, 19*(12), 716-732. https://doi.org/10.1038/s41568-019-0213-x

Willis, B. C., & Borok, Z. (2007, Sep). TGF-beta-induced EMT: mechanisms and implications for fibrotic lung disease. *Am J Physiol Lung Cell Mol Physiol, 293*(3), L525-534. https://doi.org/10.1152/ajplung.00163.2007

Wu, L., Zhu, L., Li, Y., Zheng, Z., Lin, X., & Yang, C. (2020). LncRNA MEG3 promotes melanoma growth, metastasis and formation through modulating miR-21/E-cadherin axis. *Cancer Cell Int, 20*, 12. https://doi.org/10.1186/s12935-019-1087-4

Wu, Q., Chen, D., Luo, Q., Yang, Q., Zhao, C., Zhang, D., Zeng, Y., Huang, L., Zhang, Z., & Qi, Z. (2018, Nov 28). Extracellular matrix protein 1 recruits moesin to facilitate invadopodia formation and breast cancer metastasis. *Cancer Lett, 437*, 44-55. https://doi.org/10.1016/j.canlet.2018.08.022

Xu, D., Liu, T., He, L., Han, D., Ma, Y., & Du, J. (2020, Apr 28). LncRNA MEG3 inhibits HMEC-1 cells growth, migration and tube formation via sponging miR-147. *Biol Chem, 401*(5), 601-615. https://doi.org/10.1515/hsz-2019-0230

Xu, G., Meng, L., Yuan, D., Li, K., Zhang, Y., Dang, C., & Zhu, K. (2018, Jul). MEG3/miR-21 axis affects cell mobility by suppressing epithelial-mesenchymal transition in gastric cancer. *Oncol Rep, 40*(1), 39-48. https://doi.org/10.3892/or.2018.6424

Xu, J., Lamouille, S., & Derynck, R. (2009, Feb). TGF-beta-induced epithelial to mesenchymal transition. *Cell Res, 19*(2), 156-172. https://doi.org/10.1038/cr.2009.5

Yan, X., Sabrautzki, S., Horsch, M., Fuchs, H., Gailus-Durner, V., Beckers, J., Hrabě de Angelis, M., & Graw, J. (2014, Nov 1). Peroxidasin is essential for eye development in the mouse. *Hum Mol Genet, 23*(21), 5597-5614. https://doi.org/10.1093/hmg/ddu274

Yang, Z., Bian, E., Xu, Y., Ji, X., Tang, F., Ma, C., Wang, H., & Zhao, B. (2020). Meg3 Induces EMT and Invasion of Glioma Cells via Autophagy. *Onco Targets Ther, 13*, 989-1000. https://doi.org/10.2147/ott.S239648

Yao, Y., Zhang, T., Qi, L., Zhou, C., Wei, J., Feng, F., Liu, R., & Sun, C. (2019, Oct 15). Integrated analysis of co-expression and ceRNA network identifies five lncRNAs as prognostic markers for breast cancer. *J Cell Mol Med*. https://doi.org/10.1111/jcmm.14721

Ye, X., & Weinberg, R. A. (2015, Nov). Epithelial-Mesenchymal Plasticity: A Central Regulator of Cancer Progression. *Trends Cell Biol, 25*(11), 675-686. https://doi.org/10.1016/j.tcb.2015.07.012

Yersal, O., & Barutca, S. (2014, Aug 10). Biological subtypes of breast cancer: Prognostic and therapeutic implications. *World J Clin Oncol, 5*(3), 412-424. https://doi.org/10.5306/wjco.v5.i3.412

Yin, D. D., Liu, Z. J., Zhang, E., Kong, R., Zhang, Z. H., & Guo, R. H. (2015, Jun). Decreased expression of long noncoding RNA MEG3 affects cell proliferation and predicts a poor prognosis in patients with colorectal cancer. *Tumour Biol, 36*(6), 4851-4859. https://doi.org/10.1007/s13277-015-3139-2

You, L., Wang, N., Yin, D., Wang, L., Jin, F., Zhu, Y., Yuan, Q., & De, W. (2016, Apr). Downregulation of Long Noncoding RNA Meg3 Affects Insulin Synthesis and Secretion in Mouse Pancreatic Beta Cells. *J Cell Physiol, 231*(4), 852-862. https://doi.org/10.1002/jcp.25175

Yu, M., Bardia, A., Wittner, B. S., Stott, S. L., Smas, M. E., Ting, D. T., Isakoff, S. J., Ciciliano, J. C., Wells, M. N., Shah, A. M., Concannon, K. F., Donaldson, M. C., Sequist, L. V., Brachtel, E., Sgroi, D., Baselga, J., Ramaswamy, S., Toner, M., Haber, D. A., & Maheswaran, S. (2013, Feb 1). Circulating breast tumor cells exhibit dynamic changes in epithelial and mesenchymal composition. *Science, 339*(6119), 580-584. https://doi.org/10.1126/science.1228522

Zeisberg, E. M., Potenta, S., Xie, L., Zeisberg, M., & Kalluri, R. (2007, Nov 1). Discovery of endothelial to mesenchymal transition as a source for carcinoma-associated fibroblasts. *Cancer Res, 67*(21), 10123-10128. https://doi.org/10.1158/0008-5472.Can-07-3127

Zeisberg, E. M., Potenta, S. E., Sugimoto, H., Zeisberg, M., & Kalluri, R. (2008, Dec). Fibroblasts in kidney fibrosis emerge via endothelial-to-mesenchymal transition. *J Am Soc Nephrol, 19*(12), 2282-2287. https://doi.org/10.1681/asn.2008050513

Zeisberg, M., & Kalluri, R. (2004, Mar). The role of epithelial-to-mesenchymal transition in renal fibrosis. *J Mol Med (Berl), 82*(3), 175-181. https://doi.org/10.1007/s00109-003-0517-9

Zerbino, D. R., Achuthan, P., Akanni, W., Amode, M. R., Barrell, D., Bhai, J., Billis, K., Cummins, C., Gall, A., Giron, C. G., Gil, L., Gordon, L., Haggerty, L., Haskell, E., Hourlier, T., Izuogu, O. G., Janacek, S. H., Juettemann, T., To, J. K., Laird, M. R., Lavidas, I., Liu, Z., Loveland, J. E., Maurel, T., McLaren, W., Moore, B., Mudge, J., Murphy, D. N., Newman, V., Nuhn, M., Ogeh, D., Ong, C. K., Parker, A., Patricio, M., Riat, H. S., Schuilenburg, H., Sheppard, D., Sparrow, H., Taylor, K., Thormann, A., Vullo, A., Walts, B., Zadissa, A., Frankish, A., Hunt, S. E., Kostadima, M., Langridge, N., Martin, F. J., Muffato, M., Perry, E., Ruffier, M., Staines, D. M., Trevanion, S. J., Aken, B. L., Cunningham, F., Yates, A., & Flicek, P. (2018, Jan 4). Ensembl 2018. *Nucleic Acids Res, 46*(D1), D754-d761. https://doi.org/10.1093/nar/gkx1098

Zha, F., Qu, X., Tang, B., Li, J., Wang, Y., Zheng, P., Ji, T., Zhu, C., & Bai, S. (2019, Jun 13). Long non-coding RNA MEG3 promotes fibrosis and

inflammatory response in diabetic nephropathy via miR-181a/Egr-1/TLR4 axis. *Aging (Albany NY), 11*(11), 3716-3730. https://doi.org/10.18632/aging.102011

Zhan, R., Xu, K., Pan, J., Xu, Q., Xu, S., & Shen, J. (2017, Aug 26). Long noncoding RNA MEG3 mediated angiogenesis after cerebral infarction through regulating p53/NOX4 axis. *Biochem Biophys Res Commun, 490*(3), 700-706. https://doi.org/10.1016/j.bbrc.2017.06.104

Zhang, C. Y., Yu, M. S., Li, X., Zhang, Z., Han, C. R., & Yan, B. (2017, Jun). Overexpression of long non-coding RNA MEG3 suppresses breast cancer cell proliferation, invasion, and angiogenesis through AKT pathway. *Tumour Biol, 39*(6), 1010428317701311. https://doi.org/10.1177/1010428317701311

Zhang, J., Yao, T., Wang, Y., Yu, J., Liu, Y., & Lin, Z. (2016). Long noncoding RNA MEG3 is downregulated in cervical cancer and affects cell proliferation and apoptosis by regulating miR-21. *Cancer Biol Ther, 17*(1), 104-113. https://doi.org/10.1080/15384047.2015.1108496

Zhang, X., Martinez, D., Koledova, Z., Qiao, G., Streuli, C. H., & Lu, P. (2014, Sep). FGF ligands of the postnatal mammary stroma regulate distinct aspects of epithelial morphogenesis. *Development, 141*(17), 3352-3362. https://doi.org/10.1242/dev.106732

Zhang, X., Rice, K., Wang, Y., Chen, W., Zhong, Y., Nakayama, Y., Zhou, Y., & Klibanski, A. (2010, Mar). Maternally expressed gene 3 (MEG3) noncoding ribonucleic acid: isoform structure, expression, and functions. *Endocrinology, 151*(3), 939-947. https://doi.org/10.1210/en.2009-0657

Zhang, X., Zhou, Y., Mehta, K. R., Danila, D. C., Scolavino, S., Johnson, S. R., & Klibanski, A. (2003, Nov). A pituitary-derived MEG3 isoform functions as a growth suppressor in tumor cells. *J Clin Endocrinol Metab, 88*(11), 5119-5126. https://doi.org/10.1210/jc.2003-030222

Zhang, Y., Wu, J., Jing, H., Huang, G., Sun, Z., & Xu, S. (2019, Apr). Long noncoding RNA MEG3 inhibits breast cancer growth via upregulating endoplasmic reticulum stress and activating NF-κB and p53. *J Cell Biochem, 120*(4), 6789-6797. https://doi.org/10.1002/jcb.27982

Zhang, Y. Y., & Feng, H. M. (2017). MEG3 Suppresses Human Pancreatic Neuroendocrine Tumor Cells Growth and Metastasis by Down-Regulation of Mir-183. *Cell Physiol Biochem, 44*(1), 345-356. https://doi.org/10.1159/000484906

Zhang, Z., Wang, S., & Liu, W. (2018, Sep 10). EMT-related long non-coding RNA in hepatocellular carcinoma: A study with TCGA database. *Biochem Biophys Res Commun, 503*(3), 1530-1536. https://doi.org/10.1016/j.bbrc.2018.07.075

Zhao, J., Zhang, X., Zhou, Y., Ansell, P. J., & Klibanski, A. (2006). Cyclic AMP stimulates MEG3 gene expression in cells through a cAMP-response element (CRE) in the MEG3 proximal promoter region. *Int J Biochem Cell Biol, 38*(10), 1808-1820. https://doi.org/10.1016/j.biocel.2006.05.004

Zhao, T., Su, Z., Li, Y., Zhang, X., & You, Q. (2020, Sep 14). Chitinase-3 like-protein-1 function and its role in diseases. *Signal Transduct Target Ther, 5*(1), 201. https://doi.org/10.1038/s41392-020-00303-7

Zhao, X. Y., Li, W., Lv, Z., Liu, L., Tong, M., Hai, T., Hao, J., Guo, C. L., Ma, Q. W., Wang, L., Zeng, F., & Zhou, Q. (2009, Sep 3). iPS cells produce viable mice through tetraploid complementation. *Nature, 461*(7260), 86-90. https://doi.org/10.1038/nature08267

Zheng, X., Carstens, J. L., Kim, J., Scheible, M., Kaye, J., Sugimoto, H., Wu, C. C., LeBleu, V. S., & Kalluri, R. (2015, Nov 26). Epithelial-to-mesenchymal transition is dispensable for metastasis but induces chemoresistance in pancreatic cancer. *Nature, 527*(7579), 525-530. https://doi.org/10.1038/nature16064

Zheng, Y. Z., & Liang, L. (2018, Jun). High expression of PXDN is associated with poor prognosis and promotes proliferation, invasion as well as migration in ovarian cancer. *Ann Diagn Pathol, 34*, 161-165. https://doi.org/10.1016/j.anndiagpath.2018.03.002

Zhou, Y., Yang, H., Xia, W., Cui, L., Xu, R., Lu, H., Xue, D., Tian, Z., Ding, T., Cao, Y., Shi, Q., & He, X. (2020, Mar 1). LncRNA MEG3 inhibits the progression of prostate cancer by facilitating H3K27 trimethylation of EN2 through binding to EZH2. *J Biochem, 167*(3), 295-301. https://doi.org/10.1093/jb/mvz097

Zhou, Y., Zhong, Y., Wang, Y., Zhang, X., Batista, D. L., Gejman, R., Ansell, P. J., Zhao, J., Weng, C., & Klibanski, A. (2007, Aug 24). Activation of p53 by MEG3 non-coding RNA. *J Biol Chem, 282*(34), 24731-24742. https://doi.org/10.1074/jbc.M702029200

Zhu, W., Botticelli, E. K., Kery, R. E., Mao, Y., Wang, X., Yang, A., Wang, X., Zhou, J., Zhang, X., Soberman, R. J., Klibanski, A., & Zhou, Y. (2019, Jul 10). Meg3-DMR, not the Meg3 gene, regulates imprinting of the Dlk1-Dio3 locus. *Dev Biol*. https://doi.org/10.1016/j.ydbio.2019.07.005

Zhu, X., Wu, Y. B., Zhou, J., & Kang, D. M. (2016, Jan 8). Upregulation of lncRNA MEG3 promotes hepatic insulin resistance via increasing FoxO1 expression. *Biochem Biophys Res Commun, 469*(2), 319-325. https://doi.org/10.1016/j.bbrc.2015.11.048

9 Original publications

Paper I

frontiers in Cell and Developmental Biology

ORIGINAL RESEARCH
published: 16 June 2020
doi: 10.3389/fcell.2020.00461

Expression of ncRNAs on the DLK1-DIO3 Locus Is Associated With Basal and Mesenchymal Phenotype in Breast Epithelial Progenitor Cells

*Zuzana Budkova[1], Anna Karen Sigurdardottir[1], Eirikur Briem[1], Jon Thor Bergthorsson[2], Snævar Sigurdsson[1], Magnus Karl Magnusson[3], Gunnhildur Asta Traustadottir[1], Thorarinn Gudjonsson[1,2] and Bylgja Hilmarsdottir[1,4]**

[1] Stem Cell Research Unit, Biomedical Center, Department of Anatomy, Faculty of Medicine, School of Health Sciences, University of Iceland, Reykjavik, Iceland, [2] Department of Laboratory Hematology, Landspitali – University Hospital, Reykjavik, Iceland, [3] Department of Pharmacology and Toxicology, Faculty of Medicine, School of Health Sciences, University of Iceland, Reykjavik, Iceland, [4] Department of Pathology, Landspitali – University Hospital, Reykjavik, Iceland

OPEN ACCESS

Edited by:
Zuzana Koledova, Masaryk University, Czechia

Reviewed by:
Lone Rønnov-Jessen, University of Copenhagen, Denmark
Giulia Ricci, University of Campania Luigi Vanvitelli, Italy
Zhongxin Lu, Huazhong University of Science and Technology, China

***Correspondence:**
Bylgja Hilmarsdottir
bylgjah@landspitali.is

Specialty section:
This article was submitted to Stem Cell Research, a section of the journal Frontiers in Cell and Developmental Biology

Received: *12 December 2019*
Accepted: *18 May 2020*
Published: *16 June 2020*

Citation:
Budkova Z, Sigurdardottir AK, Briem E, Bergthorsson JT, Sigurdsson S, Magnusson MK, Traustadottir GA, Gudjonsson T and Hilmarsdottir B (2020) Expression of ncRNAs on the DLK1-DIO3 Locus Is Associated With Basal and Mesenchymal Phenotype in Breast Epithelial Progenitor Cells. Front. Cell Dev. Biol. 8:461. doi: 10.3389/fcell.2020.00461

Epithelial-to-mesenchymal transition (EMT) and its reversed process mesenchymal-to-epithelial transition (MET) play a critical role in epithelial plasticity during development and cancer progression. Among important regulators of these cellular processes are non-coding RNAs (ncRNAs). The imprinted DLK1-DIO3 locus, containing numerous maternally expressed ncRNAs including the lncRNA maternally expressed gene 3 (*MEG3*) and a cluster of over 50 miRNAs, has been shown to be a modulator of stemness in embryonic stem cells and in cancer progression, potentially through the tumor suppressor role of *MEG3*. In this study we analyzed the expression pattern and functional role of ncRNAs from the DLK1-DIO3 locus in epithelial plasticity of the breast. We studied their expression in various cell types of breast tissue and revisit the role of the locus in EMT/MET using a breast epithelial progenitor cell line (D492) and its isogenic mesenchymal derivative (D492M). Marked upregulation of ncRNAs from the DLK1-DIO3 locus was seen after EMT induction in two cell line models of EMT. In addition, the expression of *MEG3* and the maternally expressed ncRNAs was higher in stromal cells compared to epithelial cell types in primary breast tissue. We also show that expression of *MEG3* is concomitant with the expression of the ncRNAs from the DLK1-DIO3 locus and its expression is therefore likely indicative of activation of all ncRNAs at the locus. *MEG3* expression is correlated with stromal markers in normal tissue and breast cancer tissue and negatively correlated with the survival of breast cancer patients in two different cohorts. Overexpression of *MEG3* using CRISPR activation in a breast epithelial cell line induced partial EMT and enriched for a basal-like phenotype. Conversely, knock down of *MEG3* using CRISPR inhibition in a mesenchymal cell line reduced the mesenchymal and basal-like phenotype of the cell line. In summary our study shows that maternally expressed ncRNAs are markers of EMT and suggests that *MEG3* is a novel regulator of EMT/MET in breast tissue. Nevertheless, further studies are needed to fully dissect the molecular pathways influenced by non-coding RNAs at the DLK1-DIO3 locus in breast tissue.

Keywords: DLK1-DIO3 locus, *MEG3*, ncRNAs, epithelial plasticity, breast progenitor cells

INTRODUCTION

Breast cancer is the most common cancer in women and the second most common cancer overall (Ghoncheh et al., 2016). Despite major advances in diagnosis and treatment of cancer in recent years, metastasis and development of resistance to cancer therapies continues to be a challenge, causing over 90% of all cancer-related deaths (Ben-Jacob et al., 2012). A major contributing factor to metastasis and drug resistance is the heterogeneity and plasticity of the cells within tumors (Dagogo-Jack and Shaw, 2018). Epithelial-to-mesenchymal transition (EMT), is a developmental process that can be hijacked by cancer cells (Zeisberg and Kalluri, 2004; Moustakas and Heldin, 2007; Radisky et al., 2007). Generally, cells undergoing EMT, acquire increased migration and invasive properties and show increased resistance to apoptosis (Robson et al., 2006; Cao et al., 2016). Through these processes, EMT is considered a major mediator of phenotypic plasticity in cancer cells, metastatic formation and drug resistance (Mani et al., 2008; Scheel and Weinberg, 2012; Ansieau, 2013; Nieto et al., 2016; Lu and Kang, 2019). Recently, hybrid E/M (or partial EMT) cells have been shown to have even more metastatic and stem cell potential compared to the full epithelial or mesenchymal phenotype (Pastushenko et al., 2018). A reversed program, mesenchymal-to–epithelial transition (MET) is considered to facilitate colonization in secondary sites and reverse the plastic mesenchymal phenotype back to an epithelial state (Lu and Kang, 2019). This, however, is debated and further studies will increase our knowledge of the role of EMT/MET in cancer progression and metastasis.

EMT can be initiated through intrinsic factors such as expression of EMT related transcription factors (SNAI1, SNAI2, TWIST1, ZEB1, or ZEB2), cadherin switch from E-cadherin (CDH1) to N-cadherin (CDH2) or through epigenetic mechanisms. It can also be brought on by extrinsic factors derived from the microenvironment, such as secreted soluble factors: transforming growth factor-β (TGF-β), epidermal growth factor (EGF), fibroblast growth factors (FGFs), hepatocyte growth factor (HGF) or Wnt signaling factors (Moustakas and Heldin, 2007; Peinado et al., 2007; De Craene and Berx, 2013; Wang and Zhou, 2013; Williams et al., 2019).

Non-coding RNAs (ncRNAs) are among intrinsic regulators of EMT (Zaravinos, 2015). It is increasingly apparent that the ncRNAs are crucial in normal development and disease, but its mechanistic mode of action is largely unknown (Liz and Esteller, 2016). The two major classes of non-coding RNAs are long non-coding RNA (lncRNAs) and microRNA (miRNAs). Accumulating evidence suggests that lncRNAs function in a broad range of cellular processes such as cell growth, survival, migration, invasion and differentiation (Mercer et al., 2009; Sun et al., 2013; Di Gesualdo et al., 2014; Fatica and Bozzoni, 2014). LncRNAs are defined by the size of their transcripts and are longer than 200 nucleotides (nt), with no protein-coding function (Eades et al., 2014). Unlike microRNAs, lncRNAs are poorly conserved, but function in a regulatory network at the transcriptional, post-transcriptional, and translational level. miRNAs are 22 nt long RNA molecules that regulate expression post-transcriptionally primarily by binding to three prime untranslated region (3′UTR) of target genes (Bartel, 2009).

The imprinted DLK1-DIO3 locus located on chromosome 14 contains three paternally expressed protein-coding genes (*DLK1*, *RTL1*, *DIO3*) and numerous maternally expressed non-coding genes, including the lncRNA maternally expressed gene 3 (*MEG3*), and a cluster of over 50 miRNAs (Zhang et al., 2010; Dill and Naya, 2018; Baulina et al., 2019; Li et al., 2019).

The DLK1-DIO3 locus has been described as an important contributor to pluripotency and stemness in embryonic stem cells (ESCs) (Kaneko et al., 2014). It discriminates between mouse induced pluripotent stem cells (iPCS) and mouse ESCs, where genes from the locus were strongly repressed in iPSC clones compared to ES clones (Liu et al., 2010; Stadtfeld et al., 2010a). Furthermore, activation of maternally expressed genes from the locus is a strong indicator of the developmental potential of iPSC (Kang et al., 2009). miRNAs from the DLK1-DIO3 locus have been shown to promote pluripotency by inhibition of differentiation and stimulation of self-renewal in mouse ES cells (Moradi et al., 2017) and were found to be increased in tumor-originating cancer cells from lung adenocarcinoma (Valdmanis et al., 2015).

MEG3 is a potential tumor suppressor gene in several cancer types, mainly through the observation that *MEG3* expression is lower in various tumor tissues compared with non-tumor tissues of the same origin (Sheng et al., 2014; Sun et al., 2014, 2016; Yin et al., 2015; Chak et al., 2017; Molina-Pinelo et al., 2018). The tumor suppressor role of *MEG3* is ascribed to stabilization of p53 with inhibition of proliferation and promotion of apoptosis (Zhang et al., 2003, 2010; Zhou et al., 2007; Wang et al., 2012; Sun et al., 2016).

MEG3 was reported to positively regulate EMT in lung (Terashima et al., 2017) and ovarian (Mitra et al., 2017) cancer. Furthermore, *MEG3* has been shown to contribute to the development of osteosarcoma through increased migration, invasion and decreased apoptosis (Wang and Kong, 2018). Higher levels of *MEG3* were detected in plasma from colorectal cancer patients compared with non-cancerous controls (Liu et al., 2019).

D492 is a primary breast epithelial cell line, immortalized with the E6 and E7 oncogenes from the human papilloma virus 16 (Gudjonsson et al., 2002). Therefore, the p53 protein, which mediates the previously described tumor suppressor role of *MEG3*, is repressed in this cell line. D492 can generate both luminal and basal/myoepithelial cells in monolayer and 3D culture, expressing luminal or myoepithelial keratins such as keratin 19 and keratin 14, respectively. Furthermore, when D492 cells are co-cultured with endothelial cells, they, can generate spindle-shaped colonies with EMT phenotype. D492M (mesenchymal) was established from one such spindle-shaped colony (Sigurdsson et al., 2011). D492M is a phenotypically stable EMT cell line. It has lost epithelial markers such as keratins, E-cadherin and TP63, and gained expression of mesenchymal markers such as N-cadherin (Sigurdsson et al., 2011; Hilmarsdottir et al., 2015). D492M has acquired classical properties of cancer stem cells, such as increased CD44/CD24 ratio, anchorage independent growth, resistance to apoptosis

and increased migration/invasion (Sigurdsson et al., 2011). D492 serves as a model for branching morphogenesis and together D492 and D492M represent a unique EMT model of isogenic cell lines with an epithelial and mesenchymal phenotype, respectively (Briem et al., 2019b). The ability of D492 to undergo mesenchymal transition upon endothelial stimulation makes it a valuable cell model to study EMT induced by extrinsic factors, although it is important to note that neither D492 nor D492M are tumorigenic in mice.

In this study, we describe a new role for the DLK1-DIO3 locus in EMT and phenotypic plasticity of breast cells. Following EMT in breast epithelial cell lines, expression of the ncRNAs at the DLK1-DIO3 locus was increased. In addition, *MEG3* was highly expressed in stromal cells in breast tissue and its expression correlated with decreased survival in breast cancer. Moreover, increased expression of the ncRNAs at the DLK1-DIO3 locus in a breast epithelial progenitor cell line promoted cellular plasticity and induced partial EMT. Collectively, our study provides a further understanding of the role of the DLK1-DIO3 locus in cellular phenotype of breast cells and might provide important insight into novel therapeutic targets aimed at overcoming heterogeneity and therapy resistance in breast cancer.

MATERIALS AND METHODS

Cell Lines

Both D492 and D492M were cultured in H14 medium, as described previously (Gudjonsson et al., 2002; Sigurdsson et al., 2011) in flasks coated with collagen I (Advanced BioMFatrix, 5005-B). HEK-293T cell were cultured in Dulbecco's Modified Eagle Medium (DMEM), high glucose, GlutaMAX (TM), pyruvate (Gibco, 31966), supplemented with 10% Fetal bovine serum (FBS), penicillin and streptomycin (Gibco, 15140-122). Primary Human umbilical vein endothelial cells (HUVECs) were obtained from Landspitali, University Hospital in Reykjavik, Iceland, (with informed consent, approved by Landspitali Ethical Committee No. 35/2013), cultured in Endothelial Growth Medium 2 (EGM2) media (Lonza, CC-3162) supplemented with growth factors and 5% FBS, further referred to as EGM5 medium as previously described (Sigurdsson et al., 2011). HMLE (Elenbaas et al., 2001) is epithelial progenitor cell line, from which was derived mesenchymal cell line HMLEmes after stable induction of EMT-TF (Mani et al., 2008). HMLE and HMLEmes were cultured in chemically defined HMLE media, containing DMEM/F12 with penicillin and streptomycin and growth factors Insulin (Sigma, I1882) 10 μg/ml, EGF (Peprotech, AF-100-15) 10 ng/ml, Hydrocortisone (Sigma, H0888) 500 ng/ml.

Primary human luminal-epithelial cells (LEP), myoepithelial cells (MEP), breast endothelial cells (BRENCs) and fibroblast were isolated from breast reduction mammoplasties (with informed consent, approved by the Icelandic National Bioethics Committee VSN-13-057) as previously described (Sigurdsson et al., 2011) and maintained in chemically defined medium 3 (CDM3) and chemically defined medium 4 (CDM4) as previously described (Pechoux et al., 1999; Ingthorsson et al., 2010). All cells were maintained in an incubator with 5% CO_2 at 37°C.

3D Cultures/Mammosphere Assays

3D cultures were carried out in a 48-well plate format (Corning, 353078) in growth factor reduced reconstituted basement membrane rBM (further referred to as Matrigel, Corning, 354230). 5–10 × 10^3 cells were seeded in 150 μl of Matrigel per well. Plate was incubated in 5% CO_2 at 37°C for 15 min to solidify the Matrigel and then 300 μl of H14 media was added on top. The cells were grown for 3 weeks and pictures were taken on day 1, 7, 14, and 21. Cell culture media was changed three times per week. The colonies were quantified at day 14. The total number of cells was converted into percentage.

For co-culture experiments, 0.5 × 10^3 of the epithelial cells were co-cultured with 1 × 10^5 of endothelial cells (HUVECs) and were resuspended in 150 μl of Matrigel. Plate was incubated in 5% CO_2 at 37°C for 15 min to solidify the Matrigel and then 300 μl EGM5 media was added on top. HUVECs cultured in Matrigel are viable, however, quiescent, having supporting role in the epithelial cells' proliferation. The effect of *MEG3* was quantified by counting all colonies bigger than 100 μm.

Total RNAseq and Analysis of the Data

The gene microarray expression analysis from D492 and D492M was published previously from our group by Sigurdsson and colleagues (Sigurdsson et al., 2011) and the total RNA-sequencing comparing D492 and D492M was published by Halldorsson and colleagues (Halldorsson et al., 2017).

The RNA was extracted using Tri-Reagent (Thermo Fisher Scientific, AM9738) from 5 replicates for each cell line. Whole Transcriptome Sequencing of $D492M^{KD-CTRL}$ and $D492M^{KD-MEG3}$ was performed in deCODE genetics (Reykjavik, Iceland). RNA sequencing reads were mapped to the reference genome (Ensembl primary assembly, version GRCh38) using STAR version 2.6.1 (Dobin et al., 2013). The program htseq-count (Anders et al., 2015) was used to quantify how many reads match each gene in an annotation file (Ensemble version GRCh38.96). The data from htseq-count was imported into R (R Development Core Team, 2015) and differential expression (DE) analysis on $D492M^{KD-CTRL}$ vs $D492^{KD-MEG3}$ was performed using DESeq2 (Love et al., 2014). Prior to DE analysis, genes with expression less than two reads were discarded. *P*-values were corrected for multiple testing using the false discovery rate (FDR) method. To compare gene expression from $D492M^{KD-CTRL}$ vs $D492M^{KD-MEG3}$ a volcano plot was generated. *P* value cut-off of 0.05 was applied. Volcano plot over all data ($p < 0.05$) was made in R using the EnhancedVolcano package from BioConductor. The top ten most upregulated and downregulated genes according log2 fold change were labeled. Gene Set Enrichment Analysis (GSEA) was applied to identify enrichment of gene signatures. Comparative analysis was investigated using the "Hallmark" database. The list of significantly expressed pathways is presented as a bar plot.

Quantitative RT-PCR Analysis

Total RNA was extracted with Tri-Reagent (Thermo Fisher Scientific, AM9738). 1 μg of RNA of each sample was reverse transcribed into complementary DNA (cDNA), using Random

Hexamers (Thermo Fisher Scientific, N8080127) and SuperScript IV Reverse Transcriptase (Thermo Fisher Scientific, 18090-200) kit and subjected to quantitative real time PCR (qRT-PCR) using Sybr Green dye Luna® Universal qPCR Master Mix (NEB, M3003L) or TaqMan probes Luna® Universal Probe qPCR Master Mix (NEB, M3004L) according to manufacturer's protocol. *GAPDH* was used as control for gene expression. For assaying the relative expression of each gene, the $2^{-\Delta\Delta Ct}$ was determined using an ABI 7500 instrument (Applied Biosystems).

List of Primers

TaqMAN: *ZEB1* (Thermo Fisher Scientific, Hs00232783_m1), *ZEB2* (Thermo Fisher Scientific, Hs00207691_m1), *SNAI1* (Thermo Fisher Scientific, Hs00195591_m1), *SNAI2* (Thermo Fisher Scientific, Hs00950344_m1), *TWIST1* (Thermo Fisher Scientific, Hs01675818_s1), *GAPDH* (Thermo Fisher Scientific, 4326317E).

SYBR Green: *KRT14* (IDT, Hs.PT.58.4592110), *KRT19* (IDT,Hs.PT.58.4188708), *MEG3* ex 10-11 (IDT, Hs.PT.58.25190740), *GAPDH* (IDT, Hs.PT.39a.22214836), *KRT5* (IDT, Hs.PT.58.14446018), *TP63* (IDT, Hs.PT.58.2966111), *CDH3* (IDT, Hs.PT.58.39234242).

Small RNAseq

The Microarray of small RNA data was published previously by our group by Hilmarsdottir and colleagues (Hilmarsdottir et al., 2015) and the small RNAseq data was published previously by Briem and colleagues (Briem et al., 2019a).

miRNA qRT PCR

Total RNA was extracted with Tri-Reagent (Thermo Fisher Scientific, AM9738). The RNA was reverse transcribed using miRCURY LNA RT Kit (Qiagen, 339340) for cDNA synthesis reactions, according to manufacturer's protocol. Quantitative RT-PCR analysis of miRNAs was performed using miRCURY LNA SYBR Green PCR Kit (Qiagen, 339346), according to manufacturer's protocol. Gene expression levels were quantified using primers for: hsa-miR-127-3p (Qiagen, YP00204048), hsa-miR-409-3p (Qiagen, YP00204358), hsa-miR-411-5p (Qiagen, YP00204531), hsa-miR-493-3p (Qiagen, YP00204557). Normalization was done with U6 snRNA (Qiagen, YP00203907). The $2^{-\Delta\Delta Ct}$ was used determined using ABI 7500 instrument (Applied Biosystems) to calculate the relative expression of each gene.

Allele Specific Expression Analysis

Total RNA was extracted with Tri-Reagent (Thermo Fisher Scientific, AM9738) and reverse transcription done using 1 μg of DNase I-treated total RNA using random hexamers (Thermo Fisher Scientific, N8080127) and SuperScript II Reverse Transcriptase (Thermo Fisher Scientific, 18064022) according to the manufacturer's instructions. PCR primers were designed using Primer3 and Pyrosequencing primers were designed using PyroMark Assay Design 2.0 (Qiagen). The reverse PCR primer had a 5′-biotin modification and was HPLC-purified. Primers were synthesized by IDT 5′-TGGCCTTTTCTTCTCCTGAA, 5′-/5Biosg/TGACACATGGAAAGCACCAT and sequencing primer 5′-TCCGGGGTTACTGCCCT-3′. Polymerase chain reactions were performed in 50 μl using 10 ng of diluted cDNA or 10 ng of DNA, 1 U DreamTaq DNA polymerase (Fermentas, EP0701), 1X PCR buffer, 200 μM of dNTPs and 0,5 μM of each PCR primer. The following PCR protocol was used: 94°C for 2 min, followed by 50 cycles of 94°C for 1 min, 60°C for 1 min, 72°C for 1 min and 72°C for 9 min. To check the quality of the amplification, PCR products were analyzed by gel electrophoresis. Pyrosequencing were sequenced using the PyroMark Q24 system (Qiagen), following the manufacturer's instructions. For the ASE SNP, DNA and RNA (cDNA) were pyrosequenced simultaneously. The proportions of individual alleles for the SNP were obtained using the PyroMark Q24 software version 1.0.10 (Qiagen). Genomic DNA from D492M was examined to confirm the heterozygosity.

Clinical Cohort

RNA from breast cancer patients (diagnosed in the years 1987–2003) and relevant patient data was obtained from the Department of Pathology Landspitali – The National University Hospital of Iceland. Informed consent was obtained from patients involved in this study according to the national guidelines. The study was approved by The Icelandic Data Protection Commission (2001/523 and 2002/463) as well as the National Bioethics Committee of Iceland (VSN-11-105-V2). 119 samples were used in the study assigned to the following subgroup: 33 luminal A, 24 luminal B, 22 Basal, 12 ErbB2, 10 Normal and 18 not classified. cDNA was synthesized from 2 μg of total RNA using Random Hexamers primers (Thermo Fisher Scientific, N8080127) and RevertAid First Strand cDNA Synthesis Kit (Thermo Fisher). *MEG3* mRNA expression level was measured with the previously described qRT-PCR primers and TBP (Applied Biosystems, 4326322E) was used as a reference gene.

Western Blot Assay

Cells were washed with cold Phosphate Buffered Saline (PBS) and lysed in radio immunoprecipitation assay (RIPA) buffer with phosphatase and protease inhibitors (Halt Protease Inhibitor Cocktail, Thermo Fisher Scientific, 78430) for 10 min on ice and scraped with cell scraper. Protein concentration was measured using Bradford reagent (BioRad, 5000002). Equal amounts of protein (5–15 μg) were separated on 10% NuPage Bis-Tris gels (Invitrogen, NP0301PK2) with NuPage MES running buffer (Thermo Fisher Scientific, NP0002) and transferred with NuPage Transfer buffer (Thermo Fisher Scientific, NP0006-1) to polyvinylidene fluoride (PVDF) membranes Millipore Imobilion-FL transfer membrane, pore size 0,45 μM (Millipore, IPFL00010). The membranes were blocked with Odyssey Blocking buffer (TBS) (LiCor, 927-500) and incubated with primary antibodies overnight at 4°C. List of antibodies: keratin 14 (KRT14; Abcam, Ab15461), keratin 19 (KRT19; Abcam, Ab7754), P-cadherin (CDH3; Cell signaling, CS2130), tumor protein p63 (TP63, Abcam, Ab124762), keratin 5/6 (KRT5/6; Invitrogen, 180267), Actin (Licor, 926-42212). Actin was used as loading control. Secondary antibodies were mouse or rabbit IRDey (Li-Cor

926-32213, 926-32212, respectively) used at 1:10.000 for 1 h at room temperature (RT) and detected and quantified using the Odyssey Infrared Imaging System (Li-Cor Fluorescent signal was detected by Odyssey image system (Li-Cor) and converted to gray scale.

Cell Migration Assay

Cell migration was examined by using trans-well Boyden chambers with 8 μm pore size (Corning, 353097). Briefly, 3×10^3 cells were resuspended in 250 μl H14 medium and seeded on the trans-well inserts in 24-well plate (Corning, 353047). H14 media with 10% FBS was added to the lower chamber, below filter. Cells were incubated for 48 h in 5% CO_2 at 37°C. Non-migratory cells from the upper part of the filter were removed with cotton swab and washed 3 times with 1× PBS. The filters were then fixed with methanol and stained with DAPI (Sigma, D9542-1MG). Cells were photographed in three random fields EVOS FL Auto 2 imaging system (ThermoFisher). Pictures were analyzed with ImageJ Software.

Low Attachment Assay

Anchorage independent growth was examined using 24-well ultra-low attachment plates (Corning, 3473). Briefly, D492 and D492M cells were single cell filtered and 500 cells/well were seeded into EGM5 media and cultured for 9 days. The growth of colonies was quantified under the microscope, counting all the colonies bigger than 40 μm.

Apoptosis Assay

Resistance to chemically induced apoptosis was examined by inducing the cells with 10 μM camptothecin [CPT, Sigma-Aldrich, C9911)] in 96-well plate format (Corning, 353072). and quantified using IncuCyte Caspase-3/7 Reagents (Essen Bioscience, 4440) on IncuCyte Zoom (Essen Bioscience) according to the manufacturer's instructions.

Lentivirus Packaging and Transfection

The packaging of lentiviral expression constructs into pseudoviral particles, was performed with the psPAX2 (Addgene, 12260) and PMDG.2 (Addgene, 12259) plasmids using Turbofect (Thermo Fisher Scientific, R05319) in HEK-293T cells. The supernatant was harvested after 48 and 72 h and filtered through 0,45 μm pore filter. For infection, cells were plated on T25 flasks, so they were 70–80% confluent following day and were infected with 1 ml of viral particles and 1 ml of fresh media in the presence of 8 μg/ml polybrene. Lentivirus-transduced cells were selected with antibiotics or sorted by FACS (Sony SH800), based on fluorescent dye to obtain stable pool of clones. The altered expression of *MEG3* was determined by qRT-PCR.

The list of lentiviral expression constructs (plasmids) used in the study and their selection marker (with final concentration in case of antibiotics): pLenti_sgRNA(MS2)_zeo (Zeocin Invitrogen 4 μl/ml), pLenti_dCas9-VP64_Blast (Blasticidin, 2 μg/ml), pLenti_dCas9-KRAB_mCherry (mCherry fluorescence), SAM MS2-P65-HSF1 Plasmids (Hygromycin 1 μl/ml).

CRISPRi/CRISPRa

To perform CRISPRi and CRISPRa, two vectors were used. First, vector with dCAS9 with effector domain KRAB (pLenti_dCas9-KRAB_mCherry, Genscript) and VP64 (pLenti_dCas9-VP64_Blast, Genscript) effector domain for CRISPRi and CRISPRa, respectively, was incorporated, using lentiviral transfection. Subsequently, vector with designed gRNA targeting specific site of our gene of interest *MEG3* was incorporated, in second round of lentiviral transfection. In case of gain of function studies with CRISPRa, one additional helper plasmid SAM (SAM MS2-P65-HSF1 Plasmids, Genscript) was used to further increase activation.

The sequence of gRNA for overexpression of *MEG3*: Guide 1: GCTCTCCGCCGTCTGCGCTA, the sequence of gRNA for downregulation of *MEG3*: Guide 2: GCGGGTGAGGGATCCTCTCGT, the sequence of gRNA for negative control: GCTTAGTTACGCGTGGACGA were cloned into pLenti_sgRNA(MS2)_zeo (Genscript).

Statistical Analysis

Statistical differences of qRT-PCRs (**Figures 1E,F**, **Figures 5A,B**, and **Figures 7A–C**) and functional assay (**Figures 8B–E**) between samples were assessed with unpaired Student *t*-test. Statistical differences in **Figure 8A** was calculated using multiple unpaired Student *t*-test per row. Statistical differences of quantifications of western blots (**Figures 7B,C**) among samples were assessed using one-way ordinary ANOVA, followed by Tukey's multiple comparison test. Statistical differences in **Figure 4A** (left) was calculated using Kruskal Wallis Test (one-way ANOVA on ranks). Statistical analysis of qRT-PCRs in **Figure 2** were assessed with One-way ANOVA with Dunnett's multiple comparisons test. All statistical analyses were performed in GraphPad Prism. *P*-values below 0,05 were considered significant ($^*p \leq 0.05$; $^{**}p \leq 0.01$; $^{***}p \leq 0.001$; $^{****}p \leq 0.0001$).

RESULTS

MEG3 Is Highly Expressed in Cell Lines With a Mesenchymal Phenotype and in the Stromal Compartment of Breast Tissue

D492 and D492M are isogenic cell lines with stem cell and mesenchymal properties, respectively. D492 cells acquire cuboidal shape in 2D culture, and form branching structures in 3D culture, akin to terminal duct lobular units (TDLU) in the breast. In contrast, D492M is elongated and spindle-shaped in 2D culture and in 3D culture it forms irregular mesenchymal-like colonies (**Figure 1A**). We have previously shown that MIR203a and the MIR200 family are downregulated in D492M and their expression is essential for the epithelial phenotype (Hilmarsdottir et al., 2015; Briem et al., 2019a). Of miRNAs upregulated in D492M, the miRNAs at the DLK1-DIO3 locus are prominent. A microarray analysis of miRNA expression demonstrated that 15 of the 25 most highly expressed miRNAs in D492M compared to D492 belong to the DLK1-DIO3

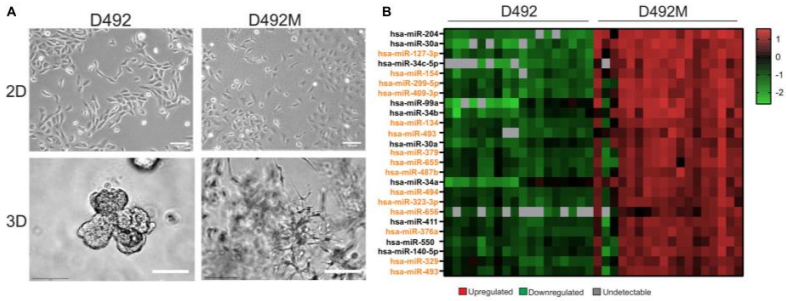

C

	lncRNA ID	D492M vs D492 - Fold change	D492M vs D492 FDR p-value correction	D492 - Normalized expression values	D492M - Normalized expression values
1	*HIF1A-AS2*	304.7	0.000	0.08	23.49
2	*MIR381HG*	217.3	0.077	0.04	8.38
3	*MIR155HG*	207.7	0.092	0.04	8.01
4	*RP11-175K6.1*	68.1	0.347	0.08	5.25
5	*LINC01551*	45.8	0.000	0.69	31.76
6	*RP11-102K13.5*	38.3	0.043	0.27	10.34
7	*MEG3*	17.9	0.000	10.64	190.67
8	*AC016831.7*	16.3	0.253	0.42	6.89
9	*MEG8*	12.0	0.000	5.05	60.60
10	*CASC19*	11.1	0.095	0.93	10.29

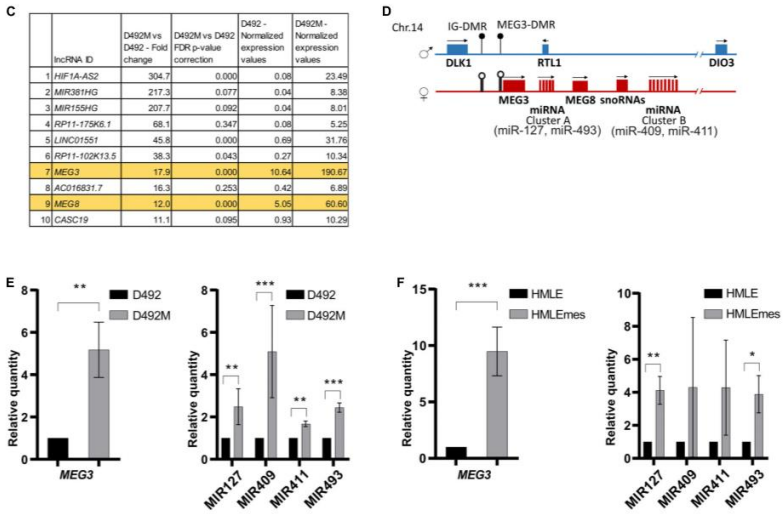

FIGURE 1 | The DLK1-DIO3 locus is upregulated in breast epithelial stem cells undergoing EMT. **(A)** D492 and D492M generate branching and mesenchymal structures in 3D culture, respectively. In 2D culture, D492 is cuboidal in shape and D492M is more spindle shaped. Scale bar = 100 μm. **(B)** Majority of the top upregulated miRNAs in D492M are from the DLK1-DIO3 locus. Microarray heat map showing top 25 upregulated miRNAs in D492M compared to D492. 15 of them are from the DLK1-DIO3 locus (highlighted in orange). **(C)** LncRNAs from the DLK1-DIO3 locus are among the most upregulated in D492M. RNAseq data showing top ten differentially expressed lncRNA, with lncRNAs from DLK1-DIO3 locus (*MEG3* and *MEG8*) highlighted in orange. **(D)** Schematic figure of the DLK1-DIO3 locus. The DLK1-DIO3 locus is located on chromosome 14 and is imprinted. It contains three paternally expressed protein coding genes (*DLK1*, *RTL1*, and *DIO3*) and many maternally expressed non-coding genes, among them lncRNAs (*MEG3* and *MEG8*) and over 50 miRNAs, among them MIR127 and MIR493 located in cluster A and MIR409 and MIR411 located in cluster B and numerous C/D-box-containing small nucleolar RNAs (snoRNAs). DMR – differentially methylated region, filled circles represent methylated DMRs, and unfilled represent unmethylated DMRs. **(E)** Upregulation of selected ncRNA from the DLK1-DIO3 locus verified with qRT-PCR. Graphs showing higher expression of *MEG3* in D492M compared to D492 (left) and higher expression of four representative miRNAs (MIR127, MIR493, MIR409, and MIR411) at the DLK1-DIO3 locus in D492M compared to D492 (right). Results shown as mean ± SD. Unpaired *t*-test was used to test significance: $^{**}p \leq 0.01$; $^{***}p \leq 0.001$; $n = 3$. **(F)** ncRNAs from the DLK1-DIO3 locus are upregulated in HMLEmes. qRT-PCR showing higher expression of *MEG3* and representative miRNAs (MIR127, MIR493, MIR409, and MIR411) from DLK1-DIO3 locus in HMLEmes compared to HMLE. Results shown as mean ± SD. Unpaired *t*-test was used to test significance: $^{*}p \leq 0.05$; $^{**}p \leq 0.01$; $^{***}p \leq 0.001$; $n = 3$.

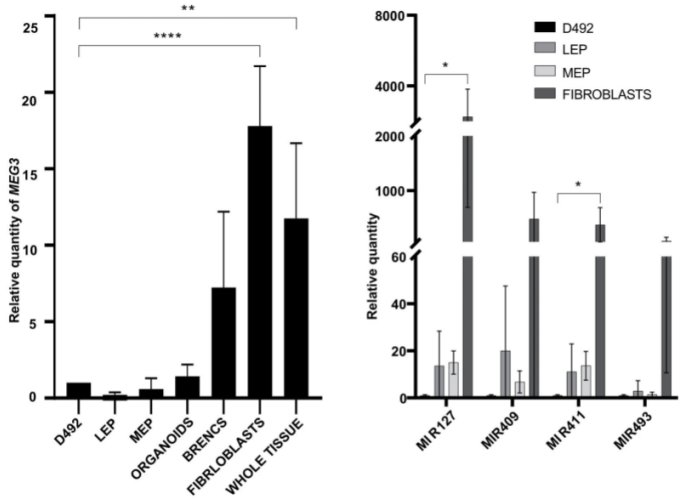

FIGURE 2 | The ncRNA from the DLK1-DIO3 locus are highly expressed in stromal cells and whole tissue compared to epithelial cells. qRT-PCR showing *MEG3* expression is higher in breast stromal cells (fibroblasts) and whole tissue than in D492 (left). (LEP – luminal epithelial cells, MEP – myoepithelial cells, BRENCs – breast endothelial cells). Results shown as mean ± SD. One-way ANOVA with Dunnett's multiple comparisons test was used to test significance: $^{**}p \leq 0.01$; $^{****}p \leq 0.0001$; $n = 3$. Expression of representative miRNAs MIR127 and MIR411 at the DLK1-DIO3 locus is higher in breast fibroblast than in D492 (right). LEP – luminal epithelial cells, MEP - myoepithelial cells. Results shown as mean ± SD. One-way ANOVA with Dunnett's multiple comparisons test was used to test significance: $^{*}p \leq 0.5$; $n = 3$.

locus (**Figure 1B**). Furthermore, small RNA sequencing revealed that 33 of the miRNAs belonging to the DLK1-DIO3 miRNA cluster have more than 1,5-fold increased expression in D492M compared to D492 (**Supplementary Figure 1**). Moreover, total RNA sequencing of D492 and D492M, revealed that *MEG3* and *MEG8* are amongst the most upregulated lncRNAs in D492M (**Figure 1C**). The non-coding part of the DLK1-DIO3 locus consists of maternally expressed lncRNAs *MEG3* and *MEG8* and miRNAs grouped into two clusters (**Figure 1D**). To confirm the sequencing results, we selected four representative miRNAs from the DLK1-DIO3 locus, two from each cluster (MIR127 and MIR493 from cluster A, MIR409 and MIR411 from cluster B). These miRNAs as well as the lncRNA *MEG3* had higher expression, as revealed by qRT-PCR, in D492M compared to D492 (**Figure 1E**). In another isogenic EMT cell model, HMLE (epithelial) and HMLEmes (mesenchymal variant) both *MEG3* and the representative miRNAs were more highly expressed in HMLEmes compared to HMLE (**Figure 1F**). Thus, our data suggests that increased *MEG3* expression is not a stochastic event but consistently associates with EMT induction in breast epithelial cell lines.

Next, we analyzed the expression of *MEG3* and miRNAs from the DLK1-DIO3 locus in primary cells from three healthy donors. We found that the expression of *MEG3* is higher in purified stromal cells (fibroblasts) than in epithelial cells (D492, luminal epithelial cells, myoepithelial cells and organoids; **Figure 2**, left). Interestingly, expression of *MEG3* in whole breast tissue lysates is closer to fibroblast expression levels than epithelial cells (**Figure 2**, left). This finding is most likely explained by the richness of stroma in normal breast tissue, whereas organoids contain only the epithelial cells. A similar pattern is seen with the four representative miRNAs, where MIR127 and MIR411 have higher expression in fibroblasts compared to their expression in D492 (**Figure 2**, right).

We next acquired a list of genes correlated the expression of MEG3 using the GOBO (Gene expression-based Outcome for Breast Cancer Online) dataset and submitted the list to DAVID (the database for annotation, visualization and integrated discovery, version 6.7) (Huang et al., 2009a,b) to identify pathways associated with *MEG3*. Herein, the expression of *MEG3* correlates with expression of extracellular matrix genes, which are in line with the observations of a high expression of *MEG3* in cells found in the stromal compartment (**Supplementary Figure 2A**). Using analysis of publicly available NGS data using MiPanda (Niknafs et al., 2018) we found positive correlation of *MEG3* with

common EMT markers in normal breast and breast cancer (**Supplementary Figure 2B**). Many of these have a correlation coefficient > 0.3 (Spearman correlation) which is considered a fair positive correlation (Chan, 2003). Interestingly, even more genes are positively correlated to *MEG3* expression in breast cancer as compared to normal breast tissue (**Supplementary Figure 2B**).

Collectively, the lncRNA *MEG3* and miRNAs from DLK1-DIO3 locus are highly expressed in the mesenchymal compartment compared to epithelial breast tissue and their expression positively correlate with numerous mesenchymal genes and EMT markers.

MEG3 Is Imprinted in Both D492 and D492M

The DLK1-DIO3 locus is imprinted and regulated by DNA methylation (Cui et al., 2018). Using pyrosequencing (Harrington et al., 2013) covering a heterozygous SNP (C/T) in *MEG3* (rs4906024) we confirmed monoallelic expression of *MEG3* in both D492 and D492M, with expression in both cell lines being from the T allele (**Figure 3**). As both cell lines are diploid at the *MEG3* locus on a DNA level a C/T ratio of 50% is expected which is consistent with the 48% C-allele prominence observed. On the mRNA deviation from expected monoallelic expression was not detected as results showed zero C allele expression in D492 and 2% in D492M. Hence, increased expression of *MEG3* in D492M is not caused by loss of imprinting. The expression remains monoallelic confirming that the increased expression originates from the non-imprinted allele.

Increased Expression of *MEG3* Is Negatively Correlated With Survival of Breast Cancer Patients

EMT has been suggested to promote metastatic behavior of epithelia-originating cancer (Felipe Lima et al., 2016) and, in addition, our data shows association of *MEG3* expression with the mesenchymal phenotype. We therefore investigated *MEG3* expression levels in different subtypes of breast cancer. We have evaluated the expression of *MEG3* in clinically well-defined breast tumors. Herein, normal like (NL) breast tumors had significantly higher expression of *MEG3* with a *p*-value of 0.0003 (**Figure 4A**, left). Survival analysis of all tumor samples showed reduced, but not significant overall survival in patients with high *MEG3* expression. However, as the normal-like tumors have in recent years been subjected to scrutiny as a possible misclassification due to low tumor cellularity and thus, high proportion of normal tissue. In light of our results showing high expression of *MEG3* in breast stromal tissue, and uncertainty that measured *MEG3* expression in the normal-like subgroup is representative of the primary tumor, we omitted NL breast tumors from the survival analysis (Elloumi et al., 2011; Prat and Perou, 2011; Yersal and Barutca, 2014). The results show significant worse overall survival of patients with high *MEG3* expression (**Figure 4A**, right). Corroborating our findings, using the GOBO database (Ringnér et al., 2011)[1], we found that high *MEG3* expression reduces distant metastasis free

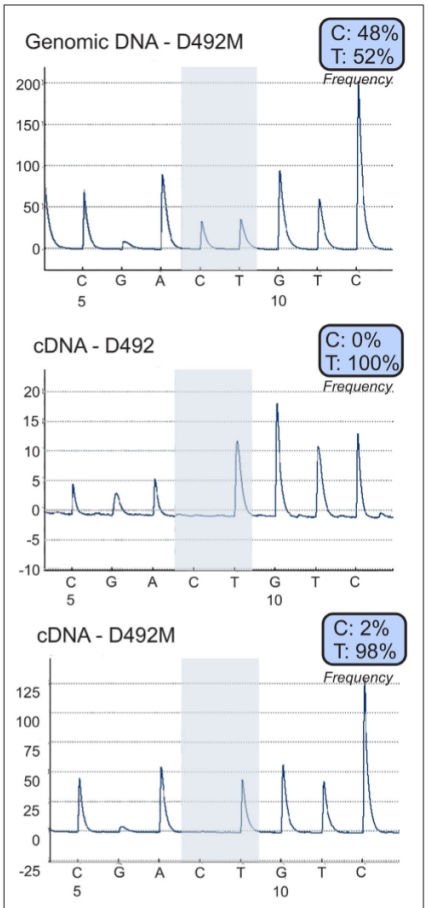

FIGURE 3 | Increased expression of *MEG3* in D492M is not caused by loss of imprinting. Allele specific expression analysis using pyro-sequencing shows that the increased expression of *MEG3* in D492M is not caused by loss of imprinting, but increased expression of the already expressed allele, the expression remains mono-allelic. Analyzed sequence: GAGCAC/TGTCCCA.

[1] http://co.bmc.lu.se/gobo/

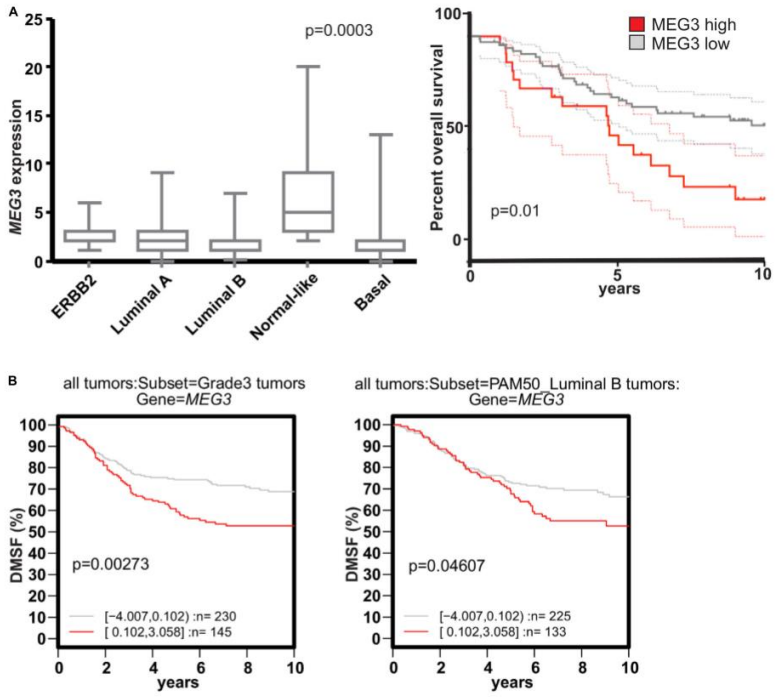

FIGURE 4 | *MEG3* expression negatively correlates with breast cancer prognosis. **(A)** High *MEG3* expression decreases overall survival in breast tumors. qRT-PCR shows that *MEG3* expression (Numbers of tumors per group: ErBB2 = 12, Luminal A = 33, Luminal B = 24, Normal = 10, Basal = 22) is significantly higher in normal-like (NL) breast cancer (left; $p = 0.0003$). High MEG3 expression is correlated with low overall patient survival (NL tumors omitted). Kruskal Wallis Test (or one-way ANOVA on ranks) was used to test the significance (right; $p = 0.01$). **(B)** High *MEG3* expression decrease distant metastasis free survival in grade three and Luminal B type tumors. Kaplan-Meier plot showing data from the online GOBO database: high expression of *MEG3* decrease DMSF (distant metastasis free survival), of poorly differentiated (grade 3) tumors (left; $p = 0.00373$) and luminal B type tumor (right; $p = 0.04607$).

survival (DMSF) of patients with poorly differentiated (grade 3) tumors (**Figure 4A**, left) and patients with luminal B tumors (**Figure 4B**, right).

Increased Expression at the DLK1-DIO3 Locus Contributes to the Basal and Mesenchymal Phenotype

To explore the functional role of *MEG3* in D492 and D492M, we established sublines with altered expression of *MEG3*. Using the CRISPRa approach (Cheng et al., 2013), we generated a D492 cell line with stable overexpression of *MEG3* ($D492^{MEG3}$). A control cell line was generated using a scrambled sgRNA ($D492^{CTRL}$). Furthermore, we used the CRISPRi approach (Gilbert et al., 2013; Qi et al., 2013), to generate knockdown of *MEG3* in D492M ($D492M^{KD-MEG3}$) and a control cell line was generated using scrambled sgRNA ($D492M^{KD-CTRL}$). The increase of *MEG3* expression was about seven-fold in $D492^{MEG3}$ compared to $D492^{CTRL}$ as determined by qRT-PCR (**Figure 5A**, left). Downregulation of *MEG3* in $D492M^{KD-MEG3}$ was more prominent, with about 20-fold reduced expression compared to $D492M^{KD-CTRL}$ (**Figure 5A**, right). Having established stable overexpression and downregulation of *MEG3* in D492 and D492M, we re-evaluated the epithelial/mesenchymal phenotypes of D492 and D492M, respectively. Based on phase contrast images, no obvious

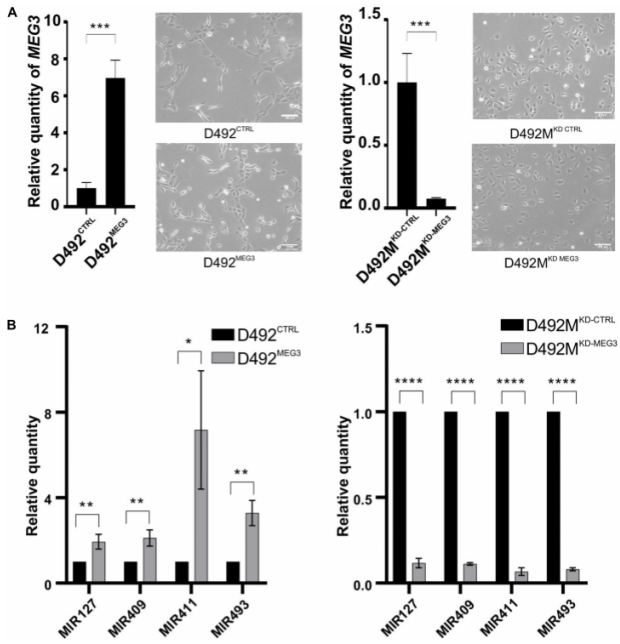

FIGURE 5 | Concomitant expression of non-coding RNAs from DLK-DIO3 locus with *MEG3*. **(A)** Overexpression and knock-down of *MEG3* in D492 and D492M, respectively. qRT-PCR confirming upregulation of *MEG3* in D492 ($D492^{MEG3}$) compared to D492 with scrambled control ($D492^{CTRL}$; left). Phase contrast pictures of $D492^{CTRL}$ and $D492^{MEG3}$ (below). qRT-PCR confirming knock-down of *MEG3* in D492M ($D492M^{KD-MEG3}$) compared to D492M with scrambled control ($D492M^{KD-CTRL}$; right). Results shown as mean ± SD. Unpaired *t*-test was used to test significance: ***$p \leq 0.001$; ****$p \leq 0.0001$; $n = 3$. Phase contrast pictures of $D492M^{KD-CTRL}$ and $D492M^{KD-MEG3}$ (below). Scale bar = 100 μm. **(B)** miRNAs form the DLK1-DIO3 locus are upregulated with overexpression of *MEG3* and downregulated with knock-down of *MEG3*. qRT-PCR shows increased expression of four representative miRNAs from the DLK1-DIO3 locus in $D492^{MEG3}$ compared to $D492^{CTRL}$ (left) and their decreased expression in $D492M^{KD-MEG3}$ compared to $D492M^{KD-CTRL}$ (right). Results shown as mean ± SD. Unpaired *t*-test was used to test significance: *$p \leq 0.05$ **$p \leq 0.01$; ****$p \leq 0.0001$; $n = 3$.

difference in phenotype could be seen between $D492^{MEG3}$ and $D492^{CTRL}$ or $D492M^{KD-MEG3}$ and $D492M^{KD-CTRL}$ (**Figure 5A**, below). Interestingly, expression of the representative miRNAs located on the DLK1-DIO3 locus is increased in $D492^{MEG3}$ compared to $D492^{CTRL}$, to similar levels as seen in D492M (**Figure 5B**, left). Conversely, the expression of representative miRNAs is downregulated in $D492M^{KD-MEG3}$ compared to $D492M^{KD-CTRL}$ (**Figure 5B**, right). Thus, it appears, that the expression of miRNAs from the DLK1-DIO3 locus is concomitant with *MEG3* expression. To test, if that holds true, we used the cBioPortal and explored correlation of *MEG3* with miRNAs using data on invasive breast cancer from the Cancer Genome Atlas (TCGA) (Cancer Genome Atlas Network, 2012) we found that of 40 miRNAs that had positive correlation over 0,3 (Person score) with *MEG3*, 30 were located at the DLK1-DIO3 locus (with other miRNAs from the locus not being in the dataset; **Table 1**). This suggests that *MEG3* may be used as a marker for the expression of ncRNAs from the DLK1-DIO3 locus.

Next, we conducted RNA sequencing of our cell lines with stably altered expression levels of *MEG3* focusing on the analysis of $D492M^{KD-CTRL}$ vs $D492M^{KD-MEG3}$. There were 1235 significantly differentially expressed genes, with symmetric distribution over genes downregulated and upregulated in $D492M^{KD-MEG3}$, shown in the volcano plot ($p < 0.05$; **Supplementary Figure 3A**), with the list of top 30 up and down-regulated genes in $D492M^{KD-MEG3}$ (**Supplementary Figure 3B**). To identify unifying biological them from RNA-sequencing data, we performed Gene Set enrichment analysis (GSEA).

TABLE 1 | MiRNAs from the DLK1-DIO3 locus positively correlate with *MEG3* expression.

Correlated gene	Location	Pearson score	*P*-value	Spearman score	*P*-value
MIR-154/154*	Chr14	0.49	7.46E−20	0.44	1.27E−15
MIR-134/134	Chr14	0.48	2.09E−18	0.44	1.22E−15
MIR-199B/3P	Chr9	0.47	4.66E−18	0.47	8.03E−18
MIR-199A-1/3P; MIR-199A-2/3P#	Chr19; Chr1	0.47	4.66E−18	0.47	8.15E−18
MIR-127/3P	Chr14	0.46	4.18E−18	0.45	3.89E−16
MIR-136/136	Chr14	0.46	1.08E−16	0.41	2.15E−13
MIR-431/431*	Chr14	0.46	7.09E−17	0.39	5.23E−12
MIR-539/539	Chr14	0.44	1.66E−15	0.43	1.21E−14
MIR-199A-1/5P; MIR-199A-2/5P#	Chr19; Chr1	0.43	1.14E−14	0.39	2.18E−12
MIR-382/382	Chr14	0.42	1.53E−14	0.41	2.71E−13
MIR-199B/5P	Chr9	0.42	2.47E−14	0.40	1.06E−12
MIR-214/214*	Chr1	0.42	6.45E−14	0.39	4.35E−12
MIR-409/3P	Chr14	0.42	3.41E−14	0.37	3.34E−11
MIR-369/3P	Chr14	0.41	1.06E−13	0.37	5.93E−11
MIR-127/5P	Chr14	0.41	1.46E−13	0.36	9.70E−16
MIR-495/495	Chr14	0.4	1.07E−12	0.39	3.84E−12
MIR-758/758	Chr14	0.4	3.97E−13	0.36	1.09E−10
MIR-381/381	Chr14	0.39	3.10E−12	0.39	2.80E−12
MIR-485/3P	Chr14	0.39	2.12E−12	0.39	5.07E−12
MIR-125B-1/125B; MIR-125B-2/125B#	Chr11; Chr21	0.39	3.92E−12	0.37	6.52E−11
MIR-337/3P	Chr14	0.39	1.80E−12	0.37	7.17E−11
MIR-493/493*	Chr14	0.38	1.15E−11	0.37	2.83E−11
MIR-369/5P	Chr14	0.38	1.68E−11	0.33	2.98E−11
MIR-379/379	Chr14	0.37	5.82E−11	0.33	4.49E−09
MIR-370/370	Chr14	0.37	2.51E−11	0.32	1.29E−08
MIR-214/214	Chr1	0.36	1.88E−10	0.35	5.19E−10
MIR-708/708	Chr11	0.35	4.91E−10	0.35	3.60E−10
MIR-432/432	Chr14	0.35	5.39E−10	0.32	1.80E−08
MIR-409/5P	Chr14	0.35	3.48E−10	0.31	6.03E−08
MIR-323/3P	Chr14	0.35	6.01E−10	0.30	1.65E−07
MIR-376C/376C	Chr14	0.34	1.40E−09	0.35	7.42E−10
MIR-889/889	Chr14	0.34	1.57E−09	0.30	1.50E−07
MIR-493/493	Chr14	0.34	1.07E−09	0.29	5.38E−07
MIR-487B/487B	Chr14	0.33	7.98E−09	0.30	1.50E−09
MIR-655/655	Chr14	0.33	6.70E−09	0.30	1.90E−07
MIR-410/410	Chr14	0.33	4.36E−09	0.29	5.07E−07
MIR-184/184	Chr15	0.31	3.50E−08	0.34	2.68E−09
MIR-411/411	Chr14	0.31	2.83E−08	0.29	3.79E−07
MIR-654/3P	Chr14	0.31	3.64E−08	0.26	4.37E−06
MIR-22/22	Chr17	0.3	1.66E−07	0.29	2.72E−07

Out of 40 miRNAs that positively correlate with MEG3 in breast cancer (with correlation over 0.3), 30 are from the DLK1-DIO3 locus, highlighted in orange (TCGA, Nature 2012 data set). #Due to sequence similarities, these two miRNAs are indistinguishable in the sequencing data used.

These gene sets consist of the defined gene lists, based on biological knowledge about biochemical pathways and co-expression data. Using the Hallmark dataset, one of the significantly, downregulated set of genes in D492M$^{KD-MEG3}$ was the epithelial-mesenchymal transition gene set, with normalized enrichment score (NES) of −2.03 and False discovery rate (FDR) q = 0.023 (**Figure 6A**). These genes define epithelial-mesenchymal transition, as in wound healing, fibrosis and metastasis. The genes belonging to this gene set are overrepresented toward the top of the ranked list, based on fold change of D492M$^{KD-CTRL}$ vs D492M$^{KD-MEG3}$ (**Figure 6B**, right). A manually curated list of mesenchymal genes from the Hallmark EMT dataset that are downregulated in D492M$^{KD-MEG3}$ is shown in **Figure 6B**, left. Further analysis of the RNA sequencing data of D492M$^{KD-MEG3}$ vs D492M$^{KD-CTRL}$, using common literature-based markers of breast tissue has showed that luminal epithelial markers *GATA3* and *MUC1* are upregulated, while myoepithelial *KRT14*, mesenchymal *VIM*, *ZEB2*, *SNAI2*, *LAMA1*, *CDH2*, and stem cell *MME*, *CTNNB1* are downregulated with knock down of *MEG3* (**Figure 6C**).

Expression of mesenchymal and basal markers was additionally confirmed on RNA level by qRT-PCR and on protein level western blot. Most of the core EMT-related transcription factors (EMT-TF) were affected by *MEG3*. D492^{MEG3} has increased expression of *SNAI2* compared to D492^{CTRL} (**Figure 7A**, left). On the other hand, D492M$^{KD-MEG3}$ has decreased expression of *SNAI2*, *ZEB1*, *ZEB2* and *TWIST1* compared to D492M$^{KD-CTRL}$ (**Figure 7A**, right). Luminal cytokeratin 19 (*KRT19*) and basal/myoepithelial cytokeratin 14 (*KRT14*) are also affected by manipulation of *MEG3* expression levels. Thus, D492^{MEG3} shows increased *KRT14* and decreased *KRT19* expression compared to D492^{CTRL} on both mRNA (**Figure 7B**, left) and protein level (**Figure 7C**, left). D492M$^{KD-MEG3}$ shows decreased *KRT14* expression compared to D492M$^{KD-CTRL}$ (**Figure 7B**, right). Furthermore, D492^{MEG3} shows increased expression of other myoepithelial markers such as *CDH3* (P-cad), *TP63* or *KRT5* compared to D492^{CTRL} as determined both at mRNA (**Figure 7D**, left) and protein level (**Figure 7E**). Also, D492M$^{KD-MEG3}$ shows decreased expression of myoepithelial markers *KRT5* on mRNA level (**Figure 7D**, right) and of TP63 on protein level (**Figure 7E**, middle) compared to D492M$^{KD-CTRL}$. This suggests that *MEG3* expression induces a shift toward a basal/myoepithelial phenotype. However, our cell lines with stably altered expression of *MEG3* do not show a significant switch in E-cadherin (CDH1) to N-cadherin (CDH2) expression (**Supplementary Figure 4**), which may explain why there are no clear changes in morphology.

MEG3 Induces Mesenchymal Properties and Stemness

As *MEG3* has previously been ascribed to have a role in pluripotency and stemness (Stadtfeld et al., 2010b; Kaneko et al., 2014), we asked how *MEG3* manipulation affects mesenchymal and stem cell properties of D492 and D492M. The expression of both aldehyde dehydrogenase (*ALDH1A3*) and integrin alpha 6 (*ITGA6*; **Supplementary Figure 6**), markers of stemness, is increased in D492^{MEG3} compared to D492^{CTRL}. Next, we employed several functional assays to assess the effect of *MEG3* levels in D492 and D492M on mesenchymal and stem cell properties. D492^{MEG3} is more resistant to chemically induced apoptosis than D492^{CTRL} (**Figure 8A**). Migration can be assessed *in vitro* using the wound healing assay or by trans-well migration

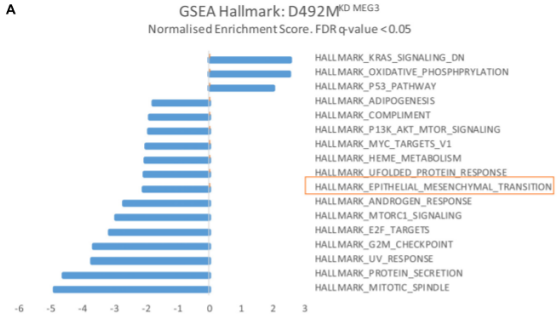

B

Gene	Name	Log2 FC	p-value
POSTN	Periostin	-2.45	$3.69x10^{-19}$
DST	Dystonin	-1.57	$2.21x10^{-9}$
IGFBP3	Insulin like grow th factor binding protein 3	-1.28	$4.99x10^{-19}$
ITGAV	Integrin alpha-V	-1.25	$1.62x10^{-42}$
ITGB1	Integrin subunit beta 1	-1.23	$1.48x10^{-56}$
VCAN	Versican	-1.19	$1.44x10^{-5}$
FERMT2	Fermitin family homolog 2	-1.07	$1.16x10^{-5}$
LAMA1	Laminin subunit alpha 1	-1.01	$2.82x10^{-26}$
COL12A1	Collagen type XII alpha 1 chain	-0.98	$9.17x10^{-19}$
CDH2	N-cadherin	-0.97	$1.21x10^{-24}$
SERPINE2	Serpine 2	-0.97	$2.42x10^{-18}$
FN1	Fibronectin 1	-0.95	$3.13x10^{-19}$
LAMC1	Laminin subunit gamma 1	-0.92	$2.61x10^{-25}$
LAMA3	Laminin subunit alpha 3	-0.92	$6.25x10^{-28}$
SERPINE1	Serpine 1	-0.9	$3.10x10^{-15}$
FBN2	Fibronectin 2	-0.89	$6.38x10^{-18}$
LAMC2	Laminin subunit gamma 2	-0.88	$1.66x10^{-22}$
VEGFC	Vascular endothelial grow th factor C	-0.74	$1.86x10^{-17}$
FGF2	Fibroblast grow th factor 2	-0.65	$3.47x10^{-11}$
SNAI2	Snail family transcriptional repressor 2	-0.63	$3.32x10^{-8}$
VIM	Vimentin	-0.49	$3.04x10^{-7}$
COL4A1	Collagen type IV alpha 1 chain	-0.48	$1.19x10^{-4}$

C

Gene	Name	Log2 FC	Marker	p-value
GATA3	GATA3	0.42	Luminal epithelial	$8.19x10^{-4}$
MUC1	Mucin 1	0.83	Luminal epithelial	$1.97x10^{-6}$
CDH2	N-cadherin	-0.97	Mesenchymal	$1.21x10^{-24}$
LAMA1	Laminin subunit alpha 1	-1.01	Mesenchymal	$2.82x10^{-26}$
SNAI2	Snail family transcriptional repressor 2	-0.63	Mesenchymal	$3.32x10^{-8}$
ZEB2	Zinc finger E-box binding homeobox 2	-0.43	Mesenchymal	$3.76x10^{-6}$
VIM	Vimentin	-0.49	Mesenchymal	$3.04x10^{-7}$
CTNNB1	Catenin beta-1	-0.3	Stem cell	$4.1x10^{-4}$
MME	Membrane metallo-endopeptidase	-2.97	Stem cell	$1.19x10^{-72}$

FIGURE 6 | Knock down of *MEG3* in D492M decrease mesenchymal markers. **(A)** Epithelial-mesenchymal transition gene set is enriched pathway in $D492M^{KD-MEG3}$ (highlighted in orange). Bar plot of Gene Set Enrichment Analysis (GSEA) with Hallmark dataset showing all significantly (False discovery rate-FDR $q \leq 0.05$) enriched pathways in $D492M^{KD-MEG3}$. Gene set Epithelial-mesenchymal transition has normalized enrichment score (NES) of –2.06 and FDR $q = 0.014$. **(B)** Knock-down of *MEG3* correlates with downregulation of mesenchymal genes relevant for breast cells. Enrichment plot showing the Enrichment Score (ES) of the genes in the Hallmark gene set Epithelial-mesenchymal transition in $D492M^{KD-MEG3}$. The genes are overrepresented toward the top the ranked list of $D492M^{KD-MEG3}$ (right). Table with relevant genes for breast cells, significantly ($p \leq 0.05$) deregulated, from the Hallmark gene list epithelial-mesenchymal transition showing Log2 fold change (FC; left). **(C)** Luminal epithelial markers (*GATA3* and *MUC1*) are upregulated, while myoepithelial (*KRT14*), mesenchymal (*CDH2*, *LAMA1*, *SNAI2*, *VIM*, and *ZEB2*) and stem cell (*CTNNB1* and *MME*) are downregulated with knock down of *MEG3*. Genes from literature-based list of markers significantly ($p \leq 0.05$) differentially expressed in $D492M^{KD-MEG3}$ vs $D492M^{KD-CTRL}$.

where the cells migrate toward a chemo-attractant. In the wound healing assay, $D492^{MEG3}$ has slightly increased migration rate compared to $D492^{CTRL}$, while $D492M^{KD-MEG3}$ has decreased migration rate compared to $D492M^{KD-CTRL}$ (**Supplementary Figure 5A**). In the trans-well migration assay, $D492^{MEG3}$ has about two-fold increased migration rate compared to $D492^{CTRL}$ and $D492M^{KD-MEG3}$ has reduced migration rate compared to $D492M^{KD-CTRL}$ (**Figure 8B**). *MEG3* manipulation, however, did not affect invasion in a transwell invasion assay (**Supplementary Figure 5B**). We performed

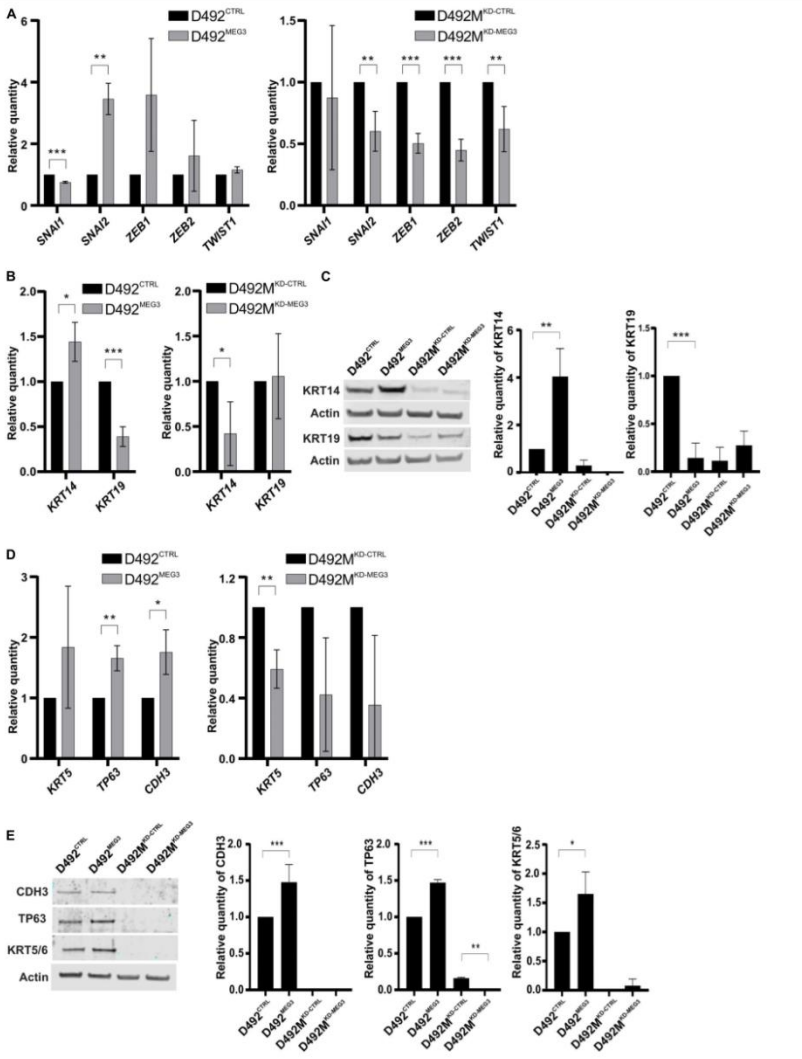

FIGURE 7 | Continued

FIGURE 7 | *MEG3* induce partial EMT. **(A)** *MEG3* increases expression of EMT transcription factors in D492 and the knock down of *MEG3* decrease expression of TF-EMT in D492M. qRT-PCR showing $D492^{MEG3}$ increased expression of transcription factors (TF) *SNAI2* compared to $D492^{CTRL}$ (left) and decreased expression of EMT related TF *SNAI2*, *ZEB1*, *ZEB2* and *TWIST1* in $D492M^{KD-MEG3}$ compared to $D492M^{KD-CTRL}$ (right). Results shown as mean ± SD. Unpaired *t*-test was used to test significance: $^{**}p \leq 0.01$; $^{***}p \leq 0.001$; $n = 3$. **(B)** *MEG3* increases expression of myoepithelial marker *KRT14* and decrease expression of luminal epithelial marker *KRT19* on mRNA level. qRT-PCR showing $D492^{MEG3}$ has increased expression of *KRT14* and decrease expression of *KRT19* compared to $D492^{CTRL}$ (left). $D492M^{KD-MEG3}$ has decreased expression of *KRT14* compared to $D492M^{KD-CTRL}$ (right). qRT-PCR results shown as mean ± SD. Unpaired *t*-test was used to test significance: $^{*}p \leq 0.05$; $^{***}p \leq 0.001$; $n = 3$. **(C)** qRT-PCR results confirmed on protein level. Representative pictures of western blot (WB) with its quantification (below). $D492^{MEG3}$ has increased protein level of KRT14 and decreased protein level of KRT19 compared to $D492^{CTRL}$. WB results shown as mean ± SD. One-way ordinary ANOVA, followed by Tukey's multiple comparison test was used to test significance: $^{**}p \leq 0.01$; $^{***}p \leq 0.001$; $n = 3$. **(D)** *MEG3* increase expression of myoepithelial markers *TP63* and *CDH3* and knock-down of *MEG3* decrease expression of myoepithelial marker *KRT5*, on mRNA level. qRT-PCR showing $D492^{MEG3}$ has increased expression of *TP63* and *CDH3* compared to $D492^{CTRL}$ (left). $D492M^{KD-MEG3}$ has decreased expression of *KRT5* compared to $D492M^{KD-CTRL}$ (right). qRT-PCR results shown as mean ± SD. Unpaired *t*-test was used to test significance: $^{*}p \leq 0.05$; $^{**}p \leq 0.01$; $n = 3$. **(E)** qRT-PCR results confirmed on protein level. Representative pictures of western blot (WB) with its quantification (below). $D492^{MEG3}$ has increased protein level of CDH3 (P-cad), TP63 (p63) and KRT5 compared to $D492^{CTRL}$. $D492M^{KD-MEG3}$ has decreased protein level of TP63 compared to $D492M^{KD-CTRL}$. WB results shown as mean ± SD. One-way ordinary ANOVA, followed by Tukey's multiple comparison test was used to test significance: $^{*}p \leq 0.05$; $^{**}p \leq 0.01$; $^{***}p \leq 0.001$; $n = 3$.

mammosphere assays in rBM (reconstituted basement membrane, Matrigel) (**Figure 8C**) and in low attachment plates (**Figure 8D**), with comparable results. $D492^{MEG3}$ increases the formation of colonies compared to $D492^{CTRL}$ while $D492M^{KD-MEG3}$ decreases the formation of colonies compared to $D492M^{KD-CTRL}$. In addition, we co-cultured $D492^{MEG3}$ with endothelial cells (HUVECs) and observed increased size of colonies and less branching compared to $D492^{CTRL}$ (**Figure 8E**). Finally, manipulation of *MEG3* levels slightly affected proliferation rate of $D492M^{KD-MEG3}$ compared to $D492M^{KD-CTRL}$ (**Supplementary Figure 5C**).

DISCUSSION

In this study, we show that ncRNAs from the DLK1-DIO3 locus are highly expressed in stromal/mesenchymal cells in the breast and positively correlate with the expression of EMT genes in breast tissue. *MEG3* expression was monoallelic in both D492 and D492M and gain and loss of function studies have shown concomitant expression of *MEG3* with miRNAs from the DLK1-DIO3 locus, indicating that *MEG3* could be used as a marker for the expression of the non-coding RNAs from the locus. *MEG3* expression was shown to be negatively correlated with survival of breast cancer patients, particularly with the luminal B subtype. Furthermore, we demonstrate that enhanced *MEG3* expression accompanied by increased expression of the ncRNAs at the DLK1-DIO3 locus, contributes to partial EMT more correctly referred to as epithelial plasticity, seen by increased expression of EMT related TFs, increase of basal/mesenchymal markers and enhanced properties such as migration, resistance to apoptosis and clonogenic capacity.

We used an isogenic breast cell line model to study the expression pattern and functional role of ncRNAs, both miRNAs and lncRNAs, in EMT. Of interest was the largest miRNA locus in the human genome and the lncRNA *MEG3*, both within the DLK1-DIO3 imprinted region on chromosome 14. The non-coding part of the DLK1-DIO3 locus has higher expression in cells with mesenchymal phenotype (D492M) compared to cells with epithelial phenotype (D492). These results were validated in primary breast tissue and in another cellular model of EMT. Furthermore, we have shown that *MEG3* expression correlates with expression of extracellular matrix proteins, which are secreted by cells with a mesenchymal phenotype, and with mesenchymal genes in breast tissue. Data from pyrosequencing demonstrate that the expression of *MEG3* is monoallelic in both D492 and D492M indicating that the increased expression of *MEG3* in D492M is not due to loss of imprinting. We have shown that *MEG3* negatively correlates with survival of luminal B breast cancer patients and patients with grade 3 breast cancer. This is in line with a recent study where high expression of *MEG3* was identified to be a negative prognostic marker for breast cancer (Yao et al., 2019).

Many studies suggest *MEG3* as a tumor suppressor, largely due to the observation that *MEG3* expression is lower in tumor tissue compared to normal tissue (Sheng et al., 2014; Sun et al., 2014, 2016; Yin et al., 2015; Chak et al., 2017; Molina-Pinelo et al., 2018). Our data demonstrates that *MEG3* expression levels are comparable in whole normal breast tissue and in stroma (fibroblasts), however, the expression of *MEG3* in epithelial cells is much lower. There was considerable variation of the *MEG3* expression in breast tissue samples that could be partially due to different proportions of subset of fibroblasts associated with ducts vs TDLUs. There are studies confirming existence of, for instance, two distinct functionally specialized lineages of lobular vs ductal fibroblast (Morsing et al., 2016) or myoepithelial cells (Fridriksdottir et al., 2017), which could be identified by specific marker expression. Importantly, relative proportions of stromal and epithelial compartment are different in normal and cancerous human breast tissue. Breast cancers arise in vast majority from epithelial cells, with TDLUs being the predominant site of breast tumor occurrence (Tabar et al., 2014). Therefore, it would be expected that expression of *MEG3* is higher in normal breast tissue, as it comprises relatively more stromal cells compared to breast cancer tissue. In line with this, expression of *MEG3* from whole breast tissue is distorted as proportions of stroma vs epithelia in normal/cancer tissue are different, resulting in misleading interpretations. Using RNA only from unsorted normal tissue will mainly represents expression of stromal cells. Therefore, it is crucial to use a proper control when comparing expression of genes in normal vs tumor tissue. Single-cell RNA-sequencing or sorted stromal and epithelial cells would give more informative results as it would enable distinctions between epithelial and stromal tissue

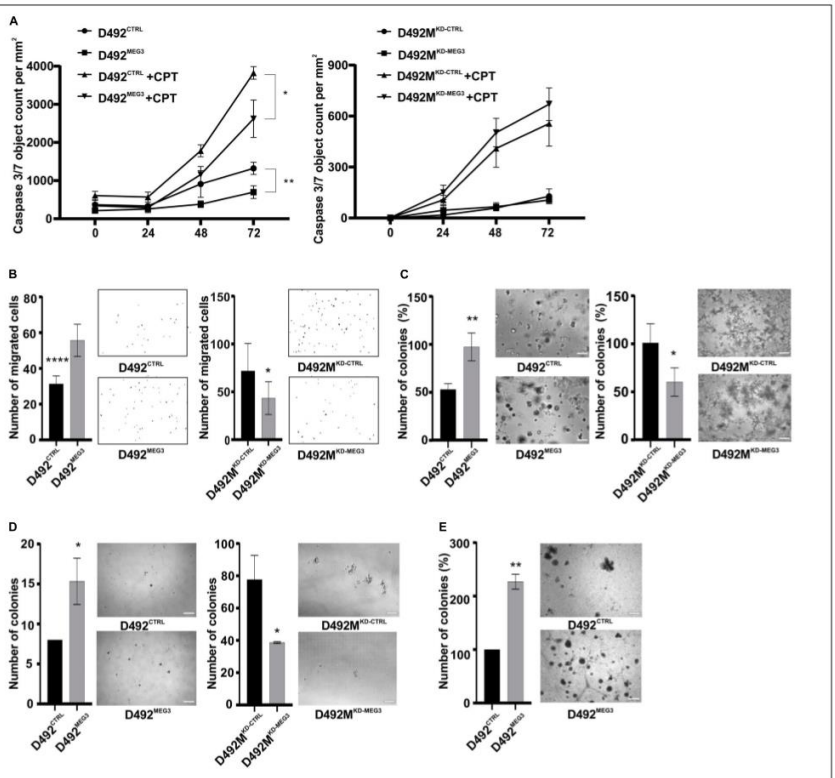

FIGURE 8 | *MEG3* increases stem cell properties. **(A)** *MEG3* increase resistance to chemically induced apoptosis. Apoptosis assay: $D492^{MEG3}$ is more resistant to chemically induced apoptosis compared to $D492^{CTRL}$ (left). Data is analyzed on Incucyte Zoom and displayed as Caspase 3/7 object count/mm^2. Results are shown as mean ± SD. Multiple unpaired Student *t*-test per row was used to test significance at 72-h time-point: $^*p \leq 0.05$; $^{**}p \leq 0.01$; $n = 6$. **(B)** *MEG3* increases migration and knock down of *MEG3* decreases migration through trans-well filters. Migration assay: $D492^{MEG3}$ has increased migration rate compared to $D492^{CTRL}$ (left), with representative pictures on side. $D492M^{KD-MEG3}$ migrates less compared to $D492M^{KD-CTRL}$ (right), with representative pictures on side. Quantification of number of migratory cells, analyzed using ImageJ software, results shown as mean ± SD. Unpaired *t*-test was used to test significance: $^*p \leq 0.05$; $^{****}p \leq 0.0001$; $n = 6$. **(C)** *MEG3* increases clonogenic capacity in 3D culture in rBM (reconstitute basement membrane). Mammosphere assay: $D492^{MEG3}$ has higher clonogenic capacity compared to $D492^{CTRL}$ (left). $D492M^{KD-MEG3}$ has lower clonogenic capacity compared to $D492M^{KD-CTRL}$ (right). Data shown as % mean ± SD, $^*p \leq 0.05$; $^{**}p \leq 0.01$; $n = 3$. Scale bar = 500 μm. **(D)** *MEG3* increases clonogenic capacity in low attachment assay. $D492^{MEG3}$ increases the formation of colonies compared to $D492^{CTRL}$ (left), with representative pictures on side. $D492M^{KD-MEG3}$ decreases the formation of colonies compared to $D492M^{KD-CTRL}$ (right), with representative pictures on side. Results shown as % of mean ± SD. Unpaired *t*-test was used to test significance: $^*p \leq 0.05$; $^{**}p \leq 0.01$; $n = 3$. Scale bars = 200 μm. **(D)** Co-culture of $D492^{MEG3}$ with endothelial cells (HUVECs) increases number and size of colonies and forms less branching compared to $D492^{CTRL}$. Results shown as % of mean ± SD. Unpaired *t*-test was used to test significance: $^{**}p \leq 0.01$; $n = 3$. Representative pictures scale bars = 200 μm.

compartments. In this paper we show that *MEG3* expression negatively correlates with survival in breast cancer, particularly in grade three tumors and the luminal B subtype. However, our study does not determine if the high *MEG3* expression represents increased stromal infiltration in the tumors or elevated expression in cancer cells.

Another reason for classifying *MEG3* as tumor suppressor is its action on stabilization of p53 (Ghafouri-Fard and Taheri, 2019). However, inactivation of p53 is a frequent event in cancer, estimated to have about 50 % occurrence (Gasco et al., 2002; Marine et al., 2006; Haupt and Haupt, 2017). The percentage is even higher, when the inactivation in p53's regulatory pathways is considered (Joerger and Fersht, 2016). Therefore, the use of cell lines which lack active p53, such as D492 and D492M, offers a different approach, more relevant for studying breast cancer signaling pathways, to study the role of DLK1-DIO3. The role of p53 in the cell is that of a tumor suppressor, impacting acts in proliferation, cell cycle and genomic stability (Mercer, 1992). In D492 cell lines, as could be expected, we did not observe effect on cell proliferation. Recently, Uroda and colleagues' stated, that cell cycle arrest by *MEG3* is exclusively p53-dependent, (Uroda et al., 2019), in line with our suggestions that *MEG3* can have a different role in cells lacking p53. Collectively, these observations could explain the conflicting results about role of *MEG3* in tumors.

Many imprinted genes are located in clusters regulated by a differentially methylated regions (DMRs) (Bartolomei and Ferguson-Smith, 2011). In our study targeting the *MEG3* promoter, we have observed concomitant expression of *MEG3* with other miRNAs from the DLK1-DIO3 locus. Our data may support previous studies showing that the *MEG3* promoter controls expression of all maternally expressed genes from the DLK1-DIO3 locus (Tierling et al., 2006; Ioannides et al., 2014; Sanli et al., 2018). Zhu et al. (2019) have shown that the MEG3-DMR overlaps with the *MEG3* gene promoter and any deletion in this region inactivates both MEG3-DMR and the *MEG3* gene. Their data shows, that it is the MEG3-DMR, not the *MEG3* gene, which regulates imprinting (and expression). Therefore, by targeting the *MEG3* promoter at the MEG3-DMR all the non-coding RNAs at the DLK1-DIO3 locus are inactivated. *MEG3* expression can be considered as a marker for the expression of other ncRNAs at the locus.

Cellular plasticity, an important contributor to heterogeneity and drug resistance in breast cancer can be conveyed through EMT/MET (Liu et al., 2014). Partial EMT (p-EMT) may reflect cellular plasticity better than full-EMT and consequently, cells possessing this state adapt more easily to a new environment, which is necessary for cancer cell invasion and metastasis (Thiery, 2002; Tam and Weinberg, 2013; Lambert et al., 2017). Notably, a recent report highlights the importance of the intermediate stages of EMT for the intravasation of tumor cells and for metastasis formation in experimental breast or skin tumors (Pastushenko et al., 2018). Similarly, another study showed that cancer cells might only reach an intermediate EMT stage allowing for increased motility, while keeping its cellular plasticity (Brabletz et al., 2018). It has also been observed that full mesenchymal phenotype (EMT), has a low capacity to form metastasis compared to p-EMT (Schmidt et al., 2015). The essential criteria for aggressive behavior does not need to be a particular phenotype, but rather enhanced cellular plasticity, as is also observed for hybrid E/M cells (Grosse-Wilde et al., 2015). Thus, EMT may be viewed as a trans-differentiation process where epithelial and mesenchymal cells interconvert by passing through an intermediate "stem-like" state (Grosse-Wilde et al., 2018).

EMT is a complex process and meta-analysis indicates that there are possibly different types of EMT (Liang et al., 2016). We have shown, that by manipulating *MEG3* expression, and thus changing the expression of the non-coding genes at the DLK1-DIO3 locus, the majority of these EMT related TFs are affected, indicating an important role of the ncRNAs the DLK1-DIO3 locus in the EMT process. One of the most typical hallmarks of EMT is downregulation of *CDH1* (E-cadherin) and epithelial-specific keratins (Peinado et al., 2007). Altered expression of *MEG3* does not lead to change of E-cadherin expression and therefore *MEG3* may have induced only a partial EMT phenotype. However, it has been shown, that cells with p-EMT phenotype display concomitant expression of epithelial and mesenchymal markers (Armstrong et al., 2011) and loss of E-cadherin is not a prerequisite for EMT (Hollestelle et al., 2013). Cells undergoing collective migration have hybrid EMT phenotype characterized by E-cadherin expression, which helps to maintain cell–cell contacts (Friedl et al., 2012; Aceto et al., 2015). Furthermore, we have shown that altered expression of *MEG3* revealed distinct luminal and myoepithelial marker expression. Increased expression of *KRT14* and decreased expression *KRT19* indicate increased myoepithelial differentiation, which has been connected to a partial EMT phenotype (Petersen et al., 2001). Study on collective migration revealed *KRT14* as a key regulator of metastasis (Cheung et al., 2016) and the same applied for collective invasion, which was facilitated by subpopulation of cells expressing *KRT14* (Cheung et al., 2013). The observed increase of myoepithelial/basal differentiation in cells with higher expression of *MEG3* was supported with altered expression of other markers such as *KRT5*, *TP63*, and *CDH3*.

A key characteristic defining breast stem cells is the ability to form of mammospheres (Dontu et al., 2003; Grosse-Wilde et al., 2015). Morel and colleagues confirmed that human mammary epithelial cells undergoing EMT exhibited better mammosphere-forming capabilities (Morel et al., 2008) and Shimono et al. have shown that mammosphere-forming activity is abrogated in both normal and malignant mammary stem cells when the EMT program is shut down (Shimono et al., 2009). In this study phenotypic differences upon altered MEG3 expression were more prominent in 3D than in 2D cell culture, where *MEG3* increased mammosphere formation ability and slightly decreases branching potential in 3D culture. Furthermore, we have shown increased expression of *ALDH1A3* and *ITGA6*, in cells with overexpression of *MEG3*, supporting role of *MEG3* in stemness.

We propose that increased expression of *MEG3*, and thus increased expression of the ncRNAs at the DLK1-DIO3 locus, in D492 leads to partial EMT phenotype/enhanced plasticity, seen by molecular changes with increased mesenchymal and myoepithelial/basal genes and increased migration and resistance to apoptosis. In contrast, the repression of *MEG3*, and the maternally imprinted ncRNAs, in D492M leads to decreased mesenchymal and basal gene expression and decreased migration and resistance to apoptosis. Nguyen-Ngoc et al.

also demonstrated, that motility can occur in cells that retain an epithelial molecular signature (Nguyen-Ngoc et al., 2012). This supports our observation, that manipulation of *MEG3* expression did not affect the morphological phenotype, but rather affected the functional phenotype. These characteristic properties of cells undergoing EMT were originally proposed to occur in breast cancer by Mani and colleagues (Mani et al., 2008), showing that stem-like and p-EMT properties share many characteristics, such as increased migration, resistance and survival (Creighton et al., 2009; Armstrong et al., 2011; Hanahan and Weinberg, 2011).

Increased understanding of branching morphogenesis in the breast and the regulation of EMT and MET may hold the key for future development of methods and drugs that neutralize the invading properties of cancer cells. Currently, there is need for biomarkers to accurately monitor the EMT/MET process that may improve treatment. Prognostic value of *MEG3* in human malignancies remains controversial and requires further investigation. Our results and conflicting data from the literature suggest that *MEG3* has a complex role in breast tissue.

DATA AVAILABILITY STATEMENT

The RNAseq data for this article has been submitted to GEO, with the GEO accession number GSE142268, see here: https://www.ncbi.nlm.nih.gov/geo/query/acc.cgi?acc=GSE142268

ETHICS STATEMENT

The studies involving human participants were reviewed and approved by Icelandic National Bioethics Committee VSN-13-057 and VSN-11-105-V2. The Icelandic Data Protection Commission (2001/523 and 2002/463) Landspitali Ethical Committee No. 35/2013. The patients/participants provided their written informed consent to participate in this study.

AUTHOR CONTRIBUTIONS

MM, TG, JB, ZB, EB, GT, and BH: conceptualization and design of the study. ZB, EB, JB, AS, and BH: data acquisition. ZB, AS, EB, GT, SS, and BH: data analysis. ZB, GT, TG, and BH: drafting the manuscript. All authors participated in data interpretation, revision of the manuscript and approved the final version to be published.

FUNDING

This work was supported by Grants from Landspitali University Hospital Science Fund, University of Iceland Research Fund, Icelandic Science and Technology Policy Council Research Fund no. 1103010061, Icelandic Science and Technology Policy – Grant of Excellence: 52144051, "Vísindasjóður Krabbameinsfélagsins" (Icelandic Cancer Society Science Fund) 2017 and 'Göngum saman', a supporting group for breast cancer research in Iceland (www.gongumsaman.is). The funders had no role in study design, data collection and analysis, decision to publish, or preparation of the manuscript.

ACKNOWLEDGMENTS

The authors would like to thank Rosa B. Barkardottir, Adalgeir Arason, Bjarni A. Agnarsson, and Oskar Thor Johannsson for their contribution to this work by providing RNA samples from breast cancer patients and pathological and clinical information. We would also like to thank Gudrun Johannesdottir for excellent technical support.

SUPPLEMENTARY MATERIAL

The Supplementary Material for this article can be found online at: https://www.frontiersin.org/articles/10.3389/fcell.2020.00461/full#supplementary-material

REFERENCES

Aceto, N., Toner, M., Maheswaran, S., and Haber, D. A. (2015). En route to metastasis: circulating tumor cell clusters and epithelial-to-mesenchymal transition. *Trends Cancer* 1, 44–52. doi: 10.1016/j.trecan.2015.07.006

Anders, S., Pyl, P. T., and Huber, W. (2015). HTSeq–a Python framework to work with high-throughput sequencing data. *Bioinformatics* 31, 166–169. doi: 10.1093/bioinformatics/btu638

Ansieau, S. (2013). EMT in breast cancer stem cell generation. *Cancer Lett.* 338, 63–68. doi: 10.1016/j.canlet.2012.05.014

Armstrong, A. J., Marengo, M. S., Oltean, S., Kemeny, G., Bitting, R. L., Turnbull, J. D., et al. (2011). Circulating tumor cells from patients with advanced prostate and breast cancer display both epithelial and mesenchymal markers. *Mol. Cancer Res.* 9, 997–1007. doi: 10.1158/1541-7786.mcr-10-0490

Bartel, D. P. (2009). MicroRNAs: target recognition and regulatory functions. *Cell* 136, 215–233. doi: 10.1016/j.cell.2009.01.002

Bartolomei, M. S., and Ferguson-Smith, A. C. (2011). Mammalian genomic imprinting. *Cold Spring Harb. Perspect. Biol.* 3:a002592.

Baulina, N., Osmak, G., Kiselev, I., Popova, E., Boyko, A., Kulakova, O., et al. (2019). MiRNAs from DLK1-DIO3 imprinted locus at 14q32 are associated with multiple sclerosis: gender-specific expression and regulation of receptor tyrosine kinases signaling. *Cells* 8:133. doi: 10.3390/cells8020133

Ben-Jacob, E., Coffey, D. S., and Levine, H. (2012). Bacterial survival strategies suggest rethinking cancer cooperativity. *Trends Microbiol.* 20, 403–410. doi: 10.1016/j.tim.2012.06.001

Brabletz, T., Kalluri, R., Nieto, M. A., and Weinberg, R. A (2018). EMT in cancer. *Nat. Rev. Cancer.* 18, 128–134. doi: 10.1038/nrc.2017.118

Briem, E., Budkova, Z., Sigurdardottir, A. K., Hilmarsdottir, B., Kricker, J., Timp, W., et al. (2019a). MiR-203a is differentially expressed during branching morphogenesis and EMT in breast progenitor cells and is a repressor of peroxidasin. *Mech. Dev.* 155, 34–47. doi: 10.1016/j.mod.2018.11.002

Briem, E., Ingthorsson, S., Traustadottir, G. A., Hilmarsdottir, B., and Gudjonsson, T. (2019b). Application of the D492 cell lines to explore breast morphogenesis, EMT and cancer progression in 3D culture. *J. Mammary Gland Biol. Neoplasia* 24, 139–147. doi: 10.1007/s10911-018-09424-w

Cancer Genome Atlas Network (2012). Comprehensive molecular portraits of human breast tumours. *Nature* 490, 61–70. doi: 10.1038/nature11412

Cao, Z., Livas, T., and Kyprianou, N. (2016). Anoikis and EMT: lethal "Liaisons" during cancer progression. *Crit. Rev. Oncog.* 21, 155–168. doi: 10.1615/critrevoncog.2016016955

Chak, W. P., Lung, R. W., Tong, J. H., Chan, S. Y., Lun, S. W., Tsao, S. W., et al. (2017). Downregulation of long non-coding RNA MEG3 in nasopharyngeal carcinoma. *Mol. Carcinog.* 56, 1041–1054. doi: 10.1002/mc.22569

Chan, Y. H. (2003). Biostatistics 104: correlational analysis. *Singapore Med. J.* 44, 614–619.

Cheng, A. W., Wang, H., Yang, H., Shi, L., Katz, Y., Theunissen, T. W., et al. (2013). Multiplexed activation of endogenous genes by CRISPR-on, an RNA-guided transcriptional activator system. *Cell Res.* 23, 1163–1171. doi: 10.1038/cr.2013.122

Cheung, K. J., Gabrielson, E., Werb, Z., and Ewald, A. J. (2013). Collective invasion in breast cancer requires a conserved basal epithelial program. *Cell* 155, 1639–1651. doi: 10.1016/j.cell.2013.11.029

Cheung, K. J., Padmanaban, V., Silvestri, V., Schipper, K., Cohen, J. D., Fairchild, A. N., et al. (2016). Polyclonal breast cancer metastases arise from collective dissemination of keratin 14-expressing tumor cell clusters. *Proc. Natl. Acad. Sci. U.S.A.* 113, E854–E863.

Creighton, C. J., Li, X., Landis, M., Dixon, J. M., Neumeister, V. M., Sjolund, A., et al. (2009). Residual breast cancers after conventional therapy display mesenchymal as well as tumor-initiating features. *Proc. Natl. Acad. Sci. U.S.A.* 106, 13820–13825. doi: 10.1073/pnas.0905718106

Cui, X., Yi, Q., Jing, X., Huang, Y., Tian, J., Long, C., et al. (2018). Mining prognostic significance of MEG3 in human breast cancer using bioinformatics analysis. *Cell. Physiol. Biochem.* 50, 41–51. doi: 10.1159/000493956

Dagogo-Jack, I., and Shaw, A. T. (2018). Tumour heterogeneity and resistance to cancer therapies. *Nat. Rev. Clin. Oncol.* 15, 81–94. doi: 10.1038/nrclinonc.2017.166

De Craene, B., and Berx, G. (2013). Regulatory networks defining EMT during cancer initiation and progression. *Nat. Rev. Cancer* 13, 97–110. doi: 10.1038/nrc3447

Di Gesualdo, F., Capaccioli, S., and Lulli, M. (2014). A pathophysiological view of the long non-coding RNA world. *Oncotarget* 5, 10976–10996. doi: 10.18632/oncotarget.2770

Dill, T. L., and Naya, F. J. (2018). A hearty dose of noncoding RNAs: the imprinted *DLK1-DIO3* locus in cardiac development and disease. *J. Cardiovasc. Dev. Dis.* 5:37. doi: 10.3390/jcdd5030037

Dobin, A., Davis, C. A., Schlesinger, F., Drenkow, J., Zaleski, C., Jha, S., et al. (2013). STAR: ultrafast universal RNA-seq aligner. *Bioinformatics* 29, 15–21. doi: 10.1093/bioinformatics/bts635

Dontu, G., Abdallah, W. M., Foley, J. M., Jackson, K. W., Clarke, M. F., Kawamura, M. J., et al. (2003). In vitro propagation and transcriptional profiling of human mammary stem/progenitor cells. *Genes Dev.* 17, 1253–1270. doi: 10.1101/gad.1061803

Eades, G., Zhang, Y. S., Li, Q. L., Xia, J. X., Yao, Y., and Zhou, Q. (2014). Long non-coding RNAs in stem cells and cancer. *World J. Clin. Oncol.* 5, 134–141.

Elenbaas, B., Spirio, L., Koerner, F., Fleming, M. D., Zimonjic, D. B., Donaher, J. L., et al. (2001). Human breast cancer cells generated by oncogenic transformation of primary mammary epithelial cells. *Genes Dev.* 15, 50–65. doi: 10.1101/gad.828901

Elloumi, F., Hu, Z., Li, Y., Parker, J. S., Gulley, M. L., Amos, K. D., et al. (2011). Systematic bias in genomic classification due to contaminating non-neoplastic tissue in breast tumor samples. *BMC Med. Genomics* 4:54. doi: 10.1186/1755-8794-4-54

Fatica, A., and Bozzoni, I. (2014). Long non-coding RNAs: new players in cell differentiation and development. *Nat. Rev. Genet.* 15, 7–21. doi: 10.1038/nrg3606

Felipe Lima, J., Nofech-Mozes, S., Bayani, J., and Bartlett, J. M. (2016). EMT in breast carcinoma-a review. *J. Clin. Med.* 5:65. doi: 10.3390/jcm5070065

Fridriksdottir, A. J., Villadsen, R., Morsing, M., Klitgaard, M. C., Kim, J., Petersen, O. W., et al. (2017). Proof of region-specific multipotent progenitors in human breast epithelia. *Proc. Natl. Acad. Sci. U.S.A.* 114, E10102–E10111. doi: 10.1073/pnas.1714063114

Friedl, P., Locker, J., Sahai, E., and Segall, J. E. (2012). Classifying collective cancer cell invasion. *Nat. Cell Biol.* 14, 777–783. doi: 10.1038/ncb2548

Gasco, M., Shami, S., and Crook, T. (2002). The p53 pathway in breast cancer. *Breast Cancer Res.* 4, 70–76.

Ghafouri-Fard, S., and Taheri, M. (2019). Maternally expressed gene 3 (MEG3): a tumor suppressor long non coding RNA. *Biomed. Pharmacother.* 118:109129. doi: 10.1016/j.biopha.2019.109129

Ghoncheh, M., Pournamdar, Z., and Salehiniya, H. (2016). Incidence and mortality and epidemiology of breast cancer in the world. *Asian Pac. J. Cancer Prev.* 17, 43–46. doi: 10.7314/apjcp.2016.17.s3.43

Gilbert, L. A., Larson, M. H., Morsut, L., Liu, Z., Brar, G. A., Torres, S. E., et al. (2013). CRISPR-mediated modular RNA-guided regulation of transcription in eukaryotes. *Cell* 154, 442–451. doi: 10.1016/j.cell.2013.06.044

Grosse-Wilde, A., Fouquier D'herouel, A., Mcintosh, E., Ertaylan, G., Skupin, A., Kuestner, R. E., et al. (2015). Stemness of the hybrid Epithelial/Mesenchymal state in breast cancer and its association with poor survival. *PLoS One* 10:e0126522. doi: 10.1371/journal.pone.0126522

Grosse-Wilde, A., Kuestner, R. E., Skelton, S. M., Macintosh, E., D'herouel, A. F., Ertaylan, G., et al. (2018). Loss of inter-cellular cooperation by complete epithelial-mesenchymal transition supports favorable outcomes in basal breast cancer patients. *Oncotarget* 9, 20018–20033. doi: 10.18632/oncotarget.25034

Gudjonsson, T., Villadsen, R., Nielsen, H. L., Ronnov-Jessen, L., Bissell, M. J., and Petersen, O. W. (2002). Isolation, immortalization, and characterization of a human breast epithelial cell line with stem cell properties. *Genes Dev.* 16, 693–706. doi: 10.1101/gad.952602

Halldorsson, S., Rohatgi, N., Magnusdottir, M., Choudhary, K. S., Gudjonsson, T., Knutsen, E., et al. (2017). Metabolic re-wiring of isogenic breast epithelial cell lines following epithelial to mesenchymal transition. *Cancer Lett.* 396, 117–129. doi: 10.1016/j.canlet.2017.03.019

Hanahan, D., and Weinberg, R. A. (2011). Hallmarks of cancer: the next generation. *Cell* 144, 646–674. doi: 10.1016/j.cell.2011.02.013

Harrington, C. T., Lin, E. I., Olson, M. T., and Eshleman, J. R. (2013). Fundamentals of pyrosequencing. *Arch. Pathol. Lab. Med.* 137, 1296–1303. doi: 10.5858/arpa.2012-0463-ra

Haupt, S., and Haupt, Y. (2017). P53 at the start of the 21st century: lessons from elephants. *F1000Res.* 6:2041. doi: 10.12688/f1000research.12682.1

Hilmarsdottir, B., Briem, E., Sigurdsson, V., Franzdottir, S. R., Ringner, M., Arason, A. J., et al. (2015). MicroRNA-200c-141 and Np63 are required for breast epithelial differentiation and branching morphogenesis. *Dev. Biol.* 403, 150–161. doi: 10.1016/j.ydbio.2015.05.007

Hollestelle, A., Peeters, J. K., Smid, M., Timmermans, M., Verhoog, L. C., Westenend, P. J., et al. (2013). Loss of E-cadherin is not a necessity for epithelial to mesenchymal transition in human breast cancer. *Breast Cancer Res. Treat.* 138, 47–57.

Huang, D. W., Sherman, B. T., and Lempicki, R. A. (2009a). Bioinformatics enrichment tools: paths toward the comprehensive functional analysis of large gene lists. *Nucleic Acids Res.* 37, 1–13. doi: 10.1093/nar/gkn923

Huang, D. W., Sherman, B. T., and Lempicki, R. A. (2009b). Systematic and integrative analysis of large gene lists using DAVID bioinformatics resources. *Nat. Protoc.* 4, 44–57. doi: 10.1038/nprot.2008.211

Ingthorsson, S., Sigurdsson, V., Fridriksdottir, A. Jr., Jonasson, J. G., Kjartansson, J., Magnusson, M. K., et al. (2010). Endothelial cells stimulate growth of normal and cancerous breast epithelial cells in 3D culture. *BMC Res. Notes* 3:184. doi: 10.1186/1756-0500-3-184

Ioannides, Y., Lokulo-Sodipe, K., Mackay, D. J., Davies, J. H., and Temple, I. K. (2014). Temple syndrome: improving the recognition of an underdiagnosed chromosome 14 imprinting disorder: an analysis of 51 published cases. *J. Med. Genet.* 51, 495–501. doi: 10.1136/jmedgenet-2014-102396

Joerger, A. C., and Fersht, A. R. (2016). The p53 pathway: origins, inactivation in cancer, and emerging therapeutic approaches. *Annu. Rev. Biochem.* 85, 375–404. doi: 10.1146/annurev-biochem-060815-014710

Kaneko, S., Bonasio, R., Saldana-Meyer, R., Yoshida, T., Son, J., Nishino, K., et al. (2014). Interactions between JARID2 and noncoding RNAs regulate PRC2 recruitment to chromatin. *Mol. Cell* 53, 290–300. doi: 10.1016/j.molcel.2013.11.012

Kang, L., Wang, J., Zhang, Y., Kou, Z., and Gao, S. (2009). iPS cells can support full-term development of tetraploid blastocyst-complemented embryos. *Cell Stem Cell* 5, 135–138. doi: 10.1016/j.stem.2009.07.001

Lambert, A. W., Pattabiraman, D. R., and Weinberg, R. A. (2017). Emerging biological principles of metastasis. *Cell* 168, 670–691. doi: 10.1016/j.cell.2016.11.037

Li, J., Shen, H., Xie, H., Ying, Y., Jin, K., Yan, H., et al. (2019). Dysregulation of ncRNAs located at the DLK1DIO3 imprinted domain: involvement in urological cancers. *Cancer Manag. Res.* 11, 777–787. doi: 10.2147/cmar.s190764

Liang, L., Sun, H., Zhang, W., Zhang, M., Yang, X., Kuang, R., et al. (2016). Meta-analysis of EMT datasets reveals different types of EMT. *PLoS One* 11:e0156839. doi: 10.1371/journal.pone.0156839

Liu, H., Ye, D., Chen, A., Tan, D., Zhang, W., Jiang, W., et al. (2019). A pilot study of new promising non-coding RNA diagnostic biomarkers for early-stage colorectal cancers. *Clin. Chem. Lab. Med.* 57, 1073–1083. doi: 10.1515/cclm-2019-0052

Liu, L., Luo, G. Z., Yang, W., Zhao, X., Zheng, Q., Lv, Z., et al. (2010). Activation of the imprinted Dlk1-Dio3 region correlates with pluripotency levels of mouse stem cells. *J. Biol. Chem.* 285, 19483–19490.

Liu, S., Cong, Y., Wang, D., Sun, Y., Deng, L., Liu, Y., et al. (2014). Breast cancer stem cells transition between epithelial and mesenchymal states reflective of their normal counterparts. *Stem Cell Rep.* 2, 78–91. doi: 10.1016/j.stemcr.2013.11.009

Liz, J., and Esteller, M. (2016). lncRNAs and microRNAs with a role in cancer development. *Biochim. Biophys. Acta* 1859, 169–176. doi: 10.1016/j.bbagrm.2015.06.015

Love, M. I., Huber, W., and Anders, S. (2014). Moderated estimation of fold change and dispersion for RNA-seq data with DESeq2. *Genome Biol.* 15:550.

Lu, W., and Kang, Y. (2019). Epithelial-Mesenchymal plasticity in cancer progression and metastasis. *Dev. Cell* 49, 361–374. doi: 10.1016/j.devcel.2019.04.010

Mani, S. A., Guo, W., Liao, M. J., Eaton, E. N., Ayyanan, A., Zhou, A. Y., et al. (2008). The epithelial-mesenchymal transition generates cells with properties of stem cells. *Cell* 133, 704–715.

Marine, J. C., Francoz, S., Maetens, M., Wahl, G., Toledo, F., and Lozano, G. (2006). Keeping p53 in check: essential and synergistic functions of Mdm2 and Mdm4. *Cell Death Differ.* 13, 927–934. doi: 10.1038/sj.cdd.4401912

Mercer, T. R., Dinger, M. E., and Mattick, J. S. (2009). Long non-coding RNAs: insights into functions. *Nat. Rev. Genet.* 10, 155–159. doi: 10.1038/nrg2521

Mercer, W. E. (1992). Cell cycle regulation and the p53 tumor suppressor protein. *Crit. Rev. Eukaryot. Gene Expr.* 2, 251–263.

Mitra, R., Chen, X., Greenawalt, E. J., Maulik, U., Jiang, W., Zhao, Z., et al. (2017). Decoding critical long non-coding RNA in ovarian cancer epithelial-to-mesenchymal transition. *Nat. Commun.* 8:1604.

Molina-Pinelo, S., Salinas, A., Moreno-Mata, N., Ferrer, I., Suarez, R., Andres-Leon, E., et al. (2018). Impact of DLK1-DIO3 imprinted cluster hypomethylation in smoker patients with lung cancer. *Oncotarget* 9, 4395–4410. doi: 10.18632/oncotarget.10611

Moradi, S., Sharifi-Zarchi, A., Ahmadi, A., Mollamohammadi, S., Stubenvoll, A., Gunther, S., et al. (2017). Small RNA sequencing reveals Dlk1-Dio3 locus-embedded MicroRNAs as major drivers of ground-state pluripotency. *Stem Cell Rep.* 9, 2081–2096. doi: 10.1016/j.stemcr.2017.10.009

Morel, A. P., Lievre, M., Thomas, C., Hinkal, G., Ansieau, S., and Puisieux, A. (2008). Generation of breast cancer stem cells through epithelial-mesenchymal transition. *PLoS One* 3:e2888. doi: 10.1371/journal.pone.0002888

Morsing, M., Klitgaard, M. C., Jafari, A., Villadsen, R., Kassem, M., Petersen, O. W., et al. (2016). Evidence of two distinct functionally specialized fibroblast lineages in breast stroma. *Breast Cancer Res.* 18:108.

Moustakas, A., and Heldin, C. H. (2007). Signaling networks guiding epithelial-mesenchymal transitions during embryogenesis and cancer progression. *Cancer Sci.* 98, 1512–1520. doi: 10.1111/j.1349-7006.2007.00550.x

Nguyen-Ngoc, K. V., Cheung, K. J., Brenot, A., Shamir, E. R., Gray, R. S., Hines, W. C., et al. (2012). ECM microenvironment regulates collective migration and local dissemination in normal and malignant mammary epithelium. *Proc. Natl. Acad. Sci. U.S.A.* 109, E2595–E2604.

Nieto, M. A., Huang, R. Y., Jackson, R. A., and Thiery, J. P. (2016). EMT: 2016. *Cell* 166, 21–45.

Niknafs, Y. S., Pandian, B., Gajjar, T., Gaudette, Z., Wheelock, K., Maz, M. P., et al. (2018). MiPanda: a resource for analyzing and visualizing next-generation sequencing transcriptomics data. *Neoplasia* 20, 1144–1149. doi: 10.1016/j.neo.2018.09.001

Pastushenko, I., Brisebarre, A., Sifrim, A., Fioramonti, M., Revenco, T., Boumahdi, S., et al. (2018). Identification of the tumour transition states occurring during EMT. *Nature* 556, 463–468. doi: 10.1038/s41586-018-0040-3

Pechoux, C., Gudjonsson, T., Ronnov-Jessen, L., Bissell, M. J., and Petersen, O. W. (1999). Human mammary luminal epithelial cells contain progenitors to myoepithelial cells. *Dev. Biol.* 206, 88–99. doi: 10.1006/dbio.1998.9133

Peinado, H., Olmeda, D., and Cano, A. (2007). Snail, Zeb and bHLH factors in tumour progression: an alliance against the epithelial phenotype? *Nat. Rev. Cancer* 7, 415–428. doi: 10.1038/nrc2131

Petersen, O. W., Lind Nielsen, H., Gudjonsson, T., Villadsen, R., Ronnov-Jessen, L., and Bissell, M. J. (2001). The plasticity of human breast carcinoma cells is more than epithelial to mesenchymal conversion. *Breast Cancer Res.* 3, 213–217. doi: 10.1186/bcr298

Prat, A., and Perou, C. M. (2011). Deconstructing the molecular portraits of breast cancer. *Mol. Oncol.* 5, 5–23. doi: 10.1016/j.molonc.2010.11.003

Qi, L. S., Larson, M. H., Gilbert, L. A., Doudna, J. A., Weissman, J. S., Arkin, A. P., et al. (2013). Repurposing CRISPR as an RNA-guided platform for sequence-specific control of gene expression. *Cell* 152, 1173–1183. doi: 10.1016/j.cell.2013.02.022

R Development Core Team (2015). *R: A Language and Environment for Statistical Computing*. Vienna: R Foundation for Statistical Computing.

Radisky, D. C., Kenny, P. A., and Bissell, M. J. (2007). Fibrosis and cancer: do myofibroblasts come also from epithelial cells via EMT? *J. Cell. Biochem.* 101, 830–839. doi: 10.1002/jcb.21186

Ringnér, M., Fredlund, E., Häkkinen, J., Borg, Å., and Staaf, J. (2011). GOBO: gene expression-based outcome for breast cancer online. *PLoS One* 6:e17911. doi: 10.1371/journal.pone.0017911

Robson, E. J., Khaled, W. T., Abell, K., and Watson, C. J. (2006). Epithelial-to-mesenchymal transition confers resistance to apoptosis in three murine mammary epithelial cell lines. *Differentiation* 74, 254–264. doi: 10.1111/j.1432-0436.2006.00075.x

Sanli, I., Lalevee, S., Cammisa, M., Perrin, A., Rage, F., Lleres, D., et al. (2018). Meg3 non-coding RNA expression controls imprinting by preventing transcriptional upregulation in cis. *Cell Rep.* 23, 337–348. doi: 10.1016/j.celrep.2018.03.044

Scheel, C., and Weinberg, R. A. (2012). Cancer stem cells and epithelial-mesenchymal transition: concepts and molecular links. *Semin. Cancer Biol.* 22, 396–403. doi: 10.1016/j.semcancer.2012.04.001

Schmidt, J. M., Panzilius, E., Bartsch, H. S., Irmler, M., Beckers, J., Kari, V., et al. (2015). Stem-cell-like properties and epithelial plasticity arise as stable traits after transient Twist1 activation. *Cell Rep.* 10, 131–139. doi: 10.1016/j.celrep.2014.12.032

Sheng, X., Li, J., Yang, L., Chen, Z., Zhao, Q., Tan, L., et al. (2014). Promoter hypermethylation influences the suppressive role of maternally expressed 3, a long non-coding RNA, in the development of epithelial ovarian cancer. *Oncol. Rep.* 32, 277–285. doi: 10.3892/or.2014.3208

Shimono, Y., Zabala, M., Cho, R. W., Lobo, N., Dalerba, P., Qian, D., et al. (2009). Downregulation of miRNA-200c links breast cancer stem cells with normal stem cells. *Cell* 138, 592–603. doi: 10.1016/j.cell.2009.07.011

Sigurdsson, V., Hilmarsdottir, B., Sigmundsdottir, H., Fridriksdottir, A. J., Ringner, M., Villadsen, R., et al. (2011). Endothelial induced EMT in breast epithelial cells with stem cell properties. *PLoS One* 6:e23833. doi: 10.1371/journal.pone.0023833

Stadtfeld, M., Apostolou, E., Akutsu, H., Fukuda, A., Follett, P., Natesan, S., et al. (2010a). Aberrant silencing of imprinted genes on chromosome 12qF1 in mouse induced pluripotent stem cells. *Nature* 465, 175–181. doi: 10.1038/nature09017

Stadtfeld, M., Maherali, N., Borkent, M., and Hochedlinger, K. (2010b). A reprogrammable mouse strain from gene-targeted embryonic stem cells. *Nat. Methods* 7, 53–55. doi: 10.1038/nmeth.1409

Sun, L., Li, Y., and Yang, B. (2016). Downregulated long non-coding RNA MEG3 in breast cancer regulates proliferation, migration and invasion by depending on p53's transcriptional activity. *Biochem. Biophys. Res. Commun.* 478, 323–329. doi: 10.1016/j.bbrc.2016.05.031

Sun, L., Luo, H., Liao, Q., Bu, D., Zhao, G., Liu, C., et al. (2013). Systematic study of human long intergenic non-coding RNAs and their impact on cancer. *Sci. China Life Sci.* 56, 324–334. doi: 10.1007/s11427-013-4460-x

Sun, M., Xia, R., Jin, F., Xu, T., Liu, Z., De, W., et al. (2014). Downregulated long noncoding RNA MEG3 is associated with poor prognosis and promotes cell proliferation in gastric cancer. *Tumour Biol.* 35, 1065–1073. doi: 10.1007/s13277-013-1142-z

Tabar, L., Dean, P. B., Yen, A. M., Tarjan, M., Chiu, S. Y., Chen, S. L., et al. (2014). A proposal to unify the classification of breast and prostate cancers based on the

anatomic site of cancer origin and on long-term patient outcome. *Breast Cancer* 8, 15–38. doi: 10.4137/bcbcr.S13833

Tam, W. L., and Weinberg, R. A. (2013). The epigenetics of epithelial-mesenchymal plasticity in cancer. *Nat. Med.* 19, 1438–1449. doi: 10.1038/nm.3336

Terashima, M., Tange, S., Ishimura, A., and Suzuki, T. (2017). MEG3 long noncoding RNA contributes to the epigenetic regulation of epithelial-mesenchymal transition in lung cancer cell lines. *J. Biol. Chem.* 292, 82–99. doi: 10.1074/jbc.m116.750950

Thiery, J. P. (2002). Epithelial-mesenchymal transitions in tumour progression. *Nat. Rev. Cancer* 2, 442–454. doi: 10.1038/nrc822

Tierling, S., Dalbert, S., Schoppenhorst, S., Tsai, C. E., Oliger, S., Ferguson-Smith, A. C., et al. (2006). High-resolution map and imprinting analysis of the Gtl2-Dnchc1 domain on mouse chromosome 12. *Genomics* 87, 225–235. doi: 10.1016/j.ygeno.2005.09.018

Uroda, T., Anastasakou, E., Rossi, A., Teulon, J. M., Pellequer, J. L., Annibale, P., et al. (2019). Conserved pseudoknots in lncRNA MEG3 are essential for stimulation of the p53 pathway. *Mol. Cell* 75, 982–995.e9. doi: 10.1016/j.molcel.2019.07.025

Valdmanis, P. N., Roy-Chaudhuri, B., Kim, H. K., Sayles, L. C., Zheng, Y., Chuang, C. H., et al. (2015). Upregulation of the microRNA cluster at the Dlk1-Dio3 locus in lung adenocarcinoma. *Oncogene* 34, 94–103. doi: 10.1038/onc.2013.523

Wang, P., Ren, Z., and Sun, P. (2012). Overexpression of the long non-coding RNA MEG3 impairs in vitro glioma cell proliferation. *J. Cell. Biochem.* 113, 1868–1874. doi: 10.1002/jcb.24055

Wang, Y., and Kong, D. (2018). Knockdown of lncRNA MEG3 inhibits viability, migration, and invasion and promotes apoptosis by sponging miR-127 in osteosarcoma cell. *J. Cell. Biochem.* 119, 669–679. doi: 10.1002/jcb.26230

Wang, Y., and Zhou, B. P. (2013). Epithelial-mesenchymal transition—a hallmark of breast cancer metastasis. *Cancer Hallm.* 1, 38–49. doi: 10.1166/ch.2013.1004

Williams, E. D., Gao, D., Redfern, A., and Thompson, E. W. (2019). Controversies around epithelial-mesenchymal plasticity in cancer metastasis. *Nat. Rev. Cancer* 19, 716–732. doi: 10.1038/s41568-019-0213-x

Yao, Y., Zhang, T., Qi, L., Zhou, C., Wei, J., Feng, F., et al. (2019). Integrated analysis of co-expression and ceRNA network identifies five lncRNAs as prognostic markers for breast cancer. *J. Cell. Mol. Med.* 23, 8410–8419. doi: 10.1111/jcmm.14721

Yersal, O., and Barutca, S. (2014). Biological subtypes of breast cancer: prognostic and therapeutic implications. *World J. Clin. Oncol.* 5, 412–424.

Yin, D. D., Liu, Z. J., Zhang, E., Kong, R., Zhang, Z. H., and Guo, R. H. (2015). Decreased expression of long noncoding RNA MEG3 affects cell proliferation and predicts a poor prognosis in patients with colorectal cancer. *Tumour Biol.* 36, 4851–4859. doi: 10.1007/s13277-015-3139-2

Zaravinos, A. (2015). The regulatory role of microRNAs in EMT and cancer. *J. Oncol.* 2015:865816.

Zeisberg, M., and Kalluri, R. (2004). The role of epithelial-to-mesenchymal transition in renal fibrosis. *J. Mol. Med.* 82, 175–181. doi: 10.1007/s00109-003-0517-9

Zhang, X., Rice, K., Wang, Y., Chen, W., Zhong, Y., Nakayama, Y., et al. (2010). Maternally expressed gene 3 (MEG3) noncoding ribonucleic acid: isoform structure, expression, and functions. *Endocrinology* 151, 939–947. doi: 10.1210/en.2009-0657

Zhang, X., Zhou, Y., Mehta, K. R., Danila, D. C., Scolavino, S., Johnson, S. R., et al. (2003). A pituitary-derived MEG3 isoform functions as a growth suppressor in tumor cells. *J. Clin. Endocrinol. Metab.* 88, 5119–5126. doi: 10.1210/jc.2003-030222

Zhou, Y., Zhong, Y., Wang, Y., Zhang, X., Batista, D. L., Gejman, R., et al. (2007). Activation of p53 by MEG3 non-coding RNA. *J. Biol. Chem.* 282, 24731–24742. doi: 10.1074/jbc.m702029200

Zhu, W., Botticelli, E. M., Kery, R. E., Mao, Y., Wang, X., Yang, A., et al. (2019). Meg3-DMR, not the Meg3 gene, regulates imprinting of the Dlk1-Dio3 locus. *Dev. Biol.* 455, 10–18. doi: 10.1016/j.ydbio.2019.07.005

Conflict of Interest: The authors declare that the research was conducted in the absence of any commercial or financial relationships that could be construed as a potential conflict of interest.

Supplementary material

Antibodies for western blot: CDH1 (E-cadherin, BD Transduction Labs, 610182), CDH2 (N-cadherin, BD Transduction Labs, 610921)

Primers for qRT-PCR: *ALDH1A3* (IDT, Hs.PT.56a.657970), *INTGA6* (IDT,Hs.PT.58.453862).

Supplementary methods

Cell proliferation assay
Cell proliferation assay was performed on IncuCyte Zoom microscope (Essen Bioscience) according to manufacturer´s protocol. Cells were plated at density 10 x 10^3/ well in 96 - well plate (Corning, 353072). Cell culture media was changed three times per week.

Cell invasion assay
Cell invasion was examined using transwell filters with 8 µm pore size (Corning, 353097) with a layer of Matrigel, diluted 1:10 with H14 media. Briefly, 3 x 10^3 cells were resuspended in 250 µl H14 medium and placed on top of Matrigel and 500 µl of H14 + 10% FBS was added to the lower chambers, bellow filter. Cell were incubated for 48 hours in 5% CO_2 at 37°C. After incubation, the Matrigel was removed as well as non-invasive cells from the upper part of the filter with cotton swab and washed in between 3 x with 1 x PBS. The filters were then fixed with methanol and stained with DAPI. Cell were photographed in three random fields. Pictures were analysed wit ImageJ Software.

Scratch wound assay
The assay was performed according to manufacturer's protocol. 6 x 10^3 cells/ well were seeded so they were 100% confluent following day into ImageLock Plates (Essen Bioscience, 4379). Woundmaker (Essen Bioscience, 4493) was used to do the scratch. The images were taken every two hours. Images were analysed as *Relative Wound Density (%)*.

Statistical analysis
Statistical differences of qRT-PCRs (Supplementary Figure 6) and functional assay (Supplementary Figure 5B) between samples were assessed with paired Student t-test. Statistical differences in Supplementary Figure 5A and 5C was calculated using multiple unpaired Student t-test per row. Statistical differences of quantifications of western blots (Supplementary Figure 4) among samples were assessed using one- way ordinary ANOVA, followed by Tukey´s multiple comparison test. *P* values below 0.05 were considered significant (*$p \leq 0.05$; **$p \leq 0.01$; ***$p \leq 0.001$; ****$p \leq 0.0001$). All statistical analysis was performed in GraphPad Prism.

Supplementary Figures

Name	Fold change	P-value
mir-370	4,49	0.0016
mir-1185-2	3,97	0.0504
mir-770	3,95	0.0166
mir-376a-2	3,74	0.0612
mir-494	3,61	0.0032
mir-382	3,46	0.0144
mir-654	3,23	0.0054
mir-541	3,20	0.2823
mir-337	3,18	0.0085
mir-485	2,80	0.0139
mir-299	2,77	0.0172
mir-1185-1	2,56	0.0547
mir-377	2,56	0.0398
mir-127	2,53	0.0307
mir-376a-1	2,47	0.0475
mir-758	2,33	0.0549
mir-493	2,32	0.0374
mir-487b	2,31	0.0563
mir-369	2,18	0.0640
mir-432	2,17	0.0738
mir-154	2,13	0.0954
mir-543	2,10	0.1642
mir-134	2,09	0.2873
mir-656	2,03	0.1442
mir-412	1,96	0.1800
mir-379	1,93	0.1593
mir-411	1,85	0.1140
mir-668	1,82	0.2650
mir-380	1,70	0.3259
mir-431	1,69	0.3057
mir-376c	1,65	0.2135
mir-381	1,55	0.5539
mir-323b	1,54	0.3447
mir-495	1,34	0.5132
mir-433	1,31	0.5713
mir-487a	1,30	0.6391
mir-655	1,28	0.5625
mir-655	1,28	0.5625
mir-410	1,26	0.5627
mir-1197	1,26	0.6935
mir-539	1,16	0.7161
mir-496	1,08	0.8971
mir-376b	1,06	0.8880
mir-136	1,01	0.8938
mir-409	-1,37	0.6847
mir-323	#N/A	#N/A
mir-329-1	#N/A	#N/A
mir-329-2	#N/A	#N/A
mir-300	#N/A	#N/A
mir-889	#N/A	#N/A
mir-544	#N/A	#N/A

Supplementary Figure 1. The ncRNAs from DLK1-DIO3 locus have increased expression in mesenchymal cells. Majority of the miRNAs from the DLK1-DIO3 locus are upregulated in D492M compared to D492. Small RNA sequencing: the list of miRNAs from the DLK1-DIO3 locus, where majority of them are upregulated in D492M.

(A)

no	term	count	%	p-value
1	Extracelllar matrix	26	1.45903	1.56E-14
2	Proteinaceous extracellular matrix	25	1.40292	2.62E-14
3	Cell adhesion	35	1.96409	1.33E-13
4	Cell attachment site	15	0.84175	1.33E-13
5	Biological adhesion	35	1.96409	1.38E-13
6	Extracelllar matrix	21	1.17845	2.06E-13
7	Extracelllar region part	38	2.13244	1.63E-12
8	Cell adhesion	25	1.40292	2.77E-12
9	Signal	71	3.98429	6.65E-12
10	Signal peptide	71	3.98429	8.99E-12
11	EGF-like domain	19	1.06622	9.40E-12
12	AGF calcium-binding	13	0.72952	1.10E-11
13	Extracellular region	54	3.0303	2.07E-11
14	EGF-like, type 3	18	1.0101	2.25E-11
15	EGF-like region, conserved site	21	1.17845	3.50E-11

(B)

Spearman correlation with *MEG3*				
	Normal breast		Breast cancer	
Mesenchymal markers	rho	p-val	rho	p-val
ACTA2	0.098	7.64E-02	0.526	1.03E-80
AXL	0.196	3.31E-04	0.455	3.36E-58
CD61 (ITGB3)	0.288	9.45E-08	0.284	3.18E-22
CDH2	0	9.99E-01	0.156	1.57E-07
FOSL2	0.451	4.97E-18	0.249	2.95E-17
FOXC1	0.138	1.20E-02	0.121	5.09E-05
FOXC2	0.304	1.57E-08	0.3	1.11E-24
LAMA1	0.236	1.42E-05	0.467	8.03E-62
LOX	0.165	2.55E-03	0.398	1.10E-43
MMP2	0.45	6.60E-18	0.656	9.34E-139
SMAD4	0.091	9.86E-02	0.017	5.81E-01
SNAI1	0.169	2.09E-03	0.163	3.82E-08
SNAI2	0.092	9.65E-02	0.469	2.01E-62
TGFB1	0.628	1.10E-37	0.508	2.59E-74
TWIST1	0.405	1.71E-14	0.516	3.14E-77
TWIST2	0.357	2.20E-11	0.636	3.81E-128
VIM	0.01	8.54E-01	0.437	2.23E-53
YAP1	-0.287	1.07E-07	0.191	1.28E-10
ZEB1	0.2	2.45E-04	0.498	3.28E-71
ZEB2	0.277	3.89E-07	0.462	3.68E-60

Supplementary Figure 2. *MEG3* correlates with expression of mesenchymal genes. **(A)** *MEG3* correlates with expression of extracellular matrix genes. MEG3 correlated pathway analysis (GOBO). **(B)** *MEG3* correlates with expression of mesenchymal genes in normal breast and breast cancer tissue. Listed mesenchymal genes shows positive correlation with *MEG3* in MiPanda dataset. The Spearman correlation above 0.3 is considered as fair positive correlation are highlighted in orange.

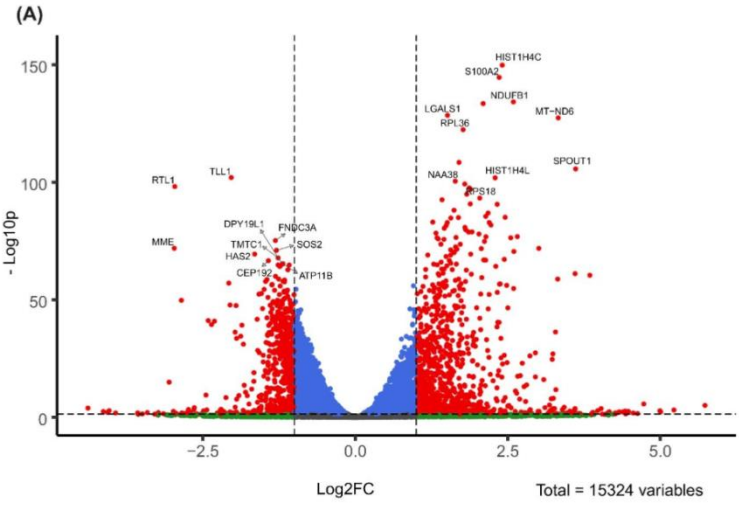
(A)
150
100
50
0
- Log10p
HIST1H4C
S100A2
NDUFB1
LGALS1
MT-ND6
RPL36
SPOUT1
NAA38
HIST1H4L
RPS18
RTL1
TLL1
DPY19L1
FNDC3A
MME
TMTC1
SOS2
HAS2
CEP192
ATP11B
−2.5
0.0
2.5
5.0
Log2FC
Total = 15324 variables

(B)

Top 30 downregulated genes in D492M$^{KD\text{-}MEG3}$

Gene	Log2 FC	p value
AC011005.1	-1.91	5.80E-10
ADGRL3	-1.77	6.60E-10
ADGRL4	-3.05	1.20E-15
CFH	-2.07	8.20E-58
CLDN24	-1.97	5.10E-05
CSMD3	-2.2	4.20E-04
DCT	-2.43	8.10E-04
EMB	-2.05	1.70E-48
GALNT3	-2.85	1.80E-50
GRIK2	-2.64	8.60E-05
HOOK1	-1.95	2.10E-08
HS6ST3	-4.38	1.30E-04
LRRCC1	-1.8	2.10E-11
MME	-2.97	1.20E-72
PKHD1L1	-2.12	4.40E-09
PKIA	-2.36	3.50E-40
POSTN	-2.45	3.70E-10
POTEE	-2.31	1.30E-41
POTEJ	-2.41	7.40E-42
RASEF	-1.86	6.70E-40
RGPD2	-1.82	2.40E-14
RGPD3	-1.88	3.30E-35
RTL1	-2.96	6.70E-99
SETSIP	-1.97	6.20E-37
SULF1	-1.96	3.00E-48
TLL1	-2.03	9.90E-103
ZC3H11B	-1.84	8.00E-32
ZDBF2	-2.74	5.10E-04
ZFY	-2.65	5.40E-04
ZNF711	-1.95	2.70E-34

Top 30 upregulated genes in D492M$^{KD\text{-}MEG3}$

Gene	Log2 FC	p value
APOA1	3.28	5.40E-37
AZU1	3.24	2.70E-04
C1orf232	2.87	5.60E-04
C1QTNF5	3.11	8.30E-05
CLDND2	3.32	1.50E-59
FFAR1	3.42	5.90E-05
FOXN1	2.95	6.80E-18
GNG8	3.21	1.40E-08
GSG1L2	3.6	2.00E-04
GUCY1A2	3.24	1.10E-27
HBZ	3.09	9.30E-17
HCRT	3.27	2.00E-04
HRC	2.86	8.10E-27
IL13RA2	3.18	6.20E-06
IYD	3.6	7.40E-04
MT-ND3	3.01	1.30E-72
MT-ND6	3.33	3.90E-128
MTRNR2L1	5.22	8.40E-04
MTRNR2L12	3.29	1.90E-12
NRXN1	4.73	2.20E-06
OR5AU1	3.39	6.10E-04
POU2F3	3.84	3.80E-61
PSORS1C2	3.23	2.30E-25
RPS29	2.95	4.00E-28
S100A8	3.25	8.90E-09
SPINK1	4.03	2.00E-04
SPOUT1	3.61	2.00E-106
TCF23	3.6	6.10E-04
TSPAN19	3.6	7.60E-62
UPK3BL1	5.73	8.90E-06

Supplementary Figure 3. RNA-sequencing analysis of D492M$^{KD\text{-}MEG3}$ vs. D492M$^{KD\text{-}MEG3}$. **(A)** Volcano plot over all data ($q < 0.05$, TPM > 1) showing symmetric distribution of the RNA-sequencing data. The top ten downregulated and top ten upregulated genes according log2 fold change in D492M$^{KD\text{-}MEG3}$ are labelled with gene names. **(B)** The table with top 30 downregulated genes in D492M$^{KD\text{-}MEG3}$ (left) and top 30, upregulated genes in D492M$^{KD\text{-}MEG3}$ (right).

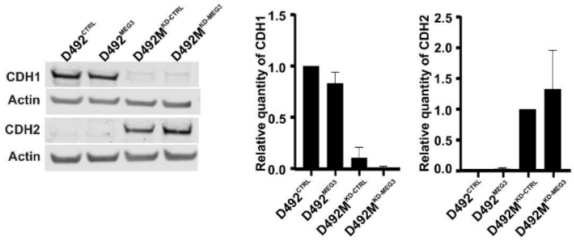

Supplementary Figure 4. *MEG3* does not change expression of CDH1 and CDH2. Representative pictures of western blot (WB) with its quantification bellow. $D492^{MEG3}$ has slightly decreased CDH1 (E-cad) on protein level compared to $D492^{CTRL}$. $D492M^{KD\text{-}MEG3}$ has slightly increased CDH2 (N-cad) on protein level compared to $D492M^{KD\text{-}CTRL}$, however with no statistical significance WB results shown as mean ± SD. One-way ordinary ANOVA followed by Tukey´s multiple comparison test was used to test significance; n = 3.

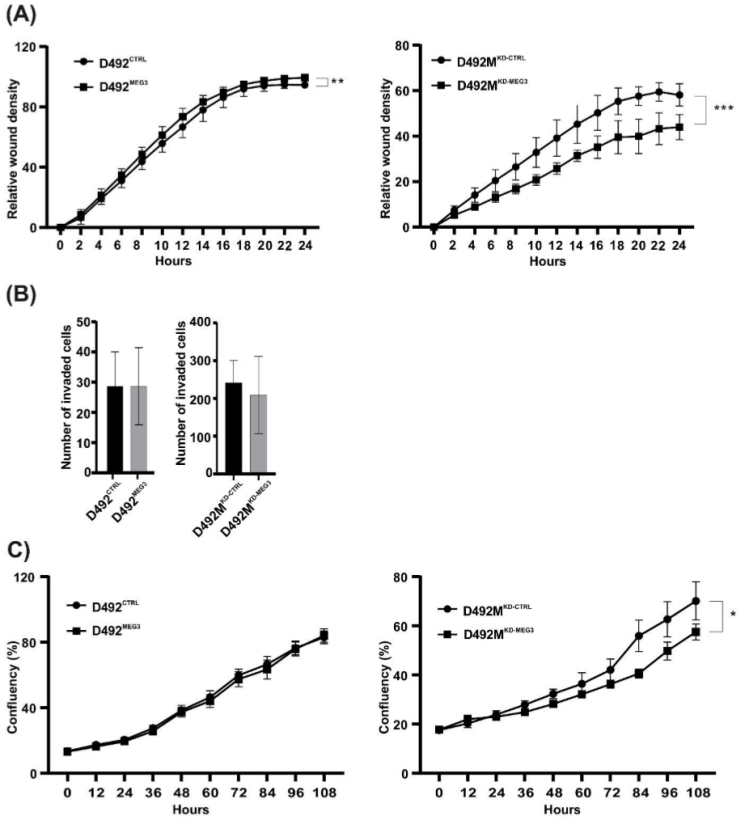

Supplementary Figure 5. *MEG3* does not influence invasion but has effect on wound healing migration. **(A)** *MEG3* slightly increase wound healing migration and knock-down of *MEG3* decrease wound healing migration. $D492^{MEG3}$ has slightly increased migration rate compared to $D492^{CTRL}$ (left). $D492M^{KD\text{-}MEG3}$ migrates less compared to $D492M^{KD\text{-}CTRL}$ (right). Data is analysed on Incucyte Zoom and results displayed as Relative wound density with mean ± SD. Multiple unpaired Student t-test per row was used to test significance, n = 6 ; ** $p \leq 0.01$; *** $p \leq 0.001$; with statistical differences at 24-hour timepoint. **(B)** *MEG3* and knock-down of *MEG3* does not have effect on invasion. $D492^{MEG3}$ has comparable invasion rate with $D492^{CTRL}$ (left). As well as $D492M^{KD\text{-}MEG3}$ has comparable invasion rate with $D492M^{KD\text{-}CTRL}$ (right). Quantification of number

of invaded cells shown as mean ± SD. Unpaired t-test was used to test significance, n = 6. **(C)** *MEG3* does not have effect on proliferation, while knock-down of *MEG3* has. Proliferation assay: $D492^{MEG3}$ has comparable proliferation rate with $D492^{CTRL}$ (left). $D492M^{KD\text{-}MEG3}$ slightly reduced proliferation rate compared to $D492M^{KD\text{-}CTRL}$ (right). Data is analysed on Incucyte Zoom and results displayed as Confluency percentage as mean ± SD. Multiple unpaired Student t-test per row was used to test significance at 24-hour time point; n = 6; $*p \leq 0.05$.

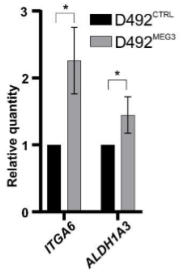

Supplementary Figure 6. *MEG3* increases expression of stem cell marker *ITGa6* and *ALDH1A3*. qRT-PCR showing $D492^{MEG3}$ has increased expression of *ITGa6* (Integrin alpha 6) and *ALDH1A3* (Aldehyde dehydrogenase) compared to $D492^{CTRL}$. Results shown as mean ± SD. Unpaired t-test was used to test significance: * $p \leq 0.05$; n = 3.

Paper II

Mechanisms of Development 155 (2019) 34–47

Contents lists available at ScienceDirect

Mechanisms of Development

journal homepage: www.elsevier.com/locate/mod

MiR-203a is differentially expressed during branching morphogenesis and EMT in breast progenitor cells and is a repressor of peroxidasin

Eirikur Briem[a], Zuzana Budkova[a], Anna Karen Sigurdardottir[a], Bylgja Hilmarsdottir[a,d], Jennifer Kricker[a], Winston Timp[e], Magnus Karl Magnusson[b,c], Gunnhildur Asta Traustadottir[a], Thorarinn Gudjonsson[a,b,*]

[a] Stem Cell Research Unit, Biomedical Center, Department of Anatomy, Faculty of Medicine, School of Health Sciences, University of Iceland, Iceland
[b] Department of Laboratory Hematology, Landspitali - University Hospital, Iceland
[c] Department of Pharmacology and Toxicology, Faculty of Medicine, School of Health Sciences, University of Iceland, Iceland
[d] Department of Tumor Biology, The Norwegian Radium Hospital, Oslo, Norway
[e] Department of Biomedical Engineering, Johns Hopkins University, USA

ABSTRACT

MicroRNAs regulate developmental events such as branching morphogenesis, epithelial to mesenchymal transition (EMT) and its reverse process mesenchymal to epithelial transition (MET). In this study, we performed small RNA sequencing of a breast epithelial progenitor cell line (D492), and its mesenchymal derivative (D492M) cultured in three-dimensional microenvironment. Among the most downregulated miRNAs in D492M was miR-203a, a miRNA that plays an important role in epithelial differentiation. Increased expression of miR-203a was seen in D492, concomitant with increased complexity of branching. When miR-203a was overexpressed in D492M, a partial reversion towards epithelial phenotype was seen. Gene expression analysis of D492M and D492M$^{miR\text{-}203a}$ revealed peroxidasin, a collagen IV cross-linker, as the most significantly downregulated gene in D492M$^{miR\text{-}203a}$. Collectively, we demonstrate that miR-203a expression temporally correlates with branching morphogenesis and is suppressed in D492M. Overexpression of miR-203a in D492M induces a partial MET and reduces the expression of peroxidasin. Furthermore, we demonstrate that miR-203a is a novel repressor of peroxidasin. MiR-203-peroxidasin axis may be an important regulator in branching morphogenesis, EMT/MET and basement membrane remodeling.

Summary statement

MiR-203a is highly upregulated during branching morphogenesis of D492 breast epithelial progenitor cells and is downregulated in its isogenic mesenchymal cell line D492M. Furthermore, miR-203a is a novel suppressor of peroxidasin (PXDN), a collagen IV crosslinking agent. MiR-203a may be an important regulator of branching morphogenesis and basement remodeling in the human breast gland, possibly through its target PXDN.

1. Introduction

Developmental events underlying breast epithelial morphogenesis are closely related to pathways important to cancer progression, *i.e.* epithelial to mesenchymal transition (EMT) and mesenchymal to epithelial transition (MET). Evidence shows that the two distinct epithelial cell lineages that make up branching morphogenesis in the breast, luminal- and myoepithelial cells, originate from common breast epithelial stem cells (Pechoux et al., 1999; Gudjonsson et al., 2002; Villadsen et al., 2007; Petersen and Polyak, 2010). These stem cells are responsible for continuous tissue remodeling throughout the reproductive period, as well as the extensive epithelial expansion and branching morphogenesis seen during pregnancy and lactation. Although, potential stem or progenitor cells have been identified in the human female breast gland there is still limited knowledge about the lineage development in the human breast. In that respect much can be learned from linage tracing studies in the mouse mammary gland. Recent studies have demonstrated that embryonic mammary gland contains homogenous basal progenitor cells that become restricted in the postnatal mammary gland (Lloyd-Lewis et al., 2018). Lilja et al. demonstrated that embryonic multipotent mammary cells become lineage-restricted early in development and that gain of function dictates luminal cell fate specification to both embryonic and basally committed mammary cells (Lilja et al., 2018). In a recent article Pal et al. demonstrated by single cell profiling of four developmental stages in the post-natal gland that the epithelium undergoes large changes in gene expression (Pal et al., 2017). In this paper they show that homogeneous basal-like expression pattern in pre-puberty was distinct to lineage-restricted programs in

* Corresponding author at: Stem Cell Research Unit, Department of Medical Faculty, Biomedical Center, University of Iceland, Vatnsmyrarvegi 16, 101 Reykjavík, Iceland.
E-mail address: tgudjons@hi.is (T. Gudjonsson).

https://doi.org/10.1016/j.mod.2018.11.002
Received 29 March 2018; Received in revised form 1 November 2018; Accepted 23 November 2018
Available online 01 December 2018

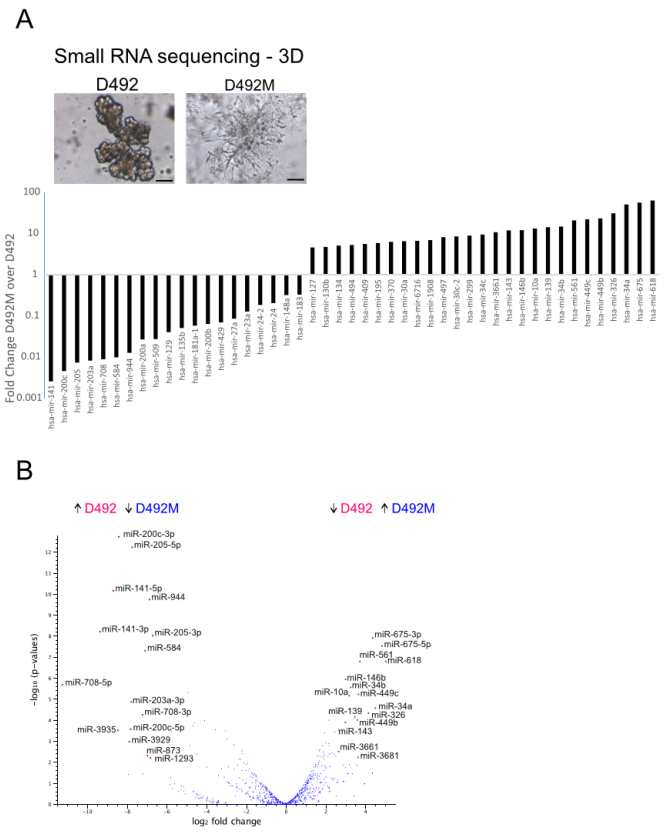

Fig. 1. Profiling miRNAs in the isogenic breast epithelial progenitor cell line D492 and its mesenchymal derivative D492M.
A) Differentially expressed miRNAs between D492M and D492 in 3D culture based on small RNA sequencing. Forty-seven miRNAs are differentially expressed between the mesenchymal (D492M) and epithelial (D492) state at day 14 in 3D culture. Twenty miRNAs are downregulated in D492M and among them are miRNAs that are important for epithelial integrity, such as the miR-200 family and miR-203a. Scale bar = 100 μm.
B) Volcano plot showing differential expressed miRNAs in D492M and D492, depicting statistical significance and high fold change in expression of epithelial associated miRNAs. Volcano plot constructed from small RNA sequencing data using fold change of expression values and p-values, enabling the visualization of the relationship between fold change and statistical significance. More extreme values on the x-axis show increased differential expression and higher values on the y-axis show increased statistical significance. The miR-200c-141 locus along with miR-205, miR-944, miR-584, miR-708 and miR-203a show the most fold change and statistical significance of the miRNAs downregulated in D492M.

puberty. Cellular linage tracing in humans is for obvious reasons not possible. However, transplantation of human breast epithelial cells into cleared mouse mammary fat pad (Lawson et al., 2015; Wronski et al., 2015) and 3D culture (Vidi et al., 2013) have to some extend unraveled the stem cell biology in the human breast gland. D492 is a breast epithelial stem cell line that generates branching *in vivo*-like structures in 3D-rBM (Gudjonsson et al., 2002; Villadsen et al., 2007; Sigurdsson et al., 2011). We have previously shown that when D492 is co-cultured

under 3D conditions, breast endothelial cells markedly stimulate their branching ability, but can also induce an irreversible EMT in the epithelial cells (Sigurdsson et al., 2011). This condition gave rise to the D492M cell line (Sigurdsson et al., 2011). In EMT, different pathways ultimately control transcriptional regulatory factors such as SNAI1, SNAI2, TWIST, ZEB1 and ZEB2 leading to increased expression of mesenchymal and decreased expression of epithelial markers (Moustakas and Heldin, 2007). Downregulation of the epithelial cell-cell adhesion proteins, such as E-cadherin, is one of the hallmarks of EMT (Peinado et al., 2007). In addition, expression of epithelial specific keratins is often greatly reduced, while expression of mesenchymal markers, such as N-cadherin, vimentin, alpha smooth muscle actin and fibronectin are increased in EMT (Moustakas and Heldin, 2007). Enhanced migration, invasion and resistance to apoptosis are also characteristic for cells that have undergone EMT (Hanahan and Weinberg, 2011). The tightly regulated process of cell conversion seen in EMT is also a critical event seen in many cancer types, including breast cancer (Petersen et al., 2001; Mani et al., 2008; Sarrio et al., 2008) and EMT is typically associated with increased aggressiveness and metastatic behavior (Hanahan and Weinberg, 2011).

Interestingly, the mesenchymal transition from D492 to D492M is accompanied by drastic changes in microRNA (miRNA) expression (Hilmarsdottir et al., 2015). MiRNAs have been described as regulators of protein expression through their ability to bind and silence mRNAs, where silencing of certain transcription factors, which are important for gene regulation, may cause marked changes in cell phenotype and fate (Hilmarsdottir et al., 2014). In recent years, miRNAs have been shown to be either tumor promoting or tumor suppressing depending on context and cancer type. For example, the miR-200 family has been linked to both stem cell regulation and cancer progression (Shimono et al., 2009). This family of miRNAs is strongly downregulated in tumors with high metastatic potential (Olson et al., 2009) and miR-200c, a member of this family, is downregulated in human breast cancer stem cells and normal mammary stem cells (Shimono et al., 2009). We have recently shown that the miRNA-200c-141 cluster is predominantly expressed in luminal breast epithelial cells, and that miRNA-200c-141 is highly expressed in D492, but not in D492M. Interestingly, overexpression of miR-200c-141 in D492M restored the luminal epithelial phenotype (Hilmarsdottir et al., 2015).

In this study, we compared the miRNA expression profile of D492 and D492M, when cultured in 3D reconstituted basement membrane matrix (3D-rBM). Small RNA sequencing revealed a striking difference in expression patterns between the two cell lines, with a number of known epithelial miRNAs, including miR-203a, downregulated in D492M. We demonstrated that miR-203a expression increases during branching morphogenesis *in vitro* similar to its expression pattern in mouse mammary gland *in vivo* (Avril-Sassen et al., 2009). Furthermore, overexpression of miR-203a in D492M induced partial phenotypic changes towards MET, reduced cell proliferation, migration, invasion, and increased sensitivity to chemically induced apoptosis. Finally, we identified miR-203a as a novel repressor of peroxidasin (PXDN), an extracellular matrix protein with peroxidase activity and a collagen IV crosslinking agent.

2. Results

2.1. Comparison of miRNA expression in the breast epithelial progenitor cell line D492 and its mesenchymal derivative D492M

D492 and D492M are isogenic cell lines with epithelial and mesenchymal phenotypes, respectively. We have previously shown a profound difference in miRNA expression between these cell lines when cultured in monolayer (Hilmarsdottir et al., 2015). Here, we conducted an expression analysis in 3D culture. Due to its stem cell properties, D492 can generate branching structures in 3D-rBM culture reminiscent of terminal duct lobular units (TDLUs) in the breast. In contrast, D492M form disorganized mesenchymal-like structures with spindle shape protrusions of cells (Fig. 1A, top). To investigate the miRNA expression patterns between D492 and D492M in 3D-rBM we performed small RNA sequencing (Fig. 1A). This revealed 47 differentially expressed miRNAs (> 1.5-fold change, $p < 0.05$ and FDR < 0.1) between D492 from (days 7, 14 and 21) and D492M at day 14 in 3D culture, where 20 of these miRNAs were downregulated in D492M. Among the most profound changes was downregulation of miR-200c, miR-141, miR-205 and miR-203a in D492M (Fig. 1A), all of which have been previously associated with epithelial integrity and repression of EMT (Gregory et al., 2008; Wellner et al., 2009; Feng et al., 2014). These miRNAs were all downregulated with high statistical significance in D492M as shown in the volcano plot (Fig. 1B). The upregulated miRNAs in D492M do not show as clear involvement in EMT as the downregulated ones.

2.2. Downregulation of miR-203a in D492M is not due to methylation of its CpG islands in the promoter area

Methylation of CpG islands in promoter areas is a common event during gene silencing. To further explore what causes downregulation of miRNAs in D492M, we explored the promoter DNA methylation status of differentially expressed miRNAs. We used the HumanMethylation450K BeadChip and looked at CpGs within 5 kb region of the promoter area of differentially expressed miRNAs. Two miRNAs did not have probes within the 5 kb region of the gene but of the 45 which did, 8 miRNAs showed differential DNA methylation between D492 and D492M (Table S2). Our data shows that promoter areas upstream of miR-200c-141 and miR-205 were methylated in D492M, but not in D492 (Fig. 2A). In contrast, the promoter area of miR-203a was not differentially methylated between D492 and D492M (Fig. 2A). Bisulfite sequencing of the promoter area of miR-200c-141, miR-205 and miR-203a confirmed that the promoter of miR-203a was unmethylated in D492M, unlike the promoters of miR-200c-141 and miR-205 (Fig. 2B). This is in contrast to previously published results in human mammary epithelial cells (HMLE) undergoing EMT (Taube et al., 2013) and some metastatic breast cancer cell lines (Zhang et al., 2011), where the promoter of miR-203a becomes methylated. Our data shows that a profound downregulation of miR-203a could be mediated through other mechanisms than DNA methylation, such as histone modifications. Indeed, miR-203a expression has been shown to be suppressed by EZH2 in prostate cancer (Cao et al., 2011). In summary, the repression of miR-203a, in endothelial induced EMT of D492 is not due to promoter methylation.

2.3. MiR-203a shows temporal changes in expression during branching morphogenesis in 3D culture and is associated with luminal breast epithelial cells

The breast gland is a dynamic organ during the reproduction period. In each menstrual cycle the breast epithelium undergoes changes associated with branching morphogenesis and if pregnancy occurs, the branching epithelium expands resulting in maximal differentiation during lactation. The glandular epithelium is then subject to apoptosis after breastfeeding during the involution phase (Javed and Lteif, 2013). Using D492 breast progenitor cells that are capable of generating branching epithelial morphogenesis in 3D-rBM, it is possible to analyze temporal changes during the branching process. To investigate if changes in miRNA expression occur during formation of TDLU–like structures in 3D-rBM, we isolated RNA from 3D-rBM cultures at days 7, 14 and 21, and performed small RNA sequencing.

Fifty-five miRNAs were differentially expressed between individual time points (> 2-fold change, FDR corrected p-value < 0.05), thereof 40 miRNAs were downregulated and 15 miRNAs were upregulated during branching (Fig. 3A). In particular, among the upregulated miRNAs were miR-141 and miR-203, which were also some of the most downregulated miRNAs in D492M (Fig. 1A). Thus, small RNA

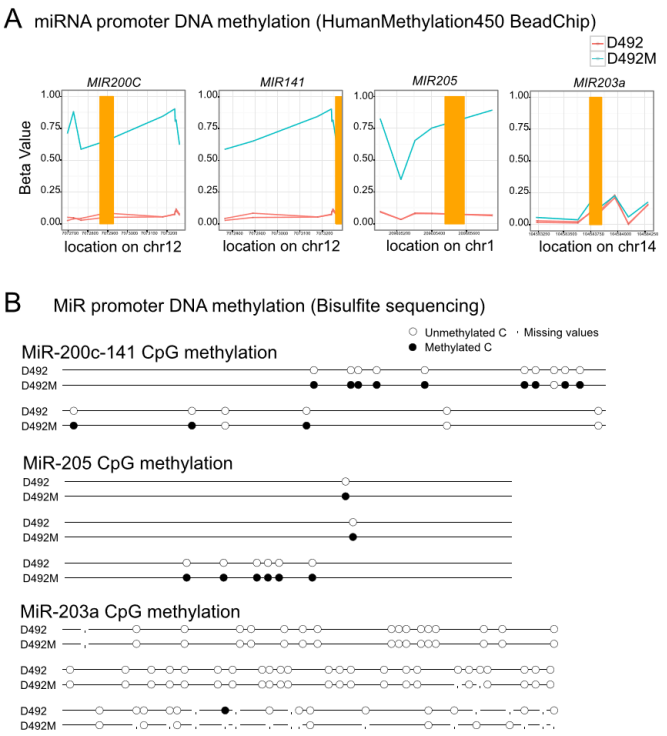

Fig. 2. miRNA promoter methylation of D492 and D492M

A) Differential DNA methylation of D492 (red) and D492M (blue). CpG methylation in the promoter area of differentially expressed miRNAs was investigated using the HumanMethylation450 BeadChip. The yellow bar represents the pre-miRNA and differential methylation is determined by a beta value > 0.2. MiR-200c, miR-141 and miR-205 are differentially methylated with more methylation in D492M, while methylation of miRNA-203a is unchanged. The expression of miR-200c-141 and miR-205 is repressed through DNA methylation, while expression of miRNA-203a is not.

B) Bisulfite sequencing of miRNA promoters in D492 and D492M. The promoters of miR-200c-141, miR-205 and miR-203a are un-methylated in D492. In D492M, the promoter of miR-203a remains un-methylated, while the promoters of miR-200c-141 and miR-205 are methylated.

sequencing, and subsequent verification with RT-qPCR, demonstrates that expression of miR-203a and miR-141 increased between time points and peaked at the late branching stage (day 21) (Fig. 3A–B). In contrast, expression of miR-205 and miR-200c was constant throughout the branching process (Fig. 3B). This indicates that miR-203a and miR-141 may play a role in differentiation of the epithelial cells during branching morphogenesis. The human breast epithelium is composed of two epithelial lineages, the luminal epithelial and the myoepithelial cells. In order to investigate whether miR-203a expression was lineage specific with either luminal- or myoepithelial cells, we sorted primary breast epithelial cells with EpCAM positive magnetic beads, as EpCAM is a luminal associated adhesion molecule that is also highly useful for antibody-based enrichment of luminal epithelial cells. We measured miR-203a expression in EpCAM high and EpCAM low cells, and demonstrated that, miR-203a expression was predominately associated with the EpCAM high luminal epithelial cells (Fig. 3C, left). There was some expression in the EpCAM low/negative myoepithelial cells, but no or little expression in endothelial cells and fibroblast (Fig. 3C, left). Due to the bipotential properties of D492 cells, they are able to generate luminal- and myoepithelial cells and differentiation of D492 branching colonies, into the two epithelial lineages, is clearly demonstrated with immunostaining against luminal- and myoepithelial markers (Gudjonsson et al., 2002). Based on EpCAM sorting of D492 cells into EpCAM high and EpCAM low fractions, we further confirmed that miR-

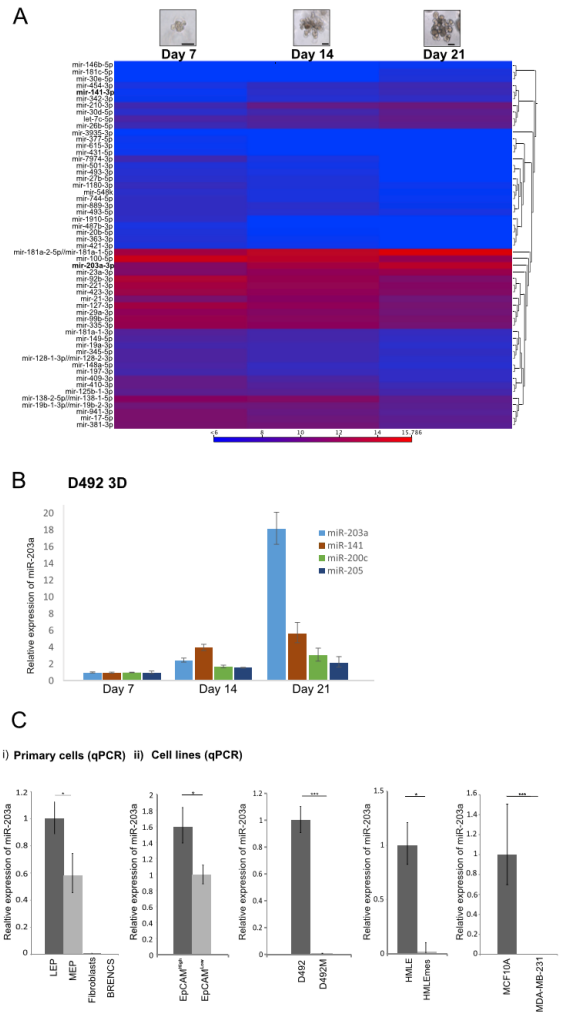

Fig. 3. MiR-203a is differentially expressed during branching morphogenesis in 3D culture.

A) Heatmap showing differentially expressed miRNAs in D492 at different time points during branching morphogenesis. Small RNA-sequencing of D492 at three different time points during branching morphogenesis at day 7, 14 and 21. miR-203a expression increases during branching of D492. Heatmap shows miRNAs with > 2-fold change in expression an FDR corrected p-values < 0.1. Scale bar = 100 μm.

B) Expression of epithelial miRNAs in D492 at different time points during branching. RT-qPCR showing that the expression of miR-203a and miR-141 significantly increases between time points during branching morphogenesis. Interestingly, expression of miR-203a increases markedly in late branching at day 21.

C) i) Expression of miR-203a in breast primary cells and D492 EpCAM sorted cells. In primary cells, miR-203a is expressed in the epithelial cells and is predominantly associated with the luminal cells but is absent in fibroblasts and endothelial cells. In D492 cells, miR-203a expression is predominantly associated with the EpCAM High cells.

ii) MiR-203a expression in breast cell lines. MiR-203a is expressed in breast cell lines with an epithelial phenotype but not with a mesenchymal phenotype. Expression of miR-203a in mesenchymal derivatives of D492 and HMLE, *i.e.* D492M and HMLEmes, is down-regulated with little or no expression in the mesenchymal state. The normal like breast cell line MCF10A has high expression of miR-203a, while the triple negative mesenchymal breast cancer cell line MDA-MB-231 has no expression of miR-203a. Results are displayed as average of three independent experiments (mean ± sd, n = 3).

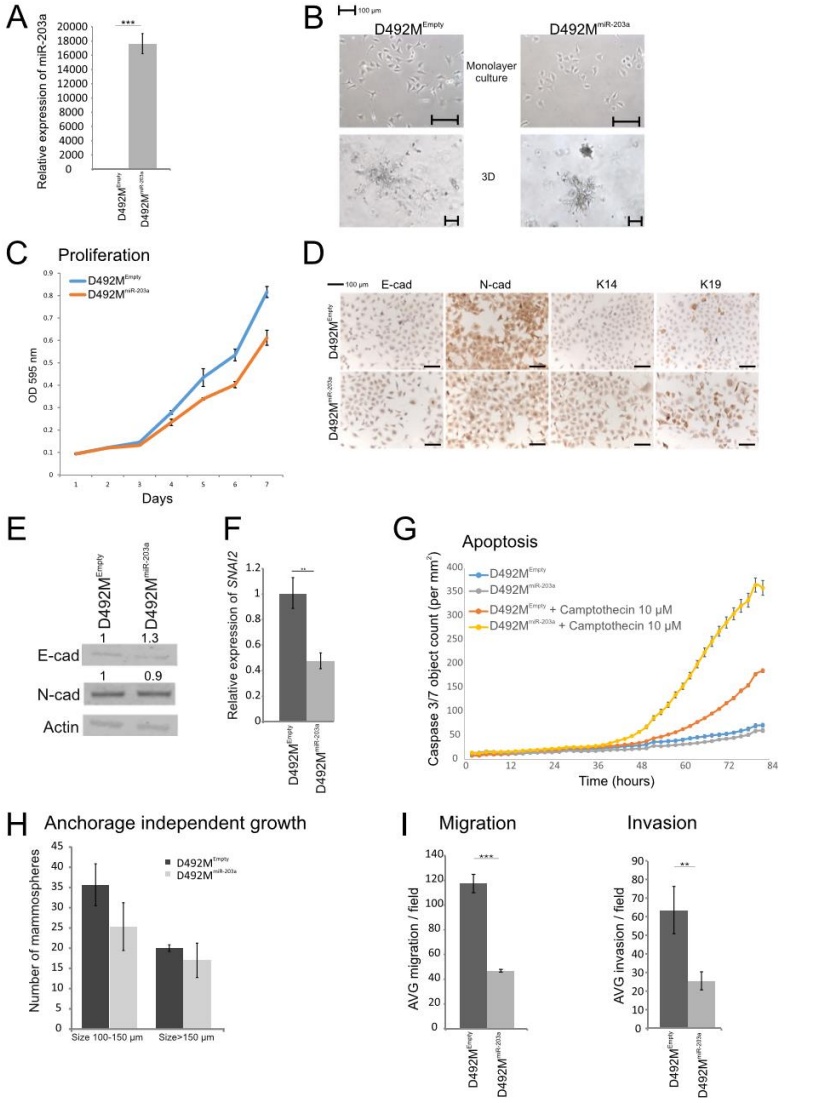

(caption on next page)

Fig. 4. Overexpression of miR-203a in D492M.
A)Overexpression of miR-203a in D492M. RT-qPCR showing 17,500-fold expression of miR-203a in D492M$^{miR\text{-}203a}$ compared to control.
B) MiR-203a increases adherence of D492M cells. Phase contrast images of monolayer cultures show that miR-203a overexpression in D492M causes cells to adhere more to each other compared to D492M^{Empty} control. Phase contrast images from 3D culture show that D492M$^{miR\text{-}203a}$ form more compact colonies, with some colonies showing protrusion of mesenchymal cells compared to control. Scale bar = 100 μm.
C) MiR-203a reduces proliferation of D492M. Reduced proliferation of D492M shown by staining with crystal violet from day 1–7 in monolayer culture. Results are shown as average of 4 replicates (mean ± SD)
D) DAB staining of monolayer cultures from D492M$^{miR\text{-}203a}$. D492M$^{miR\text{-}203a}$ cells display reduced expression of N-Cadherin but show little change in expression of E-Cadherin. Scale bar = 100 μm.
E) Western blot of E- and N-Cadherin in D492M$^{miR\text{-}203a}$. There is slightly less protein expression of N-Cadherin (10% reduction) but little change in expression of E-Cadherin in D492M$^{miR\text{-}203a}$ indicating reduced mesenchymal characteristics in D492M$^{miR\text{-}203a}$.
F) Expression of SNAI2 is reduced in D492M$^{miR\text{-}203a}$. MiR-203a, which has a known binding site in the 3′-UTR of SNAI2, significantly reduces expression of SNAI2 as determined by qPCR.
G) D492M$^{miR\text{-}203a}$ cells are more sensitive to chemically induced apoptosis. In D492M cells, miR-203a increases sensitivity to apoptosis induced by Camptothecin. Data is analyzed on IncuCyte Zoom and data is displayed as Caspase 3/7 object count/mm^2 (mean ± SEM).
H) Anchorage independent growth is reduced upon miR-203a overexpression. miR-203a reduces stem cell like properties in D492M. D492M$^{miR\text{-}203a}$ has reduced ability to generate mammospheres in low attachment assay compared to D492M^{Empty}.
I) MiR-203a reduces the ability of D492M cells to migrate and invade. D492M$^{miR\text{-}203a}$ has less ability to migrate through trans-well filter than D492M^{Empty} and D492M$^{miR\text{-}203a}$ has reduced capability to invade through Matrigel coated transwell filter. Data is shown as average number of cells per field (mean ± SEM).

203a was more associated with the luminal epithelial population in D492 (Fig. 3C, right). Differential expression of miR-203a between D492 and D492M was confirmed by RT-qPCR (Fig. 3C, right). To determine whether this was in concurrence with other breast cell lines with epithelial and mesenchymal phenotypes, we examined the expression levels of miR-203a in HMLE, its mesenchymal derivative HMLEmes (Fig. 3C, right), the normal cell-derived MCF10A, and the mesenchymal cancer cell line, MDA-MB-231 (Fig. 3C, right). Expression of miR-203a was restricted to all three cell lines with an epithelial phenotype.

2.4. MiR-203a expression reduces the mesenchymal traits of D492M cells

To analyze if the presence of miR-203a affects the phenotype of D492M, we overexpressed miR-203a in D492M (D492M$^{miR\text{-}203a}$), using a lentiviral based transfection system. D492M$^{miR\text{-}203a}$ expressed miR-203a 17,500-fold higher than control (D492M^{Empty}) (Fig. 4A). Interestingly, phase contrast images of monolayer cultures show that miR-203a overexpression in D492M causes increased adherence between cells (Fig. 4B). Furthermore, when D492M is cultivated in 3D-rBM, it forms spindle shaped mesenchymal-like colonies in contrast to D492M$^{miR\text{-}203a}$ that forms more compact colonies although the colonies still show cellular protrusions, typical of mesenchymal cells (Fig. 4B). When the cells were cultured in monolayer, overexpression of miR-203a in D492M reduces the proliferation rate of the cells (Fig. 4C). Furthermore, there was visible reduction in expression of the mesenchymal marker N-cadherin and increased expression of E-cadherin, K14 and K19 in D492M$^{miR\text{-}203a}$, indicating a moderate reduction in mesenchymal characteristics (Fig. 4D–E). The EMT transcription factor SNAI2 is a confirmed target of miR-203a, and miR-203a is in return suppressed by SNAI2 forming a negative feedback loop (Ding et al., 2013). In concordance with SNAI2 being a target of miR-203a, there was reduced expression of SNAI2 when miR-203a was overexpressed in D492M (Fig. 4F). Since the EMT phenotype has been associated with apoptosis resistance and SNAI2 is a known inhibitor of apoptosis (Inoue et al., 2002), we asked if D492M$^{miR\text{-}203a}$ cells were less resistant to chemically induced apoptosis compared to D492M^{Empty}. Indeed, D492M$^{miR\text{-}203a}$ cells were more sensitive than D492M^{Empty} to camptothecin, a chemical inducer of apoptosis (Fig. 4G).

The ability of cells to proliferate as mammospheres under non-adherent conditions has been described as a property of early progenitor/stem cells (Dontu et al., 2003). When D492 and D492M were cultured in low attachment plates both generated mammospheres but D492M generated significantly larger and a higher number of colonies (Sigurdsson et al., 2011). Interestingly, overexpression of miR-203a in D492M negatively impacts anchorage independent growth, resulting in loss of progenitor/stem cell properties indicating that miR-203a overexpression in D492M induces cellular differentiation (Fig. 4H). As mesenchymal cells have increased motility compared to epithelial cells, we analyzed the effect of miR-203a overexpression on the ability of D492M to migrate and invade. D492M$^{miR\text{-}203a}$ cells showed reduced ability to migrate through transwell filters (Fig. 4I, left) and to invade through Matrigel coated transwell filters (Fig. 4I, right) indicating a suppression of mesenchymal characteristics. Collectively, overexpressing miR-203a in D492M induced a reduction of mesenchymal characteristics, caused reduced proliferation, migration and invasion, and increased sensitivity towards chemically induced apoptosis.

2.5. Peroxidasin (PXDN) is a novel target of miR-203a

Due to the phenotypic differences between D492 and D492M in 3D culture and the fact that miR-203a is not expressed in D492M, we decided to compare the transcriptional profiling of D492, D492M and D492M$^{miR\text{-}203a}$, with emphasis on identifying novel targets of miR-203a. Herein, we identified peroxidasin (PXDN), a collagen IV cross-linking agent in the basement membrane, as the most significantly downregulated gene in D492M$^{miR\text{-}203a}$ compared to D492M (Fig. 5A). In addition, we identified three potential binding sites for miR-203a in the 3′-UTR of PXDN, one well conserved and two less conserved (Fig. 5B). To further investigate the potential interaction between miR-203a and PXDN we treated D492M and D492M$^{miR\text{-}203a}$ with miR-203a-mimic and miR-203a-inhibitor, respectively. PXDN expression was reduced (Fig. 5C, left) and increased (Fig. 5C, right) when D492M and D492M$^{miR\text{-}203a}$ were treated with miR-203a mimic and inhibitor, respectively, corroborating that miR-203a regulates PXDN expression. Furthermore, we demonstrated that PXDN expression was directly regulated by miR-203a by carrying out a dual luciferase reporter assay showing that the relative luciferase activity was significantly lower in the PXDN 3′-UTR containing the miR-203a target sequence compared with PXDN 3′-UTR with deleted miR-203a binding sequence, when transfected with miR-203a mimic (***$p < 0.001$) (Fig. 5D). This suggested that miR-203a could directly regulate the expression of PXDN through targeting its 3′-UTR. As a positive control we demonstrated significantly lower relative luciferase activity in p63 3′-UTR containing the miR-203a target sequence compared with p63 3′-UTR with deleted miR-203a binding sequence, when transfected with miR-203a mimic (**$p < 0.01$) (Fig. S1).

In order to investigate whether the observed effect of miR-203a overexpression on D492M is due to repression of PXDN, we knocked down PXDN in D492M using siRNA (Fig. S2) and analyzed the phenotypic changes in monolayer. As with miR-203a overexpression, we see reduced proliferation and increased sensitivity to chemically

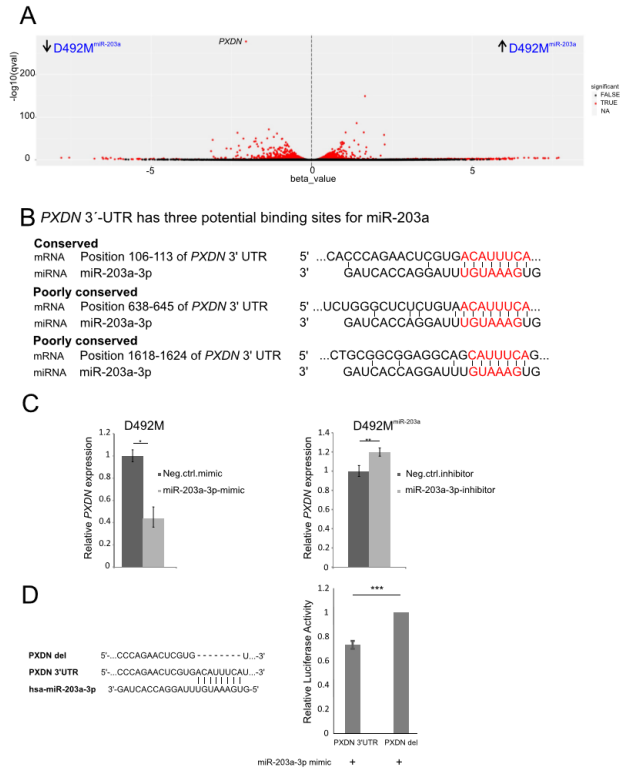

Fig. 5. Gene expression profiling of D492M overexpressing miR-203a.

A) Volcano plot showing differential expressed transcripts in D492M$^{miR\text{-}203a}$ and D492M, depicting statistical significance and high fold change in gene expression. Volcano plot was constructed from RNA sequencing data using beta and q-values from Sleuth analysis (max FDR = 0.05), enabling the visualization of the relationship between differentially expressed transcripts and statistical significance. More extreme values on the x-axis show increased differential expression and higher values on the y-axis show increased statistical significance. PXDN is the most downregulated gene when miR-203a is overexpressed in D492M.

B) PXDN 3′-UTR has three potential binding sites for miR-203a

Bioinformatics analysis reveals three potential binding sites for miR-203a in the 3′-UTR of PXDN a heme-containing peroxidase that is secreted into the extracellular matrix and is involved in extracellular matrix formation. One of the binding sites is conserved and two are poorly conserved.

C) MiR-203a regulates PXDN expression. D492M cells treated with miR-203a mimic have reduced expression of PXDN, whereas D492M$^{miR\text{-}203a}$ cells treated with miR-203a inhibitor have increased expression of PXDN. Cells were treated with miR-203a-3p mimic or inhibitor, respectively, and PXDN expression was measured by qPCR. Results are displayed as average of three independent experiments (mean ± sd, n = 3).

D) MiR-203a directly binds to its target sequence on PXDN 3′UTR. HEK293T cells transfected with miR-203a-3p mimic and pmirGLO plasmid containing the miR-203a binding site and surrounding sequence had reduced luciferase activity compared to cells transfected with the miR-203a-3p mimic and plasmid with the miR-203a binding site deleted, indicating binding of the miR-203a-3p mimic to the target sequence. Results are displayed as average of three independent experiments (mean ± SD, n = 3).

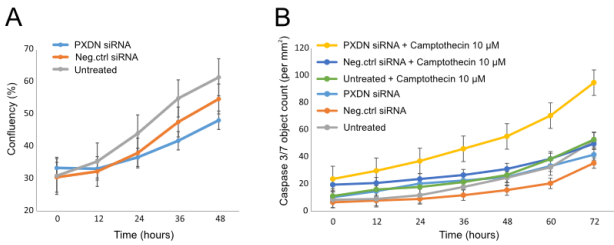

Fig. 6. PXDN repression reduces proliferation and increases sensitivity to chemically induced apoptosis.
A) PXDN silencing in D492M cells reduces proliferation. D492M cells treated with siRNA against PXDN have reduced proliferation rate compared to D492M cells treated with negative control siRNA or untreated D492M cells. Data is analyzed on IncuCyte Zoom and data is displayed as Confluency percentage (mean ± SEM). B) D492M cells with silenced PXDN are more sensitive to chemically induced apoptosis. Camptothecin induced apoptosis is increased in D492M cells with silenced PXDN, compared to cells treated with negative control siRNA and untreated D492M cells. Data is analyzed on IncuCyte Zoom and data is displayed as Caspase 3/7 object count/mm^2 (mean ± SEM).

induced apoptosis upon PXDN silencing (Fig. 6A & B), however no changes were seen in migration nor invasion (data not shown). This suggests that miR-203a mediates some of its effects, at least partly, through repression of PXDN.

Collectively, we have shown that miR-203a is a novel repressor of PXDN, a protein that plays an important role as a collagen IV cross-linking agent in the basement membrane and has been implicated in the EMT process, *i.e.* development, fibrosis and cancer.

3. Discussion

Modeling breast morphogenesis and EMT in 3D culture is an important tool to shed light on cellular and molecular mechanisms behind these developmental events and complements well *in vivo* models. Although animal models, in particular mouse models, have contributed significantly to our understanding of mammary gland morphogenesis and breast cancer, they cannot replace the necessity for using human cells due to the molecular and cellular differences in mammary gland biology between species (Dontu and Ince, 2015). Although, functionally working in similar ways during breast feeding, the mouse and human female mammary gland differ greatly. The human female breast gland is composed of ducts that end in terminal duct lobular units (TDLUs), surrounded by cellular-rich connective tissue. In contrast, the mouse mammary gland is composed of ducts that terminate in end buds, which are surrounded by adipose tissue. Thus, the histological comparison between the mouse and human mammary gland demonstrates large differences that need to be taken into account when studies are designed to explore the interactions between epithelial cells and stroma.

In this study, we have applied two isogenic breast cell lines, D492 and D492M, and 3D culture based on reconstituted basement membrane (rBM) to capture the phenotypic architecture of branching morphogenesis of breast epithelium and EMT, respectively. D492 is a breast epithelial progenitor cell line established from suprabasal epithelium of a normal breast gland (Gudjonsson et al., 2002; Villadsen et al., 2007; Sigurdsson et al., 2011). D492, was established by immortalizing cells from reduction mammoplasty using the E6 and E7 oncogenes from human papilloma virus 16. E6 and E7 target p53 and RB, respectively that without any doubt interfere with number of processes in the cells and this should be kept in mind when designing projects involving this cell line. However, D492 is non-tumorigenic, can generate both luminal and myoepithelial cells and in 3D culture generate structures reminiscent of TDLU-like structures *in vivo* and therefore remains a good tool for studying molecular mechanisms involved in these processes. D492M has a mesenchymal phenotype and is derived from D492 cells that have undergone EMT when co-cultured with breast endothelial cells (Sigurdsson et al., 2011).

In a previous work we demonstrated that overexpression of miR-200c-141 in D492M was sufficient to induce MET in D492M albeit only to luminal epithelial cells. When p63 was overexpressed in D492M containing miR-200c-141, bipotential and branching properties of D492 were restored (Hilmarsdottir et al., 2015). Recently, Wuidart et al. showed that p63 was essential for maintaining the unipotent basal fate of embryonic mouse mammary gland progenitors. Interestingly, sustained p63 expression in luminal epithelial cells reprogrammed cells towards basal cells (Wuidart et al., 2018). D492 has stem cell properties based on its ability to generate luminal and myoepithelial cells in culture and branching structures in 3D culture. It is however, possible that the immortalization using the E6 and E7 oncogenes from human papilloma virus 16 (Gudjonsson et al., 2002) and the 3D cell culture condition may contribute to the cellular plasticity of D492 and thus reflect more embryonic development of the mammary gland than postnatal development.

In this study, we analyzed differential expression of miRNAs in D492 and D492M on day 14 in 3D-rBM culture. Small RNA sequencing analysis revealed 47 differentially expressed miRNAs between D492 and D492M at day 14 in culture, of which 20 miRNAs were down-regulated in D492M. Among the most profound changes, was the downregulation of the miR-200 family, miR-205 and miR-203a in D492M. We have previously shown that these miRNAs are also down-regulated in D492M when cultured in monolayer (Hilmarsdottir et al., 2015) indicating a comparable expression pattern between 2D and 3D conditions. In the same study we demonstrated that when miR-141 and miR-200c, which are under regulation of the same promoter on chromosome 12 (Hilmarsdottir et al., 2014; Hilmarsdottir et al., 2015), were overexpressed in D492M, a reversal towards epithelial phenotype was induced, albeit only towards the luminal epithelial phenotype (Hilmarsdottir et al., 2015). Unlike miR-200c-141 and miR-205, which are both heavily methylated in D492M, we did not observe any methylation of CpG islands in the promoter area of miR-203a. The unmethylated pattern of the miR-203a promoter in D492M is opposite to what has been described in other breast cell lines with a mesenchymal phenotype (Zhang et al., 2011; Taube et al., 2013). This indicates that miR-203a down regulation in D492M may be through other processes, such as histone modification, or transcription factor repression.

Ectopic overexpression of miR-203a in D492M partially induced epithelial traits. The effect of increased miR-203a expression was

primarily evident in functional assays, where it caused reduced cell proliferation, migration, and invasion. Morphologic and gene expression changes were subtle and indicated only partial MET, as evidenced by reduced expression of N-cadherin, and SNAI2, an EMT transcription factor known to silence expression of miR-203a. Moes et al. demonstrated that overexpression of SNAI1 in MCF-7 breast cancer cells resulted in repression of miR-203 (Moes et al., 2012).

Branching morphogenesis of the D492 cells in 3D-rBM was used to mimic breast development and differentiation. We show that miR-203a expression coincides with increased differentiation status of the breast epithelial cells. In contrast, other epithelial associated miRNAs such as miR-205, miR-200c and miR-141 show constant or minimal fluctuation in expression throughout the branching period (21 days). In a miRNA expression study on mouse mammary gland development, Avril-Sassen et al. (2009) demonstrated that miR-203a showed temporal changes during different phases of mammary gland development. High expression was seen in early development and gestation followed by low expression in lactation and involution stages (Avril-Sassen et al., 2009). Reduced expression of miR-203a in lactation might be due to that fact that lactation requires functionally active p63 positive myoepithelial cells. MiR-203a is a repressor of p63 and therefore, downregulation of miR-203a is probably necessary for full activity of the myoepithelium.

Since D492 cells have stem cell properties, it is possible to separate cells into luminal epithelial and myoepithelial cells (Gudjonsson et al., 2002; Villadsen et al., 2007). Based on EpCAM, a luminal associated epithelial adhesion molecule, we separated D492 cells into two cell populations: EpCAM-high and EpCAM-low. EpCAM-high cells showed significantly higher expression of miR-203a than EpCAM-low cells. This was also confirmed in primary luminal epithelial- and myoepithelial cells. This result is in agreement with DeCastro et al. (DeCastro et al., 2013), where they demonstrated that miR-203a was significantly more expressed in mouse luminal epithelial progenitor cells and differentiated luminal epithelial cells compared to stem/basal cells. They also tested the expression levels of miR-203a in a number of normal and cancerous human breast epithelial cell lines: highest expression was predominantly in cell lines with a luminal epithelial phenotype.

To search for potential target genes for miR-203a we analyzed gene expression of D492M and D492M$^{miR\text{-}203a}$. The most significantly differential expressed gene between D492M and D492M$^{miR\text{-}203a}$ was PXDN. PXDN is a heme-containing peroxidase that produces hypobromous acid (HOBr) to form sulfilimine cross-links to stabilize the collagen IV network in the basement membrane and is believed to be important in normal development (Colon et al., 2017). PXDN has also been linked to EMT and disease conditions such as melanoma invasion and fibrosis (Tindall et al., 2005; Cheng et al., 2008; Peterfi et al., 2009; Liu et al., 2010; Tauber et al., 2010; Barnett et al., 2011; Khan et al., 2011; Bhave et al., 2012; Yan et al., 2014; Ero-Tolliver et al., 2015; Colon and Bhave, 2016; Jayachandran et al., 2016; Sitole and Mavri-Damelin, 2018).

Jayachandran et al. identified PXDN as consistently elevated in invasive mesenchymal-like melanoma cells and it was also found highly expressed in metastatic melanoma tumors. Gene silencing led to reduced melanoma invasion *in vitro* (Jayachandran et al., 2016). Moreover, Peterfi et al. have shown that PXDN is secreted from myofibroblasts and also from fibrotic kidney (Peterfi et al., 2009). Young et al. demonstrated that PXDN expression increases in PIK3CA mutant MCF10A cells and that the PXDN protein is mainly associated with secreted exosomes (Young et al., 2015). When knocking down PXDN in four basal like breast cancer cell lines, all cell lines showed reduced proliferation and when PXDN was knocked down in the luminal cell line MDA-MB-361, which expresses little PXDN, there was also reduced proliferation (Young et al., 2015). The reduced proliferation rate we saw in D492M$^{miR\text{-}203a}$, could be because of PXDN silencing by miR-203a, as we also see reduced proliferation when PXDN is transiently knocked down with silencing RNA. The fact that PXDN is overexpressed in the mesenchymal cell line D492M may link it to the EMT phenotype.

In summary, mammary gland development is mostly a post-natal process, where post-transcriptional regulation *via* miR-203a expression correlates with differentiation stages in the mammary epithelium. Using the D492 breast progenitor cells cultivated in 3D-rBM it is possible to capture the critical aspects of branching morphogenesis. Temporal changes in miR-203a expression during the *in vitro* branching process correlate well with *in vivo* conditions. Although miR-203a repression and overexpression are well documented in a number of studies, we observed only subtle changes towards MET when overexpressed in D492M. Furthermore, we have demonstrated a novel link between miR-203a and PXDN, which is highly expressed in D492M. Collectively, we conclude that miR-203a may be important to retain epithelial phenotype of breast epithelial cells, possibly through its target PXDN.

4. Material and methods

4.1. Cell culture

D492 and D492M cells were maintained in H14 medium as described previously (Sigurdsson et al., 2011). Primary luminal epithelial cells (EpCAM$^+$) and myoepithelial cells (EpCAM$^-$) were isolated from primary culture of breast epithelial cells derived from reduction mammoplasties by magnetic cell sorting (MACS) and maintained in CDM3 and CDM4, respectively, as previously described (Pechoux et al., 1999). Primary human breast endothelial cells (BRENCs) were isolated from breast reduction mammoplasties and cultured in endothelial growth medium (EGM) (Lonza) + 5% FBS (Invitrogen), referred to as EGM5 (Sigurdsson et al., 2006). Growth factor reduced reconstituted basement membrane (rBM, purchased as Matrigel, Corning #354230) was used for 3D cultures. 3D monocultures were carried out in 24-well culture plates (Corning). 1×10^4 D492 cells were suspended in 300 µl of rBM. Co-culture experiments were carried out with either 500, or 1×10^3 cells mixed with 1×10^5–2×10^5 BRENCs. 300 µl of mixed cells/rBM were seeded in each well of a 24-well plate and cultured on H14 (monoculture) or EGM5 (co-culture) for 14–21 days.

Branching, solid and spindle-like structures were isolated from 3D co-cultures with gentle shaking on ice in PBS - EDTA (5 mM) solution as previously described (Lee et al., 2007).

4.2. Small RNA sequencing

Total RNA was isolated from branching and spindle-like colonies from D492 and D492M, respectively using Tri-Reagent (Thermo Fisher Scientific, #AM9738). For D492 branching time points, RNA was isolated from 3D-rBM culture on days 7, 14 and 21 but for D492M RNA was isolated only on day 14. Samples were pooled in triplicates from each time point before small RNA library preparation. Small RNA libraries were prepared using the TruSeq Small RNA Library Kit from Illumina (#RS-200-0012) per manufacturer's protocol. The small RNA libraries were then sequenced using the Illumina MiSeq platform and V2 sequencing chemistry. FASTQ files were generated with MiSeq Reporter (Illumina, San Diego, US-CA). Small RNA sequence analysis was performed using the CLC Genomics Workbench (CLC Bio-Qiagen, Aarhus, Denmark) and miRBase – release 21 was used for annotation. Samples were normalized by totals and counts reported as reads per million. Reads above 29 nt and below 15 nt in length were discarded. Proportion-based statistical analysis was done using the test of Kal (Kal et al., 1999). Hierarchal clustering of features was performed using Log2 transformed expression values, Euclidean distance and single linkage. For the D492 and D492M comparison samples from day 7, 14 and 21 from D492 were compared to D492M sample from day 14.

4.3. DNA isolation and methylation bead chip array

D492 (1×10^4 cells) and D492M (2.5×10^4 cells) were grown in

3D-rBM in triplicate in a 24-well plate for 14 days and colonies extracted from 3D-rBM with gentle shaking on ice in PBS - EDTA (5 mM) solution as previously described (Lee et al., 2007). DNA was extracted using the PureLink Genomic DNA Mini Kit (Thermo Fisher Scientific, #K182002) and DNA was bisulfite converted using the EZ-96 DNA Methylation-Gold Kit (Zymo Research, #D5007) per manufacturer's protocols. The samples were hybridized to the Infinium HumanMethylation450 BeadChip array (Illumina, # WG-314-1003). Data was analyzed using the minfi Bioconductor package (Aryee et al., 2014).

4.4. Bisulfite sequencing

DNA (0.5–1 μg) was bisulfite converted using the EpiTect Bisulfite Kit (Qiagen, #59104). Target DNA sequences were amplified using nested PCR (see primers in Table S1). Methylation levels were analyzed by sequencing the bisulfite modified promoter regions on a 3130 Genetic Analyzer (Applied Biosystems). Methylation data from bisulfite sequencing was analyzed and visualized using the BiQ Analyzer v2.0 (Bock et al., 2005).

4.5. Quantitative reverse transcription PCR analysis

Total RNA was extracted with Tri-Reagent (Thermo Fisher Scientific, #AM9738) and

reverse transcription performed using random hexamers (Thermo Fisher Scientific, #N8080127) and SuperScript IV Reverse Transcriptase (Thermo Fisher Scientific, #18090050). The following primers were used for mRNA qRT-PCR analysis, SNAI2 (Hs00950344_m1) (Thermo Fisher Scientific, #4331182) and GAPDH as endogenous reference gene (Thermo Fisher Scientific, # 4326317E). Maxima Probe/ROX qPCR Master Mix (2×) (Thermo Fisher Scientific, # K0231) was used for TaqMan qRT-PCR analysis.

Quantitative RT-PCR analysis of miRNAs was performed using the universal cDNA synthesis kit II (Exiqon, #203301) and ExiLENT SYBR Green master mix (Exiqon, #203402). The following primer sets from Exiqon were used for miRNA qRT-PCR analysis, hsa-miR-203a (#205914), hsa-miR-141-3p (#204504), hsa-miR-200c-3p (#204482), hsa-miR-205-5p (#204487) and U6 snRNA (#203907) was used as endogenous reference. All qRT-PCRs were performed on the Applied Biosystems 7500 Real-Time PCR system and relative expression differences were calculated with the $2^{\Delta Ct}$ method.

4.6. Cloning of miR-203a into pCDH lentivector

The miR-203a miRNA construct was amplified from D492 genomic DNA using nested PCR with the following outer primers, miR-203a-outer-F 5′-ATCAGTCGCGGGACCTATG-3′ and miR-203a-outer-R 5′-GAATTCCACGGAGTTTCGAG-3′. From miR-203a-outer amplicon, *Eco*RI and *Not*I restriction sites were incorporated with PCR using the following inner primers, miR-203a-EcoRI-F-5′-TAAGCAGAA TTCaggcgagggcgtctaagg-3′ and miR-203a-NotI-R-5′-TGCTTAGCGGC CGCacctcccagcagcacttg-3′. Phusion High-Fidelity DNA Polymerase (NEB, # M0530S) was used for PCR and amplicons were purified using the GeneJET PCR purification kit (Thermo Fisher Scientific, #K0701). Double digestions of miR-203a-inner amplicon and pCDH vector (System Biosciences, #CD516B-2) were performed using EcoRI (NEB, #R0101) and NotI (Thermo Fisher Scientific, #ER0591). The miR-203a-inner amplicon was cloned into pCDH lentivector at insert-to-vector molar ratio 10:1 using T4 DNA ligase (Thermo Fisher Scientific, #15224041). Empty pCDH lentivector and miR-203a-pCDH lentivector were transformed into *E. coli* DH5alpha competent cells and inserts confirmed with colony PCR. Lentivectors were produced in cultures of DH5alpha and isolated using GeneJET Plasmid Miniprep kit (Thermo Fisher Scientific, #K0502). The cloned miR-203a insert sequence was then confirmed with sequencing. The pCDH lentivector has a RFP +Puro fusion containing the T2A element to enable co-expression of balanced levels of RFP and Puro genes. Viral particles were produced in HEK-293 T cells using TurboFect transfection reagent (Thermo Fisher Scientific, #R0531) and virus containing supernatant collected after 48 and 72 h, centrifuged and filtered through 0.45 μm filter. Target cells were transfected with virus titer in the presence of 8 μg/μl polybrene. Stable cell lines and control (empty-lentivector) cells were isolated with puromycin (2 μg/ml) (Thermo Fisher Scientific, # A1113803) followed by flow-sorting (Sony SH800), selecting for RFP expressing cells.

4.7. Immunochemistry

The following primary antibodies were used for DAB staining (Dako, # K3467), E-cadherin (BD, # 610182), *N*-cadherin (BD, # 610921), K14 (Abcam, #ab7800) and K19 (Abcam, #ab7754). Specimens were visualized on a Leica DMI3000 B inverted microscope.

4.8. Western blotting

Equal amounts (5 μg) of proteins in RIPA buffer were separated on NuPAGE™ 10% Bis-Tris Protein Gels (Thermo Fisher Scientific, #NP0302BOX) and transferred to a PVDF membrane (Millipore, #IPFL00010). Antibodies: SNAI2 (Cell Signaling, #9585) and Histone H3 (Cell Signaling, #4499). Secondary antibodies were mouse or rabbit IRDey (Li-Cor) used at 1:20,000 and detected using the Odyssey Infrared Imaging System (Li-Cor). Fluorescent images were converted to gray scale.

4.9. Proliferation assay

Cells were seeded in triplicates in 24-well plates and cultures stopped every 24 h. Cells were fixed in 3.7% formaldehyde in PBS for 10 min, washed once with 1 x PBS, stained with 0.1% crystal violet in 10% ethanol for 15 min, washed four times with water and dried. Density of cells was evaluated by extracting the crystal violet stain in 10% acetic acid and measuring optical density at 595 nm using a spectrometer. In addition, proliferation rate of D492M cells treated with siRNA was analyzed on IncuCyte Zoom (Essen Bioscience) per manufacturer's instructions.

4.10. Apoptosis assay

Resistance to chemically induced apoptosis with 10 μM camptothecin (Sigma-Aldrich, #C9911) was determined using IncuCyte Caspase-3/7 Reagents (Essen Bioscience, #4440) and imaging on IncuCyte Zoom (Essen Bioscience) per manufacturer's instructions.

4.11. Anchorage independence, migration and invasion assays

Anchorage independent growth was determined using 24-well ultra-low attachment plates (Corning, #3473), where triplicates of 500 cells of $D492M^{miR\text{-}203a}$ and $D492M^{Empty}$ were single cell filtered and cultured using EGM5 medium for 9 days.

For migration analysis, triplicates of 10,000 starved $D492M^{miR\text{-}203a}$ and $D492M^{Empty}$ cells were seeded in DMEM/F12, HEPES medium (Thermo Scientific, #31330038) on collagen I (Advanced BioMatrix, #5005-B) coated transwell filters with 8 μm pore size (Corning, #353097) with EGM5 medium in the lower chamber and incubated for 24 h. Filters were rinsed with 1 × PBS and cells on the apical layer wiped off with a cotton swab (Q-tip) and migrated cells fixed in 3.7% formaldehyde in PBS for 10 min, washed with 1 × PBS, stained with 0.1% crystal violet in 10% ethanol for 15 min and washed with water and then dried. Images were acquired and migrated cells counted, 3 images per filter.

Invasion assay was performed using transwell filters with 8 μm pore size (Corning, #353097) that were coated with 100 μl diluted Matrigel

(Corning, #354230) 1:10 in H14 media. D492M$^{miR\text{-}203a}$ and D492M^{Empty} (25,000 cells) were seeded in H14 media on top of Matrigel coated filters and H14 + 5% FBS added to the lower chamber and incubated for 44 h. Matrigel was then removed with a cotton swab and washed with PBS. Cells were fixed in 3.7% formaldehyde in PBS for 15 min and washed four times with water. Images were acquired and migrated cells counted, 3 images per filter.

4.12. PolyA mRNA sequencing and analysis

RNA was isolated from 3D and 2D cultures using the Exiqon miRCURY RNA Isolation Kit - Cell and Plant and quality control of RNA samples was performed using BioAnalyzer. Libraries were prepared using polyA mRNA library kit from Illumina and sequenced on a HiSeq sequencer from Illumina. Alignment of reads and annotation was performed using Kallisto (Bray et al., 2016) and differential expression analysis was done using Sleuth (Pimentel et al., 2017).

4.13. Transient transfection with miR-203a mimic

Briefly, D492M cells were separately transfected with 50 pmol of mirVANA miR-203a-3p mimic (Thermo Fisher, #4464066, Assay ID MC10152) and miRNA mimic negative control #1 (Thermo Fisher, #4464058) using RNAiMAX (Thermo Fisher, #13778075) per manufacturer's instructions for mirVana miRNA mimics.

4.14. Transient transfection with miR-203a inhibitor

Briefly, D492M$^{miR\text{-}203a}$ cells were separately transfected with 50 pmol of mirVANA miR-203a-3p inhibitor (Thermo Fisher, # 4464084, Assay ID MH10152) and mirVana miRNA Inhibitor, Negative Control #1 (Thermo Fisher, # 4464076) using RNAiMAX (Thermo Fisher, #13778075) per manufacturer's instructions for mirVana miRNA inhibitors.

4.15. Plasmid vector constructs and Luciferase activity assay

Synthetic oligonucleotides containing the hsa-miR203a-3p target sequence of human PXDN 3′-UTR (Position 106–113) or a deletion thereof (Table 1) were cloned into pmirGLO Dual-Luciferase miRNA Target Expression Vector (Promega Corporation, Madison, WI, USA). As a positive control we cloned the target sequence of p63 3′-UTR, a known hsa-miR203a-3p target, into pmirGLO, as well as a mismatched version of the p63 target site or a deletion thereof (Fig. S1). Correct sequence and orientation was verified by DNA sequencing (Eurofins Genomics, Ebersberg, Germany).

HEK293T cells were plated in a 96-well plate 3.0×10^4per well and incubated overnight. Cells were first transfected with hsa-miR203a-3p mimics (mirVana™ miRNA Mimics, Thermo Fisher Scientific, #4464070) with final concentration of 100 nM, using Lipofectamine RNAiMAX (Thermo Fisher Scienttific, #13778150) transfection reagent (according to manufacturer's instructions, with minor changes: using serum free and antibiotic-free high glucose DMEM medium instead of Opti-MEM® Medium). 24 h after transfection with miRNA mimics, cells were transfected (according to manufacturer's instructions) with 200 ng/well luciferase plasmids (pmirGLO constructs), using Lipofectamine 3000 (Thermo Fisher Scientific, #L3000015). After 24 h, plasmid-transfection cells were analyzed for luciferase activity using the Dual-Glo® Luciferase Assay System (Promega Corporation, Madison, WI, USA). Results are displayed as normalized firefly luciferase activity (background subtracted firefly luciferase activity/background subtracted renilla luciferase activity) for each construct. For each transfection, luciferase activity was averaged from four replicates, and three independent experiments were performed.

4.16. Transient transfection with siRNA

D492M cells were transfected with 10 nm final concentration of negative control siRNA (SilencerSelect siRNA #4390843, Ambion) and siRNA targeting PXDN (SilencerSelect siRNA #4427037, Ambion), using Lipofectamine RNAiMAX (Thermo Fisher Scienttific, #13778150), according to the manufacturer's protocol. Cells were incubated for 48 h and then the knockdown was confirmed by qRT-PCR using the following primers; Hs.PT.58.630748 (PrimeTime, IDT).

4.17. Statistics

All analyses comprised at least three independent experiments. Two-tailed student *t*-test was used to test significance ($p < 0.05$).

Supplementary data to this article can be found online at https://doi.org/10.1016/j.mod.2018.11.002.

Acknowledgements

We thank Erik Knutsen and Isac Lee for their contribution to this work.

Competing interests

No competing interests declared.

Funding

This work was supported by Grants from Landspitali University Hospital Science Fund, University of Iceland Research Fund, and Icelandic Science and Technology Policy - Grant of Excellence: 152144051. 'Göngum saman', a supporting group for breast cancer research in Iceland (www.gongumsaman.is). The funders had no role in study design, data collection and analysis, decision to publish, or preparation of the manuscript. Primary cells were received from reduction mammoplasty after acquiring informed consent from the donor. Approved by the Icelandic National Bioethics Committee VSN-13-057.

Data availability

NCBI GEO: https://www.ncbi.nlm.nih.gov/geo/query/acc.cgi?acc=GSE112306

The data discussed in this publication have been deposited in NCBI's

Table 1
Synthetic oligonucleotides containing the hsa-mir-203a-3p target sequence of human PXDN 3′-UTR/p63 3′-UTR or a deletion thereof.

PXDN 3′-UTR sense	/5Phos/AAACTAGCGGCCGCTAGTCCCAGAACTCGTGACATTTCATT
PXDN 3′-UTR antisense	/5Phos/CTAGAATGAAATGTCACGAGTTCTGGGACTAGCGGCCGCTAGTTT
PXDN del sense	/5Phos/AAACTAGCGGCCGCTAGTCCCAGAACTCGTGTT
PXDN del antisense	/5Phos/CTAGAACACGAGTTCTGGGACTAGCGGCCGCTAGTTT
p63 3′-UTR sense	/5Phos/AAACTAGCGGCCGCTAGTGAATGAGTCCTTGATTTCAAAT
p63 3′-UTR antisense	/5Phos/CTAGATTTGAAATCAAGGACTCATTCACTAGCGGCCGCTAGTTT
p63 del sense	/5Phos/AAACTAGCGGCCGCTAGTGAATGAGTCCTTGAT
p63 del antisense	/5Phos/CTAGATCAAGGACTCATTCACTAGCGGCCGCTAGTTT

Gene Expression Omnibus (Edgar et al., 2002) and are accessible through GEO Series accession number GSE112306.
(https://www.ncbi.nlm.nih.gov/geo/query/acc.cgi?acc=GSE112306).

References

Aryee, M.J., Jaffe, A.E., Corrada-Bravo, H., Ladd-Acosta, C., Feinberg, A.P., Hansen, K.D., Irizarry, R.A., 2014. Minfi: a flexible and comprehensive Bioconductor package for the analysis of Infinium DNA methylation microarrays. Bioinformatics 30 (10), 1363–1369.

Avril-Sassen, S., Goldstein, L.D., Stingl, J., Blenkiron, C., Le Quesne, J., Spiteri, I., Karagavriilidou, K., Watson, C.J., Tavare, S., Miska, E.A., Caldas, C., 2009. Characterisation of microRNA expression in post-natal mouse mammary gland development. BMC Genomics 10, 548.

Barnett, P., Arnold, R.S., Mezencev, R., Chung, L.W., Zayzafoon, M., Odero-Marah, V., 2011. Snail-mediated regulation of reactive oxygen species in ARCaP human prostate cancer cells. Biochem. Biophys. Res. Commun. 404 (1), 34–39.

Bhave, G., Cummings, C.F., Vanacore, R.M., Kumagai-Cresse, C., Ero-Tolliver, I.A., Rafi, M., Kang, J.S., Pedchenko, V., Fessler, L.I., Fessler, J.H., Hudson, B.G., 2012. Peroxidasin forms sulfilimine chemical bonds using hypohalous acids in tissue genesis. Nat. Chem. Biol. 8 (9), 784–790.

Bock, C., Reither, S., Mikeska, T., Paulsen, M., Walter, J., Lengauer, T., 2005. BiQ analyzer: visualization and quality control for DNA methylation data from bisulfite sequencing. Bioinformatics 21 (21), 4067–4068.

Bray, N.L., Pimentel, H., Melsted, P., Pachter, L., 2016. Near-optimal probabilistic RNA-seq quantification. Nat. Biotechnol. 34 (5), 525–527.

Cao, Q., Mani, R.S., Ateeq, B., Dhanasekaran, S.M., Asangani, I.A., Prensner, J.R., Kim, J.H., Brenner, J.C., Jing, X., Cao, X., Wang, R., Li, Y., Dahiya, A., Wang, L., Pandhi, M., Lonigro, R.J., Wu, Y.M., Tomlins, S.A., Palanisamy, N., Qin, Z., Yu, J., Maher, C.A., Varambally, S., Chinnaiyan, A.M., 2011. Coordinated regulation of polycomb group complexes through microRNAs in cancer. Cancer Cell 20 (2), 187–199.

Cheng, G., Salerno, J.C., Cao, Z., Pagano, P.J., Lambeth, J.D., 2008. Identification and characterization of VPO1, a new animal heme-containing peroxidase. Free Radic. Biol. Med. 45 (12), 1682–1694.

Colon, S., Bhave, G., 2016. Proprotein convertase processing enhances Peroxidasin activity to reinforce collagen IV. J. Biol. Chem. 291 (46), 24009–24016.

Colon, S., Page-McCaw, P., Bhave, G., 2017. Role of Hypohalous acids in basement membrane homeostasis. Antioxid. Redox Signal. 27 (12), 839–854.

DeCastro, A.J., Dunphy, K.A., Hutchinson, J., Balboni, A.L., Cherukuri, P., Jerry, D.J., DiRenzo, J., 2013. MiR203 mediates subversion of stem cell properties during mammary epithelial differentiation via repression of DeltaNP63alpha and promotes mesenchymal-to-epithelial transition. Cell Death Dis. 4, e514.

Ding, X., Park, S.I., McCauley, L.K., Wang, C.Y., 2013. Signaling between transforming growth factor beta (TGF-beta) and transcription factor SNAI2 represses expression of microRNA miR-203 to promote epithelial-mesenchymal transition and tumor metastasis. J. Biol. Chem. 288 (15), 10241–10253.

Dontu, G., Ince, T.A., 2015. Of mice and women: a comparative tissue biology perspective of breast stem cells and differentiation. J. Mammary Gland Biol. Neoplasia 20 (1–2), 51–62.

Dontu, G., Abdallah, W.M., Foley, J.M., Jackson, K.W., Clarke, M.F., Kawamura, M.J., Wicha, M.S., 2003. In vitro propagation and transcriptional profiling of human mammary stem/progenitor cells. Genes Dev. 17 (10), 1253–1270.

Edgar, R., Domrachev, M., Lash, A.E., 2002. Gene expression omnibus: NCBI gene expression and hybridization array data repository. Nucleic Acids Res. 30 (1), 207–210.

Ero-Tolliver, I.A., Hudson, B.G., Bhave, G., 2015. The ancient immunoglobulin domains of peroxidasin are required to form sulfilimine cross-links in collagen IV. J. Biol. Chem. 290 (35), 21741–21748.

Feng, X., Wang, Z., Fillmore, R., Xi, Y., 2014. MiR-200, a new star miRNA in human cancer. Cancer Lett. 344 (2), 166–173.

Gregory, P.A., Bert, A.G., Paterson, E.L., Barry, S.C., Tsykin, A., Farshid, G., Vadas, M.A., Khew-Goodall, Y., Goodall, G.J., 2008. The miR-200 family and miR-205 regulate epithelial to mesenchymal transition by targeting ZEB1 and SIP1. Nat. Cell Biol. 10 (5), 593–601.

Gudjonsson, T., Villadsen, R., Nielsen, H.L., Ronnov-Jessen, L., Bissell, M.J., Petersen, O.W., 2002. Isolation, immortalization, and characterization of a human breast epithelial cell line with stem cell properties. Genes Dev. 16 (6), 693–706.

Hanahan, D., Weinberg, R.A., 2011. Hallmarks of cancer: the next generation. Cell 144 (5), 646–674.

Hilmarsdottir, B., Briem, E., Bergthorsson, J.T., Magnusson, M.K., Gudjonsson, T., 2014. Functional role of the microRNA-200 family in breast morphogenesis and neoplasia. Genes 5 (3), 804–820.

Hilmarsdottir, B., Briem, E., Sigurdsson, V., Franzdottir, S.R., Ringner, M., Arason, A.J., Bergthorsson, J.T., Magnusson, M.K., Gudjonsson, T., 2015. MicroRNA-200c-141 and Np63 are required for breast epithelial differentiation and branching morphogenesis. Dev. Biol. 403 (2), 150–161.

Inoue, A., Seidel, M.G., Wu, W., Kamizono, S., Ferrando, A.A., Bronson, R.T., Iwasaki, H., Akashi, K., Morimoto, A., Hitzler, J.K., Pestina, T.I., Jackson, C.W., Tanaka, R., Chong, M.J., McKinnon, P.J., Inukai, T., Grosveld, G.C., Look, A.T., 2002. Slug, a highly conserved zinc finger transcriptional repressor, protects hematopoietic progenitor cells from radiation-induced apoptosis in vivo. Cancer Cell 2 (4), 279–288.

Javed, A., Lteif, A., 2013. Development of the human breast. Semin. Plast. Surg. 27 (1), 5–12.

Jayachandran, A., Prithviraj, P., Lo, P.H., Walkiewicz, M., Anaka, M., Woods, B.L., Tan, B., Behren, A., Cebon, J., McKeown, S.J., 2016. Identifying and targeting determinants of melanoma cellular invasion. Oncotarget 7 (27), 41186–41202.

Kal, A.J., van Zonneveld, A.J., Benes, V., van den Berg, M., Koerkamp, M.G., Albermann, K., Strack, N., Ruijter, J.M., Richter, A., Dujon, B., Ansorge, W., Tabak, H.F., 1999. Dynamics of gene expression revealed by comparison of serial analysis of gene expression transcript profiles from yeast grown on two different carbon sources. Mol. Biol. Cell 10 (6), 1859–1872.

Khan, K., Rudkin, A., Parry, D.A., Burdon, K.P., McKibbin, M., Logan, C.V., Abdelhamed, Z.I., Muecke, J.S., Fernandez-Fuentes, N., Laurie, K.J., Shires, M., Fogarty, R., Carr, I.M., Poulter, J.A., Morgan, J.E., Mohamed, M.D., Jafri, H., Raashid, Y., Meng, N., Piseth, H., Toomes, C., Casson, R.J., Taylor, G.R., Hammerton, M., Sheridan, E., Johnson, C.A., Inglehearn, C.F., Craig, J.E., Ali, M., 2011. Homozygous mutations in PXDN cause congenital cataract, corneal opacity, and developmental glaucoma. Am. J. Hum. Genet. 89 (3), 464–473.

Lawson, D.A., Werb, Z., Zong, Y., Goldstein, A.S., 2015. The cleared mammary fat pad transplantation assay for mammary epithelial organogenesis. Cold Spring Harb Protoc 2015 (12) (pdb.prot078071).

Lee, G.Y., Kenny, P.A., Lee, E.H., Bissell, M.J., 2007. Three-dimensional culture models of normal and malignant breast epithelial cells. Nat. Methods 4 (4), 359–365.

Lilja, A.M., Rodilla, V., Huyghe, M., Hannezo, E., Landragin, C., Renaud, O., Leroy, O., Rulands, S., Simons, B.D., Fre, S., 2018. Clonal analysis of Notch1-expressing cells reveals the existence of unipotent stem cells that retain long-term plasticity in the embryonic mammary gland. Nat. Cell Biol. 20 (6), 677–687.

Liu, Y., Carson-Walter, E.B., Cooper, A., Winans, B.N., Johnson, M.D., Walter, K.A., 2010. Vascular gene expression patterns are conserved in primary and metastatic brain tumors. J. Neuro-Oncol. 99 (1), 13–24.

Lloyd-Lewis, B., Davis, F.M., Harris, O.B., Hitchcock, J.R., Watson, C.J., 2018. Neutral lineage tracing of proliferative embryonic and adult mammary stem/progenitor cells. Development 145 (14).

Mani, S.A., Guo, W., Liao, M.J., Eaton, E.N., Ayyanan, A., Zhou, A.Y., Brooks, M., Reinhard, F., Zhang, C.C., Shipitsin, M., Campbell, L.L., Polyak, K., Brisken, C., Yang, J., Weinberg, R.A., 2008. The epithelial-mesenchymal transition generates cells with properties of stem cells. Cell 133 (4), 704–715.

Moes, M., Le Bechec, A., Crespo, I., Laurini, C., Halavatyi, A., Vetter, G., Del Sol, A., Friederich, E., 2012. A novel network integrating a miRNA-203/SNAI1 feedback loop which regulates epithelial to mesenchymal transition. PLoS One 7 (4), e35440.

Moustakas, A., Heldin, C.H., 2007. Signaling networks guiding epithelial-mesenchymal transitions during embryogenesis and cancer progression. Cancer Sci. 98 (10), 1512–1520.

Olson, P., Lu, J., Zhang, H., Shai, A., Chun, M.G., Wang, Y., Libutti, S.K., Nakakura, E.K., Golub, T.R., Hanahan, D., 2009. MicroRNA dynamics in the stages of tumorigenesis correlate with hallmark capabilities of cancer. Genes Dev. 23 (18), 2152–2165.

Pal, B., Chen, Y., Vaillant, F., Jamieson, P., Gordon, L., Rios, A.C., Wilcox, S., Fu, N., Liu, K.H., Jackling, F.C., Davis, M.J., Lindeman, G.J., Smyth, G.K., Visvader, J.E., 2017. Construction of developmental lineage relationships in the mouse mammary gland by single-cell RNA profiling. Nat. Commun. 8 (1), 1627.

Pechoux, C., Gudjonsson, T., Ronnov-Jessen, L., Bissell, M.J., Petersen, O.W., 1999. Human mammary luminal epithelial cells contain progenitors to myoepithelial cells. Dev. Biol. 206 (1), 88–99.

Peinado, H., Olmeda, D., Cano, A., 2007. Snail, ZEB and bHLH factors in tumour progression: an alliance against the epithelial phenotype? Nat. Rev. Cancer 7 (6), 415–428.

Peterfi, Z., Donko, A., Orient, A., Sum, A., Prokai, A., Molnar, B., Vereb, Z., Rajnavolgyi, E., Kovacs, K.J., Muller, V., Szabo, A.J., Geiszt, M., 2009. Peroxidasin is secreted and incorporated into the extracellular matrix of myofibroblasts and fibrotic kidney. Am. J. Pathol. 175 (2), 725–735.

Petersen, O.W., Polyak, K., 2010. Stem cells in the human breast. Cold Spring Harb. Perspect. Biol. 2 (5), a003160.

Petersen, O.W., Lind Nielsen, H., Gudjonsson, T., Villadsen, R., Ronnov-Jessen, L., Bissell, M.J., 2001. The plasticity of human breast carcinoma cells is more than epithelial to mesenchymal conversion. Breast Cancer Res. 3 (4), 213–217.

Pimentel, H., Bray, N.L., Puente, S., Melsted, P., Pachter, L., 2017. Differential analysis of RNA-seq incorporating quantification uncertainty. Nat. Methods 14 (7), 687–690.

Sarrio, D., Rodriguez-Pinilla, S.M., Hardisson, D., Cano, A., Moreno-Bueno, G., Palacios, J., 2008. Epithelial-mesenchymal transition in breast cancer relates to the basal-like phenotype. Cancer Res. 68 (4), 989–997.

Shimono, Y., Zabala, M., Cho, R.W., Lobo, N., Dalerba, P., Qian, D., Diehn, M., Liu, H., Panula, S.P., Chiao, E., Dirbas, F.M., Somlo, G., Pera, R.A., Lao, K., Clarke, M.F., 2009. Downregulation of miRNA-200c links breast cancer stem cells with normal stem cells. Cell 138 (3), 592–603.

Sigurdsson, V., Fridriksdottir, A.J., Kjartansson, J., Jonasson, J.G., Steinarsdottir, M., Petersen, O.W., Ogmundsdottir, H.M., Gudjonsson, T., 2006. Human breast microvascular endothelial cells retain phenotypic traits in long-term finite life span culture. In Vitro Cell. Dev. Biol. Anim. 42 (10), 332–340.

Sigurdsson, V., Hilmarsdottir, B., Sigmundsdottir, H., Fridriksdottir, A.J., Ringner, M., Villadsen, R., Borg, A., Agnarsson, B.A., Petersen, O.W., Magnusson, M.K., Gudjonsson, T., 2011. Endothelial induced EMT in breast epithelial cells with stem cell properties. PLoS One 6 (9), e23833.

Sitole, B.N., Mavri-Damelin, D., 2018. Peroxidasin is regulated by the epithelial-mesenchymal transition master transcription factor Snai1. Gene 646, 195–202.

Taube, J.H., Malouf, G.G., Lu, E., Sphyris, N., Vijay, V., Ramachandran, P.P., Ueno, K.R., Gaur, S., Nicoloso, M.S., Rossi, S., Herschkowitz, J.I., Rosen, J.M., Issa, J.P., Calin, G.A., Chang, J.T., Mani, S.A., 2013. Epigenetic silencing of microRNA-203 is required for EMT and cancer stem cell properties. Sci. Rep. 3, 2687.

Tauber, S., Jais, A., Jeitler, M., Haider, S., Husa, J., Lindroos, J., Knofler, M., Mayerhofer, M., Pehamberger, H., Wagner, O., Bilban, M., 2010. Transcriptome analysis of human

cancer reveals a functional role of heme oxygenase-1 in tumor cell adhesion. Mol. Cancer 9, 200.
Tindall, A.J., Pownall, M.E., Morris, I.D., Isaacs, H.V., 2005. Xenopus tropicalis peroxidasin gene is expressed within the developing neural tube and pronephric kidney. Dev. Dyn. 232 (2), 377–384.
Vidi, P.A., Bissell, M.J., Lelievre, S.A., 2013. Three-dimensional culture of human breast epithelial cells: the how and the why. Methods Mol. Biol. 945, 193–219.
Villadsen, R., Fridriksdottir, A.J., Ronnov-Jessen, L., Gudjonsson, T., Rank, F., LaBarge, M.A., Bissell, M.J., Petersen, O.W., 2007. Evidence for a stem cell hierarchy in the adult human breast. J. Cell Biol. 177 (1), 87–101.
Wellner, U., Schubert, J., Burk, U.C., Schmalhofer, O., Zhu, F., Sonntag, A., Waldvogel, B., Vannier, C., Darling, D., zur Hausen, A., Brunton, V.G., Morton, J., Sansom, O., Schuler, J., Stemmler, M.P., Herzberger, C., Hopt, U., Keck, T., Brabletz, S., Brabletz, T., 2009. The EMT-activator ZEB1 promotes tumorigenicity by repressing stemness-inhibiting microRNAs. Nat. Cell Biol. 11 (12), 1487–1495.
Wronski, A., Arendt, L.M., Kuperwasser, C., 2015. Humanization of the mouse mammary gland. Methods Mol. Biol. 1293, 173–186.
Wuidart, A., Sifrim, A., Fioramonti, M., Matsumura, S., Brisebarre, A., Brown, D., Centonze, A., Dannau, A., Dubois, C., Van Keymeulen, A., Voet, T., Blanpain, C., 2018. Early lineage segregation of multipotent embryonic mammary gland progenitors. Nat. Cell Biol. 20 (6), 666–676.
Yan, X., Sabrautzki, S., Horsch, M., Fuchs, H., Gailus-Durner, V., Beckers, J., Hrabe de Angelis, M., Graw, J., 2014. Peroxidasin is essential for eye development in the mouse. Hum. Mol. Genet. 23 (21), 5597–5614.
Young, C.D., Zimmerman, L.J., Hoshino, D., Formisano, L., Hanker, A.B., Gatza, M.L., Morrison, M.M., Moore, P.D., Whitwell, C.A., Dave, B., Stricker, T., Bhola, N.E., Silva, G.O., Patel, P., Brantley-Sieders, D.M., Levin, M., Horiates, M., Palma, N.A., Wang, K., Stephens, P.J., Perou, C.M., Weaver, A.M., OShaughnessy, J.A., Chang, J.C., Park, B.H., Liebler, D.C., Cook, R.S., Arteaga, C.L., 2015. Activating PIK3CA mutations induce an epidermal growth factor receptor (EGFR)/extracellular signal-regulated kinase (ERK) paracrine signaling Axis in basal-like breast Cancer. Mol. Cell. Proteomics 14 (7), 1959–1976.
Zhang, Z., Zhang, B., Li, W., Fu, L., Fu, L., Zhu, Z., Dong, J.T., 2011. Epigenetic silencing of miR-203 upregulates SNAI2 and contributes to the invasiveness of malignant breast Cancer cells. Genes Cancer 2 (8), 782–791.

Figure S1

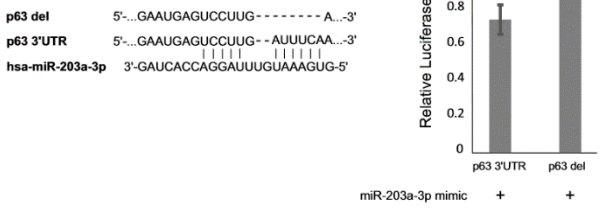
p63 del 5'-...GAAUGAGUCCUUG- - - - - - - - A...-3'
p63 3'UTR 5'-...GAAUGAGUCCUUG- - AUUUCAA...-3'
hsa-miR-203a-3p 3'-GAUCACCAGGAUUUGUAAAGUG-5'
Relative Luciferase Activity
1.2
1
0.8
0.6
0.4
0.2
0
**
p63 3'UTR
p63 del
miR-203a-3p mimic + +

Figure S2

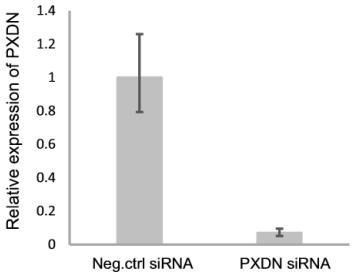
Relative expression of PXDN
1.4
1.2
1
0.8
0.6
0.4
0.2
0
Neg.ctrl siRNA
PXDN siRNA

Paper III

In Vitro Cellular & Developmental Biology - Animal (2019) 55:838–853
https://doi.org/10.1007/s11626-019-00403-x

YKL-40/CHI3L1 facilitates migration and invasion in HER2 overexpressing breast epithelial progenitor cells and generates a niche for capillary-like network formation

Erika Morera[1] · Sarah Sophie Steinhäuser[1] · Zuzana Budkova[1] · Saevar Ingthorsson[1] · Jennifer Kricker[1] · Aileen Krueger[3] · Gunnhildur Asta Traustadottir[1] · Thorarinn Gudjonsson[1,2]

Received: 10 April 2019 / Accepted: 13 August 2019 / Published online: 3 September 2019 / Editor: Tetsuji Okamoto

Abstract
Epithelial to mesenchymal transition (EMT) is a developmental event that is hijacked in some diseases such as fibrosis and cancer. In cancer, EMT has been linked to increased invasion and metastasis and is generally associated with a poor prognosis. In this study, we have compared phenotypic and functional differences between two isogenic cell lines with an EMT profile: D492M and D492HER2 that are both derived from D492, a breast epithelial cell line with stem cell properties. D492M is non-tumorigenic while D492HER2 is tumorigenic. Thus, the aim of this study was to analyze the expression profile of these cell lines, identify potential oncogenes, and evaluate their effects on cellular phenotype. We performed transcriptome and secretome analyses of D492M and D492HER2 and verified expression of selected genes at the RNA and protein level. One candidate, YKL-40 (also known as CHI3L1), was selected for further studies due to its differential expression between D492M and D492HER2, being considerably higher in D492HER2. YKL-40 has been linked to chronic inflammation diseases and cancer, yet its function is not fully understood. Knock-down experiments of YKL-40 in D492HER2 resulted in reduced migration and invasion as well as reduced ability to induce angiogenesis in an in vitro assay, plus changes in the EMT-phenotype. In summary, our data suggest that YKL-40 may provide D492HER2 with increased aggressiveness, supporting cancer progression and facilitating angiogenesis.

Keywords YKL-40/CHI3L1 · Epithelial to mesenchymal transition (EMT) · Migration · Invasive breast cancer · Angiogenesis

Introduction

Epithelial to mesenchymal transition (EMT) is a developmental process that describes the plasticity of epithelial cells to change phenotype from compact adherent epithelium to mesenchymal-like cells that have lost their polarity and cell-cell adherence (Thiery *et al.* 2009). This is an important event in normal development, during gastrulation, neural crest formation, and wound healing, but also takes place in malignant processes like fibrosis and cancer (Thiery *et al.* 2009; Nieto 2013). In cancer, EMT is associated with increased aggressiveness and it is believed to be necessary for migration and invasion of cancer cells for the initial steps in the metastatic processes (Thiery *et al.* 2009).

The EMT process is accompanied by increased expression of mesenchymal markers such as vimentin, N-cadherin, α-smooth muscle actin, fibronectin, and/or Axl, as well as decreased or absent expression of epithelial markers like cytokeratins, yet the most referenced change in EMT is the loss of E-cadherin (Peinado *et al.* 2007; Gjerdrum *et al.* 2010). EMT is known to be induced by a number of factors. It can take place due to intrinsic factors such as genetic mutations or epigenetic changes or extrinsic factors like hypoxia or inflammation that stimulate the release of signals from the stroma (Yang *et al.* 2008; Kalluri and Weinberg 2009; Polyak and Weinberg 2009). Transforming growth factor beta (TGF-β) has been

Electronic supplementary material The online version of this article (https://doi.org/10.1007/s11626-019-00403-x) contains supplementary material, which is available to authorized users.

✉ Thorarinn Gudjonsson
tgudjons@hi.is

[1] Stem Cell Research Unit, Biomedical Center, Department of Anatomy, Faculty of Medicine, School of Health Sciences, University of Iceland, Vatnsmyrarvegi 16, 101 Reykjavik, Iceland

[2] Department of Laboratory Hematology, Landspitali - University Hospital, Reykjavik, Iceland

[3] Heidelberg Institute for Stem Cell Technology and Experimental Medicine, Heidelberg, Germany

Table 1. List of primers used in this study. List of gene IDs for all target genes used and their corresponding primer IDs and supplier

Primers	Cat. number	Company
miR-200c	No. YP00204482	Qiagen
miR-203	No. 205914	Exiqon
miR-205	No. 204487	Exiqon
VEGF-A	Hs.PT.58.21234833	IDT
VEGF-C	Hs.PT.58.14602240	IDT
GUCA1C	Hs.PT.58.680712	IDT
CITED1	Hs.PT.58.1567731	IDT
MYBPH	Hs.PT.58.39772389	IDT
YKL-40 /CHI3L1	Hs.PT.58.22570467	IDT
KCNQ1OT1	Hs.PT.58.4572396.g	IDT
ERBB2	Hs.PT.58.1330269	IDT
GPR27	Hs.PT.58.38722549.g	IDT
S100A9	Hs.PT.58.20989743	IDT
DLK1	Hs.PT.58.40622309	IDT
GDF6	Hs.PT.58.20193545	IDT
PXDN	Hs.PT.58.630748	IDT
TLR4	Hs.PT.58.38700156.g	IDT
BMP4	Hs.PT.56a.3848863	IDT
CDH2	Hs.PT.58.26024443	IDT

shown to be a powerful inducer of EMT in a number of cell types (Kasai *et al.* 2005; Willis and Borok 2007; Kalluri and Weinberg 2009). Tyrosine kinase receptors and their ligands like EGF, PDGF, FGF, and HGF have also been shown to induce EMT (Kalluri and Weinberg 2009). Recently, regulatory functions carried out by non-coding RNAs have attracted the attention of researchers. Downregulation of miRNAs, especially members of the miR-200 family, miR-203, and miR-205, have been linked to EMT (Wiklund *et al.* 2010; Moes *et al.* 2012; DeCastro *et al.* 2013; Hilmarsdottir *et al.* 2014, 2015). In epithelial cells, the expression of these miRs is high but is commonly reduced or absent during EMT. Interestingly, rescue of these miRs can revert the EMT phenotype in the process mesenchymal to epithelial transition (MET) (Burk *et al.* 2008; Korpal *et al.* 2008; Hilmarsdottir *et al.* 2014). Furthermore, EMT in cells is often accompanied by increased ability to migrate and invade, as well as increased resistance to apoptosis (Thiery *et al.* 2009). For this reason, EMT has been related to aggressiveness and metastasis in cancer (Thiery 2002; Nieto 2013; Tan *et al.* 2014). The concept of cancer stem cells (CSCs) has also been linked to EMT, where EMT is an integral part of CSC plasticity and survival (Mani *et al.* 2008). Like somatic stem cells, CSCs have the capability to self-renew and their EMT phenotype is believed to be protective against external damages, which could lead to resistance to cancer therapies (Al-Hajj *et al.* 2003; Stingl 2006). In addition, CSCs as a cell population could be the cells responsible for the dissemination of cancer cells and the heterogeneity evidenced in metastasis (Brabletz 2012). Therefore, it is vital to elucidate the role of CSCs in cancer progression in order to improve efficient treatments and targeted therapy.

In breast cancer, the subtype basal-like breast cancer (BLBC) is identified as having the most undifferentiated cells and heterogeneity, which has been linked to CSCs and interestingly has a higher incidence of EMT (Mani *et al.* 2008; Morel *et al.* 2008; Sarrio *et al.* 2008). However, EMT is not exclusively found in this subtype. In luminal and HER2 breast cancers, there is an EMT-derived phenotype, although at a lower percentage (Yu *et al.* 2013; Tan *et al.* 2014).

Resistance to drugs in breast cancer may be associated with EMT-phenotype and heterogeneity of cells in the tumor. It is important to note that states of EMT are not merely defined as completely epithelial or mesenchymal; there are intermediate states of EMT that provide plasticity and advantages to cells to adapt to their microenvironment. This program is referred as partial-EMT (p-EMT) (Huang *et al.* 2013; Nieto 2013; Tam and Weinberg 2013; Yu *et al.* 2013).

The epithelial cells that reside in the breast gland are under continuous remodeling due to hormonal cycling and interactions with the surrounding stroma. This crosstalk is required in normal development and differentiation, and is utilized by tumor cells during cancer progression. Resident fibroblasts and macrophages in the stroma are able to produce growth

Table 2. List of antibodies used in this study. List of primary antibodies (protein IDs, dilution, company, and order IDs) for western blotting and IF staining for candidate proteins

Antibodies	Assay	Cat. number	Company	Dilution
Actin	WB	ab3280	Abcam	1:5000
Axl	IF	CS no. 8661	Cell Signaling	1:100
CK14	WB	ab15461	Abcam	1:1000
CK19	IF	ab7754	Abcam	1:100
E-cadherin	WB	610182	BD Transduction Labs	1:1000
Tubulin	WB	ab6046	Abcam	1:5000
Vimentin	WB	M0725	DAKO	1:1000
YKL-40 /CHI3L1	IF	MABC196	Millipore	1:100
YKL-40 /CHI3L1	WB	MABC196	Millipore	1:500

Table 3. siRNAs used for transient YKL-40 knockdown. Catalog numbers of siRNAs used as negative control and transient knock-down of YKL-40

siRNAs	Product name	Cat. number	Company
Neg Ctrl siRNA	Silencer® Select Negative Control No. 1 siRNA	4390843	ThermoFisher Scientific
YKL-40 siRNA 1	Silencer® Select CHI3L1 siRNA 1	AM16708 (ID 119124)	ThermoFisher Scientific
YKL-40 siRNA 2	Silencer® Select CHI3L1 siRNA 2	AM16708 (ID 119126)	ThermoFisher Scientific

factors and pro-inflammatory molecules, but also pro-angiogenic molecules that support the creation of new blood vessels. Fibroblasts not only interact with epithelial cells, they also activate the action of immune cells like macrophages and promote angiogenesis by cell communication with endothelial cells. The vascular endothelial growth factor (VEGF) and TGF-β are secreted by fibroblasts and macrophages, and they are able to stimulate angiogenesis. TGF-β induces the expression of VEGF that is secreted to the ECM and stimulates endothelial cells to initiate angiogenesis (Relf *et al.* 1997; Carmeliet and Jain 2000).

There is also direct interaction between epithelial cells and endothelial cells. The vascular niche plays an important role in transporting oxygen and nutrients and releasing signals for its correct morphogenesis and development. Indeed, it has also been observed that endothelial cells increase growth and branching morphogenesis of breast epithelium (Shekhar *et al.* 2000; Sigurdsson *et al.* 2006; Ingthorsson *et al.* 2010) and induce EMT (Sigurdsson *et al.* 2011). In the context of cancer, the high proliferation rate of tumor cells can lead to a reduction in oxygen concentration resulting in acidification of the surrounding stroma. In order to survive, cancer cells are able to secrete signals that induce angiogenesis, such as VEGF (Hanahan and Weinberg 2011). Receptors on endothelial cells, such as VEGFR2, are induced to trigger activation of the transcriptional machinery of angiogenesis that involves the hypoxic inducible factor 1 (HIF1) and other factors like nuclear factor κB (NF-κB) (Vegran *et al.* 2011; Sonveaux *et al.* 2012). The increase in angiogenesis ensures oxygen and a nutrient supply and therefore results in a worse prognosis of the cancer, making it an important factor to study.

D492 is a breast progenitor epithelial cell line that was established by immortalization of a suprabasal subpopulation of breast tissue from a healthy donor (Gudjonsson *et al.* 2002). As reviewed in Briem *et al.* (2019), D492 can generate both luminal and myoepithelial cells, and in 3D culture forms branching terminal ductal lobular units (TDLU) like structures (Briem *et al.* 2019). We have previously demonstrated that when D492 is co-cultured with breast endothelial cells (BRENCs), a subpopulation of cells undergoes EMT. One such subpopulation was isolated, giving rise to the D492M cell line, which has a fixed mesenchymal phenotype (Sigurdsson *et al.* 2011). In addition, we have shown that D492 cells with forced overexpression of the HER2 oncogene (D492HER2) have lost their epithelial phenotype and gained a mesenchymal one (Ingthorsson *et al.* 2015).

In this study, we have compared functional and phenotypic differences between D492M and D492HER2. We show here that D492HER2 proliferates, migrates, and invades faster than D492M. Furthermore, glucose metabolism is more dependent on glycolysis than oxidative phosphorylation in D492HER2. The comparative analysis of transcriptome revealed that a glycoprotein, YKL-40, also known as CHI3L1, is highly upregulated in D492HER2 and may contribute to the differences in tumorigenicity between the cell lines. YKL-40 has previously been linked to chronic inflammation diseases and cancer (Libreros *et al.* 2012; Jefri *et al.* 2015; Libreros and Iragavarapu-Charyulu 2015; Cohen *et al.* 2017); however, its function is not clearly understood yet. Functional studies using knockdown of YKL-40, recombinant protein, and overexpression experiments reveal that YKL-40 influences migration, invasion, and angiogenesis and induces changes in the EMT phenotype.

Material and Methods

Cell culture (2D and 3D) The main cell lines used in this project were D492 (Gudjonsson *et al.* 2002) and its EMT-phenotype-derived cell sublines D492M (Sigurdsson *et al.* 2011) and D492HER2 (Ingthorsson *et al.* 2015). For monolayer culture, flasks or plates were pre-coated with collagen I (2.2%) (no. 5005-B, Advanced BioMatrix, Carlsbad, CA). The medium used for culturing the cell lines was H14 (Blaschke *et al.* 1994), an enriched serum-free medium based on DMEM:F12 in which growth factors are added (insulin,

Table 4. gRNAs used for generating stable cell lines. Names and sequences of gRNAs used to either knockdown or overexpress YKL-40

gRNAs	Sequence	Action	Company
YKL-40/CHI3L1 KD	CCGCCATTTCTGCGCACCCA	Knockdown	
YKL-40/CHI3L1 SAM OV 1	AGTTTTGAAAACTTTGGGTC	Overexpress	Genscript
YKL-40/CHI3L1 SAM OV 2	CTGCCAGCAGAAGAGCCACT	Overexpress	Genscript

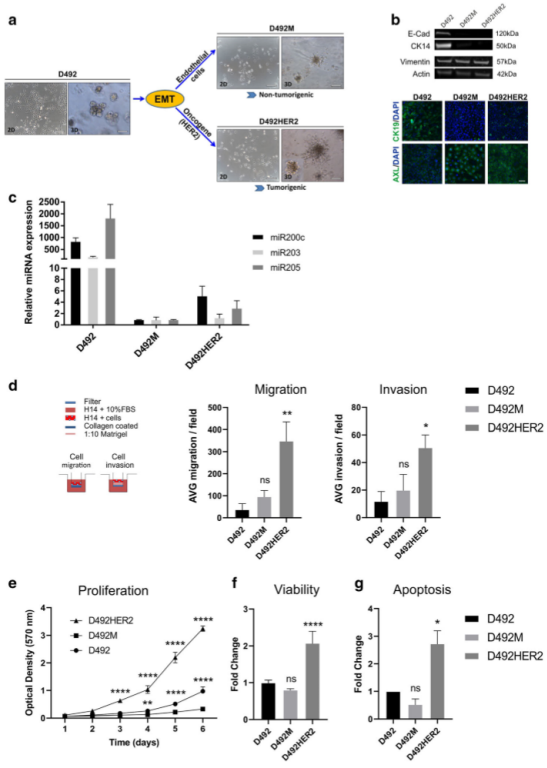

transferrin, EGF, sodium selenite (NaSel), estradiol, hydrocortisone, prolactin).

Human umbilical vein endothelial cells (HUVECs) were isolated from umbilical cords obtained from Landspitali University Hospital, Reykjavik, Iceland, with informed consent and approved by the Landspitali ethical committee (No. 35/2013). HUVECs were cultured in EGM2 + 5% FBS (no. CC-3162, Lonza).

In 3D cultures, cells were cultured in 300 µL of Matrigel (no. 354230, Corning, Corning, NY) per well, in 24-well plates (no. 353047, Corning, Corning, NY). In monoculture, 20,000 cells were embedded in reconstituted basement membrane, rBM, purchased as Matrigel (Corning no. 354230), with 500 µL of H14 media on top, while in co-cultures, 500 cells of D492 or its sublines were co-cultured with 150,000–200,000 HUVECs, embedded in Matrigel, with 500 µL of EGM2 + 5% FBS media on top.

Gene expression levels by qRT-PCR Total RNA was isolated with cold Tri-Reagent reagent (no. AM9738, Life Technologies, Carlsbad, CA). RNA precipitation was done using isopropanol and centrifugation at 14,000 rpm for 20 min.

◀ **Figure 1.** Phenotypic and functional characterization of D492M and D492HER2 cell lines. (*a*) D492M and D492HER2 are isogenic EMT-derived sublines of D492, a breast epithelial cell line with progenitor properties, which in 3D cell culture forms branching structures, resembling the TDLUs of the breast. D492M and D492HER2 were generated when D492 underwent endothelial-induced and oncogene (HER2)-induced EMT, respectively. D492M and D492HER2 show similar EMT-phenotype in 2D, but in 3D, D492M generate spindle-like colonies whereas D492HER2 generate spindle-like and grape-like colonies. D492M and D492HER2 also differ in their ability to generate tumors, as only D492HER2 is able to form tumors. *Scale bar* = 200 μm. (*b*) D492M and D492HER2 have lost expression of epithelial markers (E-cadherin, cytokeratin-14, and cytokeratin-19) and gained expression of mesenchymal markers (Axl and vimentin) as shown by western blotting and immunofluorescence. *Scale bar* = 100 μm. (*c*) D492M and D492HER2 show reduction in the expression of epithelial microRNAs such as miR-200c, miR-203, and miR-205 compared to D492. The lowest levels of expression are found in D492M (mean ± SD, $n = 2$). (*d*) In transwell migration and invasion assays, D492HER2 has an increased ability to migrate and invade compared to D492 and D492M. Results are shown as average number of cells per field (mean + SEM, $n = 3$). One-way analysis of variance (ANOVA) and Dunnett's multiple comparison test were used to test significance ($*p \leq 0.05$, $**p \leq 0.01$). (*e*) D492HER2 cells proliferate at a higher rate than D492 and D492M cells as shown by staining with crystal violet. Results are shown as average of four replicates (mean ± SD). Statistical significance was assessed using multiple *t* tests (one per *row*) ($**p \leq 0.01$, $****p \leq 0.0001$). (*f*) Furthermore, increased proliferation rate of D492HER2 compared to D492 and D492M cells was demonstrated using PrestoBlue™ Cell Viability reagent. Results are shown as average of eight replicates normalized to D492 (mean + SD). One-way analysis of variance (ANOVA) and Dunnett's multiple comparison test were used to test significance ($****p \leq 0.0001$). (*g*) In addition, D492HER2 cells are more susceptible to chemically induced apoptosis as compared to D492 and D492M cells. Caspase 3/7 luciferase activity was measured by luminescence and normalized to D492 (mean ± SEM, $n = 2$). Significance was assessed with one-way analysis of variance (ANOVA) and Dunnett's multiple comparison test ($*p \leq 0.05$).

Afterwards, RNA was washed with ethanol two times. The RNA pellet was diluted in RNAse free water. Concentration of RNA was measured using a NanoDrop® ND-1000 UV/Vis-Spectrophotometer (Thermo Fisher Scientific, Waltham, MA). For cDNA synthesis, SuperScript IV (no. 18090-200, Thermo Fisher Scientific) and random hexamer primers were used.

To quantify the expression level of genes, TaqMan (no. M3004L, NEB) or SYBR Green (no. M3003L, NEB) chemistries were used to detect gene expression. Comparative Ct values were determined using an ABI 7500 instrument (Applied Biosystems, Foster City, CA). All used primers are listed in Table 1. GAPDH was used as the reference gene.

Expression levels of miRNAs by qRT-PCR Total RNA was extracted with Tri-Reagent (no. AM9738, Thermo Fisher Scientific). The RNA was reverse transcribed using miRCURY LNA RT Kit (no. 339340, Qiagen, Hilden, Germany) for cDNA synthesis reactions. Quantitative RT-PCR analysis of miRNAs was performed using miRCURY LNA SYBR Green PCR Kit (no. 339346, Qiagen). Relative expression was calculated with the $2^{\Delta\Delta Ct}$ method. All used primers are listed in Table 1. Normalization was done with U6 (no. 203907, Exiqon, Vedbaek, Denmark).

Protein levels by Western Blot (WB) Protein isolation was done using RIPA buffer, and the concentration was measured by the colorimetric Bradford method. Equal amount of protein was loaded for each sample (5 μg) in precast NuPAGE 10% Bis-Tris gels (Invitrogen, Carlsbad, CA). Proteins were detected using IRDye secondary antibodies on an Odyssey imaging system (Li-Cor Biosciences, Lincoln, NE). Loading controls actin or tubulin were used for quantification. Antibodies used for WB are listed in Table 2.

Immunostaining Immunofluorescence (IF) was used to detect proteins and visualize their subcellular location. Cells were fixed with 3.7% paraformaldehyde (PFA) and permeabilized with 0.1% Triton X-100. Blocking with FBS was done prior to incubation with primary antibodies. Incubation was done overnight at 4°C and followed by incubation of secondary antibodies conjugated to fluorochromes Alexa Fluor-488, Fluor-546, or Fluor-647 for 1 h at room temperature. For nuclei staining, DAPI was used. Imaging was done using an EVOS FL Auto 2 Cell Imaging System (Thermo Fisher Scientific) or FV1200 Olympus inverted confocal microscope. Antibodies used for IF are listed in Table 2.

Transcriptome data analysis and classification Total RNA sequence profiles for D492, D492M, and D492HER2 were obtained from normal cell cultures and treated following the protocol detailed in Halldorsson *et al.* (2017).

Differentially expressed genes between cell lines were further classified into categories to see the biological processes that were enriched. Using a differential range from two fold change, genes were analyzed by the PANTHER analysis database (www.pantherdb.org) following instructions of Mi *et al.* (2013).

Secretome data analysis For mass spectrometry, D492 lines were grown in T175 flasks (no. 353112, Corning) and conditioned medium (CM) was collected, concentrated for 55 min using EMD Millipore Amicon™ Ultra-15 Centrifugal Filter Units (no. UFC900324, Merck Millipore, Darmstadt, Germany) followed by buffer exchange to 100 mM TRIS/HCl buffer. Triplicate samples were stored at − 80°C. Label-free relative protein quantification by nLC MS/MS after trypsin digestion was performed at the FingerPrints Proteomics Facility, University of Dundee, Dundee, UK and raw data were analyzed using MaxQuant software (version 1.6.2.1). Quantitative and statistical analyses were performed using XLStat (version 2018.1). Data were *P* value corrected (significance level 0.05)

a

Feature ID	D492 HER2 vs D492M Fold change	Higher/Lower expression confirmed by qPCR
GUCA1C	594.2	Almost not expressed
CITED1	306.1	D492HER2 > D492M
MYBPH	304.1	Similar expression
CHI3L1	199.2	D492HER2 > D492M
KCNQ1OT1	175.8	D492HER2 > D492M
ERBB2	136.1	D492HER2 > D492M
LINC00958	114.2	No
GPR27	73.3	D492HER2 > D492M
S100A9	71.0	D492M > D492HER2
DLK1	68.7	D492HER2 > D492M
More than 3.000 transcripts		
BMP4	-105.0	D492M > D492HER2
CDH2	-111.6	D492M > D492HER2
TLR4	-149.0	D492M > D492HER2
PXDN	-219.4	D492M > D492HER2
GDF6	-835.8	Similar expression

b

Enriched PANTHER GO Biological Processes in D492HER2 compared to D492M	Fold enrichment	P-value
D-aspartate transport (GO:0070777)	100	3.05E-02
inflammatory response (GO:0006954)	3.16	4.10E-04
cell chemotaxis (GO:0060326)	3.01	1.03E-02
cytokine-mediated signaling pathway (GO:0019221)	2.79	3.15E-02
regulation of neurotransmitter levels (GO:0001505)	2.72	4.02E-02
cellular response to cytokine stimulus (GO:0071345)	2.55	1.58E-02
organic anion transport (GO:0015711)	2.35	4.22E-02
cell proliferation (GO:0008283)	2.17	5.71E-03
defense response (GO:0006952)	2.09	4.70E-03
vasculature development (GO:0001944)	-2.02	4.95E-02
skeletal system development (GO:0001501)	-2.1	1.83E-02
circulatory system development (GO:0072359)	-2.23	1.84E-02
regulation of synapse structure or activity (GO:0050803)	-2.69	1.00E-02
sensory organ development (GO:0007423)	-2.77	2.85E-03
sensory organ morphogenesis (GO:0090596)	-3.54	1.44E-02
regulation of cartilage development (GO:0061035)	-4.5	3.96E-02
eye morphogenesis (GO:0048592)	-4.67	1.10E-02
negative regulation of embryonic development (GO:0045992)	-11.37	3.05E-02

c

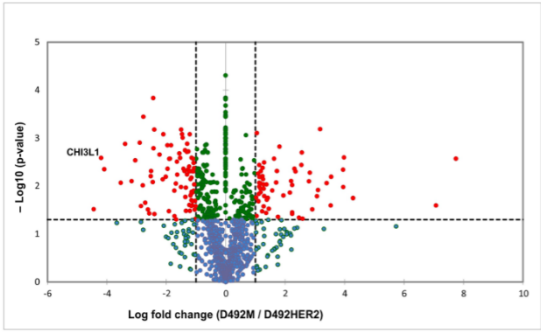

Figure 2. YKL-40 is enriched in D492HER2. *a* The analysis of transcriptome data comparing D492M and D492HER2 revealed more than 3000 transcripts differently expressed (more than two fold). YKL-40 (or CHI3L1) is more highly expressed in D492HER2 compared to D492M. *b* Classification of genes in biological processes shows an enrichment in D492HER2 compared to D492M in D-aspartate transport, inflammatory response, cell chemotaxis, cytokine-mediated signaling pathway, regulation of neurotransmitter levels, cellular response to cytokine stimulus, organic anion transport, cell proliferation, and defense response. YKL-40 is involved in the processes that require interaction with the stroma: inflammatory response, cell chemotaxis, cellular response to cytokine stimulus, and defense response (marked with *yellow*). *c* Mass spectrometry analysis of secreted proteins in CM revealed that YKL-40 is enriched in the secretome of D492HER2 compared to D492M (p value = 0.01).

and sorted based on ≥ 2-fold higher secretion (LFQ intensity) by D492HER2 compared to D492M.

Migration and invasion assays Migration and invasion assays were done in 24-well plates with transwell filter inserts (no. 353097, Corning) of 8 μm size pore diameter. Transwell inserts in the migration assay were pre-coated with collagen I (2.2%) and in the invasion assay; they were pre-coated with Matrigel diluted 1:10 in H14 media. Fifty thousand cells/transwell were seeded on the upper chamber in H14 media. In the bottom chamber, H14 was supplemented with 10% FBS as a chemoattractant. A cotton swab was used to remove non-migrated and non-invaded cells after 24 h and after 48 h, respectively. Thereafter, cells were fixed with 3.7% PFA and

stained with crystal violet (10%) or DAPI (1:5000 dilution) for 30 min. Three random pictures were taken per well and the number of cells was quantified. For DAPI-stained samples, images were converted to 8-bit in ImageJ (version 2.0.0), threshold-adjusted, and binary-converted and migratory/invasive cells were counted using the *analyze particles* function.

Proliferation assay Proliferation of cells was determined by seeding 10,000 cells/well in triplicate in 24-well plates in H14 (D492 cell lines) or EGM5 (HUVECS). Every day (2 d for HUVECs), cells were fixed and stained with crystal violet (10%). Crystal violet was diluted with acetic acid and the OD was measured at 570 nm wavelength. Alternatively, cell viability was assessed using PrestoBlue™ Cell Viability Reagent (ThermoFisher Scientific, Waltham, MA). Cells were seeded in H14 media in a 96-well plate at a density of 3000 cells/well and cultured for 4 d. PrestoBlue was added (1/10th of the total volume) to each well and incubated for 4 h, and absorbance was read on a plate reader at 570 nm and 595 nm.

Apoptosis assay To quantify apoptosis, cleavage of caspase 3/7 was measured by a luciferase assay (ApoTox-GloTM Triplex Assay, Promega, Madison, WI). Apoptosis was induced by incubating cells with 10 μM camptothecin (CPT) for 24 h according to the manufacturer's protocol. After cellular lysis, luciferase was measured with a microplate reader ModulusTM II (Turner Biosystems, Sunnyvale, CA).

Glucose consumption and lactate production measurements Glucose uptake was measured using Glucose Uptake-GloTM kit (no. J1341, Promega) following the manufacturer's protocol. Briefly, the analogue of glucose, 2-deoxyglucose (2DG), was added to the media and taken up by cells. When transported into cells, 2DG is phosphorylated to 2-deoxyglucose 6-phosphate (2DG6P) and further metabolization stimulates luciferase reactions and luminescence was measured by the microplate reader Modulus TM II (Turner Biosystems, Sunnyvale, CA).

Glucose consumption and lactate production were measured from the collected media when cells were in a high confluency. Metabolites were measured at the Analyzer machine (ABL90 FLEX Analyzer, Radiometer) at the Blood Bank of Landspitali (Reykjavik, Iceland).

Neutralization assay of YKL-40 protein A monoclonal antibody against YKL-40 (mA^{YKL40}) (MABC196, Millipore) was used to block the secretion of YKL-40 in D492HER2. The antibody was diluted in fresh H14 medium at a concentration of 10 μg/mL. Medium from cells incubated for 24 h with mA^{YKL40} was collected, and medium from non-treated D492HER2 cells was used as control. Conditioned media (CM) were used for tube formation assays (described below).

Tube formation assay on endothelial cells (angiogenesis assay in vitro) To simulate angiogenesis in vitro, 10,000–12,000 HUVECs were seeded on top of 10 μL solidified rBM in a 96-well angiogenesis plate (no. 89646, Ibidi). Controls included HUVECs cultured in EGM5 media and a dilution of 1:1 EGM5 and conditioned media (CM). Recombinant YKL-40 protein ($YKL\text{-}40^{r}$) (no. 11227H08H5, Thermo Fisher Scientific, Waltham, MA) was added to the medium at a final concentration of 100 ng/mL. After incubation overnight, the endothelial network was imaged using the EVOS FL Auto 2 Cell Imaging System. Analysis and quantification were done using the *Angiogenesis analyzer* plug-in on ImageJ software (version 2.0.0).

Transient knockdown of YKL-40 by siRNA Pre-designed siRNAs (Silencer® Select Pre-Designed, Validated and Custom siRNA, Life Technologies) against YKL-40 were used at a concentration of 10 nM in D492HER2 cells to down-regulate YKL-40. First, cells were seeded on 6-well plate (no. 353046, Corning, Corning, NY) and after 24 h, cells were transfected with the siRNA using chemical transfection with Lipofectamine® RNAiMAX (no. 13778150, Life Technologies, Carlsbad, CA). For each experiment, two different siRNAs against YKL-40 and a negative control siRNA (no. 4390843, Life Technologies, Carlsbad, CA) were used. The siRNAs are listed in Table 3. After 48 h, the knockdown was confirmed by qRT-PCR and by WB.

Generation of stable cell line with knockdown of YKL-40 in D492HER2 by CRISPR Specific gRNAs to knockdown YKL-40 were designed with the publicly available online ATUM CRISPR tool (https://www.atum.bio/). Annealing of the forward and reverse gRNA oligos was followed by ligation with the backbone vector pMLM3636. High-efficiency competent bacteria (no. C2987H, NEB) were transformed, and confirmation of successful DNA insertion was done by colony PCR. Plasmids were sequenced to confirm correct gRNA sequences. Transfection of D492HER2 was done with four plasmid gRNAs and a plasmid with only a Cas9 cassette (pST1374) using Lipofectamine® 3000 (Thermo Fisher). The control cell line was generated by transfecting the cells with only the Cas9 cassette. Selection of cells with insertion of Cas9 was done using blasticidin. Knockdown of YKL-40 in D492HER2 was confirmed by qRT-PCR and WB. Subsequently, the cell line that gave the best efficiency of knockdown was selected for further work. The sequence of this gRNA is in Table 4. It should be noted that D492HER2 is a cell line not suitable for single-cell cloning; therefore, a pool of cells was used for confirmation of knockdown and further experiments.

Generation of stable cell lines overexpressing YKL-40 in D492 and D492M by CRISPRa Overexpression of YKL-40 in D492

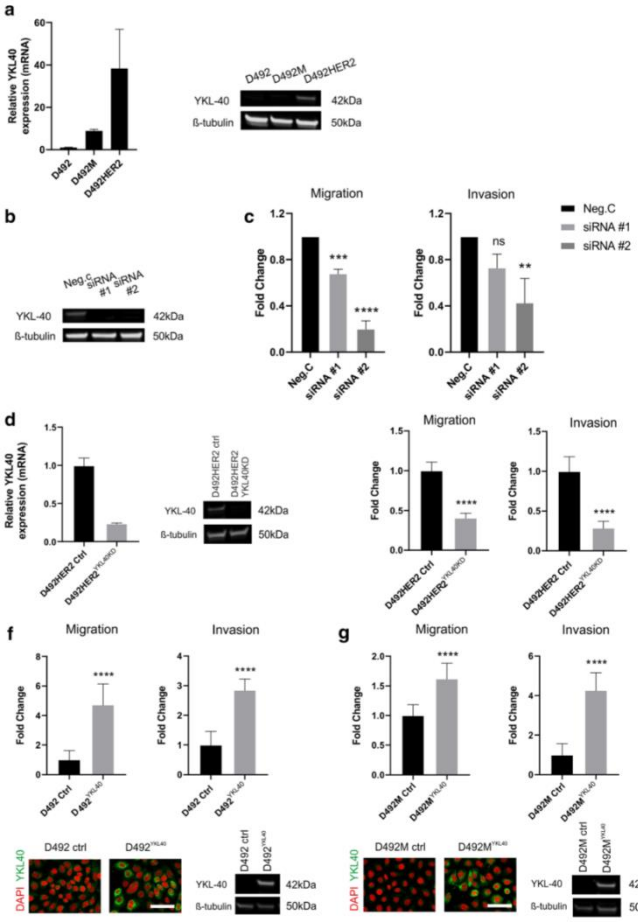

and D492M was carried out using the modified CRISPR strategy, called CRISPRa (Zhang *et al.* 2015). Two specific SAM gRNAs for YKL-40 and one empty control were purchased from Genscript containing zeomycin resistance cassettes. The gRNA sequences are listed in Table 4. Transfection of HEK293T cells was done to produce viral particles including gRNAs. Viruses collected were used to infect D492 and D492M cells that were previously transfected with dCas9-

◀ **Figure 3.** YKL-40 affects migration and invasion in D492 cell lines. *a* YKL-40 is more highly expressed in D492HER2, compared to D492 and D492M, both at mRNA and protein level. *b*, *c* Transient siRNA knock-down of YKL40 reduced the ability of D492HER2 to migrate and invade in vitro (mean ± SD, $n = 3$). Statistical significance was tested using one-way analysis of variance (ANOVA) and Dunnett's multiple comparison test (**$p \leq 0.01$, ***$p \leq 0.001$, ****$p \leq 0.0001$). *d*, *e* Knock-down of YKL-40 in D492HER2 in stable cell lines generated by CRISPR/Cas9 technology reduced the ability of D492HER2 to migrate and invade similarly to transient transfection. *f*, *g* Accordingly, overexpression of YKL40 in D492 and D492M using CRISPRa system increased their ability to migrate and invade. Overexpression of YKL-40 was confirmed by immunofluorescence staining (*Scale bar* = 100 μm) and western blotting. Migration and invasion assay results are shown as average of eight replicates (mean ± SD). Unpaired *t* test was used to test significance (**$p \leq 0.01$, ***$p \leq 0.001$, ****$p \leq 0.0001$).

VP64 to activate the promoter and later induce overexpression of the selected gene. Transduction with gRNAs was performed and selection was done with zeocin (no. R25005, Thermo Fisher Scientific). Confirmation of overexpression of YKL-40 in D492 and D492M was done by qRT-PCR, WB, and IF.

Statistical analysis One-way analysis of variance (ANOVA) using Dunnett's multiple comparison test or unpaired *t* tests were performed using GraphPad Prism to test significance. *P* values below 0.05 were considered significant (*$p \leq 0.05$, **$p \leq 0.01$, ***$p \leq 0.001$, ****$p \leq 0.0001$).

Results

Phenotypic and functional characterization of D492M and D492HER2 D492M and D492HER2 are isogenic cell lines that share a partial-EMT phenotype but are different in terms of their ability to form tumors in mice (Sigurdsson *et al.* 2011; Ingthorsson *et al.* 2015). D492M and D492HER2 are both derived from D492, a breast epithelial progenitor cell line, through endothelial-induced EMT and oncogene-induced EMT, respectively (Fig. 1*a*). D492M and D492HER2 have lost the expression of epithelial markers like E-cadherin, CK14, and CK19 and gained expression of some mesenchymal markers like vimentin and Axl, (Fig. 1*b*). MicroRNAs (miRs) such as miR-200c, miR-203, and miR-205 are frequently down-regulated in epithelial cells undergoing EMT, and this was the case for D492M and D492HER2. While D492 showed high expression of miR-200c, miR-203, and miR-205, these microRNAs were greatly reduced in D492HER2 and relatively absent in D492M (Fig. 1*c*). The difference in expression levels between D492M and D492HER2 may have been due to a more intermediate state of EMT for D492HER2. This intermediate state was also supported by the glucose metabolism (Fig. S1). These data show D492HER2 is more comparable in glucose uptake to D492 than D492M.

Further characterization demonstrated functional differences between the cell lines. Notably, D492HER2 cells migrated and invaded through transwell filters more efficiently than both D492M and D492 (Fig. 1*d*). The cell proliferation rate of D492HER2 cells was also significantly higher than in D492 and D492M cells (Fig. 1*e*, *f*). Furthermore, D492HER2 cells were more susceptible to chemically induced apoptosis than D492 and D492M cells (Fig. 1*g*), despite an apparent shift from oxidative phosphorylation to glycolysis as D492HER2 had higher glucose consumption and higher lactate production than either D492 or D492M cells (Fig. S1).

The functional differences between D492M and D492HER2 in terms of tumorigenicity prompted us to look into gene expression and secretome of D492M and D492HER2 to search for potential candidates responsible for these effects.

Transcriptome and secretome analyses show that YKL-40 is enriched in D492HER2 Next, we employed genome-wide analysis to reveal differences in gene expression in D492M and D492HER2. More than 40,000 transcripts were differentially expressed between D492M and D492HER2 and the most 15 differentially regulated genes were confirmed by qPCR (Fig. 2*a*). As expected, HER2 (ErbB2) has much higher expression in D492HER2 cells due to the ectopic overexpression of the gene (Ingthorsson *et al.* 2015). Although CITED1 was the first validated candidate, its absolute level of expression was low; thus, we focused our interest on a gene very highly expressed in D492HER2 compared to D492M (and also to D492), namely YKL-40 (also known as CHI3L1). The function of YKL-40 is not clearly understood but it has been suggested to be involved in cancer progression and other inflammation diseases (Libreros *et al.* 2012; Libreros and Iragavarapu-Charyulu 2015; Cohen *et al.* 2017) and even in EMT (Jefri *et al.* 2015).

Genes differentially expressed within the range of two fold change between D492M and D492HER2 were further classified using PANTHER analysis (Mi *et al.* 2013) in order to establish the biological processes that were enriched in each cell line. Genes more highly expressed in D492HER2 compared to D492M were shown to be involved in the following biological processes: D-aspartate transport, inflammatory response, cell chemotaxis, cellular response to cytokine stimulus, defense response, cellular response to cytokine stimulus, cell proliferation, and organic anion transport, among others (Fig. 2b). Interestingly, YKL-40 was found enriched in four of the 18 groups, as highlighted in yellow in Fig. 2b.

Complementing the gene expression data, we also measured by mass spectrometry the secretion of the proteins by D492M and D492HER2. Analysis of the total secreted

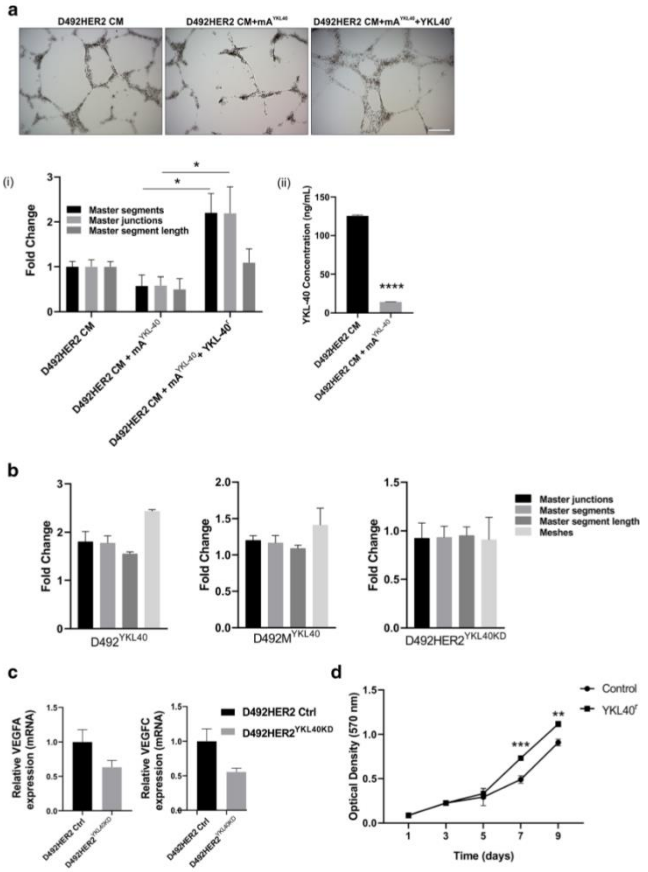

proteins in the conditioned media (CM) from D492M and D492HER2 revealed YKL-40 was found in much higher concentration in CM from D492HER2 (97.8 LFQ intensity) than D492M (5.4 LFQ intensity) (Fig. 2*c*). After these promising results, we strengthened our focus on YKL-40 as a firm candidate that could lead to differences between D492M and D492HER2.

Knockdown of YKL-40 in D492HER2 inhibits migration and invasion To explore the functional role of YKL-40 in

◀ **Figure 4.** YKL-40 expression in D492HER2 is linked to increased potential to stimulate angiogenesis. (*a*) Conditioned media (CM) from D492HER2 cells stimulates angiogenesis in an in vitro angiogenesis assay. This effect was abrogated upon YKL-40 neutralization by a monoclonal antibody (mA^{YKL40}) but rescued by the addition of recombinant YKL-40 protein ($YKL40^r$) (*Scalebar* = 200 μm). (i) Parameters of angiogenesis were measured and analyzed by ImageJ angiogenesis analyzer plug (mean ± SD) and significance was assessed with one-way analysis of variance (ANOVA) and Tukey's multiple comparison test ($*p \leq 0.05$). (ii) Decreased concentration of YKL-40 upon incubation of cells with mA^{YKL40} was verified with ELISA. Significance was tested with an unpaired t-test ($****p \leq 0.0001$). (*b*) When YKL-40 was overexpressed in D492 and D492M, there was an increase in the capillary network formation, whereas stable knockdown of YKL-40 in D492HER2 showed a tendency to reduced capillary network formation. (*c*) Knockdown of YKL-40 reduced the expression of other pro-angiogenic inducers, VEGFA and VEGFC. (*d*) Finally, recombinant YKL-40 protein ($YKL-40^r$) induced proliferation of endothelial cells when added to the media. Unpaired *t* test was used to test significance ($**p \leq 0.01$, $***p \leq 0.001$).

D492HER2, we did both transient and stable knockdown (KD). First, we confirmed the expression of YKL-40 at mRNA and protein level in D492, D492M, and D492HER2 demonstrating its abundant expression in D492HER2 (Fig. 3*a*). Transient knockdown with two different siRNAs greatly reduced YKL-40 expression in D492HER2 cells (Fig. 3*b*) and resulted in a significant decrease in migration and invasion (Fig. 3*c*). To further corroborate these effects, we generated stable YKL-40 KD using CRISPR technology in D492HER2 cells (Fig. 3*d*). Similar to transient KD of YKL-40, the stable KD cell line showed a reduction in migration and invasion compared to control D492HER2 cells (Fig. 3*e*). To analyze if overexpression of YKL-40 in D492 and D492M resulted in increased migration and invasion, we stably overexpressed YKL-40 in these cells and, indeed, this resulted in a large increase in both migration and invasion (Fig. 3*f*, *g*). No differences were seen with regard to cell proliferation regardless if YKL-40 was knocked down in D492HER2 or overexpressed in D492/D492M (data not shown). Collectively, these results demonstrate that in our cell system, YKL-40 increases migration and invasion.

YKL-40 expression in D492HER2 is linked to vascular network formation YKL-40 has previously been linked to angiogenesis (Shao *et al.* 2009, 2011). In order to see if increased expression of YKL-40 in D492HER2 was linked to increased potential to stimulate angiogenesis in an in vitro assay, we treated HUVECs on top of Matrigel with CM from D492HER2 with and without a functional blocking antibody against YKL-40 (mA^{YKL40}). Blocking YKL-40 directly reduced the ability of CM medium to induce HUVECs to form capillary-like networks. This blocking effect was reversed by adding recombinant YKL-40 protein ($YKL-40^r$) (Fig. 4*a*).

In agreement, CM from D492 and D492M stably overexpressing YKL-40 increased HUVEC network formation on top of Matrigel, whereas stable knockdown of YKL-40 in D492HER2 cells reduced HUVECs network formation (Fig. 4*b*). Additionally, the reduction of YKL-40 in the stable cell line revealed reduced expression of other pro-angiogenic genes, like VEGF-A and VEGF-C (Fig. 4*c*), suggesting a synergic pro-angiogenic effect induced in D492HER2. Furthermore, adding recombinant YKL-40 protein ($YKL-40^r$) to media not only stimulated tube formation on endothelial cells, but also increased proliferation rates of HUVECs (Fig. 4d).

YKL-40 affects phenotype of D492 cell lines when cultured in 3D culture When YKL-40 was downregulated in D492HER2 by transient or stable transfection, no phenotypic changes were seen in monolayer culture and EMT markers in immunostaining and western blot did not show any differences; thus, the EMT phenotype remained unaltered in 2D. Due to the transient nature of using siRNA, it was difficult to explore if there were any phenotypic changes occurring in 3D culture. In contrast, 3D culturing of cells with stable knockdown of YKL-40 revealed differences in phenotype of the D492 cell lines.

In 3D culture, D492HER2 formed two colony shapes, spindle-like and grape-like (Ingthorsson *et al.* 2015). Interestingly, when YKL-40 was knocked down, there was a dramatic change in the proportion of spindle-like and grape-like structures, with the proportion of grape-like structures being reduced from 21.4% to 1% (Fig. 5*a*). This subsequent change in the 3D phenotype of D492HER2 cells with knockdown of YKL-40 was similar to D492M cells that only showed a spindle-like phenotype (Sigurdsson *et al.* 2011). However, when the recombinant YKL-40 protein ($YKL-40^r$) was added to the media of D492HER2 with YKL-40 KD, the grape-like structures were rescued to 32.8% of the total 3D structures (Fig. 5*a*).

To confirm the shift to grape-like structures with the addition of YKL-40, D492M cells overexpressing YKL-40 were seeded in 3D cell culture. Remarkably, the entire cell population lost the ability to form spindle-like structures, and instead only grape-like structures were observed (Fig. 5*b*).

Discussion

In this study, we compared phenotypic and functional differences between two isogenic cell lines that share a partial-EMT phenotype but differ in terms of oncogenic properties. D492M is non-tumorigenic, whereas D492HER2 is tumorigenic. We identified YKL-40, also known as a chitinase-3-like protein 1 (CHI3L1), as a protein highly expressed and secreted in D492HER2 compared to D492M. Functional in vitro studies demonstrated that YKL-40 is involved in migration and invasion of D492HER2. Furthermore, blocking YKL-40 in conditioned media (CM) from D492HER2 reduced the ability of the

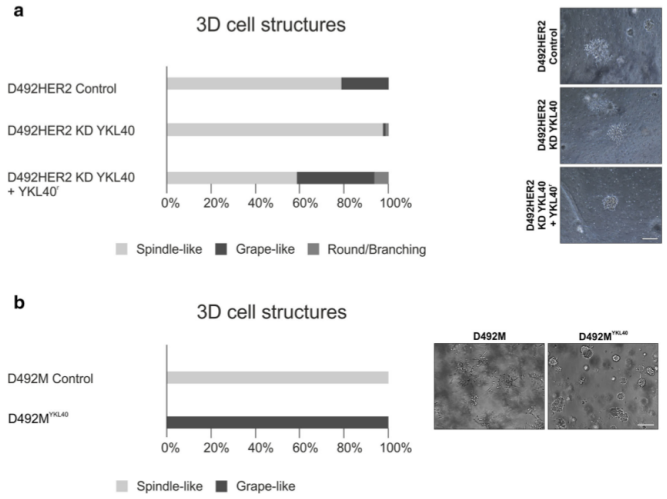

Figure 5. YKL-40 affects the phenotype of D492 cell lines in 3D. *a* CRISPR/Cas9-mediated knockdown of YKL-40 in D492HER2 cells, increased the number of spindle-like structures in a 3D culture, but grape-like structures were recovered with addition of recombinant YKL-40 protein (YKL40^r) to the media (*Scalebar* = 200 μm). *b* Overexpression of YKL-40 in D492M shifted the phenotype from spindle-like structures to grape-like structures in 3D (Scalebar = 200 μm).

D492HER2-derived CM to induce formation of capillary like network in an in vitro angiogenesis assay, which conversely can be rescued with the addition of recombinant YKL-40 protein. Finally, KD of YKL-40 in D492HER2 changed the ratio of spindle- and grape-like structures in favor of spindle-like structures, which could be reverted when the recombinant protein was added to the KD cells in 3D culture.

The term EMT is used for describing phenotypic changes where epithelial cells lose and gain epithelial and mesenchymal traits, respectively. Very rarely, a complete EMT occurs, and rather intermediate states are the most frequent phenotypes. Thus, it is common that traces of epithelial traits remain and a full mesenchymal phenotype is often incomplete resulting in a large spectrum of EMT phenotypes (Nieto 2013).

D492M and D492HER2 share some EMT properties such as loss of E-cadherin and cytokeratins and formation of a spindle-shaped phenotype in monolayer. D492M has a more fixed EMT phenotype with low or absent expression of epithelial markers, including microRNAs, and gain of mesenchymal markers (Sigurdsson *et al.* 2011; Hilmarsdottir *et al.* 2015). In a recent paper, we demonstrated that reintroduction of miR-200c-141 into D492M was sufficient to revert the phenotype to epithelial lineage, albeit only to luminal epithelial cells. Further studies demonstrated that the basal cell transcription factor P63 was necessary to recover the basal/myoepithelial phenotype. Co-transfection of miR-200c-141 and P63 into D492M was sufficient to regain the original phenotype of D492 (Hilmarsdottir *et al.* 2015). On the other hand, D492HER2 shows more intermediate EMT phenotype than D492M and could be defined as a cell line with partial-EMT (Ingthorsson *et al.* 2015). Even though D492HER2 migrates, invades, and proliferates more, it is more susceptible to apoptosis, its glucose metabolism is more similar to the one in the epithelial cell line (D492), and the expression levels of the regulatory epithelial miRNAs are reduced but not as dramatic as in the case of D492M. Moreover, there are evident phenotypic differences between these two cell lines when cultured in 3D in reconstituted basement membrane matrix, as D492M forms exclusively spindle-shaped EMT-like colonies in contrast to D492HER2 that forms mixture of spindle-shape and grape-like colonies.

Triple-negative breast cancer cell lines are often spindle-shaped with more prominent EMT phenotype in 3D rBM while cell lines with high HER2 expression are associated with grape-like phenotype (Han *et al.* 2010). We have previously shown that D492M and D492HER2 form spindle-shaped and grape-like structures in 3D rBM, respectively (Sigurdsson *et al.* 2011; Ingthorsson *et al.* 2016). That overexpression of YKL-40 in D492M shifts the phenotype toward grape-like structures may indicate that YKL-40 confers increased plasticity to D492M. Further studies in our laboratory aim to unravel whether YKL-40 expression is associated with tumorigenic potential of D492M and D492HER2.

Comparing and analyzing gene-wide expression and protein-wide secretion of D492M and D492HER2, YKL-40 was the most relevant candidate to study the differences between the cell lines. YKL-40 is a secreted glycoprotein of a still unclear function. The protein belongs to the chitinase family, but it lacks hydrolase activity (Renkema *et al.* 1998). It is expressed by several cell types including macrophages, neutrophils, epithelial cells, synovial cells, chondrocytes, smooth muscle cells, and some cancer cells (Recklies *et al.* 2002; Johansen *et al.* 2006). It is suggested to be involved in inflammation and angiogenesis, as well as survival and growth in tumors (Johansen *et al.* 2006). It is highly secreted in inflammation diseases (Roslind and Johansen 2009; Bonneh-Barkay *et al.* 2010) and some cancers, such as breast cancer, melanoma, glioblastoma, or small cell lung carcinoma (Johansen *et al.* 2006; Shao *et al.* 2011; Jefri *et al.* 2015; Libreros and Iragavarapu-Charyulu 2015). Recently, it has been linked to idiopathic pulmonary fibrosis (Zhou *et al.* 2014) and immunosuppressive effects by cancer-associated fibroblasts in breast cancer (Cohen *et al.* 2017).

We have confirmed here that changes in intrinsic expression of YKL-40 in D492HER2 lead to differences in migration and invasion behavior of the cells. When YKL-40 is downregulated by transient or stable knockdown, D492HER2 becomes less migrative and invasive. Migration and invasion are important processes that support cancer development and progression (Hanahan and Weinberg 2011) what indicates that YKL-40 may play a key role in invasiveness and dissemination of cancer cells.

YKL-40 has been previously linked to EMT in non-small cell lung cancer (Jefri *et al.* 2015), yet in our study, when YKL-40 was downregulated in D492HER2, its EMT phenotype in monolayer remained unaltered and there were no differences in expression of EMT markers. Nevertheless, high expression of YKL-40 or the addition of the recombinant protein has been related to an increase in the grape-shaped colonies in 3D cell cultures of the EMT-derived cell lines. This fact suggests that YKL-40 may have been involved in the plasticity of the cells, as the phenotype in 3D was changed when its expression was reduced in D492HER2 and then rescued when the recombinant protein was added. This is also interesting, since the grape-like structures are often associated with HER2-expressing cell lines (Kenny *et al.* 2007).

A number of papers have shown association between YKL-40 and HER2 expression in breast cancer. Wang *et al.* showed by meta-analysis of existing databases that YKL-40 is associated with poor prognosis in breast cancer patients (Wan *et al.* 2017). Kang *et al.* have demonstrated that YKL-40 expression in breast cancer is associated with Her-2 and basal-like molecular subtype of breast cancer (Kang *et al.* 2014). Also, Shao *et al.* showed an association between YKL-40 and Her2 subtype (Shao *et al.* 2011). Although, the association between YKL-40 and HER2 has been demonstrated, it is, however, to our best knowledge, still not clear if there are any direct or indirect molecular interactions between these two proteins in breast cancer. Using the breast mark database (Madden *et al.* 2013), we were however not able to link high or low expression of CHI3L1 in distinct subtype of breast cancer to increased or reduced survival.

PANTHER classification of the differentially regulated genes showed that YKL-40 is in enriched in biological processes related to interactions with the microenvironment that can support the development of tumors by cancer cells (inflammatory response, cell chemotaxis, cellular response to cytokine stimulus, and defense response). We demonstrate here that YKL-40 interacts with the microenvironment and more concretely is contributing to the angiogenesis-inducing effect of D492HER2.

We have demonstrated that YKL-40 secreted by D492HER2 has a role in angiogenesis. When YKL-40 protein is reduced in the media by a specific YKL-40 blocking antibody or stable knockdown in D492HER2, angiogenesis is decreased. Conversely, increased levels of YKL-40 in the CM by the addition of recombinant YKL-40 protein or secreted by the cell line reverted the effects to standard tube formation parameters.

Interestingly, the reduction of YKL-40 in D492HER2 by the stable knockdown cell line revealed the reduction of the expression of other pro-angiogenic genes, including VEGF-A and VEGF-C. These genes encode protein ligands that bind and activate VEGF receptor 2 (VEGFR2, Flk-1/KDR), one of the main receptors implicated in the induction of angiogenesis in endothelial cells (Carmeliet and Jain 2000; Harper and Bates 2008). Indeed, it has been shown that a monoclonal antibody against YKL-40 abolishes YKL-40-induced activation of the membrane VEGF receptor 2 and intracellular signaling mitogen-activated protein (MAP) kinase extracellular signal-regulated kinase (Erk) 1 and Erk 2 (Faibish *et al.* 2011).

However, the role of YKL-40 in cancer progression may not be exclusively derived from cancer cells and not limited to promote interactions with endothelial cells. Recently, it has been described that YKL-40 is highly secreted by fibroblasts

associated to cancer (CAFs) in breast-promoting tumor growth and facilitating metastasis. Moreover, YKL-40 released by CAFs supports recruitment of macrophages and promotes the switch to tumor-associated macrophages (TAMs) (Cohen *et al.* 2017). Furthermore, TAMs in breast cancer express YKL-40 where the secreted protein increases inflammation and angiogenesis leading to a worse prognosis and conceivably to metastasis (Shao 2013). Collectively, this suggests that YKL-40 has a complex role in malignancy that may provide the signals for further progression involving changes within cancer cells to migrate and invade and interact with cells of the surrounding stroma. Moreover, it also may provide feedback from the microenvironment to support cancer development, tumor growth, and incrementation of dissemination of cancer cells in metastasis.

Conclusion

In conclusion, our data suggest that YKL-40 may provide D492HER2 with increased aggressiveness, evidenced by enhanced migration and invasion. Furthermore, YKL-40 may also support cancer progression by facilitating angiogenesis and may therefore be of interest as a potential novel therapeutic target in HER2-positive breast cancer.

Acknowledgments This work was supported by Grants from Landspitali University Hospital Science Fund, University of Iceland Research Fund, and Icelandic Science and Technology Policy—Grant of Excellence: 152144051. 'Göngum saman,' a supporting group for breast cancer research in Iceland (www.gongumsaman.is). The funders had no role in study design, data collection and analysis, decision to publish, or preparation of the manuscript.

References

Al-Hajj M, Wicha MS, Benito-Hernandez A, Morrison SJ, Clarke MF (2003) Prospective identification of tumorigenic breast cancer cells. Proc Natl Acad Sci U S A 100(7):3983–3988

Blaschke RJ, Howlett AR, Desprez PY, Petersen OW, Bissell MJ (1994) Cell differentiation by extracellular matrix components. Methods Enzymol 245:535–556

Bonneh-Barkay D, Wang G, Starkey A, Hamilton RL, Wiley CA (2010) In vivo CHI3L1 (YKL-40) expression in astrocytes in acute and chronic neurological diseases. J Neuroinflammation 7:34

Brabletz T (2012) EMT and MET in metastasis: where are the cancer stem cells? Cancer Cell 22(6):699–701

Briem E, Ingthorsson S, Traustadottir GA, Hilmarsdottir B, Gudjonsson T (2019) Application of the D492 cell lines to explore breast morphogenesis, EMT and cancer progression in 3D culture. J Mammary Gland Biol Neoplasia 24(2):139–147

Burk U, Schubert J, Wellner U, Schmalhofer O, Vincan E, Spaderna S, Brabletz T (2008) A reciprocal repression between ZEB1 and members of the miR-200 family promotes EMT and invasion in cancer cells. EMBO Rep 9(6):582–589

Carmeliet P, Jain RK (2000) Angiogenesis in cancer and other diseases. Nature 407(6801):249–257

Cohen N, Shani O, Raz Y, Sharon Y, Hoffman D, Abramovitz L, Erez N (2017) Fibroblasts drive an immunosuppressive and growth-promoting microenvironment in breast cancer via secretion of chitinase 3-like 1. Oncogene 36(31):4457–4468

DeCastro AJ, Dunphy KA, Hutchinson J, Balboni AL, Cherukuri P, Jerry DJ, DiRenzo J (2013) MiR203 mediates subversion of stem cell properties during mammary epithelial differentiation via repression of DeltaNP63alpha and promotes mesenchymal-to-epithelial transition. Cell Death Dis 4:e514

Faibish M, Francescone R, Bentley B, Yan W, Shao R (2011) A YKL-40-neutralizing antibody blocks tumor angiogenesis and progression: a potential therapeutic agent in cancers. Mol Cancer Ther 10(5):742–751

Gjerdrum C, Tiron C, Hoiby T, Stefansson I, Haugen H, Sandal T, Collett K, Li S, McCormack E, Gjertsen BT, Micklem DR, Akslen LA, Glackin C, Lorens JB (2010) Axl is an essential epithelial-to-mesenchymal transition-induced regulator of breast cancer metastasis and patient survival. Proc Natl Acad Sci U S A 107(3):1124–1129

Gudjonsson T, Villadsen R, Nielsen HL, Ronnov-Jessen L, Bissell MJ, Petersen OW (2002) Isolation, immortalization, and characterization of a human breast epithelial cell line with stem cell properties. Genes Dev 16(6):693–706

Halldorsson S, Rohatgi N, Magnusdottir M, Choudhary KS, Gudjonsson T, Knutsen E, Barkovskaya A, Hilmarsdottir B, Perander M, Mælandsmo GM, Gudmundsson S, Rolfsson Ó (2017) Metabolic re-wiring of isogenic breast epithelial cell lines following epithelial to mesenchymal transition. Cancer Lett 396:117–129

Han, J., et al., Molecular predictors of 3D morphogenesis by breast cancer cell lines in 3D culture. PLoS Comput Biol, 2010. 6(2): p. e1000684.

Hanahan D, Weinberg RA (2011) Hallmarks of cancer: the next generation. Cell 144(5):646–674

Harper SJ, Bates DO (2008) VEGF-A splicing: the key to anti-angiogenic therapeutics? Nat Rev Cancer 8(11):880–887

Hilmarsdottir B, Briem E, Bergthorsson JT, Magnusson MK, Gudjonsson T (2014) Functional role of the microRNA-200 family in breast morphogenesis and neoplasia. Genes (Basel) 5(3):804–820

Hilmarsdottir B, Briem E, Sigurdsson V, Franzdottir SR, Ringner M, Arason AJ, Bergthorsson JT, Magnusson MK, Gudjonsson T (2015) MicroRNA-200c-141 and Np63 are required for breast epithelial differentiation and branching morphogenesis. Dev Biol 403(2):150–161

Huang RY, Wong MK, Tan TZ, Kuay KT, Ng AH, Chung VY, Chu YS, Matsumura N, Lai HC, Lee YF, Sim WJ, Chai C, Pietschmann E, Mori S, Low JJ, Choolani M, Thiery JP (2013) An EMT spectrum defines an anoikis-resistant and spheroidogenic intermediate mesenchymal state that is sensitive to e-cadherin restoration by a src-kinase inhibitor, saracatinib (AZD0530). Cell Death Dis 4:e915

Ingthorsson, S., et al., HER2 induced EMT and tumorigenicity in breast epithelial progenitor cells is inhibited by coexpression of EGFR. Oncogene, 2016. 35(32): p. 4244–55.

Ingthorsson S *et al* (2015) HER2 induced EMT and tumorigenicity in breast epithelial progenitor cells is inhibited by coexpression of EGFR. Oncogene 35(32):4244–4255

Ingthorsson S, Andersen K, Hilmarsdottir B, Maelandsmo GM, Magnusson MK, Gudjonsson T (2016) HER2 induced EMT and tumorigenicity in breast epithelial progenitor cells is inhibited by coexpression of EGFR. Oncogene 35(32):4244–4255

Ingthorsson S, Sigurdsson V, Fridriksdottir AJ, Jonasson JG, Kjartansson J, Magnusson MK, Gudjonsson T (2010) Endothelial cells stimulate growth of normal and cancerous breast epithelial cells in 3D culture. BMC Res Notes 3(1):184

Jefri M, Huang YN, Huang WC, Tai CS, Chen WL (2015) YKL-40 regulated epithelial-mesenchymal transition and migration/invasion enhancement in non-small cell lung cancer. BMC Cancer 15:590

Johansen JS, Jensen BV, Roslind A, Nielsen D, Price PA (2006) Serum YKL-40, a new prognostic biomarker in cancer patients? Cancer Epidemiol Biomark Prev 15(2):194–202

Kalluri R, Weinberg RA (2009) The basics of epithelial-mesenchymal transition. J Clin Invest 119(6):1420–1428

Kang EJ, Jung H, Woo OH, Park KH, Woo SU, Yang DS, Kim AR, Lee JB, Kim YH, Kim JS, Seo JH (2014) YKL-40 expression could be a poor prognostic marker in the breast cancer tissue. Tumour Biol 35(1):277–286

Kasai H, Allen JT, Mason RM, Kamimura T, Zhang Z (2005) TGF-beta1 induces human alveolar epithelial to mesenchymal cell transition (EMT). Respir Res 6:56

Kenny PA, Lee GY, Myers CA, Neve RM, Semeiks JR, Spellman PT, Lorenz K, Lee EH, Barcellos-Hoff MH, Petersen OW, Gray JW, Bissell MJ (2007) The morphologies of breast cancer cell lines in three-dimensional assays correlate with their profiles of gene expression. Mol Oncol 1(1):84–96

Korpal M, Lee ES, Hu G, Kang Y (2008) The miR-200 family inhibits epithelial-mesenchymal transition and cancer cell migration by direct targeting of E-cadherin transcriptional repressors ZEB1 and ZEB2. J Biol Chem 283(22):14910–14914

Libreros S, Garcia-Areas R, Shibata Y, Carrio R, Torroella-Kouri M, Iragavarapu-Charyulu V (2012) Induction of proinflammatory mediators by CHI3L1 is reduced by chitin treatment: decreased tumor metastasis in a breast cancer model. Int J Cancer 131(2):377–386

Libreros S, Iragavarapu-Charyulu V (2015) YKL-40/CHI3L1 drives inflammation on the road of tumor progression. J Leukoc Biol 98(6):931–936

Madden SF, Clarke C, Gaule P, Aherne ST, O'Donovan N, Clynes M, Crown J, Gallagher WM (2013) BreastMark: an integrated approach to mining publicly available transcriptomic datasets relating to breast cancer outcome. Breast Cancer Res 15(4):R52

Mani SA, Guo W, Liao MJ, Eaton EN, Ayyanan A, Zhou AY, Brooks M, Reinhard F, Zhang CC, Shipitsin M, Campbell LL, Polyak K, Brisken C, Yang J, Weinberg RA (2008) The epithelial-mesenchymal transition generates cells with properties of stem cells. Cell 133(4):704–715

Mi H, Muruganujan A, Casagrande JT, Thomas PD (2013) Large-scale gene function analysis with the PANTHER classification system. Nat Protoc 8:1551–1566

Moes M, Le Bechec A, Crespo I, Laurini C, Halavatyi A, Vetter G, del Sol A, Friederich E (2012) A novel network integrating a miRNA-203/SNAI1 feedback loop which regulates epithelial to mesenchymal transition. PLoS One 7(4)

Morel AP, Lievre M, Thomas C, Hinkal G, Ansieau S, Puisieux A (2008) Generation of breast cancer stem cells through epithelial-mesenchymal transition. PLoS One 3(8):e2888

Nieto MA (2013) Epithelial plasticity: a common theme in embryonic and cancer cells. Science 342(6159):1234850

Peinado H, Olmeda D, Cano A (2007) Snail, Zeb and bHLH factors in tumour progression: an alliance against the epithelial phenotype? Nat Rev Cancer 7(6):415–428

Polyak K, Weinberg RA (2009) Transitions between epithelial and mesenchymal states: acquisition of malignant and stem cell traits. Nat Rev Cancer 9(4):265–273

Recklies AD, White C, Ling H (2002) The chitinase 3-like protein human cartilage glycoprotein 39 (HC-gp39) stimulates proliferation of human connective-tissue cells and activates both extracellular signal-regulated kinase- and protein kinase B-mediated signalling pathways. Biochem J 365(1):119–126

Relf M, LeJeune S, Scott PA, Fox S, Smith K, Leek R, Moghaddam A, Whitehouse R, Bicknell R, Harris AL (1997) Expression of the angiogenic factors vascular endothelial cell growth factor, acidic and basic fibroblast growth factor, tumor growth factor beta-1, platelet-derived endothelial cell growth factor, placenta growth factor, and pleiotrophin in human primary breast cancer and its relation to angiogenesis. Cancer Res 57(5):963–969

Renkema GH, Boot RG, Au FL, Donker-Koopman WE, Strijland A, Muijsers AO, Hrebicek M, Aerts JM (1998) Chitotriosidase, a chitinase, and the 39-kDa human cartilage glycoprotein, a chitin-binding lectin, are homologues of family 18 glycosyl hydrolases secreted by human macrophages. Eur J Biochem 251(1–2):504–509

Roslind A, Johansen JS (2009) YKL-40: a novel marker shared by chronic inflammation and oncogenic transformation. Methods Mol Biol 511:159–184

Sarrio D, Rodriguez-Pinilla SM, Hardisson D, Cano A, Moreno-Bueno G, Palacios J (2008) Epithelial-mesenchymal transition in breast cancer relates to the basal-like phenotype. Cancer Res 68(4):989–997

Shao R (2013) YKL-40 acts as an angiogenic factor to promote tumor angiogenesis. Front Physiol 4:122

Shao R, Cao QJ, Arenas RB, Bigelow C, Bentley B, Yan W (2011) Breast cancer expression of YKL-40 correlates with tumour grade, poor differentiation, and other cancer markers. Br J Cancer 105(8):1203–1209

Shao R, Hamel K, Petersen L, Cao QJ, Arenas RB, Bigelow C, Bentley B, Yan W (2009) YKL-40, a secreted glycoprotein, promotes tumor angiogenesis. Oncogene 28(50):4456–4468

Shekhar MP, Werdell J, Tait L (2000) Interaction with endothelial cells is a prerequisite for branching ductal-alveolar morphogenesis and hyperplasia of preneoplastic human breast epithelial cells: regulation by estrogen. Cancer Res 60(2):439–449

Sigurdsson V, Fridriksdottir AJ, Kjartansson J, Jonasson JG, Steinarsdottir M, Petersen OW, Ogmundsdottir HM, Gudjonsson T (2006) Human breast microvascular endothelial cells retain phenotypic traits in long-term finite life span culture. In Vitro Cell Dev Biol Anim 42(10):332–340

Sigurdsson V, Hilmarsdottir B, Sigmundsdottir H, Fridriksdottir AJ, Ringner M, Villadsen R, Borg A, Agnarsson BA, Petersen OW, Magnusson MK, Gudjonsson T (2011) Endothelial induced EMT in breast epithelial cells with stem cell properties. PLoS One 6(9):e23833

Sonveaux P, Copetti T, De Saedeleer CJ, Vegran F, Verrax J, Kennedy KM, Moon EJ, Dhup S, Danhier P, Frerart F, Gallez B, Ribeiro A, Michiels C, Dewhirst MW, Feron O (2012) Targeting the lactate transporter MCT1 in endothelial cells inhibits lactate-induced HIF-1 activation and tumor angiogenesis. PLoS One 7(3):e33418

Stingl J (2006) Purification and unique properties of mammary epithelial stem cells. Nature 439:993–997

Tam WL, Weinberg RA (2013) The epigenetics of epithelial-mesenchymal plasticity in cancer. Nat Med 19(11):1438–1449

Tan TZ, Miow QH, Miki Y, Noda T, Mori S, Huang RY, Thiery JP (2014) Epithelial-mesenchymal transition spectrum quantification and its efficacy in deciphering survival and drug responses of cancer patients. EMBO Mol Med 6(10):1279–1293

Thiery JP (2002) Epithelial-mesenchymal transitions in tumour progression. Nat Rev Cancer 2(6):442–454

Thiery JP, Acloque H, Huang RY, Nieto MA (2009) Epithelial-mesenchymal transitions in development and disease. Cell 139(5):871–890

Vegran F, Boidot R, Michiels C, Sonveaux P, Feron O (2011) Lactate influx through the endothelial cell monocarboxylate transporter MCT1 supports an NF-kappaB/IL-8 pathway that drives tumor angiogenesis. Cancer Res 71(7):2550–2560

Wan G, Xiang L, Sun X, Wang X, Li H, Ge W, Cao F (2017) Elevated YKL-40 expression is associated with a poor prognosis in breast cancer patients. Oncotarget 8(3):5382–5391

Wiklund ED, Bramsen JB, Hulf T, Dyrskjot L, Ramanathan R, Hansen TB, Villadsen SB, Gao S, Ostenfeld MS, Borre M, Peter ME, Orntoft TF, Kjems J, Clark SJ (2010) Coordinated epigenetic repression of the miR-200 family and miR-205 in invasive bladder cancer. Int J Cancer 128(6):1327–1334

Willis BC, Borok Z (2007) TGF-beta-induced EMT: mechanisms and implications for fibrotic lung disease. Am J Physiol Lung Cell Mol Physiol 293(3):L525–L534

Yang MH, Wu MZ, Chiou SH, Chen PM, Chang SY, Liu CJ, Teng SC, Wu KJ (2008) Direct regulation of TWIST by HIF-1alpha promotes metastasis. Nat Cell Biol 10(3):295–305

Yu M, Bardia A, Wittner BS, Stott SL, Smas ME, Ting DT, Isakoff SJ, Ciciliano JC, Wells MN, Shah AM, Concannon KF, Donaldson MC, Sequist LV, Brachtel E, Sgroi D, Baselga J, Ramaswamy S, Toner M, Haber DA, Maheswaran S (2013) Circulating breast tumor cells exhibit dynamic changes in epithelial and mesenchymal composition. Science 339(6119):580–584

Zhang, Y., Yin, C., Zhang, T., Li, F., Yang, W., Kaminski, R. et al. (2015). CRISPR/gRNA-directed synergistic activation mediator (SAM) induces specific, persistent and robust reactivation of the HIV-1 latent reservoirs. Scientific Reports, 5(1). https://doi.org/10.1038/srep16277

Zhou Y, Peng H, Sun H, Peng X, Tang C, Gan Y, Chen X, Mathur A, Hu B, Slade MD, Montgomery RR, Shaw AC, Homer RJ, White ES, Lee CM, Moore MW, Gulati M, Lee CG, Elias JA, Herzog EL (2014) Chitinase 3-like 1 suppresses injury and promotes fibroproliferative responses in Mammalian lung fibrosis. Sci Transl Med 6(240):240ra276

Paper IV

Laboratory Investigation
https://doi.org/10.1038/s41374-020-0415-6

ARTICLE

ECM1 secreted by HER2-overexpressing breast cancer cells promotes formation of a vascular niche accelerating cancer cell migration and invasion

Sophie Sarah Steinhaeuser[1] · Erika Morera[1] · Zuzana Budkova[1] · Alexander Schepsky[1] · Qiong Wang[2] · Ottar Rolfsson[2] · Angela Riedel[3,4] · Aileen Krueger[3,4] · Bylgja Hilmarsdottir[5] · Gunhild Mari Maelandsmo[5] · Bryndis Valdimarsdottir[1] · Anna Karen Sigurdardottir[1] · Bjarni Agnar Agnarsson[6,7] · Jon Gunnlaugur Jonasson[6,7] · Saevar Ingthorsson[1] · Gunnhildur Asta Traustadottir[1] · Thordur Oskarsson[3,4,8] · Thorarinn Gudjonsson[1,2,9]

Received: 13 May 2019 / Revised: 25 February 2020 / Accepted: 26 February 2020

Abstract

The tumor microenvironment is increasingly recognized as key player in cancer progression. Investigating heterotypic interactions between cancer cells and their microenvironment is important for understanding how specific cell types support cancer. Forming the vasculature, endothelial cells (ECs) are a prominent cell type in the microenvironment of both normal and neoplastic breast gland. Here, we sought out to analyze epithelial–endothelial cross talk in the breast using isogenic non-tumorigenic vs. tumorigenic breast epithelial cell lines and primary ECs. The cellular model used here consists of D492, a breast epithelial cell line with stem cell properties, and two isogenic D492-derived EMT cell lines, D492M and D492HER2. D492M was generated by endothelial-induced EMT and is non-tumorigenic while D492HER2 is tumorigenic, expressing the ErbB2/HER2 oncogene. To investigate cellular cross talk, we used both conditioned medium (CM) and 2D/3D co-culture systems. Secretome analysis of D492 cell lines was performed using mass spectrometry and candidate knockdown (KD), and overexpression (OE) was done using siRNA and CRISPRi/CRISPRa technology. D492HER2 directly enhances endothelial network formation and activates a molecular axis in ECs promoting D492HER2 migration and invasion, suggesting an endothelial feedback response. Secretome analysis identified extracellular matrix protein 1 (ECM1) as potential angiogenic inducer in D492HER2. Confirming its involvement, KD of ECM1 reduced the ability of D492HER2-CM to increase endothelial network formation and induce the endothelial feedback, while recombinant ECM1 (rECM1) increased both. Interestingly, NOTCH1 and NOTCH3 expression was upregulated in ECs upon treatment with D492HER2-CM or rECM1 but not by CM from D492HER2 with ECM1 KD. Blocking endothelial NOTCH signaling inhibited the increase in network formation and the ability of ECs to promote D492HER2 migration and invasion. In summary, our data demonstrate that cancer-secreted ECM1 induces a NOTCH-mediated endothelial feedback promoting cancer progression by enhancing migration and invasion. Targeting this interaction may provide a novel possibility to improve cancer treatment.

Introduction

Organ morphogenesis is dependent on heterotypic interactions between multiple cell types. In breast morphogenesis, the epithelial compartment generates branching ducts that result in terminal duct lobular units (TDLU) [1]. Ducts and TDLUs are surrounded by a basement membrane, embedded in stroma consisting of extracellular matrix (ECM) as well as multiple cell types including fibroblasts, immune cells, and endothelial cells (ECs) forming the microvessels [1, 2]. Formation of TDLU is highly dependent on heterotypic interactions between the epithelial cells and the surrounding vascular-rich stroma. Multiple studies have shown that the stromal compartment plays a fundamental role when it comes to epithelial morphogenesis [2–6]. For example, the ability of breast epithelial cells to form TDLU-like structures in a 3-dimensional environment in vitro is strongly enhanced by the presence of breast ECs [2]. In

Supplementary information The online version of this article (https://doi.org/10.1038/s41374-020-0415-6) contains supplementary material, which is available to authorized users.

✉ Thorarinn Gudjonsson
tgudjons@hi.is

Extended author information available on the last page of the article

Published online: 18 March 2020

addition to its role in normal development, recent studies provide evidence that proliferation and migration of cancer cells is also largely dependent on interactions with the surrounding stroma [3, 7–9].

The tumor microenvironment is composed of a plethora of different cell types and ECM [10]. The interaction between cancer cells and cells of the microenvironment is a crucial determinant of cancer progression. Co-evolution of cancer cells and tumor stroma can lead to the generation of niches that support tumor growth, both at the primary site and at distant metastatic sites [11]. In this context, many studies have been focusing on identifying the role of tumor-associated macrophages and cancer-associated fibroblasts in cancer progression [12–16].

Recent research, however, suggests that ECs of blood vessels play a role in cancer progression that is far beyond delivering oxygen and nutrients [7, 17–20]. There is evidence that the endothelium can impact cancer progression by either preventing or supporting tumor growth and metastasis formation. An intact vasculature can keep metastatic cells in a dormant and non-proliferative state whereas a sprouting vasculature rather supports metastatic outgrowth [7, 21, 22]. Ghajar and colleagues found that endothelial-derived thrombospondin-1 induces cancer cell dormancy in breast cancer and therefore prevents outgrowth of metastasis in lung and bones [7]. However, in the presence of sprouting neovasculature this suppressive effect was lost and the endothelium now appeared to promote tumor outgrowth via TGF-b1 and periostin [7]. Therefore, an essential question to ask is how cancer cells interact with ECs in order to promote the generation of a vascular niche promoting tumor growth and cancer progression. Presently, a number of molecular mediators of angiogenesis have been identified [23]. The most commonly described candidates include vascular endothelial growth factor (VEGF), fibroblast growth factor 2 (FGF2), tumor necrosis factor alpha (TNF-a), transforming growth factor beta 1 (TGF-b1), platelet-derived growth factor (PDGF), as well as angiopoietins. Laughner et al. were able to show that HER2 signaling in breast cancer cells could increase HIF1a-mediated VEGF expression resulting in increased tumor angiogenesis [24]. Lee et al. showed that increased IL-6 secretion in breast cancer cells induces secretion of CCL5 in lymphatic endothelial cells (LEC), which in return enhances cancer cell migration [18]. Furthermore, cancer cell-secreted IL-6 increases VEGF expression in LECs, which enhances lung vascular permeability and lymph node angiogenesis and thereby promotes metastatic outgrowth [18, 19]. In addition, the NOTCH signaling pathway has recently been linked to angiogenesis [23, 25, 26]. Murtas et al. report increased NOTCH1 expression by tumor endothelium in cutaneous melanoma that was linked to increasing microvascular density [25]. This suggests that targeting the interaction between cancer cells and their niches may provide additional means to inhibit progression of cancer. However, our understanding of the generation of vascular niches and molecular interactions within the niches is generally still rudimentary.

We have previously established a breast epithelial cell line with stem cell properties, referred to as D492 [27–30]. D492 can generate both luminal and myoepithelial cells, and in 3D rBM (reconstituted basement membrane, matrigel) culture it forms branching structures reminiscent of TDLU in vivo. When D492 was co-cultured with ECs in an organoid culture, a subpopulation of D492 underwent EMT and such a structure isolated gave rise to D492M [27]. D492HER2 was generated by overexpressing the ErbB2/HER2 oncogene in D492, which then underwent oncogene-induced EMT [31]. In contrast to D492M, D492HER2 has tumorigenic properties, as evidenced by injection of cells in the mammary fat pads of NOD scid gamma (NSG) mice. The different tumorigenicities of these two isogenic EMT derivatives of D492 present an interesting research platform to study tumorigenicity, especially with regard to interaction with the endothelium.

In this study, we show that conditioned medium (CM) from D492HER2 increases endothelial network formation in vitro and induces an endothelial feedback promoting D492HER2 migration and invasion. Secretome analysis identified extracellular matrix protein 1 (ECM1) as potential pro-angiogenic factor in D492HER2. Recombinant ECM1 (rECM1) increases endothelial network formation while knockdown (KD) of ECM1 reduces the ability of D492HER2-CM to increase the endothelial network. ECM1 has previously been associated with decreased overall and distant metastasis-free survival when expressed in HER2+ breast tumors [32–34]. A role in angiogenesis and cancer cell migration and invasion has been suggested in laryngeal carcinoma, cholangiocarcinoma, gastric cancer, bladder cancer, and breast cancer [32, 35–38]. However, the mechanism through which ECM1 induces a pro-tumorigenic vascular niche promoting cancer progression is still unknown. Finally, increased expression of NOTCH1 and NOTCH3 in ECs treated with D492HER2-CM or rECM1 indicates a possible novel modulatory role of ECM1 in NOTCH signaling during angiogenesis and cancer.

Materials and methods

Cell culture

D492, D492M, and D492HER2 cells were maintained in H14 medium in tissue culture-treated T25 Falcon flasks (BD Biosciences (BD), Franklin Lakes, NJ, USA) coated with collagen I (Advanced Biomatrix, San Diego, CA, USA), as described previously [27, 31]. The cells were

grown at 37 °C and 5% CO_2 and subcultured into new flasks 1–2 times per week in a ratio of 1:10 (D492), 1:5 (D492M), or 1:15 (D492HER2). MDA-MB-231 was cultured in Gibco™ RPMI 1640 medium containing 10% fetal bovine serum (FBS) (Invitrogen), further referred to as R10F, and MCF-7 in Gibco™ DMEM:F12 medium with 10% FBS. Both cell lines were subcultured 1–2 times per week at a ratio of 1:10. Primary human umbilical vascular ECs (HUVEC) were obtained from the National University Hospital (Landspitali) Reykjavik and cultured up to passage 8 in EBM2 medium (Lonza) supplemented with growth factors and 5% FBS, further referred to as EGM5. HUVECs were subcultured 1–2 times per week at a ratio of 1:10. Culture medium was changed three times per week and routinely checked for mycoplasma contamination.

CM and mass spectrometry

D492, D492M, and D492HER2 were grown in H14 medium until 70–80% confluence. Cells were washed with 1x PBS, and half of the original volume of fresh H14 was added in order to enrich for secreted factors. After 48 h incubation at 37 °C, CM was collected, centrifuged at 2000 rpm for 3 min and sterile filtered through 0.22 µm filter unit. For endothelial network formation in 3D culture, 10,000 HUVECs were seeded in freshly collected CM (or unconditioned control H14) and fresh EGM5 medium (ratio 1:1) in a 96 well angiogenesis plate (#89646, Ibidi) on top of 10 µl solidified rBM Matrigel (#354230, Corning). For recombinant protein experiments, rECM1 (#TP723147, Origene) was added to the medium in a final concentration of 15, 30, 60, or 120 ng/ml. 60 ng/ml was then chosen as concentration for further experiments. For endothelial NOTCH inhibition, gamma-secretase inhibitor tert-Butyl (2S)-2-[[(2S)-2-[[2-(3,5-difluorophenyl)acetyl]amino]propanoyl]amino]-2-phenylacetate (DAPT) (#D5942, Sigma-Aldrich) was added to the medium in a final concentration of 20 µM. Phase-contrast images of the establishing endothelial network were taken after 4, 24, and 48 h. Images were converted to RGB color and analyzed using ImageJ Angiogenesis Analyzer macro. For mass spectrometry, D492 lines were grown in T175 flasks and CM was collected as described above, concentrated for 55 min using EMD Millipore Amicon™ Ultra-15 Centrifugal Filter Units (#UFC900324, Merck Millipore) followed by buffer exchange to 100 mM TRIS/HCL buffer. Samples (triplicates) were stored at −80 °C. Label-free relative protein quantification (LFQ) by nLC MS/MS after trypsin digestion was performed at the FingerPrints Proteomics Facility, University of Dundee, UK, and raw data were analyzed using MaxQuant software (version 1.6.2.1). Quantitative and statistical analysis was performed using XLStat (version 2018.1). Data were p value corrected (significance level 0.05) and sorted based on greter than or equal to twofold higher secretion (LFQ intensity) by D492HER2 compared with both D492 and D492M. The resulting candidate list of 77 proteins was used for GO term analysis using PANTHER database (statistical overrepresentation test). As annotation dataset we used "GO biological process complete" with Bonferroni correction for multiple testing. To investigate feedback effects of conditioned/induced ECs, CM from D492 lines was added to 40–50% confluent HUVECs (as described above) and incubated for 48 h. Cells were washed with 1x PBS, and fresh EGM5 (half volume) was added to collect conditioned endothelial-secreted factors. After 48 h, CM from induced vs. non-induced HUVECs was collected, centrifuged (2000 rpm, 3 min) and filtered (0.22 µm) and added to 40% confluent D492HER2 together with fresh H14 (ratio 1:1) for 48 h.

Migration and invasion assay

Migration was analyzed using transwell-filter units for 24-well plates with 8 µm pore size (#353097, Corning). Thirty thousand cells were seeded on top of the filter in 250 µl culture medium. For the invasion assay, filters were pre-coated with 1:10 rBM in H14 for 30 min at 37 °C. For the migration assay, cells were incubated for 24 h and for 48 h in the invasion assay. rECM1 and NOTCH inhibitor DAPT were used in the concentrations as described before. For migration towards ECs, HUVECs were grown in 500 µl EGM5 to 80% confluence in 24-well plate. Then, medium was changed to H14+ EGM5 (1:1), and D492 line cells were seeded on top of filter units (triplicates) in H14+ EGM5 (1:1). As positive control, 10% FBS was added to the medium below the filter instead of HUVECs and as negative control, medium above and below the filter unit was identical (H14+ EGM5, 1:1). For migration and invasion of D492HER2 treated with CM of induced vs. non-induced ECs, 30,000 D492HER2 cells were seeded in 250 µl H14 on top of the non-coated or rBM-coated filter units (triplicates) and 500 µl H14 containing 10% FBS as attractant was added below. For MDA-MB-231, R10F was used instead of H14 while keeping the same experimental setup. After 24 h or 48 h, non-migratory or non-invasive cells were removed from the top of the filter using Q-tips, migratory cells below the filter were fixed for 10 min with 4% PFA (#252549, Sigma-Aldrich) and stained for 30 min with 1:5000 diluted DAPI nuclear staining (20 mg/ml) (#D9542, Sigma-Aldrich). Using an EVOS FL Auto 2 Cell Imaging System (Thermo Fisher Scientific), three images per replicate were taken at ×10 magnification. Images were converted to 8-bit in ImageJ (version 2.0.0), threshold-adjusted and binary-converted. Migratory cells were counted using the "analyze particles" function.

Transient KD using siRNA

KD was performed in 24-well plate using pre-designed Silencer® Select human ECM1 siRNA (#s4441, Thermo Fisher Scientific) compared with a scrambled negative control (Silencer Select negative control No. 1, Thermo Fisher Scientific, #4390843). Cells were reverse transfected for 48 h according to the manufacturer's protocol using a siRNA concentration of 10 nM. Proliferation was monitored using an IncuCyte ZOOM 2016B System. KD was confirmed using RT-qPCR and western blotting. After 48 h, medium was changed to normal H14 and incubated for another 48 h for collection of CM as described above. Endothelial network formation was analyzed as previously described for HUVECs treated with CM from D492HER2^{siECM1} compared with control D492HER2.

Generation of stable KD and overexpression cell lines using CRISPRi/CRISPRa

In order to generate stable ECM1 KD in D492HER2 and overexpression in D492 and D492M, we used the novel CRISPRi (inhibition) and CRISPRa (activation) system. sgRNA plasmids were purchased from Genscript; for ECM1 overexpression and KD, a combination of two sgRNAs was used. Overexpression sgRNAs were predesign and located between 1 and 200 bp upstream of the ECM1 transcription start site and KD sgRNAs custom-designed to bind between 1 and 200 bp downstream. sgRNAs were cloned into the plenti sgRNA(MS2)_zeo plasmid (Genscript). As negative control, an empty plenti sgRNA(MS2)_zeo plasmid was used (Genscript). For production of lentiviral particles, HEK293T cells were used and virus was collected 48 and 72 h after transfection. D492 and D492M were first transduced with plenti dCAS9-VP64-Blast plasmid for transcriptional activation and selected with blasticidin at a concentration of 2 µg/ml for 7 days. D492HER2 were transduced with pHR-SFFV-KRAB-dCas9-P2A-mCherry plasmid for repression and sorted for mCherry expression. Next, transduction with lentivirus containing sgRNA plasmids for overexpression (D492 and D492M containing dCas9-VP64 cassette) and KD (D492HER2 containing dCas9-KRAB cassette) was performed. For both KD and OE, two different gRNAs were pooled (KD: ECM1 custom gRNA 1 and 2 (GTGGTCA GTTGCCCCAGGAT, GCCGGCCACTGAAGCTTGTC) and OE: ECM1 SAM guide RNA 1 and 2 (CATCTACA GGCTGCCTTCTG, GAAACTGAGGCACAAACTAG)). Cells were selected with 400 µg/ml (D492, D492M) or 600 µg/ml (D492HER2) zeocin (Invitrogen) for 14 days. For enhancement of ECM1 OE, D492 and D492M were then transduced with lenti MS2-P65-HSF1 Hygro plasmid, containing enhancer domains MS2, P65, and HSP1 that bind to VP64 and enhance its activation activity. Cells were selected with 100 µg/ml hygromycin (Sellekchem, #S2908) for 10–12 days. ECM1 KD or OE were validated on gene expression level using RT-qPCR.

RNA microarray

For RNA microarray analysis, D492, D492M, and D492HER2 with and without ECM1 overexpression/KD were grown until 80% confluence, fresh H14 medium was added and CM was collected after 48 h. HUVECs were grown to 40% confluence, washed with 1x PBS and CM was added together with fresh EGM5 (ratio 1:1). After 24 h, RNA was extracted using the RNeasy Mini Kit (Qiagen). Sample concentration and quality was analyzed using the Agilent 2100 Bioanalyzer System (Agilent). As RNA microarray, Affimetrix Human Clariom S Assay was performed at the sequencing core facility, German Cancer Research Center (DKFZ) Heidelberg, Germany. Raw data were analyzed using Chipster high-throughput data analysis software v3.12.

RNA, cDNA, and RT-qPCR

Total RNA was extracted with Trizol (Life Technologies) and reverse transcribed with hexanucleotides using the SuperScript® IV First-Strand Synthesis System (Invitrogen). Resulting cDNA (10 ng per reaction) was used for quantitative real-time PCR, in master mix (Life Technologies) with predesigned primer pairs ECM1 (Hs.PT.58.20438560), NOTCH1 (Hs.PT.58.23074795), NOTCH3 (Hs.PT.58.38492200), and beta-2-microglobulin (B2M) as reference gene (Hs.PT.58v.18759587). Experiments were carried out in triplicate on the 7500 Real-Time PCR System (Life Technologies). Expression levels were normalized to the reference gene, and relative mRNA differences were calculated with the ΔΔCt method according to the "Minimum Information for Publication of Quantitative Real-Time PCR Experiments" (MIQE) guidelines [39].

Protein isolation and western blotting

Protein was isolated using RIPA lysis buffer supplemented with phosphatase and protease inhibitor cocktails (Life Technologies). For western blotting, 5–10 µg protein was used per lane, unless otherwise stated. Samples were denatured using 10% mercaptoethanol at 95 °C for 5 min and run on NuPage 10% Bis-Tris gels (Life Technologies) in 2-(N-morpholino)ethanesulfonic acid running buffer. Samples were then transferred to immobilon FL polyvinylidenfluorid (PVDF) membranes (Millipore). Membranes were blocked in Li-Cor blocking buffer, and primary antibodies (ECM1:

sc-515843 (Santa Cruz), beta tubulin: ab6046 (Abcam)) were incubated overnight at 4 °C. Near-infrared fluorescence visualization was measured using Odyssey CLx scanner (Li-Cor, Cambridge, UK).

In vivo tumor formation assay

To assess tumorigenicity of D492HER2 and D492HER2 with KD of ECM1, cells were injected subcutaneously into female NSG mice, bred at the Department of Comparative Medicine, Oslo University Hospital. The mice were kept in pathogen-free environment at a constant temperature (21.5 ± 0.5 °C) and humidity (55 ± 5%); 15 air changes/h and a 12 h light/dark cycle. The animals were 5–6 weeks old and their weight was 18–20 g before they were included in experiments. Anesthesia was obtained with 5% (v/v) Sevofluran along with 1 L oxygen and 3 L nitrous oxide, given with inhalation mask. Food and water were supplied ad libitum. 5×10^5 cells in 100 µl of 1:1 mixture of PBS and Matrigel (Corning, #354248) were injected on both flanks of the animal. Tumor growth was measured twice a week using a caliper, and the tumor volume was calculated according to the formula $0.5 \times \text{length} \times \text{width}^2$. Animals were sacrificed performing cervical dislocation at the end of the experiments, or when tumor volume reached 1500 mm^3, the weight loss exceeded 20% or when they became moribund. Tumors were dissected and from each tumor one part was frozen in liquid nitrogen and the other was fixed in PFA and embedded in paraffin. All experiments involving animals have been approved by the Norwegian Animal Research Authority (ethical approval FOTS ID: 12080) and conducted according to the regulations of the Federation of European Laboratory Animals Science Association (FELASA) [40].

Immunofluorescence (IF) staining

HUVECs were grown to 80% confluence on eight-well chamber slides (#354108, Falcon), fixed with 3.7% PFA, permeabilized with 0.1% Triton X-100, and unspecific background was blocked using 10% FBS in 1x PBS. Incubation with primary antibodies for ECM1 (Sigma-Aldrich, #HPA027241), NOTCH1 (#sc-376403, Santa Cruz), and NOTCH3 (#ab23426, Abcam) was done overnight at 4 °C, followed by incubation with secondary antibodies conjugated with Alexa Fluor-488, -546, or -647 for 1 h at RT. For nuclei staining DAPI was used together with secondary antibodies at a concentration of 1:5000. Imaging was done using FV1200 Olympus inverted confocal microscope. For IHC staining, paraffin-embedded tumor tissue samples were processed in xylene and ethanol in order to remove paraffin and then rehydrated in dH2O. Following rehydration, high-temperature antigen retrieval in 1x T/E buffer was performed and samples were stained as described above. Counterstaining was performed with filtered hematoxylin for 1–2 min.

Statistical analysis

All experiments were performed at minimum in triplicate. Graphs were generated in Microsoft Excel 2015. Error bars represent the standard deviation of the mean. Statistical analysis was performed in R 3.3.3. (R Development Core team, 2013). Data were checked for normal distribution and Student's *t* test or ANOVA followed by Tukey's honest significant difference test on linear models was performed when normally distributed whereas Kruskal–Wallis chi-squared test was used when not normally distributed. The significance level was 0.05.

Results

CM from D492HER2 promotes endothelial network formation

Initially, we aimed to analyze the heterotypic interactions between normal and cancerous epithelial cells of the mammary gland and ECs. To address this, we used isogenic normal and cancerous cell lines derived from the D492 breast epithelial progenitor cell line [28, 30]. We collected CM from D492, D492M, and D492HER2 and analyzed the effect on endothelial network formation in vitro. ECs were seeded in CM from D492, D492M, and D492HER2 on top of rBM, and endothelial network formation was analyzed after 4, 24, and 48 h (Fig. 1a, b, Supplementary Fig. S1). Assessment of EC viability confirmed similar cell viability upon CM treatment compared with H14 ctrl medium (Supplementary Fig. S13). The established network of ECs treated with CM from D492HER2 but not from D492 and D492M showed significantly higher numbers of master junctions, master segments, meshes, and higher total master segment length after 4 h (Fig. 1a, b). This indicates that D492HER2-CM enhances early endothelial network formation in vitro. All quantified parameters were also significantly higher upon treatment with D492HER2-derived CM after 24 and 48 h indicating stability and persistence of the observed pro-angiogenic effect of D492HER2-CM over time (Supplementary Fig. S1).

D492HER2-induced ECs feedback on D492HER2 by promoting migration and invasion

After identifying D492HER2 as a cell line enhancing endothelial network formation, we collected CM from D492HER2-induced ECs and treated D492HER2 (Fig. 1c)

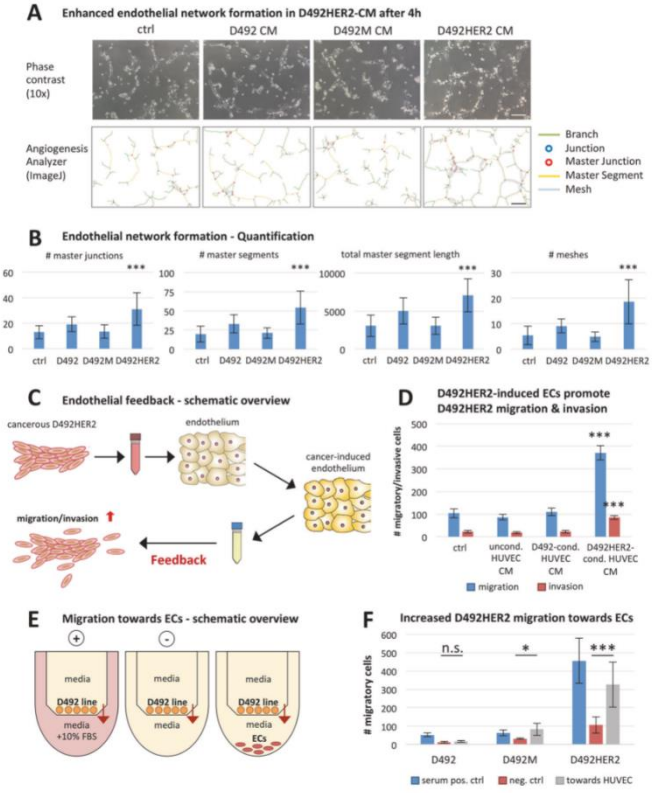

in order to investigate a possible feedback response through cellular cross talk. Interestingly, we observed that treatment with CM from D492HER2-induced ECs stimulated increased migration and invasion of D492HER2, in contrast to CM from untreated ECs and D492-induced ECs (Fig. 1d), suggesting a positive feedback. To identify whether migration of D492HER2 cells was specifically directed toward the endothelium rather than being general, we performed indirect co-culture of D492, D492M, and D492HER2 in a transwell assay with or without ECs present below the filter (Fig. 1e). When analyzing the number of migratory cells, D492HER2 in particular showed an increased migratory phenotype toward ECs below the filter (Fig. 1f), supporting the hypothesis that migration is increased toward the endothelium mediated by induced ECs. In line with this, we could see significantly more D492HER2 than D492 or D492M cells directly associated with ECs in 2D and 3D co-culture with ECs (Supplementary Fig. S2).

◀ **Fig. 1 CM from D492HER2 enhances endothelial network and induces endothelial feedback increasing D492HER2 migration/invasion. a** Enhanced endothelial network formation in D492HER2-CM after 4 h. Top: representative phase-contrast images of HUVEC endothelial network after 4 h on top of rBM in control (unconditioned) medium and conditioned medium from D492, D492M, and D492HER2. Each condition included 4–6 wells as replicates and 1–2 images were taken per well at ×10 magnification (scale bar = 100 µm). Bottom: corresponding angiogenesis images (ImageJ, angiogenesis analyzer plugin) showing branches, junctions, master junctions, master segments, and meshes. **b** Endothelial network formation—quantification. Quantification of master junctions, master segments total master segment length and meshes for each image using angiogenesis analyzer plugin (average and standard deviation per condition). Statistical analysis performed in R, one-way ANOVA, $***p < 0.001$, $**p < 0.01$, $*p < 0.05$, <0.1. **c** Endothelial feedback—schematic overview. Schematic workflow of conditioning of ECs (see "Materials and methods"). **d** D492HER2-induced ECs promote D492HER2 migration and invasion. Transwell-migration and invasion assays of D492HER2 treated with unconditioned medium, unconditioned HUVEC-CM, D492-conditioned HUVEC-CM, and D492HER2-conditioned HUVEC-CM. Number of migratory/invasive cells is shown for the different treatments (Student's *t* test, $***p < 0.001$, $**p < 0.01$, $*p < 0.05$, <0.1). **e** Migration toward ECs—schematic overview. Schematic setup of the transwell-migration assay of D492, D492M, and D492HER2 toward HUVECs seeded below the transwell filter. Migration toward HUVECs (in H14 + EGM1) was compared with migration toward 10% FBS in H14 + EGM5 (pos. ctrl) and plain H14 + EGM5 (neg. ctrl). **f** Increased D492HER2 migration toward ECs. Migration of D492, D492M, and D492HER2 toward HUVECs. Number of migratory cells is shown for the different treatments (Student's *t* test, $***p < 0.001$, $**p < 0.01$, $*p < 0.05$, <0.1).

Enrichment of angiogenesis-regulating proteins and identification of ECM1 in D492HER2 secretome

In order to identify secreted factors from D492HER2 that are mediating the observed pro-angiogenic effect, we performed label-free mass spectrometry on concentrated CM from all three D492 cell lines. In order to determine candidates involved in tumorigenicity rather than EMT phenotype, we focused on proteins higher secreted by D492HER2 compared with both D492 and D492M. We used RT-qPCR and transcriptomic data to verify secretome candidates. After correction of the data for significance (0.05 significance level) and at least twofold difference in secretion, we received a list of a total of 77 proteins more highly secreted by D492HER2 compared with D492 and D492M (Fig. 2a and Supplementary Table S1). GO term analysis showed 6.7-fold enrichment for GO term group "regulation of angiogenesis" (GO:0045765) among D492HER2-secreted candidates (Fig. 2b), consisting of seven gene members (Fig. 2c). We then compared secretion levels of these seven candidates in our secretome dataset and identified ECM1 and chitinase 3-like-1 (CHI3L1) as the two proteins with the most prominent secretion profile (Fig. 2d). Interestingly, secretion levels of commonly recognized angiogenesis inducers such as VEGFa, FGF2, or PDGF were not significantly elevated in our cell lines, suggesting a different mechanism behind the observed pro-angiogenic effect of D492HER2 secretome (Fig. 2d). CHI3L1, also known as YKL-40, is a secreted glycoprotein, which is associated with a number of biological functions and also plays a role in chronic inflammation diseases and cancer [41–43]. Recently, it has been linked to idiopathic pulmonary fibrosis [44]. Previous studies provide evidence for a role of YKL-40 in tumor angiogenesis by mediating VEGF signaling [45, 46]. ECM1 is a secreted glycoprotein, which was first identified in the mouse osteogenic stromal cell line MN7 [47]. It was initially described as modulator of proliferation and differentiation of epidermal keratinocytes and basement membrane reconstitution in the skin [48]. However, it has also been linked to angiogenesis and malignant transformation [32–34, 37, 48–50]. Interestingly, analysis to determine correlation to different gene modules using GOBO gene set analysis database (University of Lund, Sweden) revealed a significant Spearman correlation of ECM1 to the gene module "stroma" (Fig. 2e). Kaplan–Maier survival analysis revealed for both CHI3L1 and ECM1, a significant correlation of gene expression with decreased survival (Supplementary Fig. S4). However, whereas in case of CHI3L1 this correlation is not specifically associated with a certain cancer subtype, ECM1 expression is significantly correlated with decreased distant metastasis-free survival (DMSF) when expressed in HER2+ and estrogen receptor-negative (ER−) breast tumors (Fig. 2f, g, Supplementary Figs. S3 and S4) [49]. These data put together led our focus on ECM1 as the main candidate for further investigation in the context of stromal interaction.

ECM1 enhances endothelial network and induces endothelial feedback

To verify that ECM1 is involved in the inducing effects of D492HER2 on endothelial network formation and positive feedback, we investigated whether rECM1 is capable of inducing network formation and feedback as well. We treated ECs with 15, 30, 60, and 120 ng/ml of rECM1 and quantified network formation as described previously. Indeed, rECM1 had significantly increased the endothelial network formed after 4 and 24 h as quantified by numbers of master junctions, meshes, master segments, and total master segment length (Fig. 3a, b). Hereby, the strongest effect was seen for treatment with 30 and 60 ng/ml rECM1 (Fig. 3b). This indicates that the system may already be saturated at these concentrations rather than rECM1 having a dose-dependent effect. To look at the endothelial feedback, we induced ECs with 60 ng/ml rECM1 and treated D492HER2 with CM of ECM1-induced ECs (Fig. 3c). CM of ECM1-induced ECs significantly increased D492HER2 migration and invasion (Fig. 3d), confirming that ECM1 does play a role in inducing the endothelial feedback induced by D492HER2.

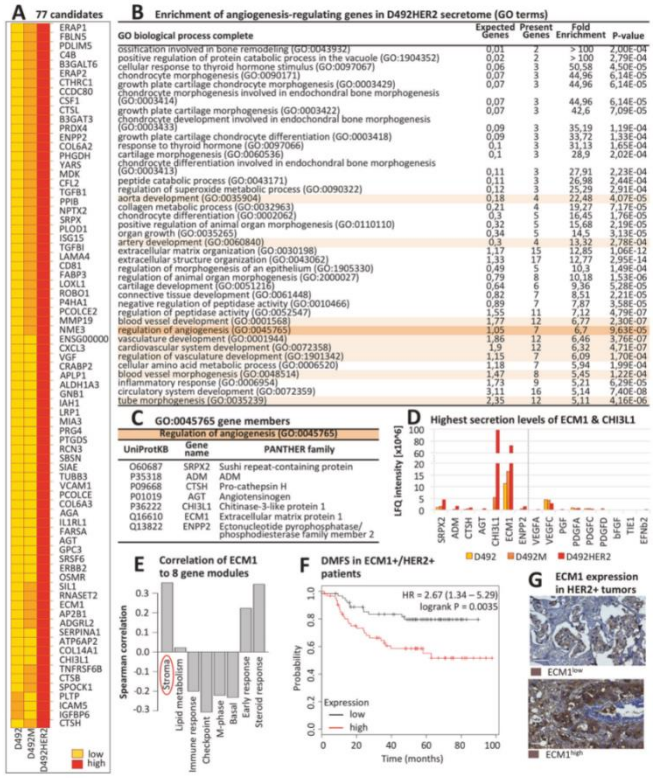

Fig. 2 Identification of ECM1 as pro-angiogenic candidate in D492HER2. **a** 77 candidates. Heat map of 77 proteins higher secreted by D492HER2 compared with both D492 and D492M (label-free mass spectrometry secretome data, $p < 0.05$, threshold fold change greater than or equal to twofold). **b** Enrichment of angiogenesis-regulating genes in D492HER2 secretome (GO terms). Enrichment of "Regulation of angiogenesis" GO term group GO:0045765 among D492HER2 secretome. Statistical overrepresentation test (Panther DB) was performed using "GO biological process complete" as annotation dataset with Bonferroni correction for multiple testing. **c** GO:0045765 gene members. Proteins part of GO term group GO:0045765 (Regulation of angiogenesis). **d** Highest secretion levels of ECM1 and CHI3L1. Secretion levels (label-free quantification LFQ) of the seven candidates from **c** (left of dotted line) compared WITH secretion levels of commonly known angiogenesis inducers (right of dotted line). **e** Correlation of ECM1 to eight gene modules. Spearman correlation of ECM1 expression to different gene modules in breast tumor samples (GOBO Genset analysis, Lund University). **f** DMFS in ECM1+/HER2+ patients. Kaplan–Meier plot of ECM1 in HER2+ tumors showing correlation of high expression with decreased distant metastasis-free survival (DMFS). **g** ECM1 expression in HER2+ tumors. ECM1 expression in representative HER2+ tumor samples showing low and high expression. Cells were counterstained with hematoxilyn. Scale bar = 100 µm.

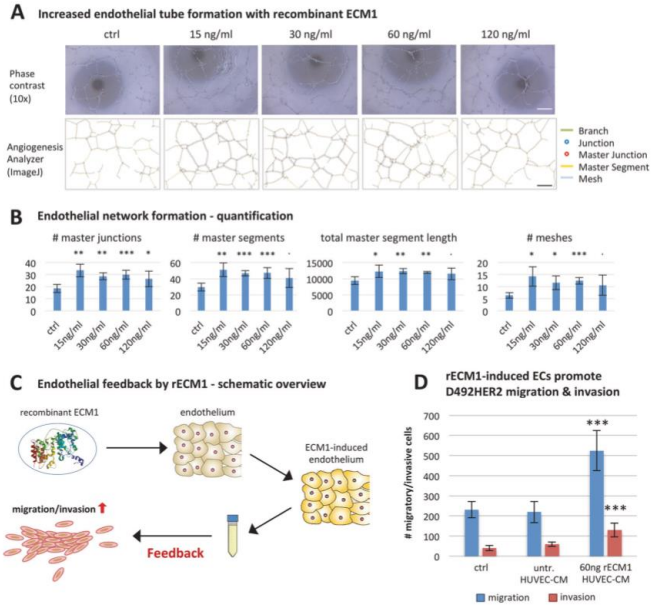

Fig. 3 Recombinant ECM1 enhances endothelial network and induces endothelial feedback increasing D492HER2 migration/invasion. a Increased endothelial tube formation with recombinant ECM1. Top: HUVEC endothelial network on top of matrigel in different concentrations of recombinant ECM1 (after 24 h). 4–6 wells as replicates per condition and 1–2 images taken per well at ×10 magnification (scale bar = 100 µm). Bottom: corresponding angiogenesis images (ImageJ angiogenesis analyzer). **b** Endothelial network formation—quantification. Quantification of master junctions, master segments, total master segment length, and meshes for each image using angiogenesis analyzer plugin. One-way ANOVA, $***p < 0.001$, $**p < 0.01$, $*p < 0.05$, <0.1. **c** Endothelial feedback by rECM1—schematic overview. Schematic workflow of conditioning of ECs using 60 ng/ml rECM1. **d** rECM1-induced ECs promote D492HER2 migration and invasion. Transwell-migration and invasion assays of D492HER2 treated with unconditioned medium, unconditioned HUVEC-CM and 60 ng rECM1-treated HUVEC-CM. Number of migratory/invasive cells shown for different treatments (Student's *t* test, $***p < 0.001$, $**p < 0.01$, $*p < 0.05$, <0.1).

To verify the activity of ECM1, we induced stable overexpression of ECM1 in D492 and D492M. CM from D492 and D492M stably overexpressing ECM1 showed pro-angiogenic properties (Fig. 4a, b). Furthermore, D492 and D492M overexpressing ECM1 show increased migration toward ECs, similar as observed for D492HER2 (Supplementary Fig. S6). Next, we generated transient KD of ECM1 in D492HER2 using siRNA (Supplementary Fig. S5) and stable KD using CRISPRi. Both transient and stable KD were successful (over 90% KD), as verified on gene as well as protein level (Supplementary Figs. S5 and S6). In accordance with the observed effects of rECM1 and ECM1 overexpression, treatment with CM from D492HER2-kdECM1 resulted in significantly lower endothelial network formation compared with control D492HER2 (Fig. 4a, b). Similar results were obtained with CM from D492HER2 with transient ECM1 KD (Supplementary Fig. S5). In addition to these results on the D492 cell lines, we investigated pro-angiogenic properties of SKBR3 (HER2+ and ECM1−) and HCC202 (HER2+ and ECM1+) breast cancer cell lines. Network formation data showed increased pro-angiogenic properties of HCC202-CM but not SKBR3-CM compared with controls, confirming the specific role of ECM1 in this context (Supplementary Fig. S10). Analysis of

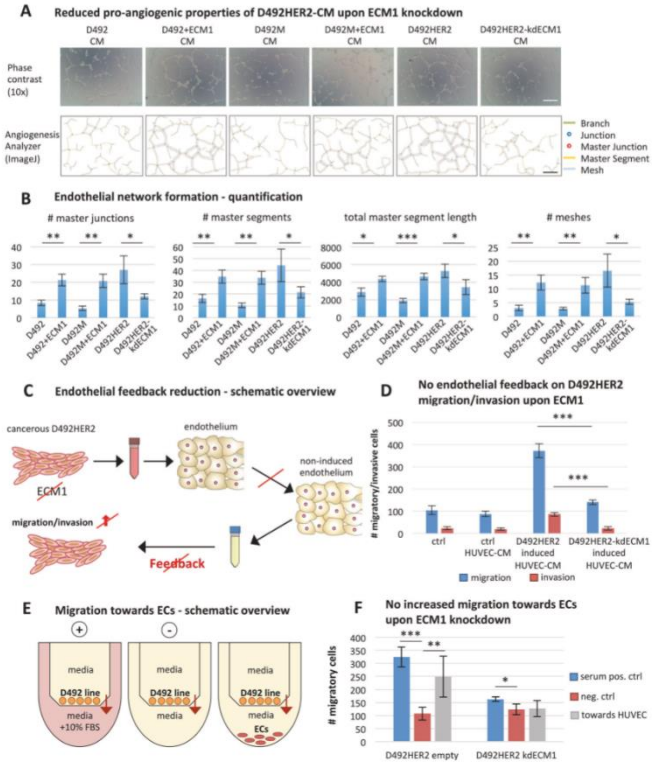

Fig. 4 ECM1 knockdown inhibits pro-angiogenic effect of D492HER2-CM and endothelial feedback on D492HER2 migration/invasion. a Reduced pro-angiogenic properties of D492HER2-CM upon ECM1 knockdown. Top: HUVEC endothelial network on top of matrigel in CM from D492 and D492M with ECM1 overexpression and D492HER2 with ECM1 knockdown compared with empty vector control (after 4 h). 4–6 wells as replicates per condition and 1–2 images taken per well at ×10 magnification (scale bar = 100 µm). Bottom: corresponding angiogenesis images (ImageJ angiogenesis analyzer). **b** Endothelial network formation—quantification. Quantification of master junctions, master segments, total master segment length, and meshes for each image using angiogenesis analyzer plugin. One-way ANOVA, $***p < 0.001$, $**p < 0.01$, $*p < 0.05$, <0.1. **c** Endothelial feedback reduction—schematic overview. Schematic workflow of conditioning of ECs using CM from D492HER2-kdECM1. **d** No endothelial feedback on D492HER2 migration upon ECM1 knockdown. Transwell-migration and invasion assays of D492HER2 treated with unconditioned medium, unconditioned HUVEC-CM, D492HER2-conditioned HUVEC-CM, and D492HER2-kdECM1-conditioned HUVEC-CM. Student's *t* test, $***p < 0.001$, $**p < 0.01$, $*p < 0.05$, <0.1. **e** Migration toward ECs—schematic overview. Schematic setup of the transwell-migration assay of D492HER2 empty ctrl. and D492HER2-kdECM1 toward HUVECs compared with pos. ctrl (10% FBS) and neg. ctrl (plain H14 + EGM5). **f** No increased migration toward ECs upon ECM1 knockdown. Migration of D492HER2 empty ctrl and D492HER2-kdECM1 toward HUVECs. Number of migratory cells for different treatments (Student's *t* test, $***p < 0.001$, $**p < 0.01$, $*p < 0.05$, <0.1).

the endothelial feedback showed that treatment of ECs with CM from D492HER2-kdECM1 did not induce an endothelial response to D492HER2 increasing cell migration and invasion (Fig. 4c, d). Also, the observed increased migration of D492HER2 toward ECs (Fig. 4c) could be depleted upon KD of ECM1, supporting the role of ECM1 in mediating the endothelial feedback and promoting migration toward the endothelium (Fig. 4e, f). These data suggest ECM1 as a specific mediator of endothelial response promoting cancer progression.

Subcutaneous injection of D492HER2 ctrl and D492HER2-kdECM1 into mice indicated a reduction in tumor volume upon ECM1 KD. However, this difference was not statistically significant (Student's t test, $p = 0.12$) (Supplementary Fig. S11). Furthermore, CD31 staining could not clearly confirm decreased angiogenesis within the tumor mass of D492HER2 with KD of ECM1 compared with D492HER2 ctrl. Interestingly though, both ctrl and kdECM1 tumors did show similar ECM1 protein expression levels although ECM1 KD had been confirmed by RT-qPCR prior injection into mice.

Triple-negative (TN) MDA-MB-231 cells also show high ECM1 expression and are capable of increasing endothelial network formation and inducing endothelial feedback

When analyzing the correlation of ECM1 and prognosis, we noted that high expression of ECM1 was not only correlated to worse survival in HER2+ breast cancer patients but also in triple-negative (TN) and generally ER− tumor patients (Supplementary Figs. S4 and S8B). In addition, correlation analysis using the Metabric discovery dataset showed a significant positive correlation between ECM1 expression and CD31 as established endothelial marker in ER− breast cancer (Supplementary Fig. S8E). Therefore, we decided to include MDA-MB-231 as TN and MCF-7 as ER+ cell line in our study. Interestingly, CM from MDA-MB-231 but not MCF-7 also increased endothelial network formation after 4, 24, and 48 h (Supplementary Figs. S8C, D, S9). Similar to D492HER2, MDA-MB-231 expresses high levels of ECM1 in contrast to MCF-7 (Supplementary Fig. S8A). Treating ECs with rECM1 also induced an endothelial feedback promoting MDA-MB-231 migration, as seen for ECM1-expressing D492HER2 (Supplementary Fig. S8F, G). Upon transient ECM1 KD in MDA-MB-231 (RT-qPCR confirmation of ECM1 KD see Supplementary Fig. S8H), its ability to increase endothelial network formation was significantly decreased (Supplementary Fig. S8I). This suggests that ECM1 might play a role in cancer progression through endothelial cross talk in a broader range of breast cancer subtypes than just HER2+.

ECM1 upregulates endothelial NOTCH1 and NOTCH3

To investigate whether treatment with D492HER2-CM upregulates commonly known angiogenesis modulators in ECs, we examined gene expression levels of endothelial VEGFa, VEGFR2 and PDGFb. However, none of these markers showed increased expression upon treatment with D492HER2-CM (Supplementary Fig. S7A).

In order to determine transcriptional changes occurring in ECs specifically in response to cancer-secreted ECM1, we performed RNA microarray analysis of ECs treated with CM from D492HER2 and D492HER2 with ECM1 KD. After p value correction and setting the fold change cutoff to twofold, analysis revealed 18 genes upregulated in ECs treated with D492HER2-CM compared with ECs treated with CM from D492HER2-kdECM1 (Supplementary Fig. S7 and Supplementary Table S2). However, the observed changes in genes expression were rather mild. One of the mildly higher expressed genes in ECs treated with D492HER2-CM was fatty acid-binding protein 4 (FABP4). FABP4 itself could not be confirmed as upregulated compared with untreated ECs, however it led our attention to the NOTCH pathway since its expression is regulated by NOTCH1 [51–53]. When investigating the expression of the NOTCH receptors 1–4 in ECs, we observed increased NOTCH1 and NOTCH3 gene and protein expression in ECs treated with D492HER2-CM and rECM1 but not with CM from D492HER2-kdECM1 (Fig. 5a).

Blocking endothelial NOTCH signaling interrupts the increase in network formation and feedback induction

Next, we wanted to investigate whether endothelial NOTCH signaling was implicated in the observed increase in endothelial network formation and the induction of an endothelial feedback promoting cancer cell migration and invasion. By blocking endothelial NOTCH using gamma-secretase inhibitor DAPT, interruption in both the increase in network formation and the feedback induction was observed. While treatment with rECM1 resulted in significantly increased numbers of master junctions, master segments, total master segment length, and number of meshes, this effect was no longer visible upon addition of DAPT (Fig. 5b, c). Compared with addition of rECM1 + DMSO, addition of rECM1 + DAPT significantly reduced numbers of master junctions ($p = 0.0004$), master segments ($p = 0.0014$), total master segment length ($p = 0.0019$), and number of meshes ($p = 0.0012$). Furthermore, CM of rECM1-induced ECs stimulated an increase in cancer cell migration and invasion whereas the addition of DAPT inhibited the induction of this feedback (Fig. 5d, e).

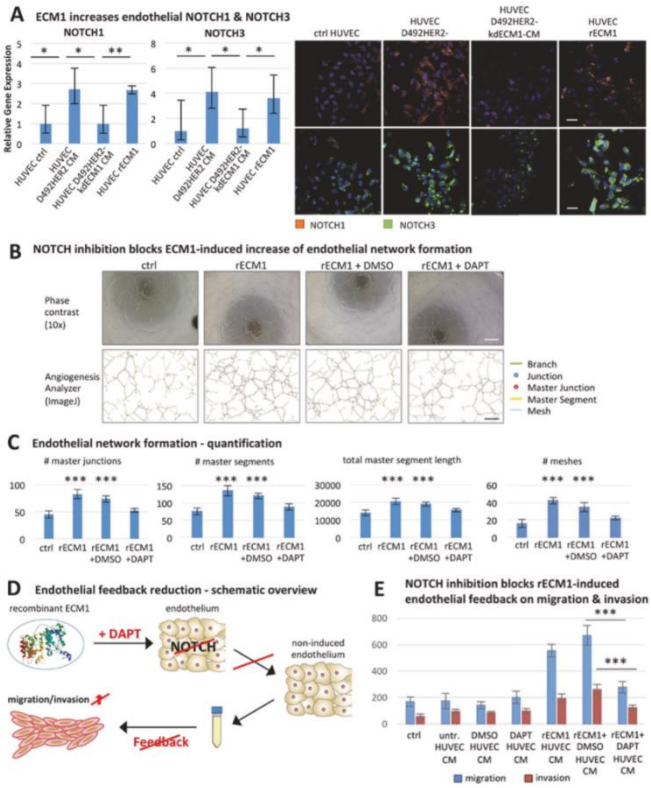

Fig. 5 Inhibition of endothelial NOTCH signaling prevents increased tube formation and feedback induction. **a** ECM1 increases endothelial NOTCH1 and NOTCH3. Increased NOTCH1 and NOTCH3 expression in HUVECs treated with D492HER2-CM and rECM1 but not D492HER2-kdECM1-CM on gene expression level (left) and protein expression level (IF staining, scale bar = 50 µm). Student's *t* test, $***p < 0.001$, $**p < 0.01$, $*p < 0.05$, <0.1. **b** NOTCH inhibition blocks ECM1-induced increase of endothelial network formation. Top: HUVEC endothelial network in H14 (ctrl), 60 ng/ml rECM1, 60 ng/ml rECM1 + DMSO and 60 ng/ml rECM1 + DAPT (20 µM) after 4 h. 4–6 wells as replicates per condition and 1–2 images taken per well at ×10 magnification (scale bar = 100 µm). Bottom: corresponding angiogenesis images (ImageJ angiogenesis analyzer). **c** Endothelial network formation—quantification. Quantification of master junctions, master segments, total master segment length, and meshes for each image using angiogenesis analyzer plugin. One-way ANOVA, $***p < 0.001$, $**p < 0.01$, $*p < 0.05$, <0.1. **d** Endothelial feedback reduction—schematic overview. Schematic workflow of treating ECs using 60 ng/ml rECM1 and blocking NOTCH signaling using DAPT (20 µM). **e** NOTCH inhibition blocks rECM1-induced endothelial feedback on migration and invasion. Transwell-migration and invasion assays of D492HER2 treated with unconditioned medium, unconditioned HUVEC-CM, DMSO-treated HUVEC-CM, DAPT-treated HUVEC-CM, 60 ng rECM1-treated HUVEC-CM, 60 ng rECM1 + DMSO-treated HUVEC-CM, and 60 ng rECM1 + DAPT-treated HUVEC-CM (NOTCH inhibition). Number of migratory/invasive cells for different treatments (Student's *t* test, $***p < 0.001$, $**p < 0.01$, $*p < 0.05$, <0.1).

Blocking endothelial NOTCH signaling therefore appears to interrupt both cancer-increased network formation as well as feedback induction. Interestingly, addition of DAPT alone to HUVEC did not affect the endothelial network (Supplementary Fig. S12) and feedback on migration and invasion (Fig. 5e). This suggests that blocking endothelial NOTCH by DAPT reduces network formation and feedback only upon elevated NOTCH signaling conditions.

Discussion

In this study, we have demonstrated that the HER2-overexpressing breast cancer cell line, D492HER2, stimulates endothelial network formation in vitro and is capable of inducing an endothelial feedback promoting cancer cell migration toward the endothelium and invasion. We have further identified ECM1 as a secreted factor in D492HER2 that plays a role in mediating both the pro-angiogenic effect of D492HER2 and the feedback induction. rECM1 increases endothelial network formation and induces the feedback while KD of ECM1 interrupts both. Furthermore, D492HER2 no longer show an increased migrative phenotype toward ECs upon ECM1 KD. However, the fact that we observed only a marginal reduction of tumor volume upon ECM1 KD indicates that it may be necessary to knockout ECM1 for in vivo studies and further to evaluate angiogenesis of the tumor-surrounding stroma. This is supported by the study of Wu and colleagues that have performed in vivo studies with ECM1 knockout rather than KD cells [54]. Interestingly, ECM1 protein expression levels were found to be similar in both ctrl and kdECM1 tumors although ECM1 KD had been confirmed by RT-qPCR prior injection into mice. Rather than suggesting no difference in tumor formation between ctrl and kdECM1 cells, these results are a possible indication that a positive selection of ECM1+ cells might have occurred in mice injected with kdECM1 cells. Therefore, our results do not necessarily stand in conflict to previously published data on ECM1 promoting tumor and metastasis formation in vivo [36–38, 54, 55]. Indeed, new studies could show that injection of equal amounts of different clones of the same breast cancer cell line MDA-MB-231 leads to formation of tumors with very few cells of one but many cells from another clone [56]. Tracing ECM1+ and ECM1− clones in vivo would offer a great approach to further investigate the occurrence of positive selection of ECM1+ clones and clarify the role of ECM1 during tumor formation.

ECM1 is a secreted glycoprotein and was first identified in the mouse osteogenic stromal cell line MN7 [47]. It was initially described as modulator of proliferation and differentiation of epidermal keratinocytes and basement membrane reconstitution in the skin [48]. However, it has also been linked to angiogenesis and malignant transformation [32–34, 37, 38, 48–50]. Han et al. demonstrated that rECM1 stimulated proliferation and blood vessel formation in the chorioallantoic membrane of chicken embryos [32] and Wang et al. found it to be expressed particularly in highly malignant breast epithelial tumors [34]. Recently, Wu et al. linked ECM1 to breast cancer progression by suggesting a role of ECM1 in facilitating metastasis through increased invasion and adhesion capacity of ECM1-expressing cancer cells [54]. These data are in line with our findings in the current study. Ferraro et al. recently showed that ECs are capable of increasing migration and invasion of SKBR3 breast cancer cells [57]. However, a direct involvement of cancer-secreted ECM1 in cancer progression through induction of an endothelial feedback supporting cancer migration and invasion has not been reported yet. Here, we show that the increased migration is directed toward the endothelium, suggesting that ECM1 may play a mediating role in inducing ECs to promote cancer cell migration from the primary tumor toward the vasculature and therefore support metastasis formation and tumor progression.

Survival analysis shows that expression of ECM1 in HER2+ breast tumors is associated with significantly reduced distant metastasis-free survival (DMFS). Therefore, targeting ECM1 in tumors overexpressing HER2 could lead to better patient prognosis. This is supported by a study of Lee et al., which showed that ECM1 regulates resistance to trastuzumab, a recombinant antibody targeting HER2 and the most common drug used in treatment of HER2+ breast cancer [49]. Interestingly, the TN breast cancer cell line MDA-MB-231 also expresses high levels of ECM1 and is capable of inducing endothelial network formation in the present study and previous studies [18, 19, 54]. KD of ECM1 in MDA-MB-231 inhibits these pro-angiogenic effects, supporting the mediating role of ECM1 in increasing the endothelial network. We also report that rECM1 is capable of inducing a positive endothelial feedback on MDA-MB-231 migration. Since expression of ECM1 also correlates with worse outcome in TN and generally ER− breast cancer, its molecular involvement in breast cancer progression might be more general rather than only limited to HER2+ cancer. Silencing of ECM1 in MDA-MB-231 led to a decrease in cancer cell migration and invasion capacity, linking its expression to increased tumor progression aggressiveness [54, 55]. Therefore, ECM1 might represent a possible therapeutic target for a broader range of breast cancer patients than just HER2+ individuals. However, the specific relationship between HER2 overexpression and ECM1 still needs to be elucidated. ECM1 expression is upregulated in several HER2+ breast cancer cell lines including ZR7530, SUM44PE, and HCC202. However, other HER2+ cell lines such as SKBR3 or BT474 show no ECM1 upregulation. However, among the breast cancer cell lines with strong ECM1 upregulation according to the GOBO database there

are numerous ER− cell lines (e.g., HCC1143, HBL100, SUM1315MO2, MDA-MB-435, and MDA-MB-231). Lee et al. report that high ECM1 expression in HER2+ breast cancer is correlated with poor prognosis and trastuzumab resistance [49]. They suggest that ECM1 may interact with EGFR family receptors that interact with HER2, attenuating therapeutic action by trastuzumab. However, the mechanisms of ECM1 expression regulation itself are not very well understood in HER2+ breast cancer. Smits et al. identified conserved potential binding sites for transcription factors of the Ap1, Ets, and Sp1 family in the human ECM1 gene in MN7 cells [58]. Ye et al. provide evidence that ECM1 is a target of miR-486-3p in cervical cancer. Overexpression of miR-486-3p thereby inhibited cell growth and metastasis by targeting ECM1 [59]. However, we could not detect differential expression of miR-486-3p between D492, D492M, and D492HER2, suggesting that ECM1 might be regulated through a different mechanism in our HER2+ breast cancer system. Generally, investigating the involvement of epigenetic regulation in modulating ECM1 expression and downstream signaling could be of great interest though as it could potentially give novel insights also in the context of cellular cross talk.

In our model, ECM1 was identified as cancer-secreted protein with pro-angiogenic properties that is capable of inducing an endothelial feedback promoting cancer cell migration toward ECs and invasion (Fig. 6). However, the molecular mechanism through which ECM1 mediates this feedback of the vascular niche on cancer progression has not been described previously. Here, we identified an upregulation of NOTCH1 and NOTCH3 receptor expression in ECs upon treatment with D492HER2-CM and rECM1 but not CM from D492HER2 with ECM1 KD. However, the initial microarray candidate, FABP4, could not be confirmed in further experiments, indicating that the subsequent downstream signaling may not involve FABP4. This would coincide with the findings that in addition to NOTCH1, also VEGFa, bFGF, and FOXO1 play potential roles in regulation of FABP4 expression [60]. So far, ECM1 has been associated with EGF signaling [49], and ITGB4/FAK/SOX2/HIF1a [36] and WNT1/ß-catenin [37] pathways, but a mediating role in NOTCH signaling has not been described. NOTCH signaling is very complex and plays a role in a large number of biological processes [61, 62]. Nevertheless, recent studies suggest NOTCH1 as a key player in inducing tumor angiogenesis and therefore promoting tumor progression in cutaneous melanoma and myeloma [25, 26]. Kalucka et al. have shown that NOTCH1 is involved in endothelial barrier function and angiogenesis by controlling fatty acid metabolism [53]. These data would support a possible involvement of endothelial NOTCH in mediating the increase in endothelial network and possibly the induction of the pro-cancerous feedback in breast cancer. Indeed, upon inhibition of endothelial NOTCH signaling, the enhancing effect of ECM1 on network formation and feedback was no longer observed, indicating the existence of a ECM1/NOTCH axis involved in mediating the cross talk between cancer cells and endothelium in terms of promoting cancer progression (Fig. 6).

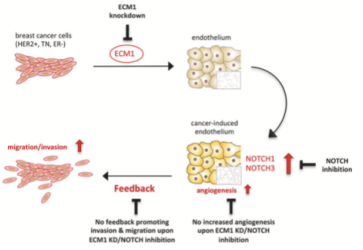

Fig. 6 Schematic summary of ECM1 inducing an endothelial feedback promoting cancer cell migration/invasion. ECM1 secreted by HER2+, TN, or ER− breast cancer cells increases endothelial network formation and induces endothelial feedback promoting cancer cell migration and invasion through upregulation of NOTCH1 and NOTCH3 expression. Knockdown of ECM1 in cancer cells and NOTCH inhibition in ECs inhibits the network formation increase and the feedback induction.

In conclusion, we have identified ECM1 as a cancer-secreted pro-angiogenic factor involved in inducing the endothelial niche to support cancer progression through increased cancer cell migration and invasion. Moreover, our data indicate a novel, mediating role of ECM1 in endothelial NOTCH signaling, which appears to be involved in mediating the induction of the cancer-promoting endothelial feedback (Fig. 6). Taken together, our findings might open up new possibilities for cancer treatment by understanding how an activated vascular niche provides positive feedback to the cancer and targeting this interaction between cancer cells and their microenvironment.

Acknowledgements We thank the FingerPrints Proteomics Facility at the University of Dundee for performing the mass spectrometry and the Center for Systems Biology at the University of Iceland for the technical support during mass spectrometry data analysis. Further, we want to thank the HI-STEM laboratory and the sequencing core facility at the German Cancer Research Center, DKFZ Heidelberg, Germany, for technical support and performing the RNA microarray. Finally, we thank Prof. Dr Haraldur Haraldsson, University of Iceland for providing primary human umbilical vascular ECs. Human umbilical vascular ECs were obtained from umbilical chords at the childbirth department, University Hospital Iceland (ethical application nr. 35/2013). This work was supported by Grants from Landspitali University Hospital Science Fund, University of Iceland Research Fund (Grant of Excellence: #152144051 Doctoral Grant: #185042051), and Icelandic Science and Technology Policy.

Compliance with ethical standards

Conflict of interest The authors declare that they have no conflict of interest. The funding body had no role in the design of the study and collection, analysis, and interpretation of data and in writing the manuscript.

Publisher's note Springer Nature remains neutral with regard to jurisdictional claims in published maps and institutional affiliations.

References

1. Hassiotou F, Geddes D. Anatomy of the human mammary gland: current status of knowledge. Clinical Anat. 2013;26:29–48.
2. Sigurdsson V, Fridriksdottir AJ, Kjartansson J, Jonasson JG, Steinarsdottir M, Petersen OW, et al. Human breast microvascular endothelial cells retain phenotypic traits in long-term finite life span culture. In Vitro Cell Dev Biol Anim. 2006;42:332–40.
3. Ingthorsson S, Sigurdsson V, Fridriksdottir A Jr., Jonasson JG, Kjartansson J, Magnusson MK, et al. Endothelial cells stimulate growth of normal and cancerous breast epithelial cells in 3D culture. BMC Res Notes. 2010;3:184.
4. Gudjonsson T, Ronnov-Jessen L, Villadsen R, Bissell MJ, Petersen OW. To create the correct microenvironment: three-dimensional heterotypic collagen assays for human breast epithelial morphogenesis and neoplasia. Methods. 2003;30:247–55.
5. Bergthorsson JT, Magnusson MK, Gudjonsson T. Endothelial-rich microenvironment supports growth and branching morphogenesis of prostate epithelial cells. Prostate. 2013;73:884–96.
6. Bissell MJ, Hall HG, Parry G. How does the extracellular matrix direct gene expression? J Theor Biol. 1982;99:31–68.
7. Ghajar CM, Peinado H, Mori H, Matei IR, Evason KJ, Brazier H, et al. The perivascular niche regulates breast tumour dormancy. Nat Cell Biol. 2013;15:807–17.
8. Erler JT, Weaver VM. Three-dimensional context regulation of metastasis. Clin Exp Metastasis. 2009;26:35–49.
9. Hoye AM, Erler JT. Structural ECM components in the pre-metastatic and metastatic niche. Am J Physiol Cell Physiol. 2016;310:C955–67.
10. Hanahan D, Coussens LM. Accessories to the crime: functions of cells recruited to the tumor microenvironment. Cancer Cell. 2012;21:309–22.
11. Oskarsson T, Batlle E, Massague J. Metastatic stem cells: sources, niches, and vital pathways. Cell Stem Cell. 2014;14:306–21.
12. Pollard JW. Macrophages define the invasive microenvironment in breast cancer. J Leukoc Biol. 2008;84:623–30.
13. Komohara Y, Jinushi M, Takeya M. Clinical significance of macrophage heterogeneity in human malignant tumors. Cancer Sci. 2014;105:1–8.
14. Komohara Y, Takeya M. CAFs and TAMs: maestros of the tumour microenvironment. J Pathol. 2017;241:313–5.
15. Shan T, Chen S, Chen X, Lin WR, Li W, Ma J, et al. Cancer-associated fibroblasts enhance pancreatic cancer cell invasion by remodeling the metabolic conversion mechanism. Oncol Rep. 2017;37:1971–9.
16. Zhang Z, Li X, Sun W, Yue S, Yang J, Li J, et al. Loss of exosomal miR-320a from cancer-associated fibroblasts contributes to HCC proliferation and metastasis. Cancer Lett. 2017;397:33–42.
17. Ghajar CM. Metastasis prevention by targeting the dormant niche. Nat Rev Cancer. 2015;15:238–47.
18. Lee E, Fertig EJ, Jin K, Sukumar S, Pandey NB, Popel AS. Breast cancer cells condition lymphatic endothelial cells within pre-metastatic niches to promote metastasis. Nat Commun. 2014;5:4715.
19. Lee E, Pandey NB, Popel AS. Crosstalk between cancer cells and blood endothelial and lymphatic endothelial cells in tumour and organ microenvironment. Expert Rev Mol Med. 2015;17:e3.
20. Lee E, Pandey NB, Popel AS. Lymphatic endothelial cells support tumor growth in breast cancer. Sci Rep. 2014;4:5853.
21. Franses JW, Baker AB, Chitalia VC, Edelman ER. Stromal endothelial cells directly influence cancer progression. Sci Transl Med. 2011;3:66ra5.
22. Franses JW, Drosu NC, Gibson WJ, Chitalia VC, Edelman ER. Dysfunctional endothelial cells directly stimulate cancer inflammation and metastasis. Int J Cancer. 2013;133:1334–44.
23. Ucuzian AA, Gassman AA, East AT, Greisler HP. Molecular mediators of angiogenesis. J Burn Care Res. 2010;31:158–75.
24. Laughner E, Taghavi P, Chiles K, Mahon PC, Semenza GL. HER2 (neu) signaling increases the rate of hypoxia-inducible factor 1alpha (HIF-1alpha) synthesis: novel mechanism for HIF-1-mediated vascular endothelial growth factor expression. Mol Cell Biol. 2001;21:3995–4004.
25. Murtas D, Piras F, Minerba L, Maxia C, Ferreli C, Demurtas P, et al. Activated Notch1 expression is associated with angiogenesis in cutaneous melanoma. Clin Exp Med. 2015;15:351–60.
26. Guo D, Li C, Teng Q, Sun Z, Li Y, Zhang C. Notch1 over-expression promotes cell growth and tumor angiogenesis in myeloma. Neoplasma. 2013;60:33–40.
27. Sigurdsson V, Hilmarsdottir B, Sigmundsdottir H, Fridriksdottir AJ, Ringner M, Villadsen R, et al. Endothelial induced EMT in breast epithelial cells with stem cell properties. PLoS ONE. 2011;6:e23833.
28. Gudjonsson T, Villadsen R, Nielsen HL, Ronnov-Jessen L, Bissell MJ, Petersen OW. Isolation, immortalization, and characterization of a human breast epithelial cell line with stem cell properties. Genes Dev. 2002;16:693–706.
29. Villadsen R, Fridriksdottir AJ, Ronnov-Jessen L, Gudjonsson T, Rank F, LaBarge MA, et al. Evidence for a stem cell hierarchy in the adult human breast. J Cell Biol. 2007;177:87–101.
30. Briem E, Ingthorsson S, Traustadottir GA, Hilmarsdottir B, Gudjonsson T. Application of the D492 cell lines to explore breast morphogenesis, EMT and cancer progression in 3D culture. J Mammary Gland Biol Neoplasia. 2019;24:139–47.
31. Ingthorsson S, Andersen K, Hilmarsdottir B, Maelandsmo GM, Magnusson MK, Gudjonsson T. HER2 induced EMT and tumorigenicity in breast epithelial progenitor cells is inhibited by coexpression of EGFR. Oncogene. 2015;35:4244–55.
32. Han Z, Ni J, Smits P, Underhill CB, Xie B, Chen Y, et al. Extracellular matrix protein 1 (ECM1) has angiogenic properties and is expressed by breast tumor cells. FASEB J. 2001;15:988–94.
33. Sercu S, Zhang L, Merregaert J. The extracellular matrix protein 1: its molecular interaction and implication in tumor progression. Cancer Invest. 2008;26:375–84.
34. Wang L, Yu J, Ni J, Xu X-M, Wang J, Ning H, et al. Extracellular matrix protein 1 (ECM1) is over-expressed in malignant epithelial tumors. Cancer Lett. 2003;200:57–67.
35. Chen H, Jia W, Li J. ECM1 promotes migration and invasion of hepatocellular carcinoma by inducing epithelial-mesenchymal transition. World J Surg Oncol. 2016;14:195.
36. Gan L, Meng J, Xu M, Liu M, Qi Y, Tan C, et al. Extracellular matrix protein 1 promotes cell metastasis and glucose metabolism by inducing integrin beta4/FAK/SOX2/HIF-1alpha signaling pathway in gastric cancer. Oncogene. 2017;37:744–55.
37. Lee KM, Nam K, Oh S, Lim J, Kim RK, Shim D, et al. ECM1 regulates tumor metastasis and CSC-like property through stabilization of beta-catenin. Oncogene. 2015;34:6055–65.
38. Wang Z, Zhou Q, Li A, Huang W, Cai Z, Chen W. Extracellular matrix protein 1 (ECM1) is associated with carcinogenesis

potential of human bladder cancer. Onco Targets Ther. 2019; 12:1423–32.
39. Bustin SA, Benes V, Garson JA, Hellemans J, Huggett J, Kubista M, et al. The MIQE guidelines: minimum information for publication of quantitative real-time PCR experiments. Clin Chem. 2009;55:611–22.
40. Guillen J. FELASA guidelines and recommendations. J Am Assoc Lab Anim Sci. 2012;51:311–21.
41. Rosenblat JD, Brietzke E, Mansur RB, Maruschak NA, Lee Y, McIntyre RS. Inflammation as a neurobiological substrate of cognitive impairment in bipolar disorder: evidence, pathophysiology and treatment implications. J Affect Disord. 2015;188:149–59.
42. Kastrup J. Can YKL-40 be a new inflammatory biomarker in cardiovascular disease? Immunobiology. 2012;217:483–91.
43. Vignon E. Is glycoprotein YKL40 a new marker for joint disorders? Joint Bone Spine. 2001;68:454–6.
44. Zhou Y, Peng H, Sun H, Peng X, Tang C, Gan Y, et al. Chitinase 3-like 1 suppresses injury and promotes fibroproliferative responses in Mammalian lung fibrosis. Sci Transl Med. 2014;6:240ra76.
45. Francescone RA, Scully S, Faibish M, Taylor SL, Oh D, Moral L, et al. Role of YKL-40 in the angiogenesis, radioresistance, and progression of glioblastoma. J Biol Chem. 2011;286:15332–43.
46. Shao R. YKL-40 acts as an angiogenic factor to promote tumor angiogenesis. Front Physiol. 2013;4:122.
47. Mathieu E, Meheus L, Raymackers J, Merregaert J. Characterization of the osteogenic stromal cell line MN7: identification of secreted MN7 proteins using two-dimensional i'olyacrylamide gel electrophoresis, western blotting, and microsequencing. J Bone Miner Res. 1994;9:903–13.
48. Oyama N, Merregaert J. The extracellular matrix protein 1 (ECM1) in molecular-based skin biology. In: Farage M., Miller K., Maibach H. (eds) Textbook of Aging Skin. Springer, Berlin, Heidelberg. 2017. p. 91–110.
49. Lee KM, Nam K, Oh S, Lim J, Kim YP, Lee JW, et al. Extracellular matrix protein 1 regulates cell proliferation and trastuzumab resistance through activation of epidermal growth factor signaling. Breast Cancer Res. 2014;16:479.
50. Sercu S, Zhang M, Oyama N, Hansen U, Ghalbzouri AE, Jun G, et al. Interaction of extracellular matrix protein 1 with extracellular matrix components: ECM1 is a basement membrane protein of the skin. J Invest Dermatol. 2008;128:1397–408.
51. Harjes U, Bridges E, Gharpure KM, Roxanis I, Sheldon H, Miranda F, et al. Antiangiogenic and tumour inhibitory effects of downregulating tumour endothelial FABP4. Oncogene. 2017;36:912–21.
52. Bruning U, Morales-Rodriguez F, Kalucka J, Goveia J, Taverna F, Queiroz KCS, et al. Impairment of angiogenesis by fatty acid synthase inhibition involves mTOR malonylation. Cell Metab. 2018;28:866.e15–80.e15.
53. Kalucka J, Bierhansl L, Conchinha NV, Missiaen R, Elia I, Bruning U, et al. Quiescent endothelial cells upregulate fatty acid beta-oxidation for vasculoprotection via redox homeostasis. Cell Metab. 2018;28:881.e13–94.e13.
54. Wu Q, Chen D, Luo Q, Yang Q, Zhao C, Zhang D, et al. Extracellular matrix protein 1 recruits moesin to facilitate invadopodia formation and breast cancer metastasis. Cancer Lett. 2018;437:44–55.
55. Gomez-Contreras P, Ramiro-Diaz JM, Sierra A, Stipp C, Domann FE, Weigel RJ, et al. Extracellular matrix 1 (ECM1) regulates the actin cytoskeletal architecture of aggressive breast cancer cells in part via S100A4 and Rho-family GTPases. Clin Exp Metastasis. 2017;34:37–49.
56. Martin-Pardillos A, Valls Chiva A, Bande Vargas G, Hurtado Blanco P, Pineiro Cid R, Guijarro PJ, et al. The role of clonal communication and heterogeneity in breast cancer. BMC Cancer. 2019;19:666.
57. Ferraro DA, Patella F, Zanivan S, Donato C, Aceto N, Giannotta M, et al. Endothelial cell-derived nidogen-1 inhibits migration of SK-BR-3 breast cancer cells. BMC Cancer. 2019;19:312.
58. Smits P, Bhalerao J, Merregaert J. Molecular cloning and characterization of the mouse Ecm1 gene and its 5' regulatory sequences. Gene. 1999;226:253–61.
59. Ye H, Yu X, Xia J, Tang X, Tang L, Chen F. MiR-486-3p targeting ECM1 represses cell proliferation and metastasis in cervical cancer. Biomed Pharmacother. 2016;80:109–14.
60. Furuhashi M, Saitoh S, Shimamoto K, Miura T. Fatty acid-binding protein 4 (FABP4): pathophysiological insights and potent clinical biomarker of metabolic and cardiovascular diseases. Clin Med Insights Cardiol. 2014;8(Suppl 3):23–33.
61. Traustadottir GA, Jensen CH, Thomassen M, Beck HC, Mortensen SB, Laborda J, et al. Evidence of non-canonical NOTCH signaling: delta-like 1 homolog (DLK1) directly interacts with the NOTCH1 receptor in mammals. Cell Signal. 2016;28: 246–54.
62. Artavanis-Tsakonas S, Rand MD, Lake RJ. Notch signaling: cell fate control and signal integration in development. Science. 1999;284:770–6.

Affiliations

Sophie Sarah Steinhaeuser[1] · Erika Morera[1] · Zuzana Budkova[1] · Alexander Schepsky[1] · Qiong Wang[2] · Ottar Rolfsson[2] · Angela Riedel[3,4] · Aileen Krueger[3,4] · Bylgja Hilmarsdottir[5] · Gunhild Mari Maelandsmo[5] · Bryndis Valdimarsdottir[1] · Anna Karen Sigurdardottir[1] · Bjarni Agnar Agnarsson[6,7] · Jon Gunnlaugur Jonasson[6,7] · Saevar Ingthorsson[1] · Gunnhildur Asta Traustadottir[1] · Thordur Oskarsson[3,4,8] · Thorarinn Gudjonsson[1,2,9]

[1] Department of Anatomy, Stem Cell Research Unit, Biomedical Center, Faculty of Medicine, School of Health Sciences, University of Iceland, Reykjavik, Iceland

[2] Center for Systems Biology, University of Iceland, Reykjavik, Iceland

[3] Heidelberg Institute for Stem Cell Technology and Experimental Medicine (HI-STEM gGmbH), 69120 Heidelberg, Germany

[4] Division of Stem Cells and Cancer, German Cancer Research Center (DKFZ), 69120 Heidelberg, Germany

[5] Department of Tumor Biology, Institute for Cancer Research, Oslo University Hospital, The Norwegian Radium Hospital, Oslo, Norway

[6] Department of Pathology, Landspitali—University Hospital, Reykjavik, Iceland

[7] Faculty of Medicine, University of Iceland, Reykjavik, Iceland

[8] German Cancer Consortium (DKTK), 69120 Heidelberg, Germany

[9] Department of Laboratory Hematology, Landspitali—University Hospital, Reykjavik, Iceland

Supplementary material

Fig. S1: CM of D492HER2 enhances endothelial network - 24 h and 48 h.

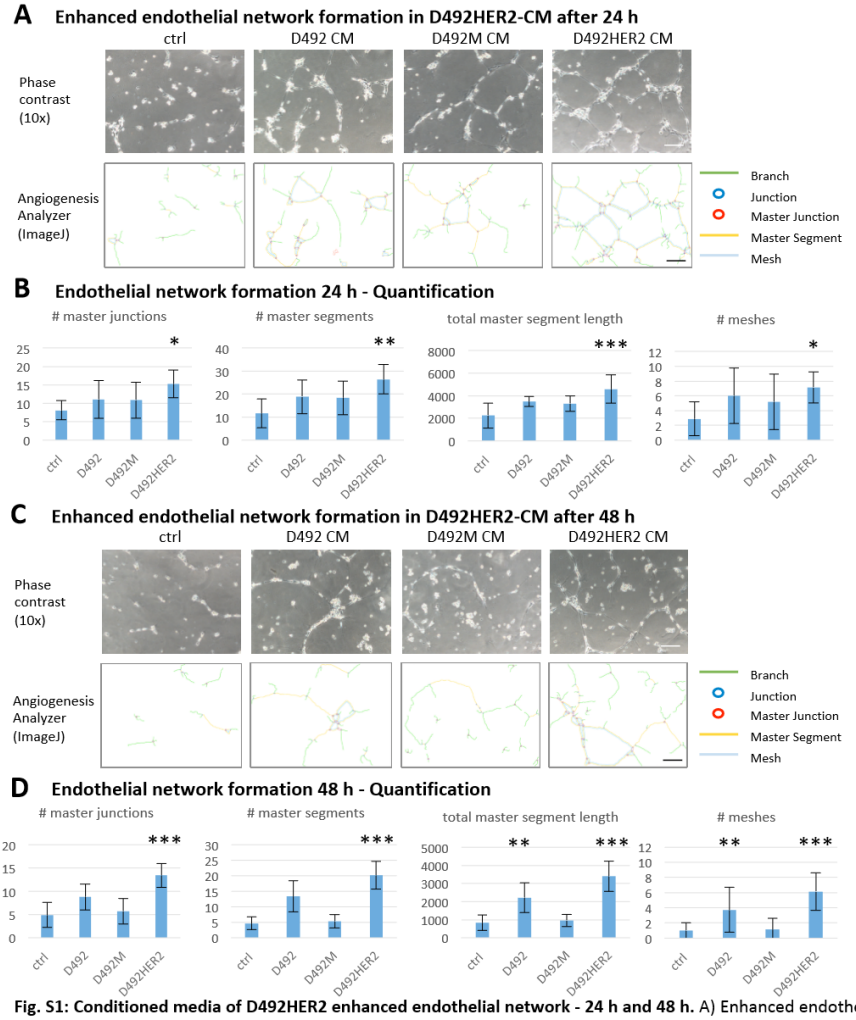

Fig. S1: Conditioned media of D492HER2 enhanced endothelial network - 24 h and 48 h. A) Enhanced endothelial network formation in D492HER2-CM after 24 h. Top: Phase-contrast images of HUVEC endothelial network after 24 h on top of matrigel in H14, D492-CM, D492M-CM and D492HER2-CM, 10x magnification (scale bar = 100 µm). Bottom: Corresponding angiogenesis images (ImageJ, angiogenesis analyzer) showing branches, junctions, master junctions, master segments and meshes. B) Endothelial network formation 24 h - Quantification. Quantification of master junctions, master segments, total master segment length and meshes (angiogenesis analyzer). Statistical analysis performed in R, one-way ANOVA, *** $p < 0.001$, ** $p < 0.01$, * $p < 0.05$, · < 0.1 . C) Enhanced endothelial network formation in D492HER2-CM after 48 h. Top: HUVEC endothelial network after 48 h (phase contrast). Bottom: Angiogenesis images. D) Endothelial network formation 48 h - Quantification. Quantification of master junctions, master segments total master segment length and meshes. One-way ANOVA, *** $p < 0.001$, ** $p < 0.01$, * $p < 0.05$, · < 0.1 .

Fig. S2: D492HER2 has increased affinity to ECs in 2D & 3D.

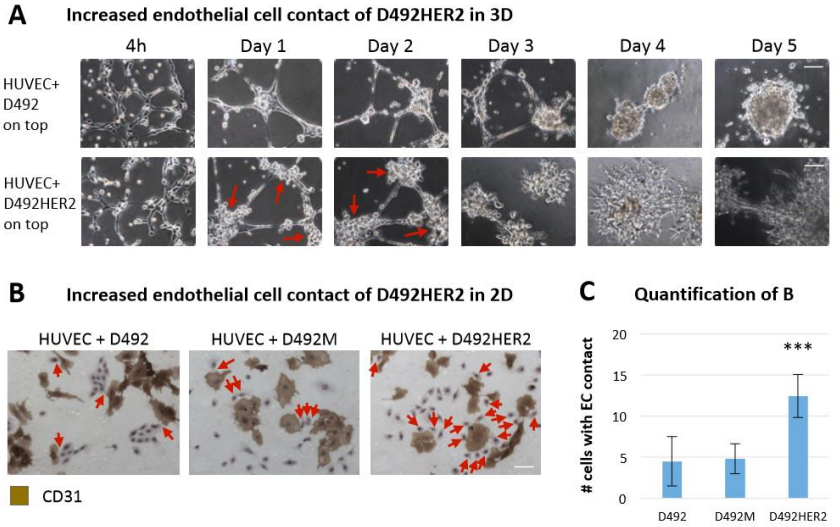

Fig. S2: D492HER2 has increased affinity to ECs in 2D and 3D. A) Increased endothelial cell contact of D492HER2 in 3D. 3D co-culture of D492 and D492HER2 with HUVEC on top of matrigel. Red arrows mark cells attached to branching points fo the endothelial network. Scale bar = 100 µm. B) Increased endothelial cell contact of D492HER2 in 2D. 2D co-culture of D492, D492M and D492HER2 with HUVEC (brown: DAB staining for CD31) for 24h. Red arrows mark cells attached to brown endothelial cells. Scale bar = 50 µm. C) Quantification of B. Mean number of cells attached to HUVEC. Statistical analyses for C) performed in R, one-way ANOVAs, *** $p < 0.001$, ** $p < 0.01$, * $p < 0.05$, · < 0.1 .

Fig. S3: Decreased DMFS when ECM1 but not CHI3L1 is expressed in HER2+ tumors (breastmark).

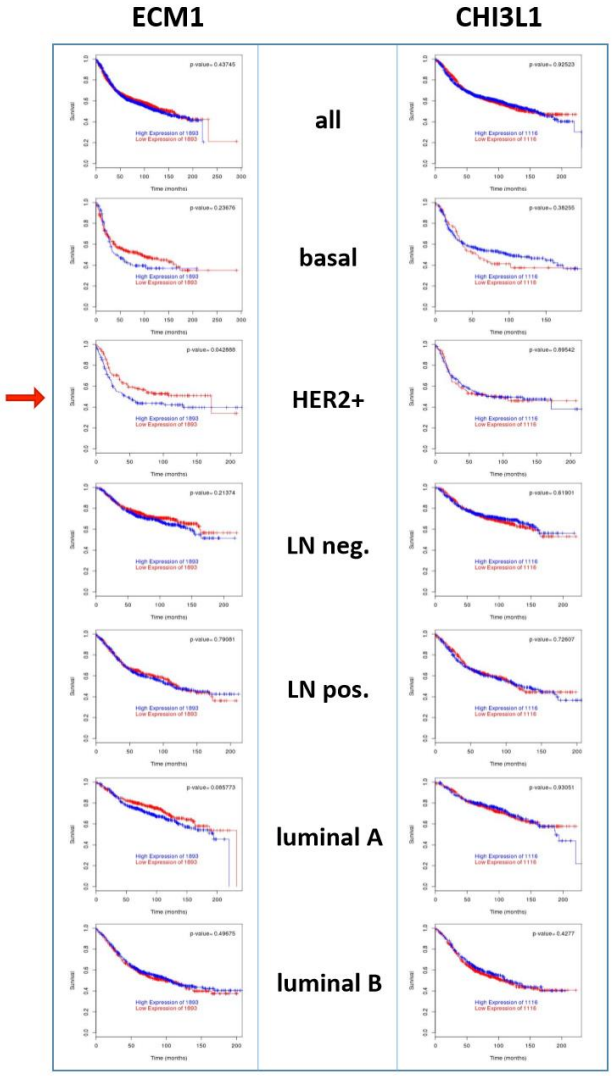

Fig. S3: Decreased DMFS when ECM1 but not CHI3L1 is expressed in HER2+ tumors (breastmark). Analysis of distant metastasis-free survival (DMFS) for ECM1 and CHI3L1 expression in different breast cancer subtypes (database breastmark).

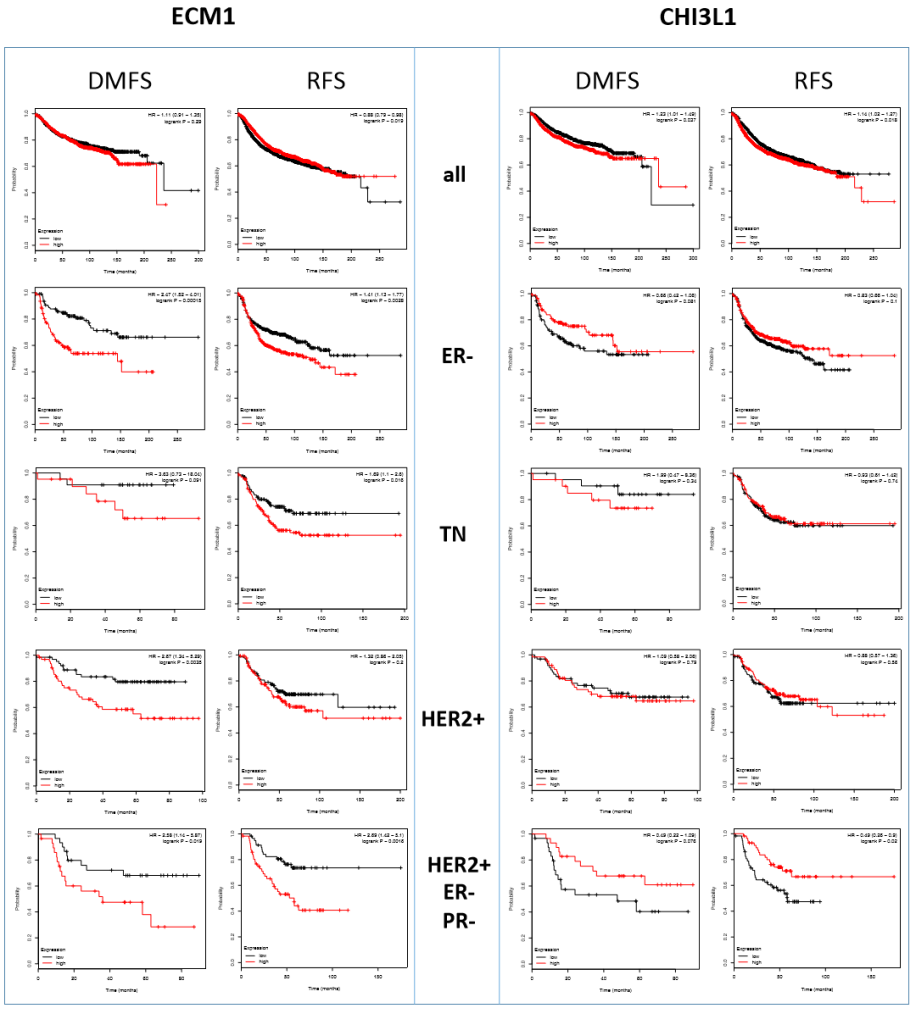

Fig. Fig. S4: Differential survival pattern for ECM1 and CHI3L1 in HER2+ and ER- tumors (KM plotter). Comparison of distant metastasis-free survival (DMFS) and relapse-free survival (RFS) for ECM1 and CHI3L1 between ER-, triple-negative (TN), HER2+ and HER2+ ER- PR- samples.

Fig. S5: Transient knockdown of ECM1 inhibits pro-angiogenic effect of D492HER2-CM.

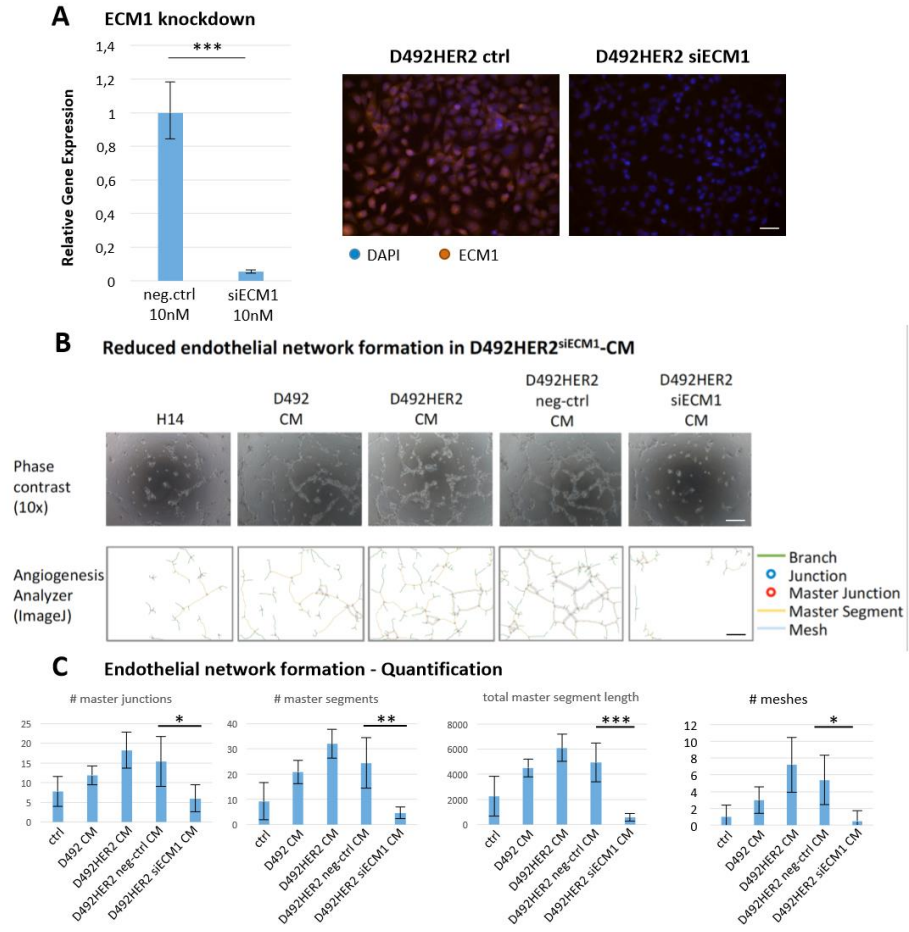

Fig. S5: Transient knockdown of ECM1 inhibits pro-angiogenic effect of D492HER2-CM. A) ECM1 knockdown. Confirmation of transient ECM1 knockdown at gene expression level (Relative Gene Expression) and protein expression level (IF staining), scale bar = 50 µm. siRNA used at a concentration of 10 nM (Student´s t-Test *** $p < 0.001$, ** $p < 0.01$, * $p < 0.05$, · < 0.1). B) Reduced endothelial network formation in D492HER2siECM1-CM. Top: HUVEC endothelial network after 4 h in H14, D492-CM, ctrl D492HER2-CM, siRNA neg. ctrl D492HER2-CM and siECM1 D492HER2-CM (phase contrast), 10x magnification (scale bar = 100 µm). Bottom: Angiogenesis images showing branches, junctions, master junctions, master segments and meshes. C) Endothelial network formation - Quantification. Quantification of master junctions, master segments total master segment length and meshes. One-way ANOVA, *** $p < 0.001$, ** $p < 0.01$, * $p < 0.05$, · < 0.1 .

Fig. S6: Increased migration of D492 and D492M overexpressing ECM1 towards ECs.

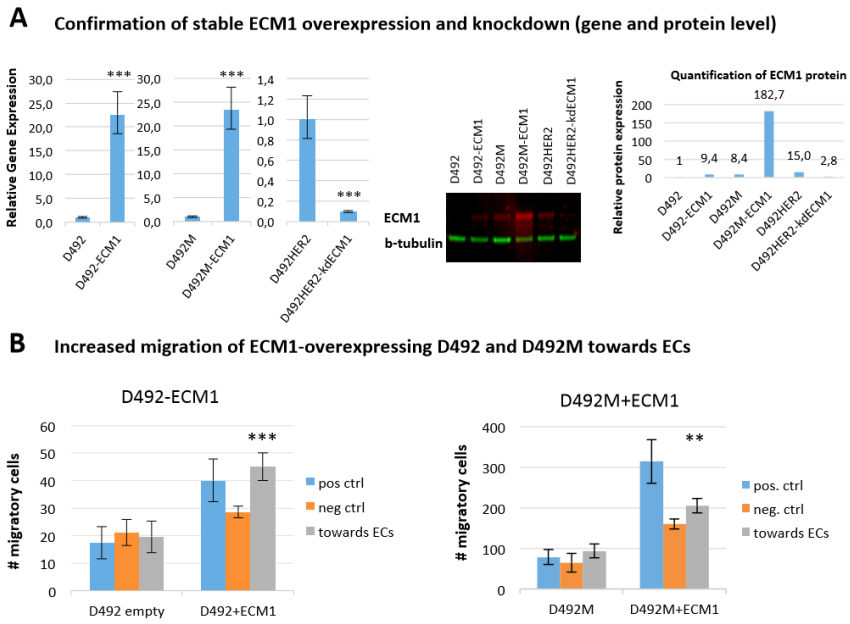

Fig. S6: Increased migration of D492 and D492M overexpressing ECM1 towards ECs. A) Confirmation of stable ECM1 overexpression and knockdown (gene and protein level). Confirmation in stable knockdown cell lines (D492+ECM1, D492M+ECM1, D492HER2-kdECM1). Left: gene expression level (relative expression), right: protein expression (western blot) and quantification. B) Increased migration of ECM1-overexpressing D492 and D492M towards ECs. Transwell-migration assay of D492 empty vector ctrl and D492HER2 with ECM1 overexpression as well as D492M empty and D492M overexpressing ECM1 towards HUVECs (80% confluent) seeded below the transwell filter. Migration towards HUVECs (in H14 + EGM1) was compared with migration towards 10% FBS in H14 + EGM5 (pos. ctrl) and plane H14 + EGM5 (neg. ctrl). Student´s t-Test (R), *** $p < 0.001$, ** $p < 0.01$, * $p < 0.05$, · < 0.1 .

Fig. S7: Mildly increased gene expression of candidates in ECs upon treatment with D492HER2-CM compared to CM from D492HER2 with ECM1 KD

A No upregulation of VEGFa, VEGFR2 or PDGFb in HUVECs treated with D492HER2-CM

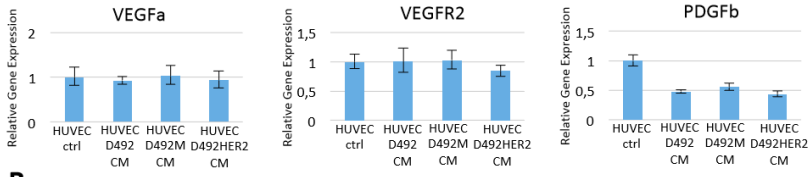

B Top 10 up- and downregulated genes in HUVECs treated with D492HER2/D492HER2-kdECM1 CM

chip.microarray 001.cel	Gene Symbol	Description	D492HER 2 CM	D492HER2-kdECM1 CM	p-value adjusted	log2 FC	FC
100287728_at	LOC100287728	uncharacterized LOC100287728	↑	↓	0	-1,06	0,48
2167_at	FABP4	fatty acid binding protein 4, adipocyte	↑	↓	5,00E-06	-0,85	0,56
84948_at	TIGD5	tigger transposable element derived 5	↑	↓	0,000565	-0,71	0,61
116441_at	TM4SF18	transmembrane 4 L six family member 18	↑	↓	0,009003	-0,61	0,65
25780_at	RASGRP3	RAS guanyl releasing protein 3 (calcium and DAG-regulated)	↑	↓	0,018059	-0,58	0,67
135924_at	OR9A2	olfactory receptor, family 9, subfamily A, member 2	↑	↓	0,018059	-0,58	0,67
8995_at	TNFSF18	tumor necrosis factor (ligand) superfamily, member 18	↑	↓	0,019042	-0,58	0,67
56911_at	MAP3K7CL	MAP3K7 C-terminal like	↑	↓	0,02629	-0,56	0,68
284349_at	ZNF283	zinc finger protein 283	↑	↓	0,029553	-0,56	0,68
359787_at	DPPA3	developmental pluripotency associated 3	↑	↓	0,030925	-0,55	0,68
597_at	BCL2A1	BCL2-related protein A1	↓	↑	0,015665	0,59	1,51
51351_at	ZNF117	zinc finger protein 117	↓	↑	0,015046	0,59	1,51
3078_at	CFHR1	complement factor H-related 1	↓	↑	0,011634	0,60	1,52
6407_at	SEMG2	semenogelin II	↓	↑	0,009003	0,61	1,53
414189_at	AGAP6	ArfGAP with GTPase domain, ankyrin repeat and PH domain 6	↓	↑	0,008609	0,62	1,54
256586_at	LYSMD2	LysM, putative peptidoglycan-binding, domain containing 2	↓	↑	0,007606	0,63	1,54
345778_at	MTX3	metaxin 3	↓	↑	0,002965	0,66	1,58
56999_at	ADAMTS9	ADAM metallopeptidase with thrombospondin type 1 motif, 9	↓	↑	0,000989	0,69	1,61
79324_at	OR51G1	olfactory receptor, family 51, subfamily G, member 1 (gene/pseudogene)	↓	↑	0,00061	0,71	1,63
5473_at	PPBP	pro-platelet basic protein (chemokine (C-X-C motif) ligand 7)	↓	↑	0,000565	0,72	1,64

C Validation of candidates from B with RT-qPCR

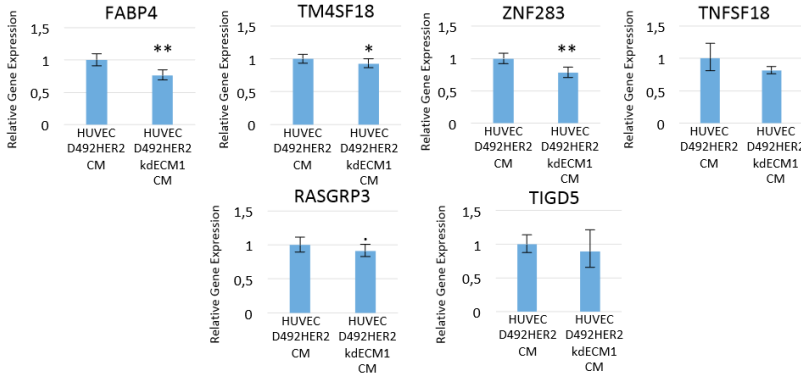

Fig. S7: Mildly increased gene expression of candidates in ECs upon treatment with D492HER2-CM compared to CM from D492HER2 with ECM1 KD. A) No upregulation of VEGFa, VEGFR2 or PDGFb in HUVECs treated with D492HER2-CM. RT-qPCR testing of common endothelial angiogenesis-regulating genes in response to CM treatment. B) Top 10 up- and downregulated genes in HUVECs treated with CM from D492HER2 vs. CM from D492HER2-kdECM1. Affymetrix human Clariom S microarray, 2-fold change threshold, p-value adjusted. C) RT-qPCR validation of candidates from A. Student´s t-Test (R), *** $p < 0.001$, ** $p < 0.01$, * $p < 0.05$, · < 0.1 .

Fig. S8: CM from MDA-MB-231 enhances endothelial network & induces endothelial feedback increasing MDA-MB-231 migration.

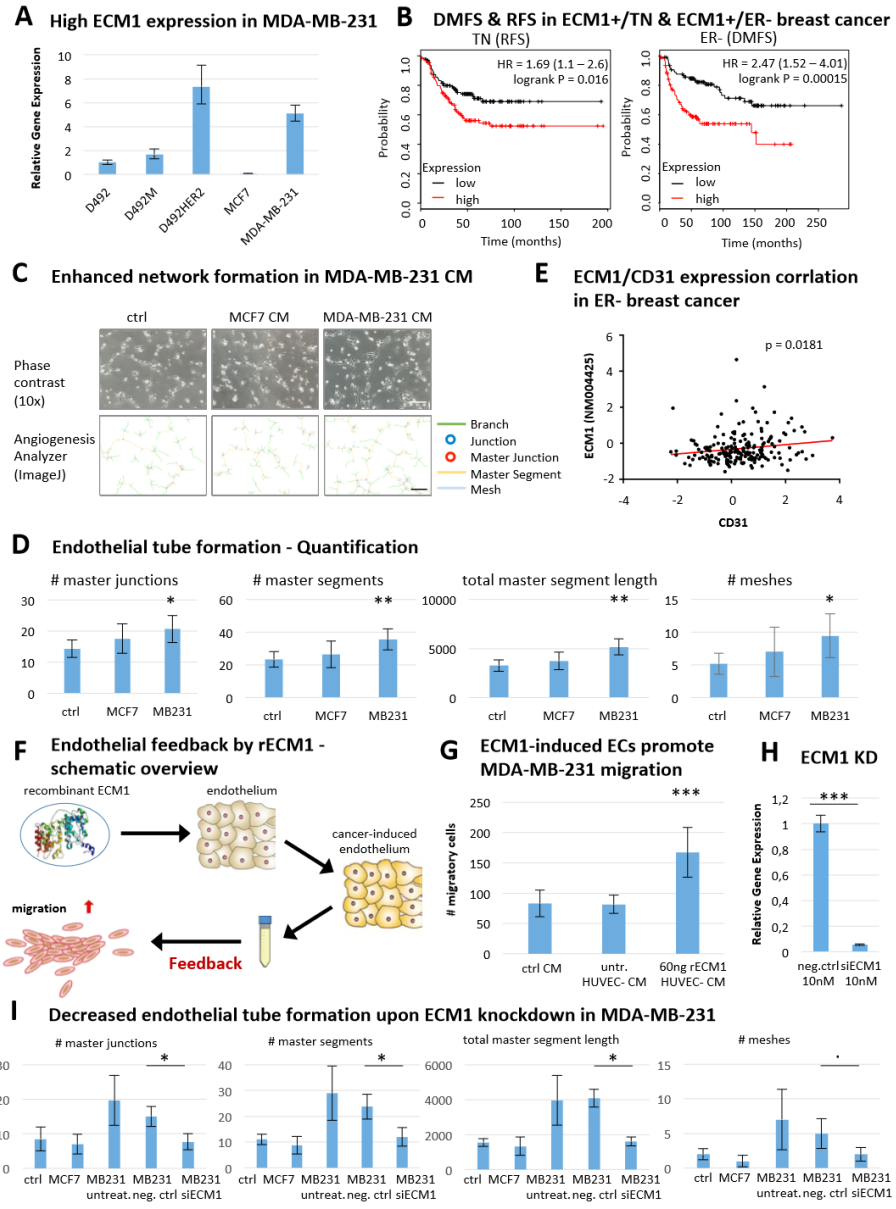

Fig. S8: CM from MDA-MB-231 enhances endothelial network and induces endothelial feedback increasing MDA-MB-231 migration. A) High ECM1 expression in MDA-MB-231. Relative Gene expression of ECM1 in MDA-MB-231 and MCF7 compared to D492, D492M and D492HER2. B) DMFS & RFS in ECM1+/TN & ECM1+/ER- breast cancer. ECM1 expression correlates with worse relapse-free survival (RFS) in triple-negative (TN) breast cancer patients and with worse distant metastasis-free survival (DMFS) in ER- breast cancer patients. C) Enhanced endothelial tube formation in MDA-MB-231 CM. Top: HUVEC endothelial network after 4h in R10F, MCF7-CM and MDA-MB-231-CM (phase contrast). 10x magnification, scale bar = 100 µm. Bottom: Angiogenesis images. D) Endothelial tube formation - Quantification. Quantification of master junctions, master segments total master segment length and meshes. One-way ANOVA, *** $p < 0.001$, ** $p < 0.01$, * $p < 0.05$, · < 0.1 . E) ECM1/CD31 expression correlation in ER- breast cancer. Correlation analysis of ECM1 and CD31 gene expression using Metabric discovery data set showing significant positive correlation (p = 0.0181) in ER- breast cancer. F) Endothelial feedback by rECM1 - schematic overview. Schematic work flow of conditioning of ECs using 60 ng/ml rECM1. G) ECM1-induced ECs promote MDA-MB-231 migration. Transwell-migration assay of MDA-MB-231 treated with unconditioned medium (R10F), unconditioned HUVEC-CM and 60 ng rECM1-treated HUVEC-CM. Number of migratory cells is shown for the different treatments. Student´s t-Test (R), *** $p < 0.001$, ** $p < 0.01$, * $p < 0.05$, · < 0.1 . H) ECM1 KD. Confirmation of ECM1 knockdown on gene expression level (RT-qPCR). Student´s t-Test (R), *** $p < 0.001$, ** $p < 0.01$, * $p < 0.05$, · < 0.1 . I) Decreased endothelial tube formation upon ECM1 knockdown in MDA-MB-231. Quantification HUVEC endothelial network after 4 h in ctrl media (R10F), MCF7-CM, ctrl MDA-MB-231-CM, siRNA neg. ctrl MDA-MB-231-CM and siECM1 MDA-MB-231-CM. One-way ANOVA, *** $p < 0.001$, ** $p < 0.01$, * $p < 0.05$, · < 0.1 .

Fig. S9: CM of MDA-MB-231 enhances endothelial network - 24 h and 48 h.

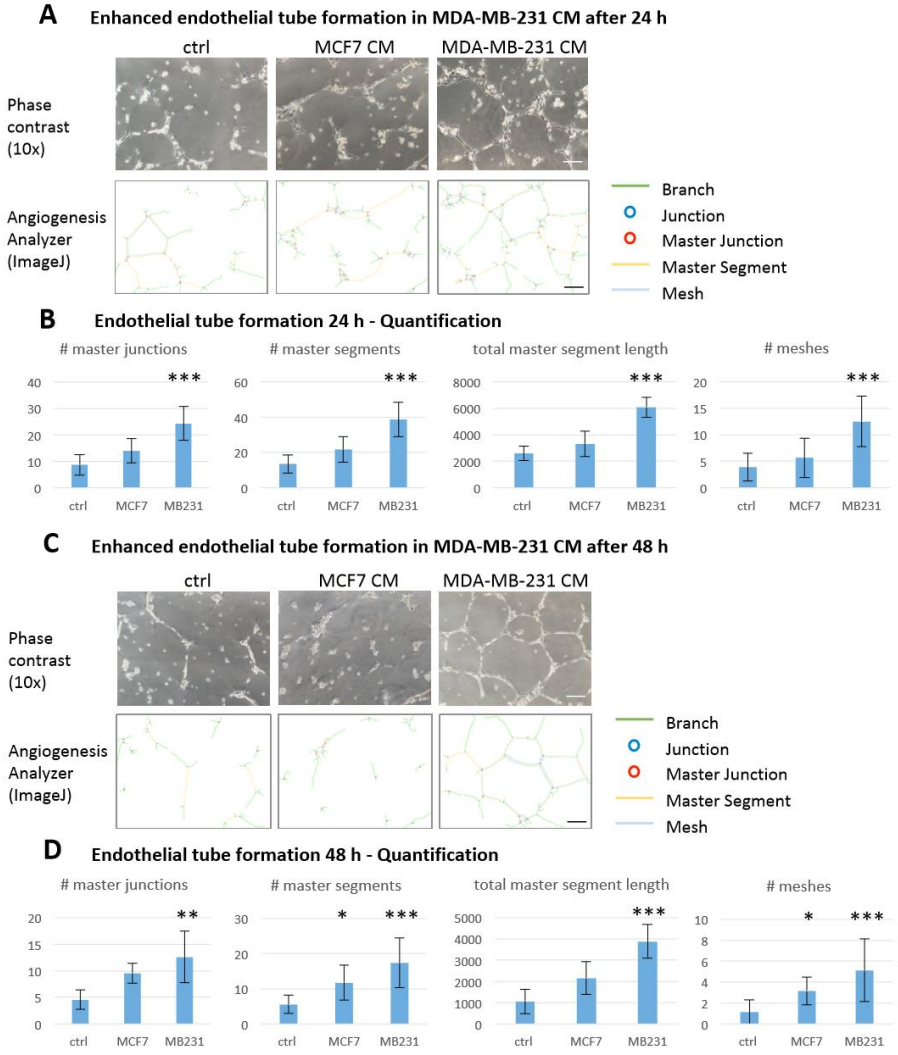

Fig. S9: Conditioned media of MDA-MB-231 enhanced endothelial network - 24 h and 48 h. A) Top: HUVEC endothelial network after 24 h in R10F, MCF7-CM and MDA-MB-231-CM (phase contrast), 10x magnification (scale bar = 100 µm). Bottom: Angiogenesis images showing branches, junctions, master junctions, master segments and meshes. B) Quantification of master junctions, master segments total master segment length and meshes. One-way ANOVA, *** $p < 0.001$, ** $p < 0.01$, * $p < 0.05$, · < 0.1 . C) Top: HUVEC endothelial network after 48 h (phase contrast). Bottom: Angiogenesis images. D) Quantification of master junctions, master segments total master segment length and meshes. One-way ANOVA, *** $p < 0.001$, ** $p < 0.01$, * $p < 0.05$, · < 0.1 .

Fig. S10: CM of HER2+/ECM1+ HCC202 cells enhances endothelial network.

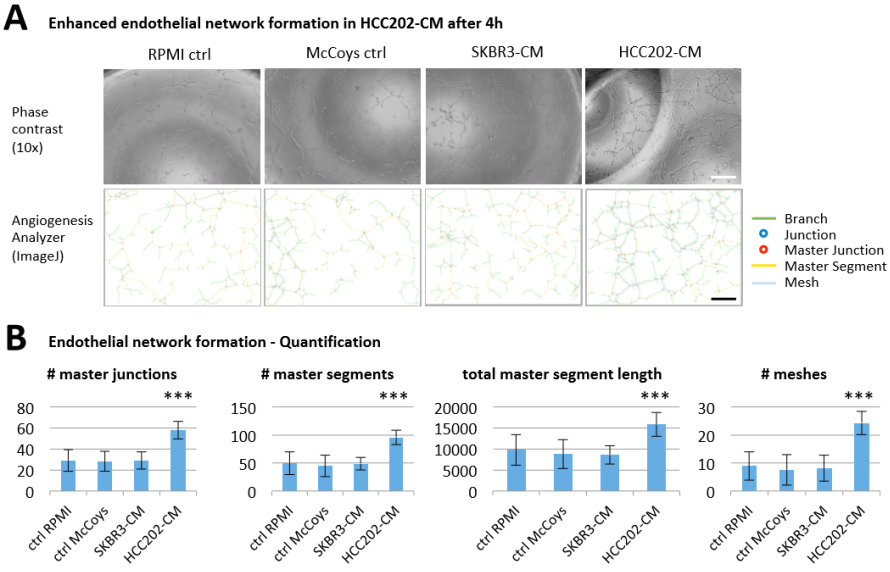

Fig. S10: CM of HER2+/ECM1+ HCC202 cells enhances endothelial network A) Enhanced endothelial network formation in HCC202-CM after 4 h. Top: Phase-contrast images of HUVEC endothelial network on top of matrigel in ctrl RPMI, ctrl McCoys, SKBR3-CM and HCC202-CM, 10x magnification (scale bar = 100 µm). Bottom: Corresponding angiogenesis images (ImageJ, angiogenesis analyzer) showing branches, junctions, master junctions, master segments and meshes. B) Endothelial network formation - Quantification. Quantification of master junctions, master segments, total master segment length and meshes (angiogenesis analyzer). Statistical analysis performed in R, one-way ANOVA, *** $p < 0.001$, ** $p < 0.01$, * $p < 0.05$, · < 0.1 .

Fig. S11: Tendency of decreased tumor volume *in vivo* upon ECM1 KD in D492HER2.

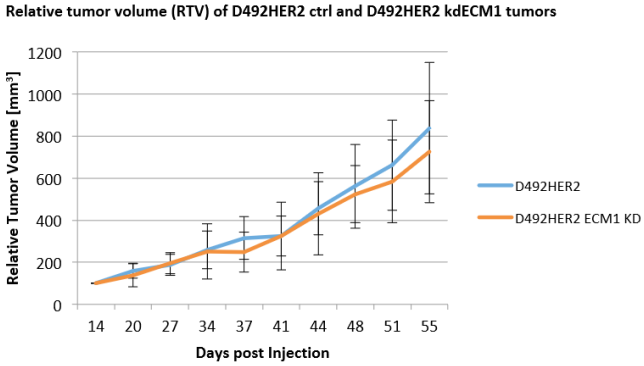

Days post injection	D492HER2 ctrl		D492HER2 kdECM1	
	RTV [mean]	RTV [SD]	RTV [mean]	RTV [SD]
14	100	0	100	0
20	154.8	35.6	138.9	55.4
27	179.5	49.6	195.5	50.4
34	256.6	84.4	251.9	131.4
37	296.2	104.7	248.3	96.0
41	317.6	90.0	324.3	161.4
44	443.5	124.7	429.9	195.0
48	542.3	192.7	523.8	135.2
51	661.1	225.0	583.7	196.3
55	837.6	312.8	726.2	243.0
58	1110.2	447.2	651.2	211.5

Fig. S11: Tendency of decreased tumor volume in vivo upon ECM1 KD in D492HER2. Relative tumor volume (RTV) of of D492HER2 ctrl and D492HER2 kdECM1 tumors. RTV calculated according to the formula 0.5 x length x width^2. Red arrow indicates timepoint chosen for analysis. Statistical analysis was performed using Students T-test, , *** $p < 0.001$, ** $p < 0.01$, * $p < 0.05$, · < 0.1 .

Fig. S12: Blocking endothelial NOTCH signaling prevents D492HER2-induced increase in endothelial network formation.

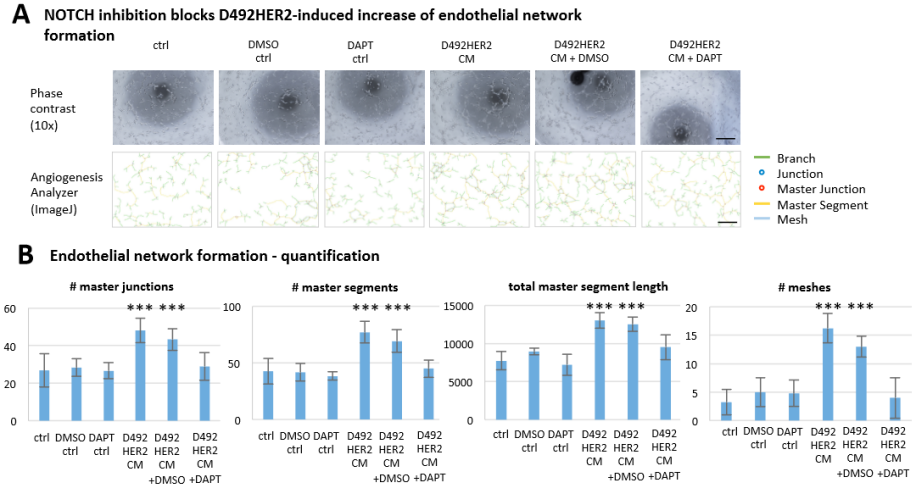

Fig. S12: Blocking endothelial NOTCH signaling prevents D492HER2-induced increase in endothelial network formation. A) NOTCH inhibition blocks D492HER2-induced increase of endothelial network formation. Top: HUVEC endothelial network in ctrl (H14), DMSO ctrl, DAPT ctrl, D492HER2-CM, D492HER2-CM+DMSO and D492HER2-CM+DAPT after 4 h. 4-6 wells as replicates per condition and 1-2 images taken per well at 10x magnification (scale bar = 100 µm). Bottom: Corresponding angiogenesis images (ImageJ angiogenesis analyzer). B) Endothelial network formation - quantification. Quantification of master junctions, master segments, total master segment length and meshes for each image using angiogenesis analyzer plugin. One-way ANOVA, *** $p < 0.001$, ** $p < 0.01$, * $p < 0.05$ · < 0.1.

Fig. S13: Similar HUVEC viability in CM vs. ctrl H14 during network formation assay on top of matrigel.

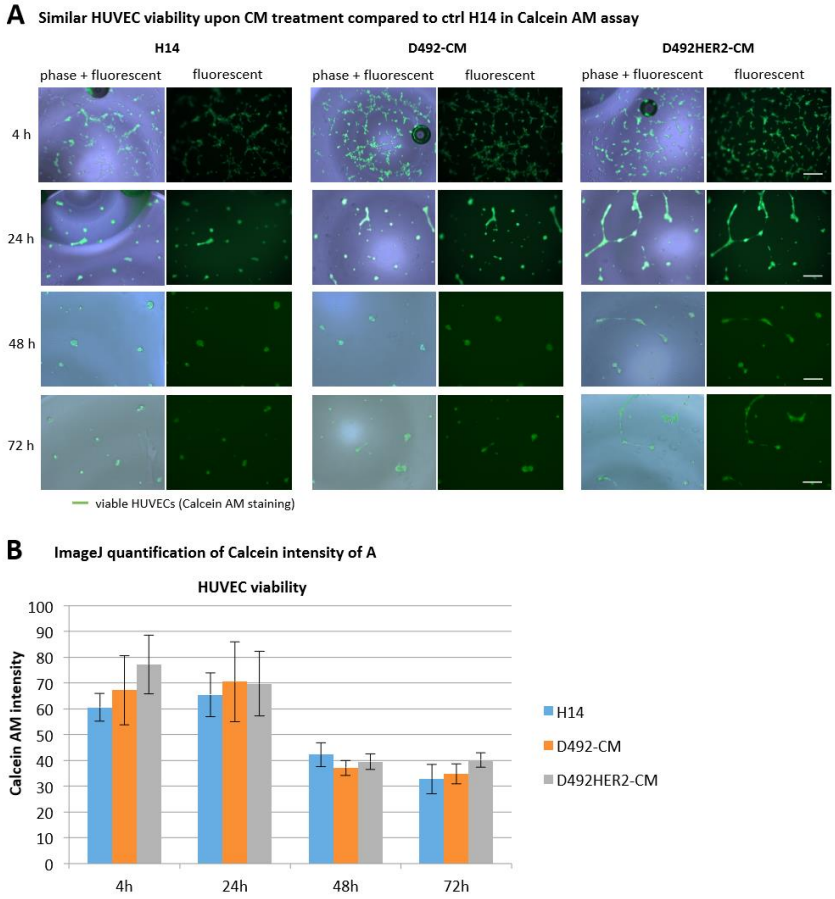

Fig. S13: Similar HUVEC viability in CM vs. H14 during network formation assay on top of matirgel. A) Similar HUVEC viability upon CM treatment compared to H14 in Calcein AM assay. HUVEC endothelial network after 4 h, 24 h, 48 h and 72 h on top of matrigel in H14 ctrl, D492-CM and D492HER2-CM, 10x magnification (scale bar = 100 µm). Left: overlay of phase contrast and fluorescent channel, Right: fluorescent channel. Calcein AM stained viable HUVECs = green. B) ImageJ quantification of Calcein AM staining intensity of HUVEC in H14, D492-CM and D492HER2-CM after 4 h, 24 h, 48 h and 72 h (n = 12).

Supplementary Table S1: Secretome data. Table includes original secretome data (tab 1) (LFQ values, mass spectrometry), lists of proteins higher secreted by D492HER2 compared to D492 (tab 2), compared to D492M (tab 3) (based on volcano plot analysis) and compared to both (tab 4, tab 5), results for enriched GO groups in proteins higher secreted by D492HER2 compared to both (tab 6) (Panther database, overrepresentation test), secretion levels of enriched GO groups and heat map analysis of proteins higher secreted by D492HER2 compared to both.

Supplementary Table S2: Microarray data. List of differentially expressed genes between all 3 replicates of HUVECs treated with D492HER2 ctrl-CM and D492HER2 kdECM1-CM. Upregulated HUVEC genes in D492HER2 kdECM1-CM (green), downregulated genes in D492HER2 kdECM1-CM (orange). Adjusted p-value, fold change (FC) and log2 FC.

Paper V

Journal of Mammary Gland Biology and Neoplasia
https://doi.org/10.1007/s10911-020-09468-x

Mammary Organoids and 3D Cell Cultures: Old Dogs with New Tricks

Jakub Sumbal[1] · Zuzana Budkova[2] · Gunnhildur Ásta Traustadóttir[2] · Zuzana Koledova[1]

Received: 24 July 2020 / Accepted: 4 November 2020

Abstract
3D cell culture methods have been an integral part of and an essential tool for mammary gland and breast cancer research for half a century. In fact, mammary gland researchers, who discovered and deciphered the instructive role of extracellular matrix (ECM) in mammary epithelial cell functional differentiation and morphogenesis, were the pioneers of the 3D cell culture techniques, including organoid cultures. The last decade has brought a tremendous increase in the 3D cell culture techniques, including modifications and innovations of the existing techniques, novel biomaterials and matrices, new technological approaches, and increase in 3D culture complexity, accompanied by several redefinitions of the terms "3D cell culture" and "organoid". In this review, we provide an overview of the 3D cell culture and organoid techniques used in mammary gland biology and breast cancer research. We discuss their advantages, shortcomings and current challenges, highlight the recent progress in reconstructing the complex mammary gland microenvironment in vitro and ex vivo, and identify the missing 3D cell cultures, urgently needed to aid our understanding of mammary gland development, function, physiology, and disease, including breast cancer.

Keywords 3D cell culture · Breast · Co-culture · Extracellular matrix · Imaging · Microenvironment · Organoid · Screening · Stromal cells

Introduction

Our bodies and organs, including mammary gland, are composed of billions of cells, which are organized in a highly defined manner in three-dimensional (3D) space to perform specific functions. The 3D organization and composition of extracellular matrix (ECM), and the identity and 3D architecture of neighboring cells, form a tissue microenvironment, which is fundamental to cell behavior and differentiation. Thus, tissue microenvironment controls tissue growth, development, homeostasis, and function, and is implicated in disease [1, 2]. Therefore, to faithfully model cell behavior and function in vitro and ex vivo, 3D cell culture techniques are required because they allow replication of crucial cell-cell and cell-ECM interactions of tissues in vivo [3]. By contrast, two-dimensional cell cultures on rigid plastic or glass surface do not provide physiologically relevant environmental context, resulting in changes in cell function [4, 5].

The 3D cell culture methods have become staples in the method toolbox of developmental and cancer biologists. In this review, we provide an overview of the 3D cell culture methods used in mammary gland biology and breast cancer research, ranging from a fairly simple cell culture in 3D ECM, through spheroid culture in suspension, to complex organotypic co-cultures of multiple cell types and organoids in 3D ECM. These methods are discussed in the context of mammary gland histology and development, and how they contributed to elucidation of cellular hierarchy, crucial morphogenetic events, function, and disease of mammary gland. We provide a short historical context to the rise of the 3D cell culture field, point out technological advances that have been essential to advanced 3D cell culture setups and analyses, and discuss current challenges and future perspectives of the 3D cell culture techniques in mammary gland biology and breast cancer research, including wishful envisioning of development of currently missing 3D cell culture types.

✉ Gunnhildur Ásta Traustadóttir
gutra@hi.is

✉ Zuzana Koledova
koledova@med.muni.cz

[1] Department of Histology and Embryology, Faculty of Medicine, Masaryk University, Brno, Czech Republic

[2] Stem Cell Research Unit, Biomedical Center, Department of Anatomy, Faculty of Medicine, School of Health Sciences, University of Iceland, Reykjavík, Iceland

Published online: 18 November 2020

Mammary Gland Histology

Mammary gland is composed of two histologically and functionally distinct tissue compartments, epithelium and stroma. The epithelium consists of two main epithelial cell types, luminal cells and basal (myoepithelial) cells, and forms a branched network of tubular structures within the stroma. While there are species-specific differences in the anatomy details, overall, the epithelial structures take few principal forms, depending on their purpose: Alveoli are spherical structures for milk production and are organized into multi-alveolar structures called lobuli. Ducts, sinuses, and cisternae serve to transport and store the milk and are shaped as tubes. Mammary stroma is a complex tissue composed of extracellular matrix (ECM) and several different cell types, including fibroblasts, adipocytes, immune cells, as well as blood vessels and nerves. Stroma provides essential regulatory, and structurally and metabolically supportive functions for the epithelium. Together with the endocrine signaling, epithelial-stromal interactions effectively coordinate mammary epithelial morphogenesis and homeostasis, and deregulation of these interactions leads to developmental defects, including lactation deficiencies, disease, and carcinogenesis (reviewed in [1, 2]).

Mouse is the most widely used experimental animal model for mammary gland biology; yet, there are important differences in the architecture of the mammary gland between mouse and human [6, 7]. Mouse mammary gland is formed by a network of ducts all leading to a single primary duct ending in the nipple. Human mammary gland is composed of several individual branched ductal networks, all leading to the nipple. The resting (non-lactating) adult human gland is more branched, containing terminal ductal lobular units (TDLUs), which represent a more advanced state of the epithelium towards the lactating architecture than the epithelium in the mouse [6, 7]. TDLUs are embedded in collagen I, hyaluronan and fibroblast-rich intralobular stroma. The lobuli are surrounded by a dense interlobular stroma, which contains less cells and more thick collagen fibers, and separates the lobuli from the adipose tissue. In contrast, mouse mammary epithelium is encircled by a relatively thin layer of periductal fibroblasts, and the stroma contains mostly adipose tissue [6, 7] (Fig. 1).

Mammary Gland Development

The sole purpose of the mammary gland, the production of milk to feed progeny, is required only in sexually mature females after they give birth to the progeny. Therefore, although the mammary gland starts developing in both sexes during embryogenesis, it fully develops and achieves full function only in females postnatally. In males, the mammary gland remains rudimentary.

Embryonic mammary gland development (reviewed in [8]) starts with formation of milk lines by slight thickening of the ectoderm. Subsequently, mammary placodes are defined, and the underlying mesenchyme condenses. The mammary placode starts to proliferate into the mammary mesenchyme, forming a primary sprout, which further grows into dermal mesenchyme, the precursor of mammary fat pad. The epithelium further bifurcates and proliferates, resulting in a rudimentary branched tree by the time of birth.

Postnatally, the mammary gland remains relatively quiescent until puberty and grows only slightly, proportionally to the growth of the organism. However, with the onset of puberty in females, the pubertal hormone stimuli awaken the dormant epithelium. The distal parts of the rudimentary epithelial branches develop into terminal end buds (TEBs), highly proliferative structures which drive mammary epithelial expansion by invasion into the fat pad and bifurcation, until a complex branched epithelial structure fills the whole fat pad by the end of puberty. Further epithelial expansion emerges with each estrus cycle (menstrual cycle in human) and further continues with pregnancy, when mammary epithelium develops into alveolar structures capable of milk production. Intriguingly, after weaning, when milk production is no longer required, secretory epithelium is destroyed, and mammary gland remodeled into a pre-pregnancy-like state via a highly controlled process of involution [7]. Together, these highly dynamic and defined postnatal changes make mammary gland an ideal model for study of morphogenesis, tissue plasticity, and of the powerful instructive role of the microenvironment in regulation of epithelial development, homeostasis, and cancer. In these efforts, 3D cell cultures have been employed and proven valuable to a great extent.

3D Cell Cultures of the Mammary Gland

The Rise of 3D Cell Culture and Organoid Techniques in the Mammary Gland Biology Field

Development of the first 3D cell culture techniques went hand-in-hand with the discovery of the crucial role that the microenvironment plays in regulation of cell function and response [9]. Beginning the twentieth century researchers realized that while cell culture on glass Petri dishes allowed cell proliferation and migration, it did not enable expression of several tissue- and function-specific markers in primary cells, such as hepatocytes or mammary epithelial cells [10, 11]. However, they discovered that culturing the cells on floating collagen gels allowed maintenance of some differentiation markers [12], including expression of some milk proteins in mammary epithelial cells in the presence of lactogenic stimuli [11]. Moreover, when mammary epithelial cells were cultured in 3D collagen gels, they self-assembled into structures similar to acini of mammary gland tissue [13]. These collagen gel cultures, which were essentially the first 3D cell cultures, suggested that ECM is a major regulator of gene expression [14], and stimulated further research

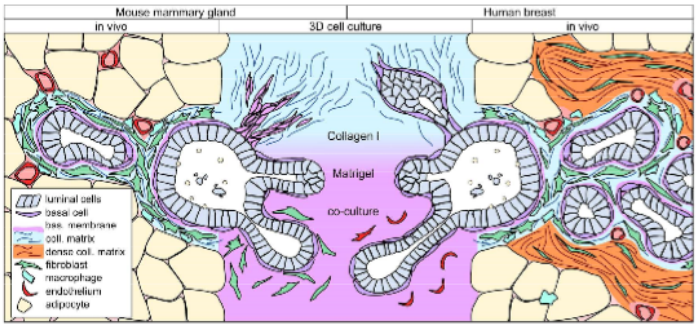

Fig. 1 3D cell cultures as models of mammary gland development and cancer. Both mouse and human mammary glands contain branched epithelial structures consisting of an inner layer of luminal cells and an outer layer of basal cells. In the mouse mammary gland, the epithelium is surrounded by a layer of periductal fibroblasts in a collagenous matrix, but the majority of the stromal volume of the non-lactating gland is taken by adipocytes. In the human breast, the epithelium is organized into terminal ductal lobular units (TDLUs), which contain a fibroblast-rich intralobular stroma around the epithelium and are further embedded in a dense collagen I-rich matrix of interlobular stroma. The adipose tissue is more separated from the epithelium in the human breast than in the mouse mammary gland. In 3D cell culture of primary epithelial organoids, Matrigel or collagen I are the most commonly used ECM. Mouse organoids efficiently branch in the Matrigel, but often lose basal cells at the tips of branches in these conditions. In fibrillar collagen I cultures, primary mouse mammary epithelium becomes invasive. In co-cultures with fibroblasts, the epithelium branches efficiently. Primary human organoids form only small buds in Matrigel and for efficient branching they require culture in floating collagen I gels. In such cultures, primary human organoids or primary human myoepithelial cells form TDLU-like structures by invasive branching morphogenesis. In co-culture with endothelial cells, human epithelial cells with stem cell properties (such as D492) efficiently form prolonged branches

into how the microenvironment regulates tissue function and morphogenesis, for which the mammary gland became one of the cardinal model systems.

A major advancement in the field of mammary 3D cell cultures involved use of laminin-rich ECM derived from Engelbreth-Holm-Swarm sarcoma [15], which revealed that basal lamina both maintains tissue-specific cell differentiation and function, and promotes epithelial cell polarization and tissue-like morphogenesis [16, 17]. Moreover, one of the first 3D primary organoid cultures were developed in the mammary gland field, when the researchers creatively combined the 3D culture in collagen gels [18] or laminin-rich gels [19] with a protocol for isolation of primary mammary epithelial tissue fragments, which had been developed almost 50 years before [20]. Altogether, these 3D cell culture and organoid cultures have formed a strong methodological basis for deciphering the complex interplay of ECM, mechanosignaling, endocrine, paracrine and juxtacrine signaling in regulation of mammary architecture and function, and for further development of more complex and physiologically more relevant 3D culture models.

3D Cell Culture Types and Techniques

In a simplistic view, any culture of cells that allows their 3D organization and/or interaction with ECM is a 3D cell culture. There are many types of 3D cell cultures based on their complexity, and on the material (both cells and ECM) and techniques used in their assembly (reviewed in [3] (Table 1)).

The 3D cell cultures can be composed of one or more cell types; in the latter case, it is often referred to as co-culture. The cells can be cultured in non-adherent conditions (suspension culture) or in the contact with ECM/scaffold. The cells can be seeded as single cells, or be pre-aggregated by several methods to form aggregates or spheroids, or as organoids (Table 1). The organoids are structures formed by two or more types of cells that by architecture and function resemble miniaturized organ units and can be of primary origin (explants) or grown from mammary stem cells in 3D ECM. Spheroids, on the other hand, are spherical masses of cells formed by proliferation or aggregation, often of only one cell type (such as breast cancer cells). Mammospheres are clonal spherical structures formed from mammary stem/progenitor cells in non-adherent conditions [21, 22]. Organotypic cultures are the most advanced 3D cell cultures that usually combine more than two types of cells (often as co-culture of organoids and stromal cells) in a 3D ECM that highly resemble the organ architecture in vivo. All these 3D cell culture types can be manually assembled using merely conventional laboratory and cell culture equipment.

In addition to manually assembled 3D cell culture techniques, two 3D cell culture technologies have been developed

Table 1 3D cell culture types

Type	Description	Strengths, special applications, weaknesses
Cellular input		
Mammary and breast cancer cell lines	immortal cell lines of normal mammary gland or mammary tumor origin	☺ availability; homogeneity across laboratories ☹ genetic and phenotypic changes due to cell culture adaptation and immortalization; missing natural heterogeneity of breast tumors
Primary cells derived from mammary gland, breast tumors, breast cancer metastases, or milk	normal mammary/breast or cancer cells isolated from freshly collected tissue (as single cells or tissue fragments) or from blood (circulating tumor cells), malignant effusion or ascites (metastatic cells), milk	☺ intact cellular genotype, phenotype and heterogeneity representing the tissue of origin (limitations in breast cancer); potential for personalized medicine applications ☹ accessibility; time consuming isolation; requirement for ethical committee approval and informed patient consent; culture conditions for breast cancer cells need further optimization
ESCs, iPSCs	pluripotent stem cells capable of differentiation to any cell type, including mammary gland cells	☺ unlimited replicative potential ☹ differentiation protocols not fully established, requirement for ethical committee approval
Complexity of cellular inputs		
monocultures	culture of one cell type or one type of tissue fragments	
co-cultures	culture of two or more different cell types or tissue fragments	☺ enable heterotypic cellular interactions
Complexity of cellular structures		
Single celled cultures	Cells seeded and cultured in 3D ECM as individual cells	☺ analysis of properties and processes of individual cells (ECM attachment, mechanism of migration etc.) ☹ epithelial cells lack proper architecture
Spheroids	spherical structures formed by cell aggregation or by clonal growth	☺ simple assembly, more realistic in modeling tumor response than 2D cultures ☹ poor cell heterogeneity, cell line-dependent architecture
Mammospheres	spherical structures formed by clonal growth of stem/progenitor cells in non-adherent conditions	☺ quantification of stem/progenitor cell potential; stem cell studies
Organoids	complex structures of two or more cell types that structurally and functionally represent miniaturized organ units or recapitulate tumors in ECM; stem cell-derived or tissue organoids	☺ recapitulate in vivo organ architecture, physiologically highly relevant
Organotypic co-cultures	co-cultures of mammary epithelial organoids/breast cancer organoids with stromal cells in ECM	☺ most realistically recapitulate in vivo organ architecture and epithelial-stromal interactions
Methods of assembly		
Manual	3D cell cultures assembled manually by pipetting in standard cell culture dishes	☺ no special equipment required
3D bioprinting	micropatterned 3D cell culture architecture generated by programmed positioning of the bioink (cells and ECM) by a 3D printer	☺ precision, consistency, and reproducibility of culture assembly
Microfluidic devices	3D cell culture in microfluidic devices per design	☺ precise control of microenvironmental conditions such as perfusion; very low consumption of culture medium

The culture types are divided according to the type of cellular input, complexity of cellular inputs, complexity of cellular structures, and methods of assembly

ECM extracellular matrix, *ESCs* embryonic stem cells, *iPSCs* induced pluripotent stem cells

to aid enhanced spatiotemporal control of cellular localization and microenvironment. They include bioprinting and microfluidic technologies (Table 1).

3D bioprinting is an additive manufacturing technology that enables formation of a complex 3D tissue architecture by precise positioning of bioink (a mixture of hydrogel scaffold and cells) to desired spatial locations with microscale precision. Several bioprinting methods exist, including inkjet, extrusion-based, and laser-assisted method [23]. Using bioprinting, both large-scale 3D mammary epithelial

structures [24, 25] and models of tissue/tumor microenvironment [26] can be assembled with consistency and reproducibility. Thus, 3D bioprinting is advantageous over manual assembling of 3D cell cultures when architectural precision, consistency and reproducibility is desired or required, such as in high-throughput drug screening [27, 28].

Microfluidic technology has contributed to 3D cell culture methods new platforms for generation of spheroids as well as devices for 3D cell culture in microchannels allowing perfusions. Microfluidic devices enable precise fluid control, and thereby control of microenvironmental conditions such as shear stress, pressure, oxygen, and nutrient or growth factor gradients in 3D cell cultures on chip [29]. Microfluidics has been useful in studies on various aspects of mammary cell and breast cancer biology, such as cell migration [30], cell-ECM interaction [31], or cell-cell interaction [32], as well as in drug screening [33, 34].

Cellular Sources for 3D Cell Cultures

Because mammary gland is an evolutionarily young organ specific for mammals, the model organisms and potential sources of primary cells for 3D culture formation are animals restricted to the class *Mammalia*. Primary human tissue is the most relevant source of cells for mammary and breast cancer 3D cell cultures because of the more straightforward application of findings from these studies to human medicine. However, it has been difficult to preserve primary human mammary tissue architecture, complexity and heterogeneity in long-term culture, and only recent advances in organoid technology have brought considerable improvements [35–38]. Moreover, use of patient tissues is associated with several other challenges, such as interpatient heterogeneity, inability to control multiple characteristics of the tissue, and administrative burden (requirement of ethical committee approval and informed patient consent).

Animal models such as mice, on the other hand, provide a virtually unlimited source of tissue with the advantages of genetic manipulation in vivo to provide source of primary tissue/cells with introduced mutations according to study requirement, use of inbred lines to reduce heterogeneity, and the option to carefully control/select for multiple variables that influence mammary tissue characteristics, such as estrus cycle phase, parity, age, stage of mammary tumor development etc. Nevertheless, other animal sources of primary cells have been explored, too. Rat mammary tissue-derived organoids have been shown to recapitulate mammary branching and lipid droplet genesis in Matrigel-based 3D cell cultures [39, 40]. Furthermore, mammosphere assay has been used to quantify mammary stem/progenitor cell potential in a wide range of mammalian species, from mouse and rat through dog and cat to water buffalo (reviewed in [41]). From several species, such as dog [42] or goat [43], mammary organoid or spheroid cultures in 3D were established. However, in general, the 3D cell culture of mouse, rat, and human mammary cells is more standardized, while the 3D cell cultures for other species are still under development.

Primary cells derived from fresh tissue samples have only a limited life span and replicative potential. Therefore, immortalization of primary cells to form cell lines with unlimited cell culture potential has been widely used. Cell lines represent a homogenous and inexpensive platform to model biological processes and have proven useful in both developmental and cancer biology. However due to adaptation to 2D culture environment, many cell lines differ genetically and phenotypically from their origin [44]. Therefore, important steps have been taken in recent years to improve culture conditions for primary mammary epithelial cells, including ER positive mammary epithelial cells [45] and putative human breast stem cells [37, 46].

Nowadays, there are many normal mammary epithelial cell lines and breast cancer cell lines available. The most widely used normal mammary epithelial cell lines include MCF10A and D492, which are both of human origin and with distinctive morphogenetic properties. MCF10A is a spontaneously immortalized human mammary epithelial cell line derived from a fibrocystic tissue [47]. In 3D Matrigel, MCF10A cells generate polarized acini-like spheroids with a hollow lumen [5, 48]. In 3D ECM consisting of Matrigel and collagen I, MCF10A cells form branched interconnected networks of cells with mixed basal and luminal phenotype that lack proper architecture of breast ducts [49].

The D492 cell line was established from normal breast tissue obtained from reduction mammoplasty by immortalization of MUC1 negative and EpCAM positive suprabasal cells [50]. D492 cells generate both luminal- and myoepithelial cells in culture and form elaborate branching structures when embedded in Matrigel [50]. Moreover, in a co-culture with breast endothelial cells, D492 cells display increased branching ability and undergo irreversible epithelial-to-mesenchymal transition (EMT), as evident by the formation of spindle-like mesenchymal colonies [51]. The propensity of D492 cells towards EMT could be linked to the method of their immortalization by human papilloma virus 16 oncogenes E6 and E7, expression of which has been correlated to EMT induction [52, 53]. Nevertheless, D492 cells have been widely used to study branching morphogenesis and cellular plasticity (reviewed in [54]).

Normal luminal epithelial cells polarize correctly and generate growth-arrested acinus-like colonies in response to cues from the basement membrane, whereas myoepithelial cells form polarized ball-like structures [5, 55]. Malignant mammary epithelial cells, on the other hand, fail to polarize and often form disorganized proliferative colonies in 3D reconstituted basement membrane matrix [5, 56]. In fact, in 3D Matrigel, breast cancer cell lines adopt one of four distinct

metabolism in lactation [91]. However, only few authors have executed concise studies on lactation itself in 3D cell cultures. Mammary epithelial line KIM2 cultured in a synthetic fat pad showed the potential to form a ductal system capable of milk production and subsequent involution [92]. Later, primary mammary organoids were demonstrated to undergo pregnancy-associated alveologenesis and milk production upon proper hormonal treatment, and an involution-like process upon withdrawal of lactation stimuli. Interestingly, after having gone through the involution-like process, these organoids were able to enter a new round of morphogenesis [64]. Importantly, the organoids derived from primary mammary tissue retain contractility of the myoepithelial layer [64, 93], another sign of physiological relevance of these organoid models.

Together, these advanced 3D cell culture models – organoids bear a potential to become a platform for research on milk production, drug testing, and are a promising source for food-production biotechnology, including infant nutrition. Although to date no protocols for human lactation organoids have been reported, suggesting that inducing lactation in human cells might be more challenging, emerging start-up companies are confidently up to the task of cultured human breast milk production [94, 95].

3D Cell Cultures in Breast Cancer Research

Breast cancer is a heterogenous disease. Breast tumors differ both between patients (intertumor heterogeneity) as well as show genomic and biological variations between cells within each tumor (intratumor heterogeneity). Intertumor heterogeneity can be classified from a histopathological perspective based on morphological differences between breast tumors (ductal carcinoma in situ, invasive ductal carcinoma or invasive lobular carcinoma) or based on their molecular signature (luminal A, luminal B, HER2 positive, triple negative, and normal-like tumors) [96, 97]. On the other hand, intratumor heterogeneity arises by tumor cell evolution in response to microenvironmental pressures in the context of different tumor etiologies [98]. Thus, tumor microenvironment shapes tumor evolution. The tumor microenvironment is comprised of ECM and of both normal and tumor-activated stromal cells, such as cancer-associated fibroblasts (CAFs), adipocytes, immune cells (such as tumor-associated macrophages), and endothelial cells [99].

Breast cancer heterogeneity and the implication of the tumor microenvironment in breast cancer progression imposes a need for experimental models that can recapitulate this complexity. Therefore, 3D cell culture methods have proven an invaluable tool for preclinical breast cancer research (Fig. 2). They bridge the gap between 2D cell cultures, which do not capture tumor heterogeneity, nor the microenvironmental influences, and animal models. Superior to drug screens in 2D cell cultures, spheroids bring another level of complexity and display a higher resistance to anti-cancer drugs [100–102]. Spheroids mimic some main features of solid tumors, such as structural organization, hypoxia, and nutrient gradients, and are widely used in drug discovery for screening of large numbers of molecules [100]. Spheroids can be established from breast cancer cell lines alone or in co-culture with stromal cells.

Still, patient-derived tumor tissue is superior to cancer cell lines in representing the actual tumor tissue. Therefore, the focus of preclinical cancer research has increasingly been shifted from using cancer cell lines towards the use of patient-derived material. As such, PDX models are advantageous due to their recapitulation of tumor-stromal interactions and representation of the heterogeneity of cancer, even after serial passaging in mice [103]. One of the major limitations of PDX models is that the immune and stromal components are of mouse instead of human origin, but this may be improved by co-engraftment of human bone-marrow cells and/or cancer-associated fibroblasts [104]. Moreover, the technique is time-consuming, laborious, inefficient and has a long culture cycle, which makes it unsuitable for high-throughput drug screening [105]. In comparison, patient-derived tumor organoid cultures or PDX organoid cultures are less time and resource demanding and have a short culture cycle, which makes them superior for biobanking, drug screening, and precision medicine (Fig. 2) [36, 105]. Organoid technology has a great potential to retain the heterogeneity of the tumor tissue [36, 59], but the organoid culture protocol requires further optimization to enable long-term culture of all breast cancer subtypes [55]. Originally-described breast cancer organoid culture medium [36] favors selective expansion of basal-like cells [55]. Moreover, primary breast cancer organoid cultures often contain also residual non-malignant mammary tissue, which severely limits their suitability for biobanking or drug screening [55].

Organoid technology is also accelerating the preclinical breast cancer research using GEMMs. GEMM-derived mammary tumor organoids can be readily established and rapidly expanded in vitro, while recapitulating the epithelial morphology and preserving the drug response of the original tumor [106]. GEMM organoids can be exposed to genetic or pharmacologic screens in vitro, and efficiently engrafted into syngeneic hosts, making them a powerful tool for rapid testing of breast cancer mechanisms [106].

Importantly, to fully capture the tumor complexity and to provide breast tumor models with the highest pathophysiological relevance, stromal microenvironment must be included in the tumor-derived cultures.

Modeling Complex Stromal Microenvironment of Normal Mammary Gland and Breast Tumors

Together with GEMMs, 3D cell cultures have been very helpful in modeling and deciphering the role of individual stromal

and the cells can be seeded on decellularized tissue-ECM sections for further studies [70]. Extracted and solubilized decellularized ECM can be added to scaffolding matrix, such as the above-mentioned alginate or peptide gels, or to Matrigel [71], to study the effect of primary ECM components (but not their primary organization) on cell behavior.

3D Cell Cultures in the Service of Research on Mammary Gland Development

Branching Morphogenesis

Branching morphogenesis is a fundamental process of mammary gland development. Branching of mammary epithelial ducts occurs first prenatally during embryonic development. Later, during puberty, the mammary epithelium is elaborated into the complex branched tree of a mature gland through a process of primary branching by bifurcation of TEBs, and secondary branching via formation of lateral branches from existing ducts. Further branching (tertiary branching) occurs during each estrous cycle and during pregnancy to expand alveolar surface for lactation.

Mechanisms regulating mammary branching morphogenesis are of great interest both for their relevance to development of other branched organs and because they are often hijacked during breast cancer invasion. 3D cell culture models allow for studies on branching morphogenesis, polarization and lumen formation, which are not possible in 2D monolayer cultures. Genetically engineered mouse models (GEMMs) have revealed several signaling pathways important for mammary gland branching morphogenesis, such as receptor tyrosine kinases EGFR, FGFR, IGFR or c-met [72–76]. To bring insights into the soluble ligands of these receptors that are involved in the branching morphogenesis, 3D cell cultures of mammary epithelium have been essential because the receptors are often promiscuous and genetic knock-out of a soluble ligand is often rescued by another from that ligand family. 3D cell cultures of primary mammary organoids have provided an important functional assay to directly assess the effect of a ligand added to a defined cell culture medium. FGF2, TGFα, EGF or neuregulin were found to promote branching of mouse mammary epithelium in Matrigel culture [19, 64, 77, 78]. Yet FGF7, FGF10, or HGF, all predicted to be important for mammary branching morphogenesis by their receptor specificity, did not induce mouse mammary organoid branching in Matrigel [19, 64, 78–80]. However, all these growth factors induce invasive branching morphogenesis of mammary epithelium in collagen I cultures [18, 81, 82]. Importantly, when comparing results from different studies, it is critical to pay attention also to the basal organoid culture medium used. Mammary epithelial response to growth factors may be modulated by other components of the medium, such as in the case of FGF7, which does not induce branching in medium containing only serum replacement, but does so in a much richer medium containing also serum and hydrocortisone [19, 38].

FGF2-induced branching of primary mouse mammary organoids has become the golden standard for ex vivo studies on mammary epithelial branching morphogenesis. Among other findings, this model has helped to shed light on the role of ERK signaling [83], ECM composition [66], and myoepithelial cell function [84] in mammary epithelial morphogenesis, and the requirement of morphogenesis for efficient lactation [64]. The model has also supported in vivo studies on pubertal mammary branching phenotypes in GEMMs [85–87], or helped to identify novel modulators of mammary branching morphogenesis by a chemical screen [88].

Nevertheless, the architecture and development of human mammary gland is different from mouse mammary gland. Among other differences, human mammary epithelium achieves a more complex and more mature architecture during puberty than mouse mammary epithelium, which remains immature until pregnancy. Thus, mouse models and mouse organoid cultures bring only limited insights into the mechanisms of human mammary development, including branching morphogenesis. Human organoid cultures provide a very useful tool to elucidate these events and to decipher interspecies differences. They revealed differential regulation of ductal morphogenesis by EGFR and FGFR2 ligands between mouse and human. While mouse organoids readily branch in response to FGFR2 ligands, human organoids require EGFR signaling for ductal outgrowth and the level of EGFR signaling regulates myoepithelial cell fate [38]. Moreover, human mammary organoid cultures in deformable collagen suggest that human mammary ducts and terminal ductal lobular units are formed by invasive branching morphogenesis, while mouse mammary ductal network is formed by non-invasive collective cell migration [37, 77].

Advanced 3D cell culture models have helped to decipher the role of stromal cells in mammary epithelial branching morphogenesis, or the mechanisms of lactation. These 3D cell culture models will be discussed in following chapters.

Lactation

While mechanisms of branching morphogenesis are well studied in 3D cell cultures, the hallmark function of mammary gland, lactation, has been much less covered by the 3D cell cultures. Importantly, the assembly of proper architecture of mammary epithelium was shown decades ago to be imperative for in vitro lactation [17]. Thus, 3D cell cultures are an essential tool for laboratory studies of lactation.

Detection of milk production, such as by immune detection of β-casein or other milk proteins, has been employed as a read-out of mammary organoid functionality in several studies [60, 89, 90]. In another study, spheroids of breast adenocarcinoma cells PMC42 were used to investigate copper

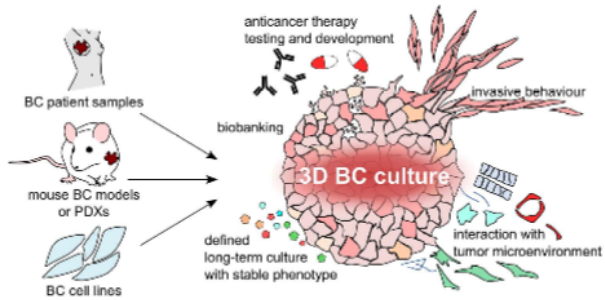

Fig. 2 Breast cancer 3D cultures. To study breast cancer in 3D cell culture, primary tumor cells can be isolated from breast cancer (BC) patients, mouse mammary tumors, or from patient-derived xenografts (PDXs). Alternatively, established breast cancer (BC) cell lines, routinely cultured and expanded in 2D, can be cultured in 3D ECM to provide more realistic and pathophysiologically relevant models of breast cancer. 3D breast cancer models such as breast cancer organoids enable long-term culture of primary tumor cells while preserving their heterogeneity and recapitulating the histopathological and genetic features of original tumors. 3D breast cancer cell models have a wide application in studies on breast cancer cell mechanisms, including invasion, metastasis formation, and interaction with tumor microenvironment, and provide a malleable platform for development and high-throughput testing of anticancer therapies because they allow more accurate prediction of the drug responses of patients

cell populations in mammary gland development and disease. In 3D ECM, mammary epithelial cells or breast cancer cells can be co-cultured with specific stromal cells of choice according to the experiment, providing a defined reductionist experimental setting in in vivo-like conditions.

For example, advanced co-cultures of primary mammary organoids with primary mammary fibroblasts have helped to understand the role of fibroblasts in regulation of mammary epithelial morphogenesis [107, 108]. When co-cultured with mammary epithelium in 3D Matrigel, mammary fibroblasts induced branching, and this process was regulated by EGFR and FGFR signaling in fibroblasts [79, 109]. To model epithelial-stromal interactions during lactation and involution in vitro, a synthetic fat pad model was developed [92, 110]. In this model, 3D scaffold of collagen and hyaluronic acid is freeze-dried to achieve proper architecture and then sequentially seeded with preadipocytic, mammary epithelial, and even monocyte/macrophage cell lines, while treated with adipogenic or lactogenic media to achieve cell functional differentiation towards cell types of the mammary gland. To interrogate the role of endothelial cells in mammary epithelial morphogenesis, 3D co-cultures of D492 cells with breast endothelial cells can be employed [51]. Recently, a biomimetic microfluidic 3D culture model was developed, in which hollow channels in collagen I ECM are coated with Matrigel and seeded with MCF10A cells to form a duct-like structure, or with primary human dermal microvascular cells to form a vessel-like structure [111]. This model facilitates studies on paracrine signaling between mammary epithelium and endothelium.

To aid research on the role of microenvironment in breast cancer disease, there have been major efforts to reproduce breast tumor microenvironment in vitro (reviewed in [112]). Multiple studies have adopted the co-culture approach, in which only breast cancer cells were cultured in 3D ECM environment, while the stromal cells were cultured in a transwell that allowed only paracrine signaling but avoided cell-cell contact between the epithelial/cancer and stromal compartments. However, to reproduce the epithelial-stromal interactions in breast cancer using 3D cell cultures more realistically, cellular contacts should be enabled. First, both breast cancer cells and stromal cells can be seeded as single-celled suspensions in ECM [113, 114]. Another common approach has been aggregation of breast cancer cell lines into spheroids and their co-culture with endothelial or fibroblasts cell lines [115]. Alternatively, the breast cancer cells have been aggregated together with endothelial or fibroblast cells by various methods, including aggregation in non-adherent plates, such as coated with agar [116], the hanging-drop method [117, 118], magnetic levitation [119], or microprinting [120]. Recently, there has been a major progress towards development and use of pathogenetically highly-relevant 3D co-cultures of primary tumor-derived organoids and stromal cells, including immune cells or cancer-associated fibroblast [121–123]. These 3D co-culture models enable dissection of dynamic changes in tumor environment, associated with tumor progression and metastasis, including immune cell suppression or education [121, 123]. An interesting model of primary tumor fragment co-culture with adipocytes in anisotropic collagen scaffolds, on the other hand, faithfully mimics

collagen orientation in the tumor invasive front and thus enables quantification of invasive potential of primary tumors and testing the response of invading cells on therapeutic drugs [124]. Altogether, 3D co-cultures derived from patient tumors represent a promising tool for precision medicine, including drug-efficacy testing for personalized therapy.

In order to gain increased control over spatial distribution of cells and ECM, and biophysical and biochemical factors in models of the tumor microenvironment, bioprinting (reviewed in [125]) and microfluidics have been explored. Using bioprinting, cells can be quite precisely distributed in 3D according to experimental needs. For instance, breast cancer cells can be spatially positioned onto ex vivo microvascular networks from rat mesentery for studies on cancer cell migration, invasion, angiogenesis and lymphangiogenesis [126]. Furthermore, 3D bioprinting scaffolds can be tailored for in vitro modeling of the breast cancer ECM, such as by adjusting scaffold material, the pore size, fiber density, and orientation of the layers [125]. Microfluidics has been widely used to study extravasation and metastasis [127, 128].

The Synergy of Mouse Models and Organoids

3D cell cultures are a great alternative to excessive use of animal models for many applications from basic through cancer research to toxicology studies. However, mouse models do have their indisputable place in mammary gland biology and breast cancer research for their high physiological relevance that is still far ahead of any in vitro organotypic culture. In fact, mouse models and primary 3D cultures benefit from each other greatly.

First, GEMMs carrying fluorescent labels of cells are a great source of organoids for time-lapse confocal imaging, especially for imaging over several days, when fluorescent dyes are continuously diluted out. Also, different cells types can be marked with different fluorophores to facilitate analysis of their contribution to resulting phenotype, such as the role of basal cell during mammary organoid branching morphogenesis or invasion [77, 84, 129] (Fig. 3A). Furthermore, organoids from inducible fluorescent reporter mouse models can be used for live visualization of lineage tracing [89] (Fig. 3B). Conceptually similar is the use of mammary tissue-derived epithelial organoids from inducible breast cancer GEMMs for controlled induction of oncogene activity, such as for residual disease modeling ex vivo [130].

Furthermore, mammary organoid cultures and co-cultures can help to decipher mechanisms of genetic knock-out/knock-down in mouse models. For instance, when a conventional genetic knockout results in mammary developmental phenotype, organotypic 3D cell culture can be used to visualize organ morphogenesis within controlled environment, and thus test the potential systemic effect (such as through changes in endocrine regulation of mammary gland development). Furthermore, the organotypic 3D co-cultures enable investigation of contribution of the epithelial and stromal compartment to the phenotype; the epithelial organoids can be cultured alone, or in the presence of the stromal cells (incl. specific stromal cell types). This approach has been used to identify the causative role of stromal cells in knock-out mouse models [109, 131] (Fig. 3C). Conversely, primary mammary cells can be expanded and genetically manipulated ex vivo as organoids and then transplanted into a cleared mammary fat pad for rapid generation of somatic GEMMs [132] (Fig. 3D).

Techniques for Imaging of 3D Cell Cultures

Imaging techniques are essential to analysis of 3D cell cultures. They provide the critical readout of cellular architecture, function and identity in the 3D cell cultures. Brightfield microscopy allows assessment of gross morphology of individual cells, spheroids or organoids in 3D cell cultures, including during live cell imaging. Fluorescence microscopy (epifluorescence, laser-scanning or spinning disc confocal, light-sheet, or multiphoton microscopy) enables a more detailed characterization of cellular composition, including cell type identification in organoid cultures and organotypic co-cultures. Electron microscopy (scanning and transmission electron microscopy) provides insights into ultrastructure of cells or fine surface morphological details of cells, organoids or ECM. Moreover, when selecting the appropriate imaging method, besides the level of morphological and histological detail achievable, compatibility with live cell imaging, phototoxicity, or requirement of special sample preparation must be carefully considered (Table 2).

Live-Cell Imaging of Organoids

3D cultures provide the possibility to observe, in real time, processes that are naturally buried deep in the tissue. Epithelial morphogenesis usually occurs in relatively long time, oscillating from days to weeks, and there are multiple issues that need to be taken into consideration [133]. First, the phototoxicity resulting from oxygen radical formation can be a limiting factor for imaging dependent on laser illumination. This could be overcome by either lowering the exposure time, laser power, or frequency of image taking. However, a compromise between the quality/detail and low phototoxicity/cell viability will always be required. A practical way how to observe long-term morphogenesis with low phototoxicity is the use of bright field or differential interference contrast imaging, either to capture the morphogenesis itself, or to identify a shorter window for more detailed imaging. Bright-field live-cell imaging has been successfully used to visualize branching of organoids and collective cell migration [77, 84, 134], cell invasion into ECM [84, 131], epithelial interaction with stromal cells [79] and at a high frame rate it was used to visualize myoepithelial cell contraction [64, 93]. Furthermore, bright-field imaging is a

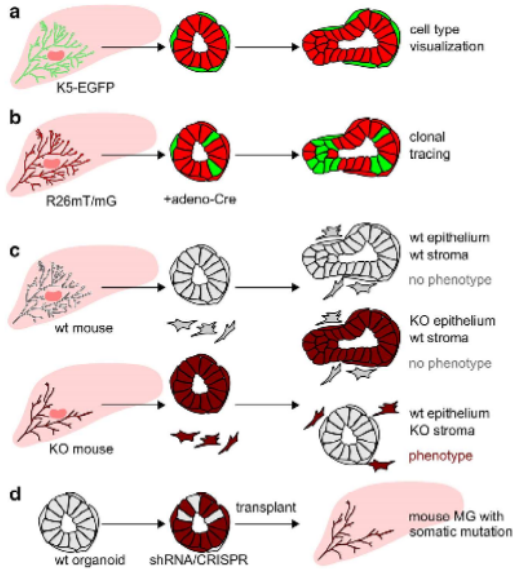

Fig. 3 Examples of synergistic use of genetic mouse models (GEMMs) and 3D organoid cultures. A, B. GEMMs carrying constitutively expressed (**a**) or conditionally expressed (**b**) fluorescent labels can be used as source of fluorescently labeled cells/organoids for cell type visualization (**a**) and clonal tracing (**b**) during ex vivo culture. **C.** 3D organoid (co-)cultures enable deciphering the causative cell types responsible for the phenotype observed in conventional knockout models. In this scheme, the phenotype of decreased epithelial branching and fat pad invasion in KO mammary gland during puberty is caused by a defect in stromal cells. **D.** Primary cells/organoids can be genetically modified ex vivo and transplanted into cleared mammary fat pad to create somatic GEMMs for further investigation

promising source for high-throughput drug screening, when coupled with automated image analysis [135, 136].

Confocal live-cell imaging greatly enhances the morphological detail acquired. However, it requires genetic fluorescent markers or live-cell imaging dyes. Moreover, the phototoxicity of lasers must be taken into considerations [133]. With the right settings, single cells can be imaged in the tissue context of organoids in 3D over time (providing a 4D measurement) to study morphogenesis, signaling, or interaction with the surrounding tissue [77, 129]. Advanced microscopy techniques, such as light-sheet microscopy or computational post-processing of epifluorescence images enable long-term imaging without worries about laser-induced damage to observed cells [137].

Imaging of Fixed Organoids

When the highest possible detail is needed, analysis of fixed samples might be necessary. Fixed samples provide a wide possibility to stain 3D cell cultures with dyes that are either cytotoxic themselves (e.g. phalloidin) or require cytotoxic

Table 2 Comparison of imaging method applicability for 3D cell culture analysis

Microscopy technique	live imaging	resolution	depth of imaging	phototoxicity	sample preparation	costs of imaging
1. bright-field	possible	low	N/A	negligible	easy	low
2. epifluorescence	possible	low	N/A	low	moderate	low
3. laser scanning conf.	possible	high	low	high	moderate	middle
4. spinning disc conf.	possible	high	low	low	moderate	high
5. light-sheet	possible	high	high	low	laborious	high
6. multiphoton	possible	high	very high	low	moderate	high
3 to 6 with clearing	impossible	high	very high	N/A	moderate to laborious	high
7. SEM	impossible	high	N/A	N/A	laborious	middle
8. TEM	impossible	ultra-high	N/A	N/A	laborious	middle

preparation before staining (e.g. cell permeabilization before immunolabeling of specific proteins). Furthermore, clearing can be applied to fixed samples to enhance imaging resolution and imaging depth of studied 3D cell cultures. There are many methods for tissue clearing that are far beyond the scope of this article (for a review, see [138, 139]). Some of these clearing methods, such as using a fructose-glycerol clearing agent, have already been successfully employed to clear mammary organoids [140]. Additionally, proper mounting of the sample can enable shortening the working distance of the objective used, thus enabling the use of higher magnification [67, 140]. Moreover, transmission electron microscopy can be used to unveil cell ultrastructure of 3D cell cultures [17, 63].

Conclusions and Future Perspectives

3D cell culture models have greatly facilitated dissection of mechanisms that regulate mammary gland development and disease. Recent developments in 3D cell culture techniques have culminated in optimization of organotypic cultures that realistically mimic cellular architecture and function of postnatal mammary gland and breast tumor tissues ex vivo and in vitro.

Mammary organotypic 3D cultures conveniently enable reconstitution of pathophysiologically highly relevant models of mammary gland or breast tumors from genetically manipulated cells and from different combinations of cell types, together with introduction of alterations to ECM composition, architecture, stiffness, or other microenvironmental characteristics according to experimental needs, while being amenable to imaging. In fact, time-lapse live-cell imaging of organoid cultures have provided invaluable insights into processes of normal development and tumorigenesis, which are in vivo inaccessible to human eye. Moreover, patient-derived breast tumor organoids have provided a new tool for dissection of tumor heterogeneity, mechanisms of tumorigenesis, and a platform for precision medicine. Emerging 3D organotypic co-cultures have revealed important insights into the roles of stromal cells in mammary gland development and breast cancer. However, long-term co-culture of multiple cell types remains a challenge – both from the perspective of optimal culture conditions as well as from the perspective of imaging.

One particularly underdeveloped field in the 3D cell culture models of the mammary gland are models of embryonic development. In this field, explant cultures of embryonic mammary gland have dominated. However, we envisage future development of embryonic organotypic cultures, which will help to shed light on the earliest processes of mammary morphogenesis, such as specification of mammary epithelial and stromal lineages or instructive signals for embryonic branching morphogenesis. Moreover, ESCs and iPSC-derived organoids offer a great platform for modeling of mammary lineage specification as well as disease modeling that remains to be exploited. Meanwhile, advances in material science, additive manufacturing, microfluidics, automatization, or imaging technologies keep providing novel materials, technologies and methods for building and analysis of 3D cell cultures, inspiring development of novel culture types and setups, and the approaches to their assembly and analysis.

The recent re-discovery of the organoid technology that first emerged three decades ago in the mammary gland biology field, and development of protocols for culture of a wide range of "organs in a dish" has taken the bioscientific world by storm. The organoid technologies have won their place in the scientific spotlight and hold promise for new scientific discoveries, biotechnology applications, and personalized medicine. Hop on the organoid technology train, it will bring you closer to your new scientific discoveries and achievements!

Funding This work was supported by grants from The Science Fund of the Icelandic Cancer Society (G.A.T.), and the Grant Agency of Masaryk University (projects no. MUNI/A/1382/2019 and MUNI/G/1446/2018), and by funds from the Faculty of Medicine, Masaryk University to junior researcher Z.K. (ROZV/28/LF/2020).

Compliance with Ethical Standards

Conflict of Interest The authors declare that they have no conflict of interest.

Ethics Approval Not applicable.

Availability of Data and Material Not applicable.

Code Availability Not applicable.

References

1. Nelson CM, Bissell MJ. Of extracellular matrix, scaffolds, and signaling: tissue architecture regulates development, homeostasis, and cancer. Annu Rev Cell Dev Biol. 2006;22:287–309.
2. Wiseman BS, Werb Z. Stromal effects on mammary gland development and breast cancer. Science. 2002;296:1046–9.
3. Koledova Z. 3D cell culture: an introduction. Methods Mol Biol. 2017;1612:1–11.
4. Bissell MJ. The differentiated state of normal and malignant cells or how to define a "normal" cell in culture. Int Rev Cytol. 1981;70:27–100.
5. Petersen OW, Rønnov-Jessen L, Howlett AR, Bissell MJ. Interaction with basement membrane serves to rapidly distinguish growth and differentiation pattern of normal and malignant human breast epithelial cells. Proc Natl Acad Sci USA. 1992;89:9064–8.
6. Dontu G, Ince TA. Of mice and women: a comparative tissue biology perspective of breast stem cells and differentiation. J Mammary Gland Biol Neoplasia. 2015;20:51–62.
7. McNally S, Stein T. Overview of mammary gland development: a comparison of mouse and human. Methods Mol Biol. 2017;1501:1–17.
8. Robinson GW. Cooperation of signalling pathways in embryonic mammary gland development. Nat Rev Genet. 2007;8:963–72.

9. Simian M, Bissell MJ. Organoids: a historical perspective of thinking in three dimensions. J Cell Biol. 2017;216:31–40.
10. Bissell DM, Tilles JG. Morphology and function of cells of human embryonic liver in monolayer culture. J Cell Biol. 1971;50:222–31.
11. Emerman JT, Pitelka DR. Maintenance and induction of morphological differentiation in dissociated mammary epithelium on floating collagen membranes. In Vitro. 1977;13:316–28.
12. Michalopoulos G, Pitot HC. Primary culture of parenchymal liver cells on collagen membranes: morphological and biochemical observations. Exp Cell Res. 1975;94:70–8.
13. Hall HG, Farson DA, Bissell MJ. Lumen formation by epithelial cell lines in response to collagen overlay: a morphogenetic model in culture. PNAS. 1982;79:4672–6.
14. Bissell MJ, Hall HG, Parry G. How does the extracellular matrix direct gene expression? J Theor Biol. 1982;99:31–68.
15. Orkin RW, Gehron P, McGoodwin EB, Martin GR, Valentine T, Swarm R. A murine tumor producing a matrix of basement membrane. J Exp Med. 1977;145:204–20.
16. Barcellos-Hoff MH, Aggeler J, Ram TG, Bissell MJ. Functional differentiation and alveolar morphogenesis of primary mammary cultures on reconstituted basement membrane. Development. 1989;105:223–35.
17. Li ML, Aggeler J, Farson DA, Hatier C, Hassell J, Bissell MJ. Influence of a reconstituted basement membrane and its components on casein gene expression and secretion in mouse mammary epithelial cells. PNAS. 1987;84:136–40.
18. Simian M, Hirai Y, Navre M, Werb Z, Lochter A, Bissell MJ. The interplay of matrix metalloproteinases, morphogens and growth factors is necessary for branching of mammary epithelial cells. Development. 2001;128:3117–31.
19. Fata JE, Mori H, Ewald AJ, Zhang H, Yao E, Werb Z, et al. The MAPK(ERK-1,2) pathway integrates distinct and antagonistic signals from TGFalpha and FGF7 in morphogenesis of mouse mammary epithelium. Dev Biol. 2007;306:193–207.
20. Lasfargues EY. Cultivation and behavior in vitro of the normal mammary epithelium of the adult mouse. Anat Rec. 1957;127:117–29.
21. Dontu G, Abdallah WM, Foley JM, Jackson KW, Clarke MF, Kawamura MJ, et al. In vitro propagation and transcriptional profiling of human mammary stem/progenitor cells. Genes Dev. 2003;17:1253–70.
22. Shaw FL, Harrison H, Spence K, Ablett MP, Simões BM, Farnie G, et al. A detailed mammosphere assay protocol for the quantification of breast stem cell activity. J Mammary Gland Biol Neoplasia. 2012;17:111–7.
23. Murphy SV, Atala A. 3D bioprinting of tissues and organs. Nat Biotechnol. 2014;32:773–85.
24. Ling K, Huang G, Liu J, Zhang X, Ma Y, Lu T, et al. Bioprinting-based high-throughput fabrication of three-dimensional MCF-7 human breast Cancer cellular spheroids. Engineering. 2015;1:269–74.
25. Reid JA, Mollica PA, Bruno RD, Sachs PC. Consistent and reproducible cultures of large-scale 3D mammary epithelial structures using an accessible bioprinting platform. Breast Cancer Res. 2018;20:122.
26. Zhou X, Zhu W, Nowicki M, Miao S, Cui H, Holmes B, et al. 3D bioprinting a cell-laden bone matrix for breast Cancer metastasis study. ACS Appl Mater Interfaces. 2016;8:30017–26.
27. Mazzocchi A, Soker S, Skardal A. 3D bioprinting for high-throughput screening: Drug screening, disease modeling, and precision medicine applications. Applied Physics Reviews. American Institute of Physics. 2019;6:011302.
28. Knowlton S, Onal S, Yu CH, Zhao JJ, Tasoglu S. Bioprinting for cancer research. Trends Biotechnol. 2015;33:504–13.
29. Shang M, Soon RH, Lim CT, Khoo BL, Han J. Microfluidic modelling of the tumor microenvironment for anti-cancer drug development. Lab Chip. 2019;19:369–86.
30. Peela N, Sam FS, Christenson W, Truong D, Watson AW, Mouneimne G, et al. A three dimensional micropatterned tumor model for breast cancer cell migration studies. Biomaterials. 2016;81:72–83.
31. Gioiella F, Urciuolo F, Imparato G, Brancato V, Netti PA. An engineered breast Cancer model on a Chip to replicate ECM-activation in vitro during tumor progression. Adv Healthc Mater. 2016;5:3074–84.
32. Choi Y, Hyun E, Seo J, Blundell C, Kim HC, Lee E, et al. A microengineered pathophysiological model of early-stage breast cancer. Lab Chip. 2015;15:3350–7.
33. Lanz HL, Saleh A, Kramer B, Cairns J, Ng CP, Yu J, et al. Therapy response testing of breast cancer in a 3D high-throughput perfused microfluidic platform. BMC Cancer. 2017;17:709.
34. Mi S, Du Z, Xu Y, Wu Z, Qian X, Zhang M, et al. Microfluidic co-culture system for cancer migratory analysis and anti-metastatic drugs screening. Sci Rep. 2016;6:35544.
35. Rosenbluth JM, Schackmann RCJ, Gray GK, Selfors LM, Li CM-C, Boedicker M, et al. Organoid cultures from normal and cancer-prone human breast tissues preserve complex epithelial lineages. Nat Commun Nature Publishing Group. 2020;11:1–14.
36. Sachs N, de Ligt J, Kopper O, Gogola E, Bounova G, Weeber F, et al. A Living Biobank of Breast Cancer Organoids Captures Disease Heterogeneity. Cell. 2018;172:373–386.e10.
37. Linnemann JR, Miura H, Meixner LK, Irmler M, Kloos UJ, Hirschi B, et al. Quantification of regenerative potential in primary human mammary epithelial cells. Development. 2015;142:3239–51.
38. Pasic L, Eisinger-Mathason TSK, Velayudhan BT, Moskaluk CA, Brenin DR, Macara IG, et al. Sustained activation of the HER1–ERK1/2–RSK signaling pathway controls myoepithelial cell fate in human mammary tissue. Genes Dev. 2011;25:1641–53.
39. Darcy KM, Black JD, Hahm HA, Ip MM. Mammary organoids from immature virgin rats undergo ductal and alveolar morphogenesis when grown within a reconstituted basement membrane. Exp Cell Res. 1991;196:49–65.
40. Darcy KM, Zangani D, Shea-Eaton W, Shoemaker SF, Lee PP, Mead LH, et al. Mammary fibroblasts stimulate growth, alveolar morphogenesis, and functional differentiation of normal rat mammary epithelial cells. In Vitro Cell Dev Biol Anim. 2000;36:578–92.
41. Rauner G, Ledet MM, de Walle GRV. Conserved and variable: understanding mammary stem cells across species. Cytometry Part A. 2018;93:125–36.
42. Cocola C, Molgora S, Piscitelli E, Veronesi MC, Greco M, Bragato C, et al. FGF2 and EGF are required for self-renewal and Organoid formation of canine Normal and tumor breast stem cells. J Cell Biochem. 2017;118:570–84.
43. Ogorevc J, Zorc M, Dovč P. Development of an in vitro goat mammary gland model: Establishment, characterization, and applications of primary goat mammary cell cultures. In: Kukovics S, editor. Goat Science. IntechOpen; 2017. https://doi.org/10.5772/intechopen.71853.
44. Keller PJ, Lin AF, Arendt LM, Klebba I, Jones AD, Rudnick JA, et al. Mapping the cellular and molecular heterogeneity of normal and malignant breast tissues and cultured cell lines. Breast Cancer Res. 2010;12:R87.
45. Fridriksdottir AJ, Kim J, Villadsen R, Klitgaard MC, Hopkinson BM, Petersen OW, et al. Propagation of oestrogen receptor-positive and oestrogen-responsive normal human breast cells in culture. Nat Commun. 2015;6:8786.

46. Fridriksdottir AJ, Villadsen R, Morsing M, Klitgaard MC, Kim J, Petersen OW, et al. Proof of region-specific multipotent progenitors in human breast epithelia. Proc Natl Acad Sci U S A. 2017;114:E10102–11.
47. Soule HD, Maloney TM, Wolman SR, Peterson WD, Brenz R, McGrath CM, et al. Isolation and characterization of a spontaneously immortalized human breast epithelial cell line, MCF-10. Cancer Res. 1990;50:6075–86.
48. Debnath J, Muthuswamy SK, Brugge JS. Morphogenesis and oncogenesis of MCF-10A mammary epithelial acini grown in three-dimensional basement membrane cultures. Methods. 2003;30:256–68.
49. Qu Y, Han B, Yu Y, Yao W, Bose S, Karlan BY, et al. Evaluation of MCF10A as a reliable model for Normal human mammary epithelial cells. PLoS One. 2015;10:e0131285.
50. Gudjonsson T, Villadsen R, Nielsen HL, Rønnov-Jessen L, Bissell MJ, Petersen OW. Isolation, immortalization, and characterization of a human breast epithelial cell line with stem cell properties. Genes Dev. 2002;16:693–706.
51. Sigurdsson V, Hilmarsdottir B, Sigmundsdottir H, Fridriksdottir AJR, Ringnér M, Villadsen R, et al. Endothelial induced EMT in breast epithelial cells with stem cell properties. PLoS One. 2011;6:e23833.
52. Hellner K, Mar J, Fang F, Quackenbush J, Münger K. HPV16 E7 oncogene expression in normal human epithelial cells causes molecular changes indicative of an epithelial to mesenchymal transition. Virology. 2009;391:57–63.
53. Jung Y-S, Kato I, Kim H-RC. A novel function of HPV16-E6/E7 in epithelial-mesenchymal transition. Biochem Biophys Res Commun. 2013;435:339–44.
54. Briem E, Ingthorsson S, Traustadottir GA, Hilmarsdottir B, Gudjonsson T. Application of the D492 cell lines to explore breast morphogenesis, EMT and Cancer progression in 3D culture. J Mammary Gland Biol Neoplasia. 2019;24:139–47.
55. Goldhammer N, Kim J, Timmermans-Wielenga V, Petersen OW. Characterization of organoid cultured human breast cancer. Breast Cancer Res. 2019;21:141.
56. Lee GY, Kenny PA, Lee EH, Bissell MJ. Three-dimensional culture models of normal and malignant breast epithelial cells. Nat Methods. 2007;4:359–65.
57. Kenny PA, Lee GY, Myers CA, Neve RM, Semeiks JR, Spellman PT, et al. The morphologies of breast cancer cell lines in three-dimensional assays correlate with their profiles of gene expression. Mol Oncol. 2007;1:84–96.
58. Powley IR, Patel M, Miles G, Pringle H, Howells L, Thomas A, et al. Patient-derived explants (PDEs) as a powerful preclinical platform for anti-cancer drug and biomarker discovery. Br J Cancer. 2020;122:735–44.
59. Whittle JR, Lewis MT, Lindeman GJ, Visvader JE. Patient-derived xenograft models of breast cancer and their predictive power. Breast Cancer Res. 2015;17:17.
60. Qu Y, Han B, Gao B, Bose S, Gong Y, Wawrowsky K, et al. Differentiation of human induced pluripotent stem cells to mammary-like Organoids. Stem Cell Reports. 2017;8:205–15.
61. Cregan MD, Fan Y, Appelbee A, Brown ML, Klopcic B, Koppen J, et al. Identification of nestin-positive putative mammary stem cells in human breastmilk. Cell Tissue Res. 2007;329:129–36.
62. Streuli CH. Cell adhesion in mammary gland biology and neoplasia. J Mammary Gland Biol Neoplasia. 2003;8:375–81.
63. Ewald AJ, Huebner RJ, Palsdottir H, Lee JK, Perez MJ, Jorgens DM, et al. Mammary collective cell migration involves transient loss of epithelial features and individual cell migration within the epithelium. J Cell Sci. 2012;125:2638–54.
64. Sumbal J, Chiche A, Charifou E, Koledova Z, Li H. Primary Mammary Organoid Model of Lactation and Involution. Front Cell Dev Biol. 2020;8:68.
65. Brownfield DG, Venugopalan G, Lo A, Mori H, Tanner K, Fletcher DA, et al. Patterned collagen fibers orient branching mammary epithelium through distinct signaling modules. Curr Biol. 2013;23:703–9.
66. Nguyen-Ngoc K-V, Ewald AJ. Mammary ductal elongation and myoepithelial migration are regulated by the composition of the extracellular matrix. J Microsc. 2013;251:212–23.
67. Miller DH, Sokol ES, Gupta PB. 3D primary culture model to study human mammary development. Methods Mol Biol. 2017;1612:139–47.
68. Chaudhuri O, Koshy ST, Branco da Cunha C, Shin J-W, Verbeke CS, Allison KH, et al. Extracellular matrix stiffness and composition jointly regulate the induction of malignant phenotypes in mammary epithelium. Nat Mater. 2014;13:970–8.
69. Ashworth JC, Thompson JL, James JR, Slater CE, Pijuan-Galitó S, Lis-Slimak K, et al. Peptide gels of fully-defined composition and mechanics for probing cell-cell and cell-matrix interactions in vitro. Matrix Biol. 2020;85–86:15–33.
70. Wishart AL, Conner SJ, Guarin JR, Fatherree JP, Peng Y, McGinn RA, et al. Decellularized extracellular matrix scaffolds identify full-length collagen VI as a driver of breast cancer cell invasion in obesity and metastasis. Sci Adv. 2020;6:43.
71. Schedin P, Mitrenga T, McDaniel S, Kaeck M. Mammary ECM composition and function are altered by reproductive state. Mol Carcinog. 2004;41:207–20.
72. Bonnette SG, Hadsell DL. Targeted disruption of the IGF-I receptor gene decreases cellular proliferation in mammary terminal end buds. Endocrinology. 2001;142:4937–45.
73. Gamer OB, Bush KT, Nigam KB, Yamaguchi Y, Xu D, Esko JD, et al. Stage-dependent regulation of mammary ductal branching by Heparan sulfate and HGF-cMet signaling. Dev Biol. 2011;355:394–403.
74. Lu P, Ewald AJ, Martin GR, Werb Z. Genetic mosaic analysis reveals FGF receptor 2 function in terminal end buds during mammary gland branching morphogenesis. Dev Biol. 2008;321:77–87.
75. Parsa S, Ramasamy SK, De Langhe S, Gupte VV, Haigh JJ, Medina D, et al. Terminal end bud maintenance in mammary gland is dependent upon FGFR2b signaling. Dev Biol. 2008;317:121–31.
76. Sebastian J, Richards R, Walker M, Wiesen J, Werb Z, Derynck R, et al. Activation and function of the epidermal growth factor receptor and erbB-2 during mammary gland morphogenesis. Cell Growth Differ. 1998;9:777–85.
77. Ewald AJ, Brenot A, Duong M, Chan BS, Werb Z. Collective epithelial migration and cell rearrangements drive mammary branching morphogenesis. Dev Cell. 2008;14:570–81.
78. Jardé T, Lloyd-Lewis B, Thomas M, Kendrick H, Melchor L, Bougaret L, et al. Wnt and Neuregulin1/ErbB signalling extends 3D culture of hormone responsive mammary organoids. Nat Commun. 2016;7:13207.
79. Sumbal J, Koledova Z. FGF signaling in mammary gland fibroblasts regulates multiple fibroblast functions and mammary epithelial morphogenesis. Development. 2019;146:dev185306.
80. Zhang X, Martinez D, Koledova Z, Qiao G, Streuli CH, Lu P. FGF ligands of the postnatal mammary stroma regulate distinct aspects of epithelial morphogenesis. Development. 2014;141:3352–62.
81. Niranjan B, Buluwela L, Yant J, Perusinghe N, Atherton A, Phippard D, et al. HGF/SF: a potent cytokine for mammary growth, morphogenesis and development. Development. 1995;121:2897–908.
82. Pavlovich A, Boghaert E, Nelson CM. Mammary branch initiation and extension are inhibited by separate pathways downstream of TGFβ in culture. Exp Cell Res. 2011;317:1872–84.

83. Huebner RJ, Neumann NM, Ewald AJ. Mammary epithelial tubes elongate through MAPK-dependent coordination of cell migration. Development. 2016;143:983–93.
84. Sirka OK, Shamir ER, Ewald AJ. Myoepithelial cells are a dynamic barrier to epithelial dissemination. J Cell Biol. 2018;217:3368–81.
85. Soady KJ, Tomillo G, Kendrick H, Meniel V, Olijnyk-Dallis D, Morris JS, et al. The receptor protein tyrosine phosphatase PTPRB negatively regulates FGF2-dependent branching morphogenesis. Development. 2017;144:3777–88.
86. Tang C, van den Bijgaart RJE, Looman MWG, Tel-Karthaus N, de Graaf AMA, Gilfillan S, et al. DC-SCRIPT deficiency delays mouse mammary gland development and branching morphogenesis. Dev Biol. 2019;455:42–50.
87. Xu W, Gulvady AC, Goreczny GJ, Olson EC, Turner CE. Paxillin-dependent regulation of apical-basal polarity in mammary gland morphogenesis. Development. 2019;146:9.
88. Basham KJ, Kieffer C, Shelton DN, Leonard CJ, Bhonde VR, Vankayalapati H, et al. Chemical genetic screen reveals a role for Desmosomal adhesion in mammary branching morphogenesis. J Biol Chem. 2013;288:2261–70.
89. Jamieson PR, Dekkers JF, Rios AC, Fu NY, Lindeman GJ, Visvader JE. Derivation of a robust mouse mammary organoid system for studying tissue dynamics. Development. 2017;144:1065–71.
90. Mroue R, Inman J, Mott J, Budunova I, Bissell MJ. Asymmetric expression of connexins between luminal epithelial- and myoepithelial- cells is essential for contractile function of the mammary gland. Dev Biol. 2015;399:15–26.
91. Freestone D, Cater MA, Ackland ML, Paterson D, Howard DL, de Jonge MD, et al. Copper and lactational hormones influence the CTR1 copper transporter in PMC42-LA mammary epithelial cell culture models. J Nutr Biochem. 2014;25:377–87.
92. Campbell JJ, Botos L-A, Sargeant TJ, Davidenko N, Cameron RE, Watson CJ. A 3-D in vitro co-culture model of mammary gland involution. Integr Biol (Camb). 2014;6:618–26.
93. Zhou T, Lu Y, Xu C, Wang R, Zhang L, Lu P. Occludin protects secretory cells from ER stress by facilitating SNARE-dependent apical protein exocytosis. PNAS. 2020;117:4758–69.
94. TurtleTree Labs [Internet]. [cited 2020 Oct 2]. Available from: https://turtletreelabs.com/.
95. Mother cultured breastmilk | BIOMILQ | United States [Internet]. BIOMILQ. [cited 2020 Oct 2]. Available from: https://www.biomilq.com.
96. Perou CM, Sørlie T, Eisen MB, van de Rijn M, Jeffrey SS, Rees CA, et al. Molecular portraits of human breast tumours. Nature. 2000;406:747–52.
97. Sørlie T, Perou CM, Tibshirani R, Aas T, Geisler S, Johnsen H, et al. Gene expression patterns of breast carcinomas distinguish tumor subclasses with clinical implications. Proc Natl Acad Sci USA. 2001;98:10869–74.
98. Nowell PC. The clonal evolution of tumor cell populations. Science. 1976;194:23–8.
99. Hirata E, Sahai E. Tumor microenvironment and differential responses to therapy. Cold Spring Harb Perspect Med. 2017;7:7.
100. Breslin S, O'Driscoll L. The relevance of using 3D cell cultures, in addition to 2D monolayer cultures, when evaluating breast cancer drug sensitivity and resistance. Oncotarget. 2016;7:45745–56.
101. Imamura Y, Mukohara T, Shimono Y, Funakoshi Y, Chayahara N, Toyoda M, et al. Comparison of 2D- and 3D-culture models as drug-testing platforms in breast cancer. Oncol Rep. 2015;33:1837–43.
102. Lovitt CJ, Shelper TB, Avery VM. Doxorubicin resistance in breast cancer cells is mediated by extracellular matrix proteins. BMC Cancer. 2018;18:41.
103. Hidalgo M, Amant F, Biankin AV, Budinská E, Byrne AT, Caldas C, et al. Patient-derived xenograft models: an emerging platform for translational cancer research. Cancer Discovery. 2014;4:998–1013.
104. Dobrolecki LE, Airhart SD, Alferez DG, Aparicio S, Behbod F, Bentires-Alj M, et al. Patient-derived xenograft (PDX) models in basic and translational breast cancer research. Cancer Metastasis Rev. 2016;35:547–73.
105. Yang L, Liu B, Chen H, Gao R, Huang K, Guo Q, et al. Progress in the application of organoids to breast cancer research. J Cell Mol Med. 2020;24:5420–7.
106. Duarte AA, Gogola E, Sachs N, Barazas M, Annunziato S, de Ruiter JR, et al. BRCA-deficient mouse mammary tumor organoids to study cancer-drug resistance. Nat Methods. 2018;15:134–40.
107. Koledova Z. 3D Coculture of mammary Organoids with Fibrospheres: a model for studying epithelial-stromal interactions during mammary branching morphogenesis. Methods Mol Biol. 2017;1612:107–24.
108. Koledova Z, Lu P. A 3D fibroblast-epithelium co-culture model for understanding microenvironmental role in branching morphogenesis of the mammary gland. Methods Mol Biol. 2017;1501:217–31.
109. Koledova Z, Zhang X, Streuli C, Clarke RB, Klein OD, Werb Z, et al. SPRY1 regulates mammary epithelial morphogenesis by modulating EGFR-dependent stromal paracrine signaling and ECM remodeling. Proc Natl Acad Sci U S A. 2016;113:E5731–40.
110. Campbell JJ, Davidenko N, Caffarel MM, Cameron RE, Watson CJ. A multifunctional 3D co-culture system for studies of mammary tissue morphogenesis and stem cell biology. PLoS One. 2011;6:e25661.
111. Kutys ML, Polacheck WJ, Welch MK, Gagnon KA, Koorman T, Kim S, et al. Uncovering mutation-specific morphogenic phenotypes and paracrine-mediated vessel dysfunction in a biomimetic vascularized mammary duct platform. Nat Commun. 2020;11:3377.
112. Bahcecioglu G, Basara G, Ellis BW, Ren X, Zorlutuna P. Breast cancer models: engineering the tumor microenvironment. Acta Biomater. 2020;106:1–21.
113. Pallegar NK, Garland CJ, Mahendralingam M, Viloria-Petit AM, Christian SL. A novel 3-dimensional co-culture method reveals a partial Mesenchymal to epithelial transition in breast Cancer cells induced by adipocytes. J Mammary Gland Biol Neoplasia. 2019;24:85–97.
114. Shekhar MPV, Werdell J, Tait L. Interaction with endothelial cells is a prerequisite for branching ductal-alveolar morphogenesis and hyperplasia of Preneoplastic human breast epithelial cells: regulation by estrogen. Cancer Res Am Assoc Cancer Res. 2000;60:439–49.
115. Swaminathan S, Cranston AN, Clyne AM. A three-dimensional in vitro Coculture model to quantify breast epithelial cell adhesion to endothelial cells. Tissue Eng Part C: Methods. 2019;25:609–18.
116. Holliday DL, Brouilette KT, Markert A, Gordon LA, Jones JL. Novel multicellular organotypic models of normal and malignant breast: tools for dissecting the role of the microenvironment in breast cancer progression. Breast Cancer Res. 2009;11:R3.
117. Ren J, Smid M, Iaria J, Salvatori DCF, van Dam H, Zhu HJ, et al. Cancer-associated fibroblast-derived gremlin 1 promotes breast cancer progression. Breast Cancer Res. 2019;21:109.
118. Upreti M, Jamshidi-Parsian A, Koonce NA, Webber JS, Sharma SK, Asea AA, et al. Tumor-endothelial cell three-dimensional spheroids: new aspects to enhance radiation and drug therapeutics. Transl Oncol. 2011;4:365–76.

119. Jaganathan H, Gage J, Leonard F, Srinivasan S, Souza GR, Dave B, et al. Three-dimensional in vitro co-culture model of breast tumor using magnetic levitation. Sci Rep. 2014;4:6468.
120. Ham SL, Thakuri PS, Plaster M, Li J, Luker KE, Luker GD, et al. Three-dimensional tumor model mimics stromal – breast cancer cells signaling. Oncotarget. 2017;9:249–67.
121. Chan IS, Knútsdóttir H, Ramakrishnan G, Padmanaban V, Warrier M, Ramirez JC, et al. Cancer cells educate natural killer cells to a metastasispromoting cell state. J Cell Biol. 2020;219:9.
122. Chatterjee S, Bhat V, Berdnikov A, Liu J, Zhang G, Buchel E, et al. Paracrine Crosstalk between Fibroblasts and ER+ Breast Cancer Cells Creates an IL1β-Enriched Niche that Promotes Tumor Growth. iScience. 2019;19:388–401.
123. Phan-Lai V, Florczyk SJ, Kievit FM, Wang K, Gad E, Disis ML, et al. Three-dimensional scaffolds to evaluate tumor associated fibroblast-mediated suppression of breast tumor specific T cells. Biomacromolecules. 2013;14:1330–7.
124. Hume RD, Pensa S, Brown EJ, Kreuzaler PA, Hitchcock J, Husmann A, et al. Tumour cell invasiveness and response to chemotherapeutics in adipocyte invested 3D engineered anisotropic collagen scaffolds. Scientific Reports. Nat Publ Group. 2018;8:12658.
125. Belgodere JA, King CT, Bursavich JB, Burow ME, Martin EC, Jung JP. Engineering breast cancer microenvironments and 3D bioprinting. Front Bioeng Biotechnol. 2018;6:66.
126. Burks HE, Phamduy TB, Azimi MS, Saksena J, Burow ME, Collins-Burow BM, et al. Laser direct-write onto live tissues: a novel model for studying Cancer cell migration. J Cell Physiol. 2016;231:2333–8.
127. Bersini S, Jeon JS, Dubini G, Arrigoni C, Chung S, Charest JL, et al. A microfluidic 3D in vitro model for specificity of breast cancer metastasis to bone. Biomaterials. 2014;35:2454–61.
128. Coughlin MF, Kamm RD. The use of microfluidic platforms to probe the mechanism of Cancer cell extravasation. Adv Healthcare Mater. 2020;9:1901410.
129. Neumann NM, Perrone MC, Veldhuis JH, Huebner RJ, Zhan H, Devreotes PN, et al. Coordination of Receptor Tyrosine Kinase Signaling and Interfacial Tension Dynamics Drives Radial Intercalation and Tube Elongation. Dev Cell. 2018;45:67–82.e6.
130. Havas KM, Milchevskaya V, Radic K, Alladin A, Kafkia E, Garcia M, et al. Metabolic shifts in residual breast cancer drive tumor recurrence. J Clin Invest. 2017;127:2091–105.
131. Feinberg TY, Zheng H, Liu R, Wicha MS, Yu SM, Weiss SJ. Divergent Matrix-Remodeling Strategies Distinguish Developmental from Neoplastic Mammary Epithelial Cell Invasion Programs. Dev Cell. 2018;47:145–160.e6.
132. Zhang Z, Christin JR, Wang C, Ge K, Oktay MH, Guo W. Mammary-stem-cell-based somatic mouse models reveal breast Cancer drivers causing cell fate Dysregulation. Cell Rep. 2016;16:3146–56.
133. Ewald AJ. Practical considerations for long-term time-lapse imaging of epithelial morphogenesis in three-dimensional organotypic cultures. Cold Spring Harb Protoc. 2013;2013:100–17.
134. Huebner RJ, Lechler T, Ewald AJ. Developmental stratification of the mammary epithelium occurs through symmetry-breaking vertical divisions of apically positioned luminal cells. Development. 2014;141:1085–94.
135. Borten MA, Bajikar SS, Sasaki N, Clevers H, Janes KA. Automated brightfield morphometry of 3D organoid populations by OrganoSeg. Sci Rep. 2018;8:5319.
136. Hasnain Z, Fraser AK, Georgess D, Choi A, Macklin P, Bader JS, et al. OrgDyn: Feature and model based characterization of spatial and temporal organoid dynamics. Bioinformatics. 2020;36:3292–94.
137. Alladin A, Chaible L, Garcia del Valle L, Sabine R, Loeschinger M, Wachsmuth M, et al. Tracking cells in epithelial acini by light sheet microscopy reveals proximity effects in breast cancer initiation. Postovit L-M, White RM, Rios A, editors. eLife. 2020;9:e54066.
138. Richardson DS, Lichtman JW. Clarifying tissue clearing. Cell. 2015;162:246–57.
139. Richardson DS, Lichtman JW. SnapShot: Tissue Clearing. Cell. 2017;171:496–496.e1.
140. Dekkers JF, Alieva M, Wellens LM, Ariese HCR, Jamieson PR, Vonk AM, et al. High-resolution 3D imaging of fixed and cleared organoids. Nat Protoc. 2019;14:1756–71.